An Exploration of Joint Likelihood Spatio-temporal Point Process Models in the Study of Animal Movement and Habitat Selection

Megan R. Morton

Submitted in fulfilment of the requirements for the
Degree of Doctor of Philosophy by Research in
Statistics

School of Mathematics and Statistics
College of Science and Engineering
University of Glasgow

January 30, 2026

Abstract

Industrial development and increased resource demand as a result of human population growth are drastically altering the environment, disrupting the balance of ecosystems relied upon for key services and increasing instances of human-wildlife conflict, risks of zoonotic infection, and instability of food source populations. Models of animal movement, space-use, and habitat selection provide insight which can be used to safeguard against these risks, by informing the conservation and management of wild and domesticated species.

Historically, different approaches to habitat selection modelling have been developed independently in relation to different systems and data structures. Recently, demonstrations of the equivalence of point process methods to various approaches used in the analysis of species distribution and movement data has posited spatial and spatio-temporal point processes as a unifying framework for habitat selection modelling. The history of point process literature has been largely theoretical, due to a lack of available computationally efficient methods for fitting these models to large and complex datasets. However, this has changed with the recent development of the Integrated Nested Laplace Approximation (INLA) method for inference and its associated software packages `R-INLA` and `R-inlabru`. Data integration has also become a topic of current research interest in species distribution and movement ecology, promoting the emergence of joint likelihood models as a key framework for ongoing development in this area. Consequently, there is a demand in the ecological literature for demonstrations of the applications of joint likelihood spatio-temporal point process models to large and complex ecological datasets. This forms the underlying motivation for this thesis, which provides an exploration of the use of these methods in modelling animal movement, space use, and habitat selection, with applications in different areas of ecology.

The work included in this thesis is presented in the form of three case studies, which each

demonstrate a different methodological framework and ecological application for joint likelihood spatio-temporal point process modelling of habitat selection data. Chapter 2 demonstrates a marked point process approach to modelling the spread of a reintroduced population of Eurasian crane (*Grus grus*). Chapter 3 compares between habitat selection models at different organisational scales to analyse cattle (*Bos taurus*) tracking data, with applications in livestock management. Chapter 4 introduces the novel implementation of a joint likelihood framework for integrating survey and telemetry data in `R-inlabru` and demonstrates the advantages of this approach using simulated data. Finally, the approach developed in Chapter 4 is applied to real data in Chapter 5, in which it is used to understand habitat selection in a semi-domesticated reindeer (*Rangifer tarandus tarandus*) population in an area of land-use conflict.

Overall, this thesis provides an exploration of different approaches and applications for joint-likelihood spatio-temporal point process modelling of animal movement, space-use, and habitat selection. This includes novel methodological contributions, such as extensions to the unique integration scheme used in the GF-iSSA movement model; and the implementation of the first individual-level continuous-time habitat selection model in `R-inlabru`. Key themes of accounting for availability; the impacts of spatial, temporal, and organisational scale on inference; and the balance between model complexity, interpretability, and computational efficiency are investigated throughout. Main results provide insights into the relationship between model complexity and performance; and the relevance of the spatial scales of heterogeneity in covariate structure, and of representations of availability, on habitat selection inference.

Contents

List of Tables

List of Figures

Acknowledgements

Firstly, I would like to thank my primary supervisor, Prof. Janine Illian, for her invaluable guidance and support throughout my doctoral journey. Your belief in me has provided me with so many opportunities for professional development over the last 4 years and has built my confidence as a researcher. More than this, you have shown me what it is to be a mentor, and I am endlessly grateful for the kindness, patience, and encouragement you have shown me.

I would also like to thank my secondary supervisor, Prof. Jason Matthiopoulos for his insightful feedback and advice, which have been crucial to the creation of this doctoral thesis. I am truly grateful to have had the opportunity to work with you, and have learned so much from you over this time.

Thank you to the Engineering and Physical Sciences Research Council for providing the funding which allowed me to complete this PhD. Thank you also to the School of Mathematics and Statistics for providing travel funding with which I have been able to present my work at workshops and conferences.

Thank you to my co-authors of the publication on the work included in Chapter 2, Dr Óscar Rodríguez de Rivera (University of Exeter) and Dr Andrea Soriano-Redondo (University of Extremadura), for their contributions to the published work. Thanks again to Andrea for providing and advising on the crane occupancy data.

Thank you to Dr Caren Pauler and Dr Manuel Schneider from Agroscope (Switzerland) for providing and advising on the cattle tracking data used in Chapter 3, and to all in the Grazing Systems group at Agroscope for providing a warm welcome to Switzerland during my visit there.

Thank you to Prof. Paul Blackwell (University of Sheffield) and Dr Théo Michelot (Dalhousie University) for sharing their expertise and for insightful discussions on movement modelling. Thank you to Prof. Finn Lindgren and Man Ho Suen (University of Edinburgh) for generously giving their time and expert advice, which greatly aided in the implementation of the joint Langevin movement model in `R-inlabru` (Chapter 4).

Thank you to Prof. Juha Heikkinen and Dr Jouko Kumpula from the Natural Resources Institute Finland (LUKE) for providing and advising on the reindeer tracking data used in Chapter 5. Thank you also to the reindeer herders of the Oraniemi herding district for enabling the GPS tracking of reindeer.

Thank you to all of the researchers who attended the *"Spatial Point Processes and Beyond..."* group meetings for the warm company and interesting discussions over the years.

Thank you to my friends for their love and laughter. Thanks especially to Millie and Kirsty for always being there for me - I am so lucky to call you my best friends.

Thank you to my family for their unwavering support, encouragement, love, and fun. Thank you, Mum and Dad, for encouraging me to follow my interests in life and for believing in me. Thank you, Emma and Zoe, for always listening. I feel deeply blessed to call you all family.

Finally, thank you to my wonderful husband, Callum. Your love, empathy, humour, and care have got me through the hard times on this journey and I would never have been able to get to this point without you. Thank you for sharing this life with me. *Above all, to love and to cherish*

science, which is a unique system for the measurement of doubt, always rejoices in a good question

– Martin Brasier

transit nebula sol restat

Declaration of Originality

I, Megan Ruth Morton (née Laxton), certify that the thesis presented here for examination for a PhD degree of the University of Glasgow is solely my own work other than where I have clearly indicated that it is the work of others (in which case the extent of any work carried out jointly by me and any other person is clearly identified in it) and that the thesis has not been edited by a third party beyond what is permitted by the University's PGR Code of Practice.

I declare that the thesis does not include work forming part of a thesis presented successfully for another degree. I declare that this thesis has been produced in accordance with the University of Glasgow's Code of Good Practice in Research. I acknowledge that if any issues are raised regarding good research practice based on review of the thesis, the examination may be postponed pending the outcome of any investigation of the issues.

The work presented in Chapter 2 has been published in the Methods in Ecology and Evolution journal with the title "Balancing structural complexity with ecological insight in spatio-temporal species distribution models" (Laxton et al., 2023b), and is jointly authored by Dr Óscar Rodríguez de Rivera (University of Exeter), Dr Andrea Soriano-Redondo (University of Extremadura), and Prof. Janine Illian (University of Glasgow). The code used in the analysis in Chapter 2 is available on Zenodo (Laxton et al., 2022a). A transformed version of the data is available on Dryad (Laxton et al., 2022b). These data have been randomly transformed to prevent an exact identification of nest locations and avoid potential disturbance to cranes during the breeding period.

I contributed a poster presentation on the work presented in Chapter 3 to the 16th Workshop on Spatial Statistics and Image Analysis in Biology (SSIAB16) in Smögen, Sweden in 2025. I delivered a contributed talk on the work presented in Chapter 4 at the 15th Workshop on Spatial Statistics and Image Analysis in Biology (SSIAB15) in Grenoble, France in 2023. I also delivered poster presentations on this work at: the 11th International Conference on Spatio-Temporal Modelling (METMA XI) in Lancaster, UK in 2024; the International Statistical Ecology Conference (ISEC) in Swansea, UK in 2024; and the Association for the Study of Animal Behaviour (ASAB) winter meeting in Edinburgh, UK in 2022. I delivered a contributed talk on some of the work presented in Chapter 5 at the British Ecological Society's Movement Ecology special interest group (BES Move) annual meeting in 2022.

Abbreviations

AR1 - First-order Auto-regressive

CTCRW - Continuous-time Correlated Random Walk

DIC - Deviance Information Criterion

GAM - Generalised Additive Model

GF-iSSA - Gaussian Field Integrated Step Selection Analysis

GLM - Generalised Linear Model

GLMM - Generalised Linear Mixed Model

GMRF - Gaussian Markov Random Field

GPS - Global Positioning System

GRF - Gaussian Random Field

HPP - Homogeneous Poisson Process

IID - Independent and Identically Distributed

INLA - Integrated Nested Laplace Approximation

IPP - Inhomogeneous Poisson Process

ISDM - Integrated Species Distribution Model

iSSA - Integrated Step Selection Analysis

JAGS - Just Another Gibbs Sampler

JSDM - Joint Species Distribution Model

LGCP - Log Gaussian Cox Process

LGM - Latent Gaussian Model

MAP - Maximum A Posteriori

MCMC - Markov Chain Monte Carlo

MPP - Marked Point Process

PC - Penalising Complexity

RSA - Resource Selection Analysis

RSF - Resource Selection Function

SCR - Spatial Capture Recapture

SDM - Species Distribution Model

SPDE - Stochastic Partial Differential Equation

SSA - Step Selection Analysis

SSF - Step Selection Function

WAIC - Watanabe-Akaike Information Criterion

Chapter 1

Introduction

This thesis explores the use of joint likelihood spatio-temporal point process methods for modelling animal movement, spatial distribution, and habitat selection. It focuses on issues of model complexity, spatio-temporal scale, data integration, and availability in a range of applied ecological modelling contexts. This chapter will provide an introduction to: the ecological aims of habitat selection modelling; data types, collection methods, and processes impacting data structure; methods used in habitat selection analysis; Bayesian inferential methods; Integrated Nested Laplace Approximation (INLA) and associated `R` packages which use this method for inference; and the topic of joint likelihood models. Lastly, the thesis structure, key themes, and overall aims are presented.

1.1 Motivations for Understanding Habitat Selection

As the human population grows, cities expand to provide housing, increased demand means that agricultural practices become more intensive, and waste and its management become an increasing problem. Industrial development and urban sprawl, deforestation, monoculture farming, pesticide runoff, pollution, marine debris, global warming and greenhouse gas emissions, are all issues contributing to the reduction of suitable habitat for wildlife (Hald-Mortensen, 2023). Carefully balanced ecosystems are disrupted, populations diminished or exterminated, and key ecosystem services lost. This can have disastrous and often unforeseen consequences for the environment, and in turn impacts the human population through the loss of food and water stability, increasing human-wildlife conflict and the risk of zoonotic infection, and exacerbating the effects of climate change such as natural disasters (i.e., by reducing the buffering effects stable ecosystems have to deal with these). Understanding how animals use a space, how abundant a population is, and its preferred environmental conditions can improve the effectiveness of conservation measures aimed to protect species from extinction, contributing to the safeguarding of ecosystems and the vital services they provide.

In the world of reintroduction biology, emphasis is balanced between *in situ* and *ex situ* conservation. Captive populations require appropriate husbandry and stimulation, in order to ensure the efficacy of captive breeding programmes. Natural behavioural responses, such as hunting and predator avoidance, must also be encouraged to ensure the survival of individuals following

release. Management practices require an understanding of the natural behaviours and fitness requirements of the wild population, in order to replicate these in a captive environment (Rabin, 2003). Further to this, the successful release and establishment of captive populations, into original habitats which experienced extirpation, or into new environments, requires an understanding of the spatial behaviours and needs of the study species (Seddon, Armstrong, and Maloney, 2007). Typical home range or territory areas, mobility, site fidelity, and dispersal are all aspects of movement behaviour which need to be considered when planning reintroduction. Knowledge of species habitat requirements is also vital to the apportionment of protected areas or spatial planning of other conservation management practices, to ensure survival of the reintroduced species.

Another aspect of animal movement behaviour which has implications for human populations is understanding habitat connectivity and movement corridors. Habitat is often not only lost but fragmented into smaller areas or 'patches', where interstitial areas are unsafe or impossible for individuals in the population to cross. Populations will make use of movement corridors, which provide connectivity between habitat patches. Identification of these movement corridors is important in a number of contexts. Movement corridors can be manmade structures, the use of which by wildlife clashes with their original purpose and can create conflict. One example of this is the use of roads. Roads can also serve as sources of anthropogenic disturbance and as barriers to movement, and animals attempting to cross them create traffic collisions (Lundqvist, 2007; Shepard et al., 2008). In these instances, areas of high usage can be identified, and appropriate alternative movement corridors created to ensure the protection and safety of humans and wildlife (i.e., wildlife crossings). Loss of habitat connectivity can have drastic implications for wild populations, which experience genetic bottlenecking and drift, reduction in fitness through inbreeding, or loss of key population dynamics such as those connecting source and sink populations (Allee, 1938). Protecting areas of connectivity, and habitat patches themselves, can ensure the long-term protection of a wild population's gene pool.

The adaptation of species to urban environments brings risks and benefits, increasing instances of human-wildlife conflict but also providing ecosystem services (Soulsbury and White, 2015). Human-wildlife conflict is a particular issue in agricultural environments, where the loss

of wild prey species leads to livestock predation, or the loss of natural forage leads to crop loss and trampling (Mattisson, Odden, and Linnell, 2014; Heggenes et al., 2017). Aside from ensuring that designated protected areas contain the environmental conditions that wild populations need, understanding animal movement can also be used to inform management aimed to reduce instances of human-wildlife conflict (Pekarsky et al., 2021).

Increased human-wildlife conflict and the encroachment of human populations on wild systems also increases the risk of zoonotic infection. Again, understanding the habitat requirements of animals can reduce instances of human-wildlife conflict, so reduce this risk (Soulsbury and White, 2015). For known disease vectors, understanding habitat selection, spatial distribution, and movement in these species can aid in understanding of disease transmission and spread (Pepin et al., 2015). Modelling animal space-use can also aid in evaluating existing management practices applied to vector populations to mitigate disease risk. For example, Woodroffe et al. (2006), demonstrated that culling, which aimed to control spread of bovine tuberculosis by reducing badger populations, actually increased the home range sizes of remaining badgers, influencing contact rates with livestock and so increasing the risk of disease spread.

Habitat selection, spatial distribution, and movement are not uniquely useful to understand for wildlife, but are also important factors in the agricultural and fisheries sectors. In the fisheries sector, abundance is a key factor in the determination of stocking densities, to protect food source populations from overfishing (Paradinas et al., 2015; Murphy, 2020). Abundance is a characteristic drawn from an overall population, which will vary in spatial distribution according to biotic and abiotic conditions. Thus, the accuracy of abundance estimates are improved through an understanding of habitat selection and how population densities vary in space. Fisheries can rely on populations which are at risk from the introduction of invasive species, so understanding the spatial distribution and habitat selection of invasive populations can aid in their eradication and management (Gutowsky et al., 2020).

In agriculture, particularly when herbivorous livestock are grazed in upland or rangeland systems, as opposed to intensive farming practices, understanding animal space-use can inform management practices, leading to improved animal welfare, economic stability and environmental impact (Homburger et al., 2015). Distribution of water and mineral sources, fencing, pasture

rotation, can all be used to increase uniformity of space-use, leading to increased stocking rates and decreased damage to vegetation and soil structures (Probo et al., 2013). Similarly, in the management of semi-domesticated species, understanding habitat selection, movement, and spatial distribution is vital to navigating land-use conflict and resource sharing (Skarin et al., 2015; Horstkotte et al., 2023).

Overall, understanding habitat selection, space-use, and movement in wild and domesticated animal populations has an extensive and varied range of applications in conservation, urban planning, epidemiology, fisheries, and agriculture. The impacts of this type of research include: conservation of wild ecosystems and key ecosystem services; prevention of human-wildlife conflict; safeguarding of food source populations; and reduction in the risk of zoonotic infection. Understanding how animals move and use their environment is integral to navigating the challenges presented by climate change and population growth in the Anthropocene.

1.2 Collecting Habitat Selection Data

Different methods are used to collect information for the analysis of animal spatial distribution, habitat selection, and movement, which result in different data structures and vary in their advantages and disadvantages. A general trend across all types of data in this area is that technological advancement and the automation of data collection and processing is allowing datasets to become larger and larger (Mccrea et al., 2023). Data generally fall somewhere along a spectrum of spatio-temporal and organisational scale, between long-term population-level observations, and short-term individual-level observations. Here, the different data types and their methods for collection are explored.

Population-level data on spatial distribution are often collected using surveys: an umbrella term for structured sampling methods wherein a given area is monitored and the spatial location of detected individuals is recorded. Observations are collected by human observers (on-foot, or shipboard) or using aerial imagery, via drones or other aircraft. A defining feature of this type of data is that it provides a snapshot of the overall distribution of the population of interest, and that sampling is performed either only once, or is repeated at a coarse temporal interval. Structured surveys are usually expensive and labour intensive to conduct, thus reducing the spatial coverage

and temporal frequency of data collection. Often, the area of interest is large or heterogeneous in terms of accessibility, and so is usually broken up into smaller subsets using subplots, line, or point transects. Thus, the information collected is subject to a spatially-varying observation process: sampling, though often systematic or random, is not uniform across space. This can have implications for inference if not properly accounted for during analysis.

Technological advancement has enabled the compilation and transfer of data collected by citizen scientists: opening up survey data to a larger number of observations that would not previously have been possible to collect. Citizen science data can be less reliable than structured survey data, due to the inexpertise of observers. Errors in the detection or identification of species of interest are more common in this type of data, although do still occur in structured survey data. Citizen science data are also more likely to be subject to preferential sampling, wherein sampling efforts are focused on areas where the species is already thought to or known to occur. Sampling distribution is also subject to other biases, such as accessibility or distance to population centres (Panunzi et al., 2025a). As such, citizen science data are also subject to a spatially-varying, and often complex and unknown observation process.

Information on population spatial distribution can also be collected passively, through the use of records (e.g., fisheries), reports from centres such as veterinary practices, governmental institutions, or hospitals (e.g., cases of zoonotic infection or injurious human-wildlife conflicts), or via the provenance of museum specimens. In these instances, the sampling process can be even more varied and elusive than in citizen science, as the actual spatial distribution of sampling methods is often unknown (Ribeiro et al., 2023).

Observations of animal occurrence can also be collected through stationary system networks such as camera traps, acoustic telemetry receivers, echolocation click detectors, or insect traps (Pepin et al., 2015; Lavender et al., 2022; Williamson et al., 2022a). Similar to point transects in structured surveys, these data collection networks break up a spatial area into smaller subsets for observation. However, the data collected will sometimes differ in temporal structure compared to survey data, as sequential observations of the same individual can be observed, to make up a movement track or encounter history (as in spatial capture recapture (SCR), Linden, Sirén, and Pekins, 2018; Hostetter et al., 2022). As such, these sampling methods may provide information

on spatial distribution at the population or individual-level.

Other methods of collecting individual-level data involve following a single individual through space, and recording a sequence of observations of its spatial location through time. This was previously carried out via human observation, which had associated issues with labour cost, accessibility, and observers influencing the behaviour of the monitored individuals (Bailey et al., 2018). Automation of data collection with the advent of tracking devices transformed this practice, removing these issues and allowing for the collection of much larger datasets. Recording devices utilise radio and satellite technologies to transmit locations, and include VHF and GPS tracking collars or tags fitted or attached to the monitored individuals. Although data are not subject to the same detection errors or complex observation processes as population-level data, there is an associated level of error in the observed location, which varies by device (Turner et al., 2000). This type of data is often collected at a much finer temporal frequency as compared to population-level data, so can provide more detailed information on animal space-use. However, fiscal constraints usually limit the number of individuals that can be monitored, meaning that a smaller subset of the population is observed.

Understanding habitat selection requires not only observation of the spatial location of an individual or population, but the conditions of the environment which it occupies. Environmental variable data has also undergone a transformation in terms of size and resolution. Previously, static vegetation surveys would be labour intensive to conduct, and provide low spatial coverage. However, satellite technology, remote sensing, and climate models have allowed for the compilation of large datasets, containing information on environmental conditions covering wide spatial areas at fine temporal frequencies (Rhodes et al., 2022).

In summary, information used to understand animal habitat selection, spatial distribution, and movement can come from a wide range of sources with varying associated errors and biases. Recent advances in technology have transformed the size of datasets in many areas, meaning that ecological data have become much larger and more complex than in previous years.

1.3 Considerations in Habitat Selection Modelling

Due to the complex nature of sampling methods used to collect animal location data, and the fact that modelling often aims to understand processes which exist in the context of space and time, there are a number of factors which need to be considered when fitting a habitat selection model. Some of these key considerations are introduced here.

1.3.1 Spatial, Temporal, and Organisational Scale

Ecological processes take place in the context of space and time, and so the spatial and temporal scales at which data collection and analysis take place will influence inferences made about these processes. In ecology, the effect of scale on results remained largely unexplored until pivotal discussions in the late 1980's (Addicott et al., 1987; Wiens, 1989; Levin, 1992). Since then, research has developed in the areas of scale-optimisation (Jackson and Fahrig, 2015; Paton and Matthiopoulos, 2015), inter-scale comparison (Thompson and Mcgarigal, 2002; Mayor et al., 2009), and the inclusion of multiple scales within a single model (Compton, Rhymer, and Mccollough, 2002; Graf et al., 2005; Sánchez, Cushman, and Saura, 2014; Mcgarigal et al., 2016; Timm et al., 2016; Crosby and Porter, 2018; Klaassen and Broekhuis, 2018; Sarkar et al., 2018; Li et al., 2021; Sun, Long, and Jia, 2022).

Measures of scale do not just include spatial grain or temporal frequency, but also the organisational scale at which data are collected or analysis is performed. In habitat selection modelling, inferences are usually made at one of two organisational scales: the individual-level and the population-level. These organisational scales are intrinsically linked to spatio-temporal scale, as population-level models usually cover a wider spatial domain at a coarser temporal interval, giving an overview of the overall long-term distribution of a population, as compared to individual-level models, which provide detailed high-frequency insight into individual movement.

The scale at which a system is analysed can influence the inferences made about the processes operating within that system (Chase and Leibold, 2002; Compton, Rhymer, and Mccollough, 2002; Paton and Matthiopoulos, 2015). Scale choice is dependent on ensuring representation of the process of interest, but is restricted by resource allocation and computational feasibility. As

scale-dependency impacts all of inference in habitat selection modelling, it is an area of interest to determine biologically relevant scales for modelling, or to investigate the influence of scale on results (Decesare et al., 2012; Jackson and Fahrig, 2015).

In this thesis, scale is determined and investigated in a number of ways. In Chapter 2 modelling is performed at the level of habitat patches, encompassing a biologically relevant scale for habitat selection analysis. In Chapter 3, models are compared across varying organisational, spatial, and temporal scales, with the aim of describing the impacts of data granularity on inference at different levels of selection. Finally, in Chapters 4 and 5, a joint modelling framework is used to integrate data and share parameter estimation across different organisational scales.

1.3.2 Spatio-temporal Autocorrelation

Tobler's First Law of Geography describes the phenomenon that data points are more similar when they are closer together in physical space (Tobler, 1970). This is also known as spatial autocorrelation; a dependence in the spatial structure between locations meaning that their similarity is defined by a declining function of the Euclidean distance between them. Habitat selection data consists of observed locations of animals in space (and time), so is subject to this effect (Kneib, Müller, and Hothorn, 2008). Other spatial and spatio-temporal correlation structures also arise in habitat selection data as a result of complex underlying ecological processes, such as interaction with conspecifics, dispersal limitations, or interspecific competition (Lichstein et al., 2002; Storch et al., 2003; Miller, 2012).

Several methods for modelling habitat selection at the population-level are based on an assumption that the observations being modelled are independent (see Section 1.4). Failing to account for unexplained spatial or temporal correlation structures in species distribution modelling can lead to spurious significance and an increase in the rate of Type I errors (false positives) in the interpretation of explanatory variables (Segurado, Araujo, and Kunin, 2006; Dormann, 2007; Dormann et al., 2007). In some cases, it can also lead to incorrect inference on the direction of the effect of an environmental covariate (Kühn, 2006).

This thesis explores varying methods to account for different spatial and spatio-temporal correlation structures in animal location data, including: spatial and spatio-temporal random

effects in Chapters 2, 4 and 5; and Markov properties in movement modelling in Chapters 3, 4 and 5.

1.3.3 The Observation Process

As described in Section 1.2, data collected for habitat selection modelling, particularly at the population-level, is subject to the constraints of the sampling method, or observation process. Often, structured surveys are labour-intensive and costly to conduct, so use a stratification of the area of interest for data collection. Other methods of data collection, such as citizen science data, are subject to different biases in accessibility or preferential sampling (Panunzi et al., 2025a).

Animal habitat preferences are related to environmental conditions using locations in space (and time). If data are distributed not only as a function of underlying processes of interest (i.e., habitat selection), but also as a function of the observation process, failing to take this into account can lead to biased inference (Chadwick et al., 2024). Accounting for sampling effort clarifies whether a cluster of observations is observed in an area because environmental conditions are preferable, or whether this is a location where more intensive sampling took place. Similarly, in terms of background information, accounting for the observation process differentiates between areas where the species of interest is absent because of habitat avoidance, and areas where no sampling took place.

The analysis performed in this thesis utilises the `R-inlabru` package for inference (Bachl et al., 2019). This is introduced fully in Section 1.6.5. This software package was originally developed with accounting for spatially-varying observation processes for ecological data in mind, and a number of applied examples have since been developed (Yuan et al., 2017; Ribeiro et al., 2023; Panunzi et al., 2025b). The topic of accounting for the observation process is revisited in Chapters 2 and 4.

1.3.4 Availability

Principally, habitat selection analysis assumes that the observed locations of an animal are indicative of its preference (or avoidance) of a given set of environmental conditions. However, methods for analysis often operate under the assumption that the full spatial domain of interest is available to the animal, which is unrealistic, given that animal locations are subject to geograph-

ical inaccessibility and movement limitations, such as mobility (Paton and Matthiopoulos, 2015; Matthiopoulos et al., 2020).

Given the temporal interval over which movement is modelled, the area accessible to an animal will depend on its mobility. At the individual-level, this can be interpreted as the average distance over which the individual can travel in a given timeframe. At the population-level, if a population only occupies a small portion of the domain of interest, then its spread through the spatial domain over time is restricted by dispersal ability, which can be a combination of effects of mobility and density dependence (Matthiopoulos et al., 2020).

Variations in the definition of the area available to an individual or population can drastically alter inferences about habitat selection behaviour (Beyer et al., 2010). Crucially, accurately representing available space creates the distinction between absence of observed locations due to habitat avoidance, and absence of observations due to inaccessibility. Without this distinction, inferences made about the relationship between response data and environmental covariates may be inaccurate.

This thesis explores the theme of accounting for availability in habitat selection modelling through a number of methods. In Chapter 2, availability at the population-level is represented through habitat patch density and dispersal limitations, estimated using spatial and spatio-temporal random effects. In Chapter 3, availability is accounted for through a bespoke integration scheme, which combines individual mobility restrictions with physical barriers to movement. Finally, in Chapters 4 and 5, availability is incorporated through a diffusivity parameter related to individual mobility, included in representations of movement behaviour and environmental variables.

1.3.5 Model Complexity

As environmental and ecological datasets become larger and more complex, and more advanced methods for analysis become available, models of species distribution, movement, and habitat selection are becoming more complex (Mccrea et al., 2023). Increasing model complexity can improve biological realism, predictive accuracy, and model fit, but comes at a cost to interpretability and computational efficiency. It is therefore of interest to understand how complex model components and structures can be used to improve ecological insight, but where a balance

can be struck to avoid complexity for complexity's sake. The topic of model complexity is explored throughout this thesis, with particular emphasis in Chapter 2, and with parallel themes in Chapters 3-5.

1.4 Approaches for Habitat Selection Modelling

Historically, spatial and spatio-temporal models have been developed separately for specific data structures, systems, and applications. As such, habitat selection modelling has largely developed independently based on the organisational-scale of interest, and can broadly be classed into two categories: species distribution models or resource-selection for population-level data, and movement models or step-selection for individual-level data. As well as estimating habitat selection parameters, population-level models can be used to predict abundance and large-scale spatial distribution, and individual-level models can be used to predict small-scale spatial distribution and movement characteristics.

1.4.1 Data Processing

Data to which habitat selection models are fitted usually consist of the observed locations of an individual or population in space (and time). The structure of data, and thus the method generally used for analysis, is dependent on both the sampling method, and sometimes processing steps which are applied prior to model fitting. Population-level observations can take the form of presence-absence or occupancy data (wherein sampling locations are recorded alongside species occurrence in terms of presence or absence) or presence-only data (wherein only observations of species presence are recorded). Population-level observations obtained using citizen science or through passive records are often presence-only. Presence-only data with accompanying information on sampling effort and underlying environmental conditions in the wider area can also be referred to as presence-background data. Individual-level observations are usually presence-only, as tracked animals typically do not make up the full population, and so observations only consist of the locations of tracked individuals. However, some methods for individual identification can be used alongside sampling to obtain presence-absence information at the individual level, for example in spatial capture-recapture.

When analysing spatial distribution and habitat preference, the absence of a species, indicating avoidance of a given habitat type, is just as important as presence of the species, indicating preference for a given set of environmental conditions. Some methods attempt to supplement presence-only data by generating pseudo-absences, while others define the spatial area of the 'background'. Individual-level tracking data are often processed by adding pseudo-absences: generated locations describing the area assumed to be available to the individual at the time of observation, but not chosen by the individual. However, the number and location of pseudo-absence points is a topic of debate in ecology, as inferences on species-habitat relationships can be biased or artificially inflated with different numbers or distributions of pseudo-absences (Hazen et al., 2021). Point process modelling, which emerges as a theme here, has been shown to solve the issue of determining number and location of pseudo-absences, by absorbing representations of availability into the definition of continuous space, which can be based on a deterministic integration scheme (Warton and Shepherd, 2010; Michelot et al., 2024).

For population-level data, background 'absence' information is often generated through a uniform sampling of a user-specified observation window or spatial domain (although more complex pseudo-absence approaches are also used, see Barbet-Massin et al., 2012). This is done explicitly or implicitly within the model structure, and so becomes a model assumption which is often violated by practitioners when animal mobility and the observation process are not taken into account (e.g., in MaxEnt, Phillips et al., 2009). Methods have been developed to account for spatially-varying detection probabilities in point process models, therefore resolving the issue of accounting for the observation process in the representation of background information (Bachl et al., 2019).

In addition to the generation of background information or pseudo-absences, raw presence-only data are also often subject to other forms of processing prior to analysis, to deal with the discretisation of space or time. Population-level data are often modelled using a gridded discretisation of space, meaning that point locations of observations are amalgamated into occupancy or count information at the grid resolution. For individual-level inference, discrete-time methods of analysis rely on a regular temporal frequency of sequential observations, so data are often regularised through spatial interpolation. Discretisation, whether in space or time, influences

the scale at which inference can be made, and can often be arbitrary to the process of interest, hindering ecological insight (Jackson and Fahrig, 2015; Mcgarigal et al., 2016; Michelot and Blackwell, 2019). Modelling in continuous-space, or in continuous-time, addresses the issue of scale-dependency in inference.

1.4.2 Individual-Level (Movement) Models

'Movement modelling' is a term which encompasses a wide range of model types including: mechanistic models of physiological movement; models which provide descriptions of space use such as home range or the locations of migratory sites; models which describe long-term changes in population space-use; movement kernels which estimate individual-level movement parameters such as velocity or distribution of turning angles; and context-aware movement models, which combine movement modelling with habitat selection parameter estimation. As the scope of movement modelling is so wide, this section will only provide an introduction to the types of approach used in this thesis - specifically, individual-level context-aware movement models without state or behavioural classification. For example, approaches incorporating classification of the behavioural state of animals, such as Hidden Markov Models (HMMs), and closely related State Space Models (SSMs) are widely used in ecology, but are not covered here (though see Patterson et al. (2017) for an overview of these approaches). The approaches covered in this section form the basis of individual-level habitat selection modelling using tracking data, and can be split into categories by their typical use of discrete- or continuous-time.

Discrete-time Modelling: Step Selection Analysis (SSA)

Modelling the sequential track of observed locations of an animal in discrete-time necessitates the partitioning of the track into distinct movement steps. Tracks are usually discretised at the temporal frequency of the observations, and steps are described using two parameters: step length and turning angle. Step length describes the Euclidean distance between successive locations (namely the current location at time t and previous observation at time $t-1$), so provides an indication of the distance travelled over a movement step. Turning angle describes the short-term directional persistence of movement (Mcclintock et al., 2014). The direction of movement between the observation at time $t-2$ and that at time $t-1$ is determined, as is the direction

between observations at $t-1$ and t. Then, the angle between the previous and new directions is calculated, providing insight into the tortuosity of movement. Usually, the step length parameter is modelled with a Gamma, exponential, or Weibull distribution, and turning angle is modelled with a von Mises or wrapped Cauchy distribution (Michelot et al., 2024).

A step selection function (SSF) is used to model the likelihood of moving to the spatial location x_{t+1} given the previous locations $x_{1:t} = \{x_1, ..., x_t\}$, which is defined as

$$p\left(x_{t+1} \mid x_{1:t}\right) = \frac{w\left(x_t, x_{t+1}\right) \phi\left(x_{t+1} \mid x_{1:t}\right)}{\int_\Omega w\left(x_t, z\right) \phi\left(z \mid x_{1:t}\right) dz}, \tag{1.1}$$

where Ω is the study region, w is a habitat selection function, usually the exponential of an additive combination of environmental variables, ϕ describes movement, usually as a function of step length and turning angle, and the denominator represents a normalising constant (Michelot et al., 2024).

Existing literature employs a number of approaches to performing inference using the general framework described in Equation 1.1 (Michelot et al., 2024). Many approaches incorporate a use-availability design, wherein observed steps are compared to generated pseudo-absences in a conditional logistic regression, as introduced by Fortin et al. (2005) and formalised by Forester, Im, and Rathouz (2009). Although, the method used to generate this background information is a topic of debate in animal movement literature (Hazen et al., 2021).

Muff, Signer, and Fieberg, 2019 describe the conditional logistic regression implementation of the SSF model, accounting for multiple individuals and including a pseudo-absence representation of availability (instead of assuming the full study region is available, as in Equation 1.1). Using conditional logistic regression, each observed step is modelled conditional on a set of time- and individual-specific available steps. Let $n \in 1, ..., N$ represent an individual which has been observed at times $t = 1, ..., T_n$, and $j = 1, ..., J_{n,t}$ represent locations that were either used ($y_{ntj} = 1$) or available ($y_{ntj} = 0$) to individual n at time t. Usually, the total number of available points is kept constant between individuals and timepoints, so the total number of locations $J_{n,t}$ can be written as J for notational simplicity. Then, the probability that individual n selects location j at time t depends on the habitat variables x_{ntj}, given the possible choices

$x_{nt} = \left\{x_{nt1}, ..., x_{ntJ}\right\}$, and is described by

$$\Pr\left(y_{ntj} = 1 \mid x_{nt}\right) = \pi_{ntj} = \frac{\exp\left(\beta^T x_{ntj}\right)}{\sum_{j=1}^{J} \exp\left(\beta^T x_{ntj}\right)}, \tag{1.2}$$

where β represents covariate effects to be estimated. The model can be fitted using a stratified proportional hazards model, although this prohibits the inclusion of random effects (Muff, Signer, and Fieberg, 2019).

Muff, Signer, and Fieberg (2019) demonstrate an equivalence between the commonly used conditional logistic regression approach described in Equation 1.2 and Poisson regression with fixed stratum-specific intercepts (i.e., for each set of time- and individual-specific available locations), extending the approach to account for individual variability in behaviour in terms of movement and habitat selection. Thus, probability of use (as described in Equation 1.2) can be rewritten as

$$\Pr\left(y_{ntj} = 1 \mid x_{nt}\right) = \frac{\exp\left(\alpha_{nt} + \beta^T x_{ntj}\right)}{\sum_{j=1}^{J} \exp\left(\alpha_{nt} + \beta^T x_{ntj}\right)}, \tag{1.3}$$

where α_{nt} are specific intercepts for each set (or stratum) of used and available locations associated with each step. The model in Equation 1.3 is named the conditional Poisson model, and gives equivalent parameter estimates to the conditional logistic regression model, but within the more flexible GLM framework which allows for the inclusion of random effects (i.e., as a Generalized Linear Mixed Model (GLMM)).

Using the equivalence demonstrated by Muff, Signer, and Fieberg (2019), Arce Guillen et al. (2023) reformat step selection analysis into a formulation in which each location at each time point is interpreted as an observation from an inhomogeneous Poisson process (IPP). Thus, the presence-absence framework is transformed to presence-background, where availability is accounted for through a unique integration scheme. The GF-iSSA approach is introduced in more detail in Chapter 3 (Arce Guillen et al., 2023).

Continuous-time Modelling: Diffusion Based Movement Models

Continuous-time movement models are usually based on diffusion processes (continuous-time random walks). Diffusion-based models of animal movement are generally considered technically challenging to implement for applied users, and less interpretable than their discrete-time counterparts, hindering the uptake of these methods in movement ecology (Mcclintock et al., 2014; Patterson et al., 2017). Despite this, various diffusion-based models have been applied to a range of applications in modelling animal movement.

The simplest diffusion process is Brownian motion, which is usually denoted $W(\cdot)$, as it is also referred to as the Wiener process (Patterson et al., 2017). This is the continuous-time version of a random walk model. Using a 2D Brownian motion, $W(t) = \{x, y\}$, which starts at location $\mathbf{0}$ at time 0, the trajectory follows a Gaussian distribution

$$W(t + \Delta t) - W(t) \sim \mathrm{N}(0, \Delta t \Sigma), \tag{1.4}$$

where Σ is a variance-covariance matrix (or in the 1D case, a variance), which is usually defined as $\Sigma = \sigma^2 I_d$, where I_d is the identity matrix of order d. This extremely simplistic model does not account for directional persistence or environmental impacts on animal movement, so would only be of use in the unrealistic scenario wherein an individual moves randomly over a homogeneous environment. However, it provides a framework which allows for additional complexity to be built in, leading to more realistic and useful models of movement behaviour.

Brownian motion forms the basis for more complex diffusion-based movement models, which build upon this initial formulation. Complexity is built in to the structure to allow for environmental and social influences on movement behaviour, as well as building in intrinsic features like directional persistence.

The Ornstein-Uhlenbeck (OU) process builds on Brownian motion by incorporating drift toward a central location (Patterson et al., 2017). It is a mean-reverting Gaussian process, so has a tendency to drift towards its long-term mean. The equilibrium distribution of an individual following an OU process in d dimensions is

$$U(t) \sim \mathrm{N}(\mu, \Lambda), \tag{1.5}$$

where $U(t)$ and μ are d-dimensional vectors and Λ is a $d \times d$ covariance matrix. The conditional distribution of the process at a future timepoint, given its current value, can be written as

$$U\left(t+s\right) \mid U(s) \sim \mathrm{N}\left(e^{Bt}U(s) + \left(1 - e^{Bt}\right)\mu, \Lambda - e^{Bt}\Lambda e^{B't}\right), \tag{1.6}$$

where B is a $d \times d$ stable matrix ($e^{Bt} \to 0$ as $t \to \infty$). Therefore there is an attraction towards the centre of the process, μ, the rate of which is controlled by B, with random variation according to Λ. This attraction, or drift, to the centre is paralleled by central tendencies in animal movement behaviour, such as home ranging or central place foraging. The OU process has been extended for various applications in animal movement modelling, formulating the model in terms of velocity to account for directional persistence (Johnson et al., 2008), or building in additional processes to account for behavioural switching (Blackwell, 1997; Michelot and Blackwell, 2019).

Another way to approach using diffusion processes to model animal movement, but still keeping Brownian motion as a key component, is to define them in terms of a Stochastic Differential Equation (SDE, Patterson et al., 2017). A general SDE can be defined as

$$dX(t) = A\left(t, X(t)\right)dt + B\left(t, X(t)\right)dW(t), \tag{1.7}$$

where A is the drift coefficient which represents the rate of change of the process, and B is the diffusion coefficient which scales the randomness introduced by Brownian motion, $W(t)$.

One such example is the Langevin diffusion, a stochastic process with a stationary distribution, which is used to link individual-level movement to population-level space use (Michelot et al., 2019). Let $\mathbf{X}_t \in \mathbb{R}^d$ be the location of an individual in d dimensional space at time $t \geq 0$, and $\pi : \mathbb{R}^d \to \mathbb{R}$ be its utilisation distribution. Then, in a steady-state regime, the utilisation distribution is the probability density function π which satisfies

$$\mathbb{P}\left(\mathbf{X}_t \in A\right) = \int_A \pi(z)dz, \tag{1.8}$$

for any area $A \subset \mathbb{R}^d$. Therefore, the utilisation distribution represents the (time-invariant) steady-state behaviour of the process, as defined over the spatial domain A. Then, the continuous-time location process of the individual $\mathbf{X}_t$ can be described with a Langevin diffusion for the density π, defined as the unique solution to the SDE

$$d\mathbf{X}_t = \frac{1}{2}\nabla \log \pi\left(\mathbf{X}_t\right) dt + dW_t, \tag{1.9}$$

with initial condition $\mathbf{X}_0 = \mathbf{x}_0$, where W_t is a d-dimensional Brownian motion, and ∇ is the gradient operator. The movement model therefore incorporates drift, like the OU process, but instead of simply to a central location, drift is towards a steady-state distribution, which can be modelled as a function of environmental covariates. Chapters 4 and 5 use a model of animal movement based on the Langevin diffusion process. Importantly, the approach introduced in Chapter 4 uses an inhomogeneous Poisson process (IPP) to model the utilisation distribution. The joint Langevin movement model is introduced in more detail in Section 4.2.

1.4.3 Population-Level (Species Distribution) Models

Population-level models of habitat selection are usually called Species Distribution Models (SDM), but are also referred to as Resource Selection Analyses (RSA), particularly when they are fitted to tracking data. Population-level models are fitted to presence-absence or presence-only data, and are formulated in discrete or continuous-space. They aim to provide an understanding of habitat selection at the population-level, as well as predicting the distribution of a population in space (and time). A wide range of methods exist for population-level habitat selection modelling, including: generalised linear models (GLM) and their extension generalised additive models (GAM); logistic regression; machine learning methods such as MaxEnt and random forests; and point process methods. Point processes have been proposed as a unifying framework in species distribution modelling as they provide a link between different approaches to modelling population-level data of different types and scales (Miller et al., 2019). Here, three commonly used approaches to modelling habitat selection at the population-level are described.

Poisson Generalised Linear Models

One approach to modelling presence-only data is to discretise space into a regular grid, and then model the count of observations per grid cell using a Poisson distribution. As described in Aarts, Fieberg, and Matthiopoulos, 2012, using this approach, cells are split into used U (those containing observations) and available A (all cells, including those with no observations). Let Y_j be the number of observations within a grid cell j, and X contains the value of spatial covariates either measured at the centre of the grid cell, or averaged across the cell. The Poisson log-likelihood is

$$l_{\text{PGLM}}(\beta; X) \propto \sum_{m=1}^{M} \log\left(\lambda\left(X_m^U\right)\right) - \sum_{j=1}^{N} \lambda\left(X_j^A\right), \tag{1.10}$$

where N is the total number of grid cells (i.e., representing both used and available areas), M is the number of used points (i.e., where observation of an individual occurred), X_m^U describes environmental conditions in a given m used cell, and X_j^A describes environmental conditions in a given j cell (all cells in the grid $j = 1, ..., N$). The expected density, λ_j, of observations in a grid cell j is modelled as a Poisson rate, defined as the exponential of the linear predictor

$$\lambda_j = \exp\left(\beta X_j + \log(\alpha)\right), \tag{1.11}$$

where $\log(\alpha)$ is the offset term containing the spatial area of the grid cell.

The definition of the log-likelihood in Equation 1.10 includes the assumption that the intensity function $\lambda\left(X_S\right)$ is constant within a grid cell, and so the Poisson likelihood function can be viewed as an approximation to a spatially continuous, unconditional inhomogeneous Poisson process (Aarts, Fieberg, and Matthiopoulos, 2012).

Weighted Distribution Theory (WDT) for Point Data

Presence-only data are often processed for modelling by adding pseudo-absences; points which represent the 'absence' of an observation, generated randomly using the distribution of the presence observations. Habitat selection can then be modelled as a function of this combination of observed and generated data. The Weighted Distribution Theory (WDT) describes the habitat

selection function as a set of weights that connects the distribution of available habitat to the distribution of used habitat, by representing the relative selection probabilities of available resources (Lele and Keim, 2006). Let $\boldsymbol{C}(s)$ describe the environmental covariates at location s, $a(s)$ describe the distribution of available locations in space (typically a constant within the domain of availability, $\boldsymbol{G}$, so that $a(s) = 1/|\boldsymbol{G}|$), and $w(\boldsymbol{C}(s), \beta)$ be the habitat selection function (Fieberg et al., 2021). Then, the utilisation distribution is described by

$$u(s) = \frac{w(\boldsymbol{C}(s), \beta)\, a(s)}{\int_{g \in G} w(\boldsymbol{C}(g), \beta)\, a(g) dg}, \tag{1.12}$$

where integration is performed over the available geographical area $\boldsymbol{G}$, and g is a dummy variable which acts as a placeholder for all possible locations within $\boldsymbol{G}$ during integration, allowing integration over the full spatial area.

Fieberg et al. (2021) demonstrate that the utilisation distribution as described using WDT is consistent with a conditional likelihood for an inhomogeneous Poisson process (IPP).

Logistic Regression

For presence-absence (occupancy) data, the occurrence of a population is observed at a number of detection sites, where the presence of the species of interest is equal to 1 and the absence is equal to 0. Similarly, presence-only data with added pseudo-absences can also be thought of in the same way (e.g., in resource selection functions of tracking data, Muff, Signer, and Fieberg, 2019). This data structure can be used to quantify the occupancy probability (relative to the available area defined by pseudo-absences) at each site, or the probability of use at each available location, as a function of environmental covariates using logistic regression, which assumes a logit link (Aarts, Fieberg, and Matthiopoulos, 2012).

Let $j = 1, ...\boldsymbol{J}$ represent a set of available locations (or detection sites). Then, the probability that a point y_j with covariate vector c_j is used (or the occurrence probability of the point) can be modelled as

$$\text{logit}(\Pr(y_j = 1 \mid c_j)) = \beta^T c_j, \quad y_j \sim \text{Bernoulli}(\Pr(\text{y}_\text{j} = 1 \mid \text{c}_\text{j})), \tag{1.13}$$

where β^T is the transposed of the covariate vector β that is the target of interest (Muff, Signer,

and Fieberg, 2019).

This method becomes equivalent to a log-linear IPP model when the number of available points (or detection sites) is large (Warton and Shepherd, 2010). Alternatively, the approach can be extended to a marked point process model, wherein the probability of use (or occurrence) is modelled as a mark dependent on the underlying distribution of the available points (detection sites), modelled as an inhomogeneous Poisson process (IPP). This is demonstrated in Chapter 2.

1.4.4 Spatial Point Processes

As mentioned in the preceding sections, the most common approaches to habitat selection modelling of population-level data have been demonstrated to be equivalent to using a point process model (Warton and Shepherd, 2010; Aarts, Fieberg, and Matthiopoulos, 2012; Fieberg et al., 2021). Similarly, point process modelling can also be used to describe habitat selection at the individual-level (Arce Guillen et al., 2023).

In the simplest case, a spatial point process $\mathbf{X}$ is a finite random subset of a given bounded region $S \subset \mathbb{R}^2$. A realisation of this process is a spatial point pattern $x = x_1, ..., x_n$ of $n \geq 0$ points contained in S (Møller and Waagepetersen, 2004). The distribution of the number of points $n(\mathbf{X})$ can be used to specify the distribution of the point process, and for each $n \geq 1$, conditional on $n(\mathbf{X}) = n$, the joint distribution of the n points in $\mathbf{X}$. Equivalently, the distribution of variables $N(B) = n(\mathbf{X}_B)$ can be specified for subsets $B \subseteq S$, where $\mathbf{X}_B = \mathbf{X} \cap B$.

In a spatial point process, the expected density of points at spatial location $s \in S$ is described by the intensity $\Lambda(s)$.

The Poisson Process

If points in a point process arise independently and at random, the intensity λ can be described by a homogeneous Poisson distribution, so the process is referred to as a homogeneous Poisson process (HPP). A Poisson process $\mathbf{X}$ defined on S and with intensity measure μ and intensity function ρ satisfies for any bounded region $B \subseteq S$ with $\mu(B) > 0$,

1. $N(B)$ is Poisson distributed with mean $\mu(B)$,

2. conditional on $N(B)$, the points in $\mathbf{X}_B$ are IID with density proportional to $\rho(u), u \in B$.

Within a homogeneous Poisson process, the locations of points are assumed to follow complete spatial randomness, i.e., reflecting a lack of interaction between the points (Møller and Waagepetersen, 2004). In other words, a homogeneous Poisson point process has a constant rate of intensity, meaning that the average density of points is uniform across space. Homogeneous Poisson processes are mathematically tractable so attractive for modelling, but this independence property is not realistic when applied to ecological systems. For example, when modelling the spatial distribution of a population of organisms, spatial interaction amongst individuals (e.g., competition, facilitation), and other factors (e.g., symbiotic relationships, conspecific preferences) can influence spatial distribution. The Poisson process can be extended to account for this heterogeneity in point pattern intensity using an inhomogeneous point process (IPP), such as a Cox process, wherein point pattern intensity (Λ) can be spatially varying. This is discussed further in Section 1.6.1.

Thinned Point Processes

In most applications, spatial point processes are fitted to data wherein a realisation of the process (the point pattern, or spatial distribution of observations) is observed over a known observation window, W. Both the observed point locations, and the absence of points where observation was possible (i.e., within W) are sources of information used to describe the underlying point process. If sampling or detection is not perfect over the domain of interest, so some points are missing from the set of observations, then the observed pattern arises from a thinned point process. Accounting for spatially varying detection probabilities in point process models is a speciality of the `R-inlabru` package (see Section 1.6.5, Bachl et al., 2019).

Marked Point Processes

In a marked point process, the locations of points are modelled alongside one or more dependent 'marks': quantitative or qualitative features of the objects or events found at the point locations, which are dependent on the point spatial structure (Illian, Sørbye, and Rue, 2012). A marked point process model is a joint likelihood model wherein the distribution of the points is modelled simultaneously alongside the marks. Sometimes, the marks are the feature of interest, and so a marked point process model can be seen as a model of the marks which takes the dependence

on the underlying spatial structure of the points into account. Marked point process models are discussed further in Chapter 2.

Applications of Spatial and Spatio-temporal Point Processes

Spatial and spatio-temporal point process models have been proposed as a unifying framework for modelling species distributions and habitat associations (Miller et al., 2019; Matthiopoulos et al., 2022). It has been demonstrated that the varying approaches to modelling species distributions can be thought of as special cases of the same underlying approach; an inhomogeneous Poisson point process (IPP, Warton and Shepherd, 2010; Aarts, Fieberg, and Matthiopoulos, 2012; Fieberg et al., 2021). This has also been translated to models of individual-level selection (Muff, Signer, and Fieberg, 2019; Arce Guillen et al., 2023).

The history of point process modelling has been largely theoretical, due to a lack of available software for computationally efficient fitting of these complex spatial and spatio-temporal models to large datasets (Illian, Sørbye, and Rue, 2012). However, this has changed in recent years, resulting in the relevance of point process methodology being recognised by the ecological community, and intensifying the need for demonstrations of the various ways in which point process methodology can be applied (Illian and Burslem, 2017). In this thesis, each chapter demonstrates a different approach to incorporating point process methodology in habitat selection models. Chapter 2 uses a marked point process model to predict the spatio-temporal distribution of a population. Chapter 3 applies the discrete-time GF-iSSA movement model, and compares this to an RSA approach using an IPP. Finally, Chapters 4 and 5 use an IPP model to describe the utilisation distribution in a continuous-time movement modelling framework. Therefore, this thesis provides an overview to a broad range of uses for point process modelling of animal space-use and habitat selection at different organisational scales.

1.5 Bayesian Inference

Bayesian statistics is a method for statistical analysis which incorporates prior knowledge about parameters of interest and updates this with observed data. It differs from classical, Frequentist statistics in that: (1) instead of evaluating the probability of the data given the model, it evaluates the probability of the model given the data; (2) it has a different definition of probability; (3) it

incorporates prior beliefs instead of only using observed data; and (4) it treats model parameters as random variables instead of estimates of fixed, true values (Ellison, 2004). Bayesian inference is a preferred method in many areas of ecology, as it allows for more interpretable uncertainty quantification and the creation of adaptive models, which can be continually updated with new evidence. However, fully Bayesian inferential methods are often computationally costly, which has historically been a barrier to applied hierarchical Bayesian modelling.

Bayesian statistics aims to make probabilistic statements about unknown parameter values θ, given observed data y. This can be done using Bayes theorem (Bayes, 1763), wherein the posterior density $p(\theta \mid y)$ is computed from the prior $p(\theta)$ and likelihood $p(y \mid \theta)$

$$p(\theta \mid y) = \frac{p(\theta)\, p(y \mid \theta)}{p(y)}, \tag{1.14}$$

where $p(y) = \int_\theta p(\theta) p(y \mid \theta)$. Removing the normalising constant $p(y)$ (the integral over all possible values of θ) from the denominator gives the unnormalised posterior density

$$p(\theta \mid y) \propto p(\theta)\, p(y \mid \theta), \tag{1.15}$$

wherein the unnormalised posterior is given proportional to the product of the prior and likelihood (Gelman et al., 2015). This definition can be used to define a probabilistic interpretation of values of θ, for example, the % probability that the true value is contained within a given range. Thus, point estimates (e.g., mean, median, mode) and associated posterior intervals can be used for parameter interpretation and communication of uncertainty. Often, the posterior distribution is not available in closed form, and credible intervals are derived from simulation-based samples of the posterior (Section 1.5.1), or using approximation methods (Section 1.5.2).

1.5.1 Markov Chain Monte Carlo (MCMC)

Markov chain Monte Carlo (MCMC) is a simulation-based method for Bayesian inference. Probabilistic statements about parameter values are made by sequentially sampling from approximate distributions and correcting the samples drawn in order to improve the approximation of the target posterior distribution (Gelman et al., 2015). As sampling is performed iteratively, over time,

the approximate distributions from which samples are drawn will converge towards the target distribution. Given a long enough running time, the difference between $p(\theta|y)$ and the distribution of samples should be minimal enough that inference can be performed using the sample distribution. Therefore, point estimates and uncertainty intervals computed from the sample distribution should give an accurate description of the true underlying process.

The basis of the MCMC approach relies on the creation of a Markov process whose stationary distribution is the target $p(\theta|y)$. Then, if simulation is performed for long enough, the distribution of samples should reflect the true distribution. The number of iterations and appropriate 'burn-in' period must be defined to give the process enough time to produce accurate results. Since MCMC is an iterative process, appropriate initial values also need to be specified to give chains a good starting point.

The general method of MCMC can be performed using many different algorithms, which provide variations suited to different modelling problems. Here, a commonly used algorithm, the Gibbs sampler, is explained in more detail.

Gibbs Sampler

The Gibbs sampler, or 'alternating conditional sampling' (Geman and Geman, 1984) is an MCMC algorithm wherein θ is split into a d-dimensional vector $\theta = (\theta_1, ..., \theta_d)$. Each sample of each subvector θ_j is drawn conditional on the value of all of the others. Thus, for each iteration t of the algorithm, there are d steps. For each iteration, θ_j^t is sampled from the conditional distribution (given all the other components of θ)

$$p(\theta_j^t \mid \theta_{-j}^{t-1}, y), \tag{1.16}$$

where θ_{-j}^{t-1} represents all the components of θ except θ_j, at their current values

$$\theta_{-j}^{t-1} = (\theta_1^t, ..., \theta_{j-1}^t, \theta_{j+1}^{t-1}, ..., \theta_d^{t-1}), \tag{1.17}$$

where θ_{-j}^{t-1} includes the values of all the already updated components for iteration t, and the values at iteration $t-1$ for the components which haven't yet been updated (Gelman et al., 2015). Gibbs sampling is particularly useful for complex, high-dimensional distributions.

Software Platforms for MCMC

There are multiple popular software platforms for performing Bayesian inference using MCMC. These include Just Another Gibbs Sampler (JAGS, Plummer, 2012); Numerical Inference for Statistical Models for Bayesian and Likelihood Estimation (NIMBLE, De Valpine et al., 2017); and Stan (Carpenter et al., 2017).

JAGS is a software program for the analysis of Bayesian hierarchical models using MCMC which uses Gibbs sampling as its core algorithm (Plummer, 2012). Although most of the analysis in this thesis is performed using the INLA method for inference, JAGS is used for comparison in Chapter 4, Section 4.3.5.

1.5.2 Integrated Nested Laplace Approximation (INLA)

Bayesian inference for applied ecological problems has historically been restricted by the computational cost of inferential methods. Accurate estimation of posterior densities from simulation-based methods (such as MCMC) require a long running time, to ensure the stationary distribution of interest, from which samples are drawn, has been achieved. When research aims to interpret intricate ecological systems, large datasets and complex models are predominant. This often means that fully Bayesian inferential methods are prohibitively long-running for use in applied ecological modelling.

An alternative to MCMC which solves the computational efficiency problem is to use approximate methods for Bayesian inference. Integrated Nested Laplace Approximation (INLA) is a method that can be used for inference from the wide class of structured additive regression models which fall under the heading of latent Gaussian models (Rue, Martino, and Chopin, 2009). As opposed to sampling the full posterior using MCMC algorithms, INLA is used to approximate the posterior marginals of latent Gaussian models in a computationally efficient way.

It is important to note that the error in MCMC methods can be made arbitrarily small, but that this is reflected through an increase in model running times. Approximate inference using INLA can have a lower approximation bias than MCMC error *for a given computational cost* (Rue, Martino, and Chopin, 2009). Thus, from the perspective of the end-user (with large datasets, complex models, and limitations on project timelines), INLA is almost always preferable to MCMC for

accurate and efficient Bayesian inference from latent Gaussian models.

Latent Gaussian Models

Latent Gaussian models are a large, general class of models which are made up of conditionally independent observations which belong to an exponential family and follow a probability distribution that depends on parameters (following a Gaussian distribution, also called the latent Gaussian random field (GRF)) and hyperparameters (not necessarily Gaussian). Latent Gaussian models can be defined using a three-stage hierarchical framework (Rue et al., 2017). Let y be the observations, which are conditionally independent given the latent GRF $\mathcal{X}$ and hyperparameters θ_1. Then

$$y \mid \mathcal{X}, \theta_1 \sim \prod_{i \in \mathcal{I}} p\left(y_i \mid \mathcal{X}_i, \theta_1\right), \tag{1.18}$$

where $\mathcal{X}_i$ is the i-th component of the latent GRF which describes the underlying dependence structure of the data. The latent GRF is decribed as

$$\mathcal{X} \mid \theta_2 \sim \mathcal{N}\left(\mu\left(\theta_2\right), Q^{-1}\left(\theta_2\right)\right). \tag{1.19}$$

The hyperparameters which control the likelihood, θ_1, and the latent GRF, θ_2, combine to give the hyperparameter vector $\theta = \left(\theta_1, \theta_2\right)$. The joint posterior density of $\mathcal{X}$ and θ can be given as

$$p\left(\mathcal{X}, \theta \mid y\right) \propto p(\theta)\, p(\mathcal{X} \mid \theta) \prod_{i \in \mathcal{I}} p(y_i \mid \mathcal{X}_i, \theta). \tag{1.20}$$

Latent Gaussian models can be expressed using a linear predictor which is an additive combination of fixed and random effects, where all model components (except for hyperparameters) are Gaussian. The linear predictor η_i of an LGM can be expressed as

$$\eta = \alpha + \sum_j \beta_j z_{ij} + \sum_k f_{k, j_k(i)}, \tag{1.21}$$

when a joint Gaussian prior is assumed for the overall intercept term α and the parameters of the fixed linear effects β of the covariates z. A range of Gaussian processes f_k can be included in

the model, including random spatial and auto-regressive temporal models.

INLA relies on a property found in most latent Gaussian models that the latent field $\mathcal{X}$ has conditional independence, and thus is a Gaussian Markov random field (GMRF) with a sparse precision matrix. This enables the use of sparse matrix methods for numerical computation. This feature, alongside the condition that the number of hyperparameters θ is small (also a common property of latent Gaussian models), contributes to the computational efficiency of the method.

Classical INLA

When the INLA method was first developed by Rue, Martino, and Chopin (2009), it originally utilised Laplace approximation to estimate the joint posterior density of the latent GRF and hyperparameters $p(\mathcal{X}, \theta \mid y)$, as written in Equation 1.20. The Laplace approximation is given by

$$\begin{aligned} \pi(x, \theta|y) &\propto \pi(y|\mathcal{X}, \theta)\, \pi(\mathcal{X}, \theta) \\ &\propto \pi(y|\mathcal{X}, \theta)\, \pi(\mathcal{X}|\theta)\, \pi(\theta), \\ p(\theta \mid y) &= \left. \frac{p(\mathcal{X}, \theta \mid y)}{p_G(\mathcal{X} \mid \theta, y)} \right|_{\mathcal{X}=\mu(\theta)} \end{aligned} \tag{1.22}$$

where $p_G(\mathcal{X} \mid \theta, y)$ is a Gaussian approximation of the density, $\pi(\mathcal{X}|\theta, y)$, and all is evaluated at $\mu(\theta)$; its mode. This approximation was then used to compute the posterior marginal distributions for the latent GRF and hyperparameters using nested, numerical integration. The GRF is represented with a GMRF during computation; this approximation is explored further in Section 1.6.2, (Lindgren, Rue, and Lindström, 2011).

The classical INLA method can be summarised in three main steps:

1. Use the Laplace approximation (Equation 1.22) to approximate the posterior marginal of the hyperparameters.

2. Compute the simplified Laplace approximation of the latent Gaussian field for selected values of the hyperparameters.

3. Combine the previous two steps using numerical integration.

This nested approach contributed to the accuracy of the classical INLA methodology. The simplified Laplace approximation used in INLA corrects for location and skewness in the Gaussian

marginals, to provide a more accurate approximation than the original naive Gaussian.

The outputs from INLA are posterior marginal distributions for the latent Gaussian random field and hyperparameters. Values of interest such as means and quantiles can then be derived from these marginals.

Updated INLA

Recently, the INLA inferential method has been updated to improve its stability and reduce computational cost. Van Niekerk et al. (2023) proposed a new framework for approximate Bayesian inference using INLA, removing the linear predictor from the latent field to improve computational efficiency, but using a low-rank Variational Bayes correction to maintain accuracy.

In the updated INLA formulation, the latent field $\mathcal{X}$ has a 0 mean Gaussian prior, and the n linear predictors are defined as

$$\eta = A\mathcal{X}, \tag{1.23}$$

where A is a sparse design matrix that links the linear predictors to the latent GRF. The joint posterior density defined in Equation 1.20 is updated to become

$$p(\mathcal{X}, \theta \mid y) \propto p(\theta)\, p(\mathcal{X} \mid \theta) \prod_{i \in \mathcal{I}}^{n} p(y_i \mid (A\mathcal{X})_i, \theta). \tag{1.24}$$

However, this formulation could lead to inaccurate results, so a correction is applied to the posterior means of the latent GRF using low-rank Variational Bayes (Van Niekerk and Rue, 2024).

The updated INLA method can be summarised in the below steps:

1. Formulate the latent GRF without linear predictors, instead using a sparse design matrix to link linear predictors to the latent GRF (Equation 1.23).

2. Derive the joint density of the latent GRF, hyperparameters and data (Equation 1.24).

3. Approximate the posterior using Laplace approximation (Equation 1.22).

4. Apply a Variational Bayes correction to the posterior means of the latent GRF (Van Niekerk

and Rue, 2024).

5. Compute the posterior marginals using numerical integration of the Gaussian conditional marginals.

The work in Chapter 2 was carried out prior to the default implementation of updated INLA in the R-INLA package, and so this chapter uses the classical INLA method for inference (Van Niekerk et al., 2023). Chapters 3-5 all use the updated INLA method.

1.6 Spatial Point Process Modelling with R-INLA

R-INLA is a software package in the R programming language, which is used for Bayesian computing with the INLA method (Rue, Martino, and Chopin, 2009; Rue et al., 2017; R Core Team, 2025). Among other applications, it provides a computationally efficient Bayesian framework that can be used to fit spatial and spatio-temporal point process models to large datasets.

1.6.1 Log Gaussian Cox Processes (LGCP)

Log Gaussian Cox processes (LGCP) are a special case of latent Gaussian models - which makes them suitable for fitting with INLA - where the random intensity function forms the latent Gaussian structure (Cox and Isham, 1980; Illian and Burslem, 2017). LGCP are doubly stochastic point processes in which the intensity function is modelled as

$$\log\left(\Lambda(s)\right) = \mathcal{X}(s), \tag{1.25}$$

where $\mathcal{X}(s)$ is a Gaussian random field, $s \in \mathbb{R}^2$, so for any location $s_1, ..., s_l$ the vector $\mathcal{X}(s_1), ..., \mathcal{X}(s_l)$ follows a multivariate normal distribution (Møller, Syversveen, and Waagepetersen, 1998). The exponential is used to keep values of $\Lambda(s)$ positive-definite.

The theoretical framework of LGCP is well suited to spatial and spatio-temporal problems in ecology, as the modelled point pattern forms a Poisson process, given the latent Gaussian random field which describes random intensity. In practice, Cox process models are difficult to fit to point pattern data due to intractable likelihoods (Illian et al., 2013). Therefore, prior to implementation in the INLA framework, only simple Cox process models were fitted in an

applied context, and joint modelling was prohibitively computationally expensive. When fitting LGCP with INLA, the the continuous Gaussian random field is approximated by a Gaussian Markov random field (GMRF) with local dependence structure. Therefore, INLA allows for the computationally efficient modelling of spatial and spatio-temporal point process models using LGCP.

The analyses performed in this thesis all incorporate an LGCP: as a marked point process model in Chapter 2; via the GF-iSSA approach and also in the RSA model in Chapter 3; and to describe the utilisation distribution in the joint Langevin movement model in Chapters 4 and 5.

1.6.2 Stochastic Partial Differential Equations

For continuous spatial and spatio-temporal models in INLA, such as LGCP, the Stochastic Partial Differential Equation (SPDE) approach can be used to approximate continuous-space (Lindgren, Rue, and Lindström, 2011). The SPDE approach works by approximating a Gaussian random field by its corresponding Gaussian Markov random field, and then using the GMRF to represent the GRF in computation (Simpson, Lindgren, and Rue, 2012; Miller, Glennie, and Seaton, 2020). The Markov property of the GMRF greatly improves computational efficiency. A GRF with Matérn covariance is the solution to a certain type of SPDE. Since the covariance structure of the GRF is known to be Matérn, the SPDE behind this can be approximated. From this, the corresponding GMRF can be estimated.

The solution to the SPDE is represented using the finite element method as the sum of weighted basis functions, where the weights follow a Gaussian distribution. The basis functions are carefully chosen to preserve the sparse structure of the precision matrix for the GRF, which provides a link between the continuous field and a GMRF, giving computational advantages. The basis functions are defined at a set of mesh nodes, with the overall mesh providing a representation of continuous-space. The mesh is a division of the spatial domain into a set of non-intersecting triangles, which only meet at most at a common edge or vertex. The number of basis functions (and associated weights) is the same as the number of vertices in the mesh. The mesh provides a lower bound to the spatial resolution of analysis, so therefore must be fine enough so that no further changes in results are observed when a finer mesh is used (Lindgren,

Rue, and Lindström, 2011; Dambly et al., 2023).

The solution to the SPDE is given as

$$u(s) = \sum_{k=1}^{m} \psi_k(s) w_k, \tag{1.26}$$

where $s \in D$, ψ_k are basis functions, w_k are Gaussian distributed weights, m represents the number of vertices in the triangulation.

The piece-wise linear basis functions can be used to approximate the process at any point inside the triangulated domain. The joint distribution for the weights determines the full distribution in the continuous domain.

Using a GRF to Account for Spatial Autocorrelation

A spatio-temporal point pattern is a realisation of an underlying point process, which describes the relative pattern of locations of observations in space and time. Point process modelling relies on the assumption that each point (observation) is independent conditional on point process intensity. The violation of this assumption can lead to spurious significance in the interpretation of parameters, and Type I errors. Therefore, any correlation between points should be explained by the intensity function. This can incorporate the effects of known environmental covariates, but can also include a structure to account for residual spatial autocorrelation. Using INLA, residual spatial autocorrelation in point pattern intensity can be accounted for using a Gaussian random field (GRF). The GRF can be approximated in continuous-space using the Stochastic Partial Differential Equation (SPDE) approach, which makes complex modelling feasible by vastly reducing computational cost (Lindgren, Rue, and Lindström, 2011).

Accounting for spatial autocorrelation via the inclusion of a spatially structured random effect can reduce the risk of spurious significance and improve spatial prediction. However, there is a risk of spatial confounding, wherein there is multicollinearity between fixed effects and the spatial random effect, creating biased estimates of the fixed effects. Similar issues can also arise wherein the GRF is overfitted to the data (Illian et al., 2014). The risk of spatial confounding can be reduced by using GRFs in a controlled way, through PC-priors or restricted spatial regression (Hodges and Reich, 2010; Simpson et al., 2017).

1.6.3 Priors

As R-INLA operates in a Bayesian framework, it allows for the incorporation of prior beliefs in modelling. There are several kinds of prior, based on differing levels of existing knowledge on a subject. Objective (or non-informative) priors are highly design dependent and do not require knowledge of the study system. This type of prior can be generalised across several models, but does little to update the model, meaning that models rely heavily on the sampled data. Informative priors, or expert priors, allow for the incorporation of known information about a study system, but are often misinterpreted when lifted from existing literature (Simpson et al., 2017). The use of interpretable default priors provides an attractive alternative.

When a model is too complex, or when a prior defines a spatial effect at too fine a spatial scale, overfitting occurs (Illian, Sørbye, and Rue, 2012). Overfitted model predictions rely too heavily on the data collected, and so can't be extrapolated to similar study areas because they are too specific (Illian et al., 2014). One method to avoid overfitting in INLA involves the specification of variance-partitioning based priors, the details of which are discussed further in Ferrari and Ventrucci (2024). A common approach to avoid including unnecessary complex components in a model, in order to avoid overfitting, involves using Penalised Complexity (PC) priors (Simpson et al., 2017).

Penalised Complexity Priors

Penalised Complexity (PC) priors are interpretable default priors which operate under the principle of Occam's razor, working to reduce deviation away from the most parsimonious model unless complexity is supported by the data (Blangiardo et al., 2013; Simpson et al., 2017). The prior is placed not on a parameter, but on the divergence of a model component from the simplest base model. Specifically, a prior is put on a flexibility parameter ξ for a model component with density $p(y|\xi)$.

The construction of PC-priors is based on the following four principles:

1. Parsimony (Occam's razor)

   The PC-prior approach is designed to penalise model complexity (deviation from a simpler base model) to prioritise a more parsimonious model formulation. This is achieved

by measuring complexity, as in principle 2, and penalising it with a constant rate, as in principle 3. The user defining the prior chooses the scale of penalisation, as in principle 4.

2. Measure of complexity

   In the construction of PC-priors, the complexity of a model component with density f over a model component with density g is measured. The measure d used for this is based on the Kullback-Leibler divergence between f and g and is calculated as

$$d(f\|g) = \sqrt{2\text{KLD}(f\|g)}, \tag{1.27}$$

   where $\text{KLD}(f\|g)$ denotes the KL divergence between f and g.

3. Constant rate penalisation

   In order to ensure that deviation from the base model is penalised in the same way everywhere in the parameter space, an exponential prior with rate parameter λ on the distance space is used

$$p(d) = \lambda \exp(-\lambda d). \tag{1.28}$$

4. User defined scaling

   To allow the user to prescribe the degree of informativeness of the prior the parameter λ in Equation 1.28, they choose U and α in the following equation

$$P(Q(\xi) > U) = \alpha, \tag{1.29}$$

   where $Q(\xi)$ is an interpretable transformation of ξ. Equation 1.29 describes the likelihood α that ξ is in the tail of the distribution (i.e., bigger than a threshold U). In other words, the user decides where the tails of the prior distribution are located and how sure they are about this decision.

Each model component requires its own PC-prior (hence its own flexibility parameter). However, PC-priors remain consistent throughout reparameterisation (even if the significance of a

model component's effect changes, its PC-prior will remain invariant). This is beneficial, as the PC-priors are resistant to iteration so do not have to be computed with every new model arrangement.

Since PC-priors operate under the principle of Occam's razor, they only enable increased complexity in a model (i.e., the inclusion of complex model components) if this is supported by strong evidence from the data. In this way, PC-priors can be used to justify model selection, as they provide a systematic approach to assessing the level of complexity needed in a model.

PC-Priors for GRF Parameters

PC-priors can be specified to inform the Matérn covariance structure of a Gaussian random field included as a spatial random effect in INLA. This is carried out using a reparameterisation of κ and τ from the Matérn covariance function to a range and variance (Blangiardo et al., 2013). The PC-prior is specified on the joint density of the spatial range (ρ) and marginal standard deviation (σ^2). The spatial range gives an indication of the spatial span of the covariance structure, and the standard deviation provides the degree of spatial variability. The hyper-parameters (R and S) for this prior are set indirectly by specifying the lower tail quantile and probability for the range, and the upper tail quantile and probability for the standard deviation (Laxton et al., 2023a).

Priors are specified on the range using

$$P(\rho < \rho_0) = p_\rho, \tag{1.30}$$

where ρ_0 corresponds to the lower tail quantile for the range, and p_ρ corresponds to the probability that the actual range value (ρ) is less than ρ_0.

Similarly, variance priors are specified using

$$P(\sigma > \sigma_0) = p_\sigma, \tag{1.31}$$

where σ_0 corresponds to the upper tail quantile for the standard deviation, and p_σ corresponds to the probability that the actual standard deviation (σ) is greater than σ_0.

When using PC-priors in this way, the effects of complex model components like spatial or spatio-temporal Gaussian random fields will only be included when this is supported by the data

(Simpson et al., 2017). For the Matérn field, PC-priors penalise complexity away from the base model which represents the instance where the Gaussian random field has close to no impact; the limiting case with $\sigma^2 \to 0$ and $\rho_s \to \infty$. This is essentially a spatially constant random field with infinite range and zero variance.

1.6.4 Model Comparison in R-INLA

When comparing a number of models of the same type fitted to the same dataset, it can be of interest to perform a quantitative assessment which places models on the same scale, for comparison. However, when using quantitative measures for model assessment, it is important to incorporate a balance for model complexity, as prioritising only fit to data will result in highly data-specific models with poor predictive accuracy (Gelman, Hwang, and Vehtari, 2014). Measures of the Deviance Information Criterion (DIC) and Watanabe-Akaike (or Widely Applicable) Information Criterion (WAIC) are computed by default when fitting models in R-INLA (Spiegelhalter et al., 2002; Watanabe, 2010). These are commonly used Bayesian criteria for assessing a model's goodness of fit, whilst taking into account the complexity of the model required (in terms of the effective number of parameters). Lower values of DIC and WAIC indicate more probable model predictions, so in comparative analyses the model with the lowest DIC or WAIC value is chosen as optimal (Gelman, Hwang, and Vehtari, 2014).

DIC

DIC uses data-based bias correction to penalise model complexity (in terms of the effective number of parameters), and is based on the posterior mean $\hat{\theta}_{Bayes} = E(\theta|y)$ (Spiegelhalter et al., 2002). The criterion is defined as

$$\text{DIC} = -2\log\left(p\left(y \mid \hat{\theta}_{Bayes}\right)\right) + 2p_{DIC}, \tag{1.32}$$

where y is a vector of observations, p is the number of model parameters, and p_{DIC} is the effective number of model parameters calculated using simulation (Gelman et al., 2015).

WAIC

WAIC can be more robust than DIC, particularly for complex or hierarchical models, because it makes use of the full posterior distribution (Watanabe, 2010). In Gelman et al. (2015), WAIC is defined as

$$\text{WAIC} = -2\text{lppd} + 2p_{WAIC2}, \tag{1.33}$$

where lppd is the log pointwise predictive density, and p_{WAIC2} is the effective number of model parameters, calculated using a measure of variance summed over the data.

DIC is used for model comparison in Chapter 3, as recommended in Arce Guillen et al. (2023), and WAIC is used for model comparison in Chapter 2. Both measures provide proxies for cross-validation, wherein subsets of the data are removed from model fitting to test for predictive accuracy. As such, these measures are poorly understood in the context of point process models, which can be thought of as having essentially one observation: the overall distribution of points in the observation window (Illian and Burslem, 2017). Therefore, in Chapters 2 and 3 these model comparison measures are considered as one feature within an overall assessment, and not used for definite model selection.

1.6.5 `R-inlabru`

`R-inlabru` is a package in the `R` software language, which is a wrapper around and extension to the `R-INLA` package (Bachl et al., 2019; Lindgren et al., 2024; R Core Team, 2025). While `R-inlabru` uses `R-INLA` - and thus the INLA method for inference - internally, the syntax of `R-inlabru` code was designed to be more concise and user-friendly. Therefore, `R-inlabru` is a more accessible package for use in applied contexts.

Further to this, `R-inlabru` has additional flexibility which allows it to handle more complex modelling problems than `R-INLA`. It extends the class of models that can be fitted using the INLA methodology by allowing the predictor to be a non-linear (deterministic) funtion of the latent Gaussian parameters (Bachl et al., 2019). This is achieved using an inferential approach wherein model configurations are linearised and fitted iteratively, named iterated INLA (Lindgren et al.,

2024). Allowing non-linear predictors means that R-inlabru can be used in a wider range of complex applications than the R-INLA package.

The Iterative, Linearised INLA Method

In INLA, the sparse desgin matrix A links the latent GRF $\mathcal{X}$ which describes the parameters in the model to the linear predictor η of an LGM (see Equation 1.23). INLA can be used for models with non-linear predictors by allowing the predictor η to be a deterministic function of the parameter vector.

The iterative linearised INLA method is performed using the following steps:

1. Approximate the nonlinear model with its linearisation (based on first-order Taylor approximation).

2. Posit an initial linearisation point using a fixed point iteration method, so that the resulting conditional posterior mode of the linearised model is the same as the linearisation point.

3. Apply the INLA method to obtain posteriors, and choose the next linearisation point as the point that minimises a norm of the difference between the linearised and non-linear predictors (using an approximate line search method).

4. Repeat step 3 iteratively, until convergence to a given tolerance is achieved.

The non-linear feature of R-inlabru enables a wider range of complex models to be fitted using the INLA method (Lindgren et al., 2024). R-inlabru extends the range of ecological applications for which INLA can be used for inference, as complex spatial and spatio-temporal patterns in both the underlying process and its detection can be modelled (Bachl et al., 2019). All of the analyses in this thesis are carried out in the R-inlabru software package. (with the exception of Section 4.3.5, in which models are compared to a JAGS implementation).

1.6.6 Habitat selection modelling with R-INLA and R-inlabru

The INLA approach has been used for inference in various species distribution, movement, and habitat selection models with applications in different disciplines such as conservation, fisheries

science, invasive species research, and epidemiology. A few of these numerous applications are summarised here.

INLA provides a computationally efficient framework for modelling species distributions from large and complex spatio-temporal occupancy data (Belmont et al., 2024). This includes integrated species distribution models (ISDMs), wherein multiple sources of presence-only data are combined in a single model, such as in Martino et al. (2021), Morera-Pujol et al. (2023), Paradinas et al. (2023), and Panunzi et al. (2025b). It also extends to joint species distribution models (JSDMs), which model co-occurence of multiple species (e.g., Sadykova et al., 2017).

INLA has also been used to model geostatistical data such as that collected using passive acoustic telemetry, with applications in estimating distributions of threatened (e.g., Griffin et al., 2019) and invasive species (e.g., Gutowsky et al., 2020). Similar applications have been demonstrated using location data collected at echolocation-click detectors (Williamson et al., 2022a). Murphy (2020) constitutes another example of geostatistical modelling, using trawl survey data to predict distribution and abundance of species supporting industrial fisheries. Geostatistical modelling has also been used in the application of epidemiology, for example by Pepin et al. (2015), who fit a spatio-temporal model of disease spread from vector surveillance data (mosquito traps).

Other complex spatio-temporal models in INLA include that of Schrödle, Held, and Rue (2012), who present an areal-data spatio-temporal model of disease spread, with applications in assessing the impact of agricultural practices on the spread of infection in livestock. Paradinas et al. (2015) develop a complex spatio-temporal modelling approach to describe the abundance and occurrence of fisheries resource species. Williamson et al. (2022b) and Torney et al. (2023) both provide examples of fitting point-process methods in INLA to aerial-survey data, for the prediction of species distribution and abundance. Features describing movement and space-use behaviours have also been linked to social network positioning using INLA (Albery et al., 2021).

In terms of modelling spatio-temporal tracking data, resource selection analyses have been implemented in INLA, using binomial models of tracking locations and generated 'absence' data (for example, Muff, Signer, and Fieberg, 2019; Wall et al., 2024). Another example of modelling tracking data with INLA comes from Liu et al. (2016), who focus on correcting biases for path reconstruction with irregularly spaced temporal data. Johnson, London, and Kuhn

(2011) demonstrate the implementation of a continuous-time correlated random walk (CTCRW) to estimate movement parameters in INLA. Carson and Flemming (2014) group raw tracking data into encounter events, which are then modelled as a function of fixed and random effects in INLA, to provide an understanding of the environmental drivers of seal encounters. Discrete-time modelling of individual-level habitat selection using tracking data has been demonstrated by Arce Guillen et al. (2023), who implement a step-selection model in `R-inlabru`. To the author's knowledge, continuous-time modelling of individual-level habitat selection has not yet been demonstrated in the INLA framework. Therefore, the implementation of the joint Langevin movement model in `R-inlabru` in Chapter 4, and its application to real data in Chapter 5, represent a novel contribution to this research area.

1.7 Joint Likelihood Models

Joint models are complex models which require multiple likelihoods, and in which parameter estimation can be shared across likelihoods in a joint likelihood function. Joint models can be used to explicitly model different aspects of data (for example, separating the distributions of marks and points in a marked point process, Illian, Sørbye, and Rue, 2012), or to combine multiple data streams (also termed data integration or data fusion). Joint modelling can aid in managing missing or incomplete data, or in balancing biases from different data sources. Joint models are flexible because they are able to handle complex data structures, can be more efficient than multi-step approaches, and solve issues with propagating uncertainty.

Joint models are generally more complex than single-likelihood models, so come with the disadvantages of being more computationally costly to implement. They are also subject to more complex assumptions, and can be less interpretable than single-likelihood models, so may be considered more inaccessible for applied users. Despite these drawbacks, joint likelihood modelling opens up a range of possibilities in ecological data analysis.

In the world of community ecology, joint models allow for the integration of data on the spatial or spatio-temporal distribution of multiple species into a single model (joint species distribution modelling, or JSDM, Poggiato et al., 2021). This can improve predictions of spatial distribution by accounting for species co-occurrence patterns which are not explained by envi-

ronmental variables. JSDMs can also help to uncover the drivers of co-occurence, by describing shared responses to environmental variables (Pollock et al., 2014; Sadykova et al., 2017).

Joint likelihood methods also form the basis for a range of data-integration approaches in ecology (Miller et al., 2019). In these approaches, multiple data streams are combined into a joint likelihood model, and shared parameter estimation maximises the combined fit to all data. Joint modelling is often used to balance biases of different data sources, account for missing data, or combine data at different spatial, temporal, and organisational scales (Blackwell and Matthiopoulos, 2024). In the world of species distribution modelling, joint likelihood models (often termed integrated species distribution models, or ISDMs) can be used to combine reliable, structured survey data (usually covering a small or stratified domain) with more widespread, but often less reliable and subject to different sources of bias, citizen science data (Miller et al., 2019). Habitat selection modelling has also recently benefitted from the development of joint likelihood methods which combine data collected at different organisational scales, such as population-level survey data and individual-level telemetry data (Blackwell and Matthiopoulos, 2024; Buderman et al., 2025; Lauret et al., 2025). The integration of animal movement data as an additional data stream is also a feature in much of the spatial capture-recapture (SCR) literature (Tenan et al., 2017; Linden, Sirén, and Pekins, 2018; Hostetter et al., 2022; Badger et al., 2024).

In animal movement modelling, joint likelihood methods can be used to bring together multiple likelihoods which could typically only be used to analyse the movement of one individual in a single-likelihood approach (for example, Arce Guillen et al., 2023). Habitat selection parameter estimation can be shared across likelihoods, therefore providing descriptions of shared responses to environmental variables. This information can be easier to interpret than comparing varied estimates from multiple individual models.

In point process modelling, joint likelihood methods can be used to jointly model the point pattern of observed locations and environmental covariates which are measured at different spatial locations, for example at weather stations (Illian, Sørbye, and Rue, 2012). This removes the initial step of interpolating covariates to obtain values at the point locations, and accounts for covariate measurement error. In addition, marked point process approaches can be used to jointly model the distribution of point locations and multiple dependent marks. Where the marks are the

feature of interest, the dependence on the spatial distribution of point pattern intensity is taken into account. This has a range of applications in ecology, wherein processes of interest are often subject to complex spatial or spatio-temporal correlation structures.

Joint models take many forms, and provide a framework for complex modelling with varied applications in ecology. In this thesis, various uses for joint modelling are explored. Chapter 2 includes a marked point process model, allowing key ecological processes driving population spread to be explicitly modelled and used to improve prediction. Chapter 3 incorporates a joint likelihood to simultaneously model discrete-time movement from multiple individuals, producing shared estimates of habitat selection parameters. Finally, Chapters 4 and 5 present an approach for data integration, where a joint likelihood habitat selection model is used to combine population-level and individual-level data streams.

1.8 Summary of Thesis

1.8.1 Thesis Structure

The remainder of this thesis is organised into 5 chapters, containing 3 case studies. The content of the thesis is arranged as follows:

Chapter 2: titled *"Patch-Level Habitat Selection and Dispersal in a Reintroduced Population: A Spatio-temporal Marked Point Process Model in* `R-inlabru`*"*, contains the first case study which demonstrates the use of a marked point process approach with an application in reintroduction biology.

Chapter 3: titled *"Scale-Dependent Habitat Selection in a Domesticated Population: Gaussian Field Integrated Step Selection Analysis in* `R-inlabru`*"*, contains the second case study, in which a discrete-time individual-level model and a population-level model are applied in an agricultural setting.

Chapter 4: titled *"Combining Local and Global Scale Habitat Selection: Implementing the Langevin Movement Model in* `R-inlabru`*"*, translates a newly developed joint likelihood for the integration of survey and tracking data for implementation in the `R` software

package `R-inlabru`.

Chapter 5: titled *"Habitat Selection and Distribution of a Semi-Domesticated Population: Application of the Langevin Diffusion Movement Model"*, makes up the third case study, in which the model developed in Chapter 4 is fitted to tracking data from a semi-domesticated population.

The thesis concludes with Chapter 6, a discussion of the key findings from Chapters 2-5.

1.8.2 Case Studies: Key Themes

The case studies presented in Chapters 2, 3, and 5 have been selected to provide a varied exploration of key ecological and statistical themes pertaining to spatio-temporal modelling in ecology. These include: varying ecological applications and aims in habitat selection modelling; handling differing data structures; joint modelling; point process modelling; model complexity; spatio-temporal scale; data integration; and availability.

The species of interest in each of the case studies represent a different type of population and application of habitat selection modelling. Chapter 2 investigates the dispersal of a population of Eurasian crane (*Grus grus*) which have been recently reintroduced to a wild setting and are monitored for the purpose of conservation. The main aim of Chapter 2 is to predict population spread. In contrast, Chapter 3 analyses habitat selection in a fully domesticated population, wherein models are fitted to data from 3 breeds of cattle (*Bos taurus*) grazed in mountain rangeland pastures. Chapter 3 aims to improve understanding of pasture utilisation, with impacts in ecological and economic stability, and animal welfare. The final case study, Chapter 5 focuses on a semi-domesticated population of reindeer (*Rangifer tarandus tarandus*) during a free-ranging period with minimal management. Chapter 5 aims to provide insight into long-term habitat selection for different land-use types, in order to improve the sustainability of management practices. Each case study provides a different perspective on the aims of habitat selection modelling and the restrictions and parameters of interest in varying applications.

Further to their aims and applications, the case studies in Chapters 2, 3, and 5 also differ in data type and structure. The data analysed in Chapter 2 are presence-absence data collected at a coarse spatio-temporal scale. Conversely, the data analysed in Chapter 3 are presence-only

tracking observations, collected at a fine spatio-temporal resolution. The data analysed in Chapter 5 are also presence-only tracking observations, but are subsetted to create a combination of fine-scale individual-level data, and coarse-scale population-level data. Overall, the case studies comprise a varied exploration of different data types and how they are analysed in habitat selection modelling.

The models fitted in Chapters 2, 3, and 5 are all joint likelihood models which utilise point process methodology and are fitted using the `R` package `R-inlabru` (Bachl et al., 2019; R Core Team, 2025). However, each case study contains a different method for analysis. In Chapter 2, a marked point process model is fitted, wherein the joint structure allows for the simultaneous modelling of the underlying distribution of points (habitat patch locations) with the likelihood of the associated marks (species occurrence). Chapter 3 uses a point-process model of step-selection, wherein a joint likelihood approach allows for the inclusion of multiple individuals in the model (GF-iSSA, Arce Guillen et al. (2023)). Finally, Chapter 5 uses a joint model for the integration of two data streams, where one likelihood is a point process fitted to population-level data, and the other is a diffusion based movement model of individual-level data. The approach used in Chapter 5 is developed in Chapter 4. The two individual-level movement models presented in Chapters 3 and 5 also provide examples of discrete-time (Chapter 3) and continuous-time (Chapter 5) movement modelling. Overall, the case studies in Chapters 2, 3, and 5 are all joint likelihood spatio-temporal point process models which use `R-inlabru` for inference, but each one varies in model structure.

Each of the case studies in Chapters 2, 3, and 5 contain a comparison of multiple models, but with the aim of evaluating a different question from the larger discipline of spatio-temporal modelling in ecology. In Chapter 2, models of varying levels of structural complexity are compared to investigate the role of complexity in model fit and predictive accuracy. Chapter 3 poses the question of how varying spatial scale and temporal frequency impacts inference. Finally, Chapter 5 compares different types of model for different levels of selection, and investigates how models with multiple data streams compare to those with a single data stream. The questions of model complexity, scale, and data integration are subjects of current interest and development in statistical ecology (Jackson and Fahrig, 2015; Matthiopoulos et al., 2022; Mccrea et al., 2023).

Each of the case studies in Chapters 2, 3, and 5 demonstrates a different approach to accounting for availability, or animal mobility, in habitat selection modelling. Chapter 2 incorporates a Gaussian random field to estimate and account for overall restrictions on population dispersal ability. Alternatively, Chapter 3 accounts for individual mobility restrictions through a unique integration scheme. Chapter 5 also accounts for restrictions in individual mobility, but instead uses a Gaussian kernel transformation. Each case study presents a different approach to handling the ubiquitous problem of availability in spatial models of animal movement and distribution.

1.8.3 Summary

This thesis aims to enhance understanding of joint likelihood spatio-temporal point process methods for habitat selection modelling, as motivated by the emergence of these methods as a unifying framework for analysis in this area and the need for applied demonstrations of their implementation (Illian and Burslem, 2017; Miller et al., 2019; Matthiopoulos et al., 2022). It focuses on demonstrating applications of this model type in a range of ecological contexts, creating extensions to current methods, and developing novel implementations for statistical inference and prediction using an accessible software platform. It explores questions of complexity, spatio-temporal scale, data integration, and availability which are central to rapidly evolving areas of statistical ecology. Overall, it provides substantial methodological advancements for applied modelling of spatial distribution, movement, and habitat selection.

Chapter 2

Patch-Level Habitat Selection and Dispersal in a Reintroduced Population: A Spatio-temporal Marked Point Process Model in `R-inlabru`

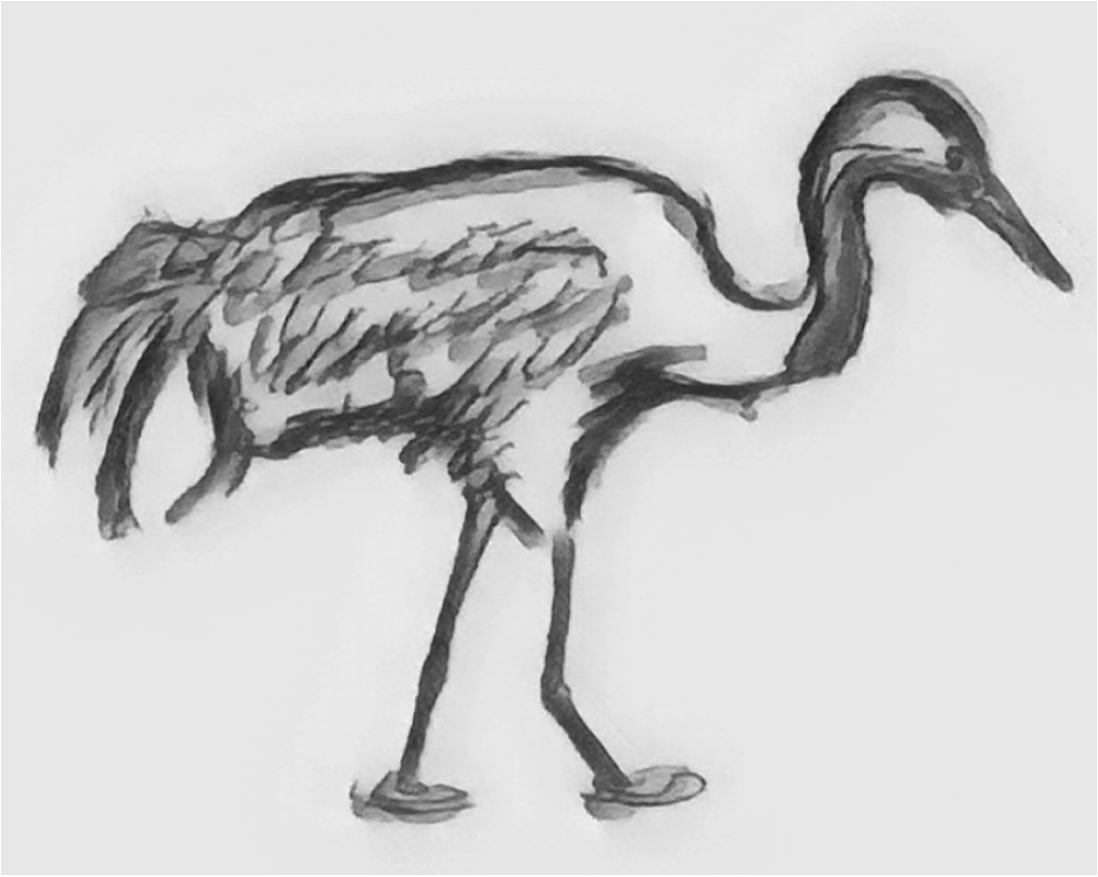

2.1 Introduction

The following chapter contains a case study fitting a joint likelihood spatio-temporal point process model (a marked point process) to data from a reintroduced population. It aims to estimate habitat selection and predict spread of the reintroduced population, whilst accounting for availability in terms of habitat patches and dispersal restrictions.

2.1.1 Habitat Selection and Dispersal in Reintroduction Biology

Urban expansion and increased demand for resources are just some of the factors that have led to the reduction and fragmentation of suitable habitat for wild populations, and increased anthropogenic disturbance in remaining protected areas. This highlights the insufficiency of *in situ* conservation alone, with an increasing demand for *ex situ* methods such as captive breeding and reintroduction (Pritchard et al., 2011). However, historically, many attempts at reintroduction have been unsuccessful, causing a serious blow to fragile populations of threatened species (Armstrong and Seddon, 2008). In addition, reintroduction projects are often labour-intensive and so economically costly, augmenting the need for *a priori* assessment of the potential success of reintroduction, which is dependent on an understanding of a population's needs and behaviours (Bleisch et al., 2017). Understanding of the spread and establishment of reintroduced populations can be gained from *post hoc* analysis of reintroduction data, so this provides a vital source of information in the development of reintroduction biology (Seddon, Armstrong, and Maloney, 2007).

Habitat selection modelling for reintroduced species is subject to a range of challenges, as the reintroduced population is not observed during a period of spatial equilibrium, but of range expansion (Planillo et al., 2023). It is often not well understood how a species will behave in a new environment, and it can be difficult to define the dispersal limitations of a reintroduced population, as movement can be influenced by several factors such as site fidelity, density dependence, and social bonding (Haydon et al., 2008). Instead of trying to define dispersal limitations entirely using insubstantial prior information, it can instead be useful to capture availability restrictions using a random effect in the model. This allows for the estimation of dispersal limitations using

a combination of observed data and priors.

2.1.2 Complexity in Species Distribution Modelling

Methods for collecting ecological data are developing rapidly, allowing for the automated collection of location data, and improved availability and resolution of environmental information. This, coupled synergistically with the development of technology used for analysis, means that larger and more complex models are becoming more widespread in ecological research (Mccrea et al., 2023). However, increasing the structural complexity of a model can reduce interpretability, particularly when there is a lack of ecological justification for the inclusion of additional model components. Hence increased model complexity is only relevant if the more complex models provide additional insight into ecological processes as compared to simpler models, which are often computationally cheaper (Bolker, 2009). In defense of model complexity, more complex models may provide improved predictive accuracy or parameter estimation; be subject to less restrictive assumptions; and account for dynamics of intricate ecological processes in a more biologically realistic way than simpler models.

Species distribution models aim to provide insight into the spatio-temporal distribution and habitat selection of a population, so are often constructed as complex spatio-temporal models. Spatio-temporal random effects can be used to account for sources of spatio-temporal autocorrelation, such as missing covariates or correlated data structures. In this context, more complex models can also improve ecological insight by accounting for less tangible processes driving species distribution than environmental covariates, such as demography (Pagel and Schurr, 2012), dispersal (Iverson, Schwartz, and Prasad, 2004; Elith and Leathwick, 2009), and physiology (Buckley et al., 2011). However, incorporation of random effects can result in spatial confounding with covariates and overfitting to data (Sørbye et al., 2019).

2.1.3 Case Study

This chapter explores the effect of structural complexity on predictive accuracy and ecological insight in a spatio-temporal species distribution model, related to a model that has previously been fitted (Soriano-Redondo et al., 2019). The analysis performed in Soriano-Redondo et al. (2019) consists of a spatio-temporal marked point process model fitted in R-INLA (Rue, Martino,

and Chopin, 2009). Here, the approach is revisited by fitting a similar model and comparing it to new models with variations in level of complexity, using R-inlabru for model fitting and inference.

The marked point process model is an extension to the point process model, wherein the object or event locations are modelled alongside some properties of the events or objects (Illian, Sørbye, and Rue, 2012). These properties can be qualitative or quantitative and are commonly referred to as 'marks'. If a dependency between the values of a mark and the point distribution is assumed, these can be jointly modelled with two or more dependent likelihoods. Hence the marked point process model is a joint likelihood point process.

In the model formulation described here, the spatio-temporal structure of the marks (independent of point distribution) and the spatio-temporal structure of the points are represented with different Gaussian random fields in a shared representation of continuous-space and discrete-time (using the SPDE approach, Lindgren, Rue, and Lindström, 2011).

The ecological context of the case study aims to estimate habitat selection and predict population spread of the Eurasian crane (*Grus grus*) following reintroduction of the population to the UK. Habitat availability and dispersal limitations are accounted for through the modelling framework.

2.1.4 Aims

This chapter aims to demonstrate the use of a marked point process model to predict the spatio-temporal spread of a reintroduced population. It will:

1. fit four model variations related to a joint likelihood spatio-temporal marked point process model to population-level presence-absence data, in order to predict population spread of a reintroduced species;

2. demonstrate the use of complex model components (spatial and spatio-temporal random fields) to represent availability in terms of population dispersal ability and density of available habitat patches; and

3. compare model performance, in terms of fit and predictive accuracy, across four models

with different levels of structural complexity.

2.2 Methods

2.2.1 Data Background

This analysis investigates the spatial distribution of a resident breeding population of Eurasian crane (*Grus grus*) in England following the return of the species to the UK in 1979 (Stanbury, 2011), with the aim of predicting the distribution of the population in future years. Breeding pairs of cranes are only found in wetland habitats, which creates a spatial restriction on the suitable habitat available to the species, although little is known about its dispersal ability. The distribution of wetland locations in England is heterogeneous, with various underlying factors creating a clustered structure of habitat patches. Thus, the distribution of the crane population throughout the UK and its future spread is dependent on the availability of suitable wetland habitat. Due to this known species habitat selection, data on crane presence were collected only at wetland locations, and not in interstitial areas. This type of data can be modelled as a marked point process in `R-inlabru`, in order to infer habitat selection and predict species distribution, whilst accounting for known species habitat requirements and observation processes. Specifically, the observation process is modelled as reflected in the wetland locations as a point pattern, jointly modelled with the presence-absence of nesting cranes as a mark.

The dataset includes information on a small breeding population which naturally settled in the UK in 1979 after earlier extirpation of the species, as well as animals used in a reintroduction project in 2010-2014. It also includes records for 2 526 wetlands in England derived from the UK Land Cover Map 2007 (Morton et al., 2011) and the Wetland Vision map of current wetlands (Hume, 2008). While the UK Land Cover Map 2007 assigns the dominant habitat to a 25m raster grid, the Wetland Vision map determines the boundaries of the major wetland areas in England at a landscape-scale. Combining both sources provides an approximation of most available wetland patches in England. This selection was reduced by eliminating wetlands in moorland areas since cranes in the UK are only nesting in lowland wetland areas (Stanbury and Sills, 2012). Wetland patches smaller than 5 ha were also removed, as estimates show that cranes required at least 8

ha to nest (Johnsgard, 1983). The fine grain of this classification allows the wetland areas to be treated as points, since extensive wetland regions are fragmented by other types of habitats, roads or other human infrastructure, and are indeed composed by multiple smaller wetland areas. Each wetland area has associated information: its spatial coordinates, data on the presence or absence of breeding pairs of cranes, wetland extent, perimeter-to-area ratio, and the proportion of urbanised areas in a 10km surrounding terrestrial buffer. Of the 2 526 wetland locations (which remained consistent over all years of observation), cranes were observed to be present in 8 wetlands in 2011, 7 in 2012, 8 in 2013, 9 in 2014, and 12 in 2015. As some wetlands were occupied by cranes for multiple years, cranes were observed to occupy a total of 16 unique wetlands over the 5-year observation window. Figure 2.1 shows the spatial distribution of the data over time.

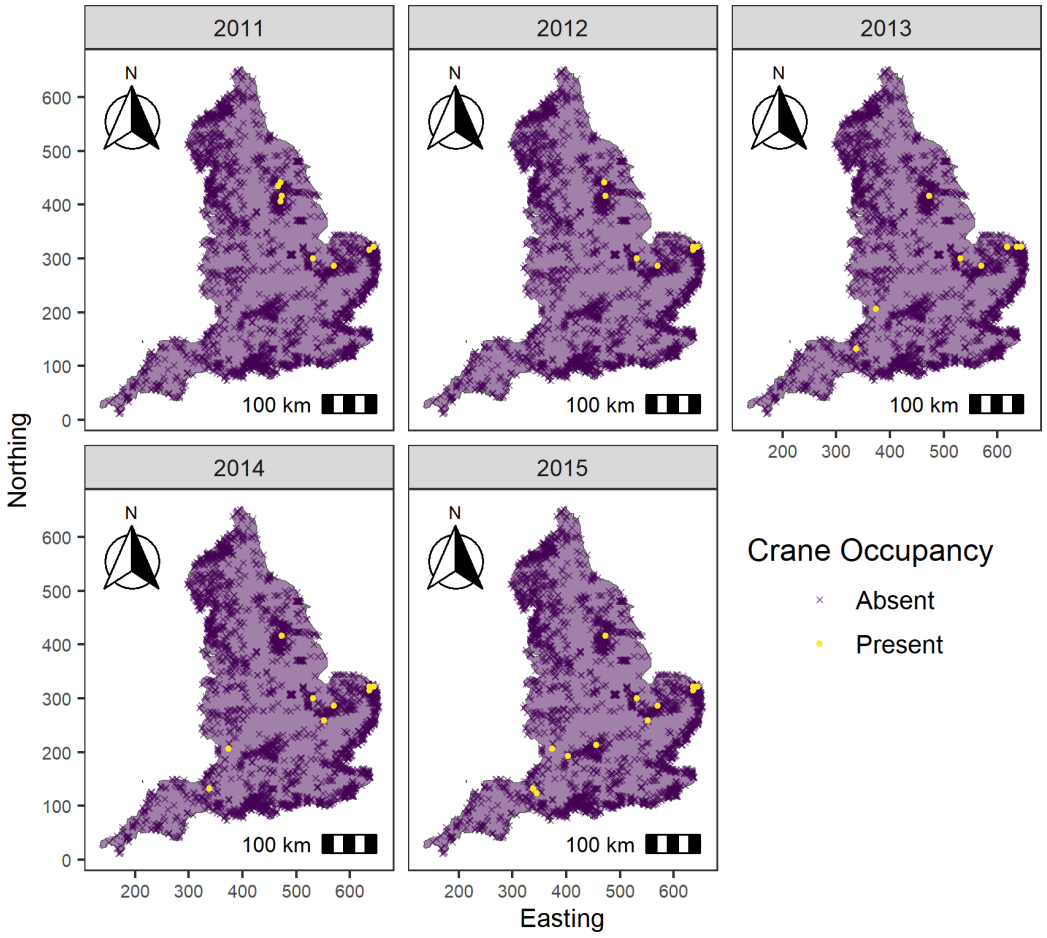

Figure 2.1: Distribution of wetland locations and observed crane presences in England 2011-2015. Purple background colour is used for visual clarity, and does not represent a value on the colour scale.

2.2.2 Modelling Strategy

To evaluate the structure of the model in Soriano-Redondo et al. (2019) this analysis demonstrates two modelling approaches with the aim of estimating the spatio-temporal distribution of cranes in England. The first approach makes use of a single Gaussian random field to represent spatio-temporal correlation in the distribution of the observed population of cranes. The second is a marked point process approach, which incorporates a second Gaussian random field, accounting for the spatial distribution of wetlands (which remains constant over time). Within these modelling frameworks, differences arising from the inclusion of a temporal correlation structure via a first-order autoregressive (AR1) process, where estimates for each year are dependent on the immediately previous year, are compared to treating each year of data as independent and identically distributed (IID). Therefore the overall modelling strategy included 4 models, which are summarised in Table 2.1.

Table 2.1: Description of 4 models of crane distribution, fitted in R-inlabru.

Modelling Approach	Temporal Correlation	$\text{logit}^{-1}(P(s,t))$
Geostatistical	IID	$\beta_0 + \sum_{i=1}^{I} \beta_i x_i(s,t) + M(s,t)$
	AR1	$\beta_0 + \sum_{i=1}^{I} \beta_i x_i(s,t) + M(s,t)$
Marked Point Process	IID	$\beta_0 + \sum_{i=1}^{I} \beta_i x_i(s,t) + \zeta G(s) + M(s,t)$
	AR1	$\beta_0 + \sum_{i=1}^{I} \beta_i x_i(s,t) + \zeta G(s) + M(s,t)$

Model fitting and inference were carried out in R version 4.1.1 (R Core Team, 2021) using the packages R-inlabru version 2.3.1.9000 (Bachl et al., 2019) and R-INLA version 21.02.23 (Rue, Martino, and Chopin, 2009).

2.2.3 Single-Field Models

In order to explore what level of model complexity is needed to answer relevant ecological questions based on the crane data, the initial model is a relatively simple spatio-temporal model in continuous-space. To improve understanding of the spatio-temporal distribution of cranes across England, the fact that cranes will only nest in wetland habitats is initially ignored, and a model containing a single spatio-temporal Gaussian random field is constructed. This is essentially a model of geo-referenced (binomial) data (often referred to as a geostatistical model) with a

single likelihood, which does not take the observation process into account and assumes that crane presence is equally likely across England. Here, crane presence is modelled as a binomial distribution

$$O_{s,t} \sim \text{Bernoulli}\left(P(s,t)\right), \tag{2.1}$$

where the occurrence of cranes $O_{s,t}$ at each location s, in each year t can be considered an individual Bernoulli trial with probability $P(s,t)$. Here, the location s is a vector representing coordinates s_1 and s_2 in two-dimensional space. Note that for larger-scale models, location could also be represented on the sphere (Simpson et al., 2016).

The probability of crane presence P in a location s at time t is denoted by $P(s,t)$ and is dependent on the observed distribution of the existing population in space and time, as well as the effect of environmental covariates. It is defined as

$$P(s,t) = \text{logit}^{-1}\left(\beta_0 + \sum_{i=1}^{I} \beta_i x_i(s,t) + M(s,t)\right), \tag{2.2}$$

where β_0 represents an intercept term and $x_i(s,t)$ is the value of each covariate i at location s and time t. The environmental covariates included in the model were: density of surrounding urbanised areas (within a 10km terrestrial buffer), wetland perimeter-to-area ratio, and wetland extent. The values of these covariates were standardised using the Z-score formula prior to inclusion in the model, in order to improve the stability of numerical computation. The regression coefficient β_i of each covariate is estimated in the model. The separable spatio-temporal Gaussian random field $M(s,t)$ represents the spatial structure in distribution of the observed crane population in space and time unexplained by the intercept and covariates. The Gaussian random field $M(s,t))$ is approximated using an SPDE. Penalised complexity (PC) priors defining a likely minimum spatial range of 200km and maximum standard deviation of 1.5 were used to inform this covariance structure, according to ecological understanding of the distances across which values may be correlated, and the extent to which values may vary. Two options are explored for the temporal element of this field, (1) incorporating a random effect in which each year of data is considered independent and identically distributed (IID) and (2) modelling temporal correlation

between consecutive years with a first-order autoregressive (AR1) process.

2.2.4 Marked Point Process Models

The binomial presence-absence model in Equations 2.1 and 2.2 captures the spatial correlation structure in the occurrence of breeding pairs of cranes, but ignores the distribution of suitable habitat patches (wetlands). However, sampling only took place in locations where cranes would be expected to nest, i.e., the locations of wetlands. This observation process could also be interpreted as preferential sampling (Diggle, Menezes, and Su, 2010; Pennino et al., 2019). In this example, crane detectability is assumed to be known, as due to the large size of the animals they are easy to detect. This means that detectability is not overestimated even though preferential sampling is not accounted for, because absence of cranes in unsampled areas is known, not incorrectly assumed. However, with rare or small organisms that are more difficult to detect, it may be of interest to use models to predict and estimate abundance across space. In these cases, such a model would likely predict presence where the species of interest does not occur, and overestimate abundance as a result. Despite the certainty of detection of cranes here, the distribution of wetlands is still an important factor in determining species distribution, as it represents habitat selection. This can be accounted for through modelling the data using a marked point process, by jointly modelling the distribution of wetlands as a point process, and the presence-absence of breeding pairs of cranes as a binomial mark. The presence-absence of cranes can be viewed as a mark on the wetland point process; a feature which only occurs at the point locations, and so is dependent on the underlying spatial structure of the points. In this second approach, the model presented in Equation 2.2 is extended to include the density of available wetland habitat. This model structure is taken from Soriano-Redondo et al. (2019), and the models developed here are based on those created by Soriano-Redondo et al. (2019), in order to evaluate the advantages and disadvantages of including complex model components.

The point pattern of wetland locations is modelled as a log Gaussian Cox process in `R-inlabru`. The distribution of wetlands is assumed to be independent conditional on the point process intensity $\Lambda(s)$

$$\Lambda(s) = \exp\left(\alpha_0 + G(s)\right), \tag{2.3}$$

where the log-intensity of the spatial point process model is given by an intercept term α_0 and a spatial Gaussian random field $G(s)$. Since it is not of interest to gain an understanding of the underlying drivers of wetland distribution in this context, covariates that would help to explain wetland spatial distribution are not included in the model. However, this could be easily done. Additionally, wetland density is assumed to be constant over time. This is a reasonable simplification for the data presented here, but could easily be adapted to allow for changing wetland distributions with a spatiotemporal field.

The probability of crane presence $P(s,t)$ is dependent on both the distribution of wetlands in space, and the distribution of the existing crane population in space and time

$$P(s,t) = \text{logit}^{-1}\left(\beta_0 + \sum_{i=1}^{I} \beta_i x_i(s,t) + \zeta G(s) + M(s,t)\right), \tag{2.4}$$

where wetland density is incorporated into the model through the inclusion of the spatial Gaussian random field $G(s)$ multiplied by a scaling parameter ζ, which determines the strength and direction of the interaction between wetland density and crane presence. When $\zeta = 0$, Equation 2.4 becomes equivalent to Equation 2.2 (i.e., wetland density does not affect crane presence). A prior is placed on ζ to provide stability due to convergence issues. This ensures a simple interpretation of the interaction between $G(s)$ and crane presence (i.e., positive effect of high density as opposed to negative effect of low density). The spatio-temporal Gaussian random field $M(s,t)$ represents the distribution of the observed crane population in space and time, independent of wetland distribution. As in the binomial presence-absence model, both an AR1 and IID temporal correlation structure are considered for $M(s,t)$. However, the point pattern of wetland locations does not change between years, and so represents a constant restriction on species distribution. Therefore, $G(s)$ is a purely spatial Gaussian random field, and does not incorporate a temporal element. This represents an improvement in computational efficiency compared to the model structure in Soriano-Redondo et al. (2019), which includes a spatio-temporal field instead of a spatial one.

2.3 Results

In both the binomial presence-absence model (Equation 2.2) and marked point process model (Equation 2.4) which incorporated an AR1 temporal correlation structure, the correlation parameter for the AR1 process, ρ_t, (which is bounded between -1 and 1) was estimated to be extremely high (Table 2.2). This indicates a very strong temporal correlation across years. Due to this strong temporal correlation, the model estimated the same spatial structure in the mark random field $M(s,t)$ and predictions of crane probability of presence across all 5 years considered in the study. The estimated spatial distribution of the mark random field $M(s,t)$ for the marked point process models with AR1 temporal structure can be seen in Figure 2.2. For comparison, see Figure 2.3, which contains the estimated spatial distribution of the mark random field $M(s,t)$ for the marked point process models with IID temporal structure. The estimated fields from the IID model were smoother than those from the AR1 model, and differed between years.

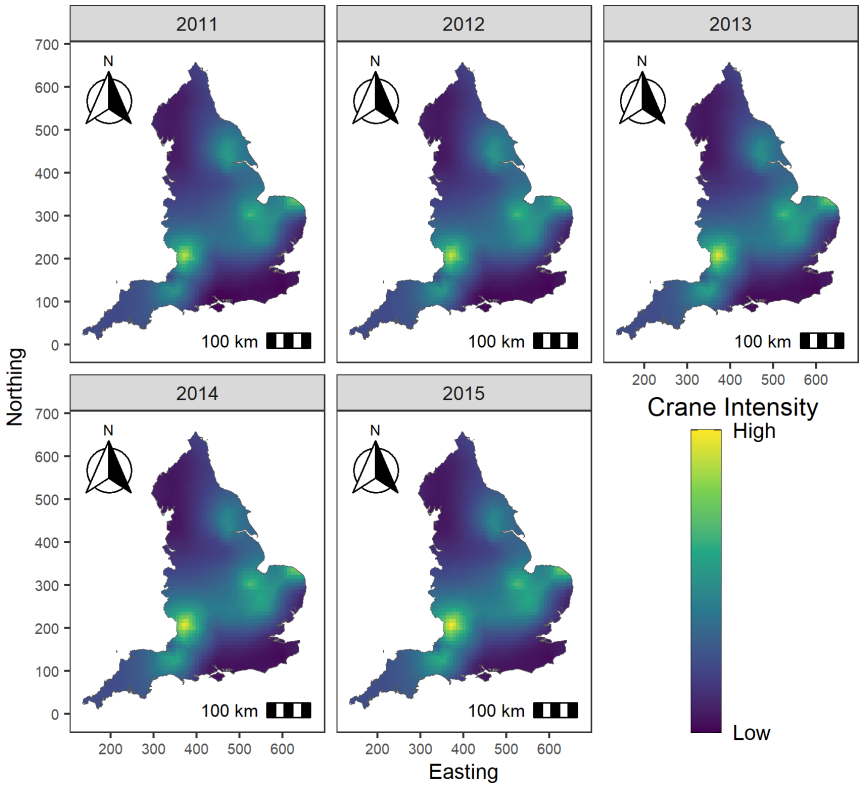

Figure 2.2: Estimated mark random field ($M(s,t)$) for 2011-2015 from the marked point process model with AR1 temporal structure. Colour scale is given in low-high intensity as interest is in relative differences across space and not absolute values.

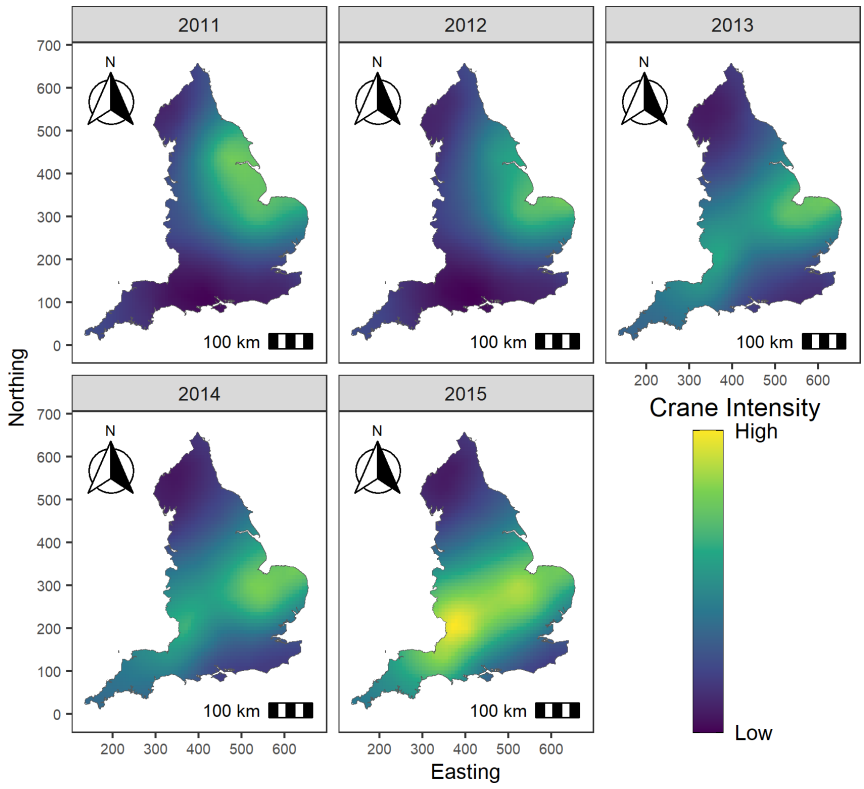

Figure 2.3: Estimated mark random field ($M(s,t)$) for 2011-2015 from the marked point process model with IID temporal structure. Colour scale is given in low-high intensity as interest is in relative differences across space and not absolute values.

The estimates from the marked point process AR1 model constituted a spatial structure reflecting an average of all years of data, as opposed to accurately representing changes in spatial structure each year (Figures 2.2 and 2.3). This behaviour is matched in the single-likelihood models with AR1 temporal structure (see Appendix A). Such averaged estimates may be inaccurate when interpreting within-year spatial effects, and so from this point onwards, graphical representations of results are provided for the models which treat each year of data as IID only.

In the marked point process and binomial presence-absence models, the mark random field $M(s,t)$ represents the spatial distribution of the crane population each year (Figure 2.4 (b)). This constrains predictions to near where nesting pairs of cranes have been observed, and without it the species could be predicted to occur in areas of suitable environmental conditions, but that are an unrealistic distance from the established population.

The marked point process models also contain a point random field $G(s)$, which models the spatial distribution of wetlands (Figure 2.4 (a)). The strength and direction of the interaction

between wetland density and probability of crane presence is estimated through the scaling parameter ζ. In the models containing the point random field, ζ is estimated as a positive effect with 95% credible intervals above zero (Table 2.2). This means that probability of crane presence is estimated to be higher in areas of high wetland density, as opposed to low density areas. Without the inclusion of the point random field (as in the binomial presence-absence model), predictions of species distribution could be correlated across wide expanses of interstitial habitat, and are not assumed to depend on the density of suitable habitat patches. Using a random effect allows for the spatial range of the impact of habitat availability to be estimated in the model, as compared to including wetland density as a fixed effect, which would require the spatial scale of the buffer region to be determined *a priori*.

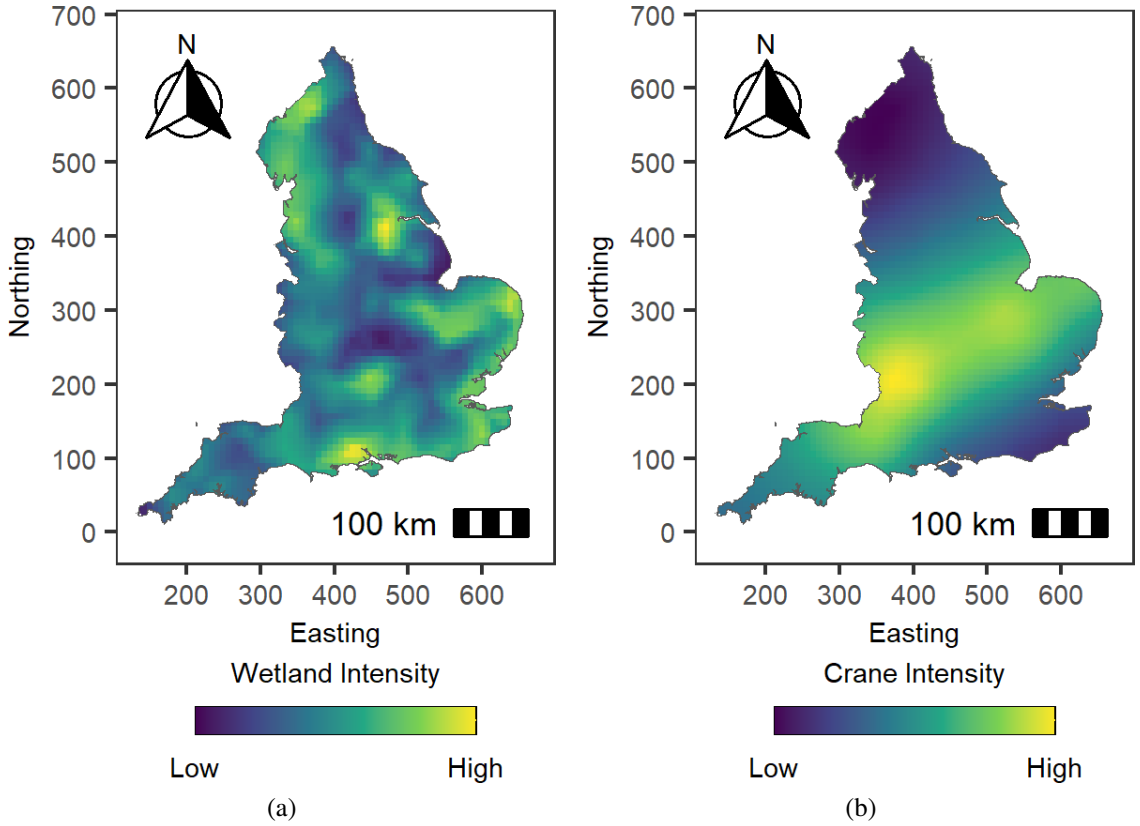

Figure 2.4: Estimated (a) point random field ($G(s)$) and (b) mark random field ($M(s,t)$), both for 2015 from the marked point process model with IID temporal structure. Colour scale is given in low-high intensity as interest is in relative differences across space and not absolute values.

Estimated regression coefficients were similar across all models for both wetland perimeter-to-area ratio and wetland extent. For all models, wetland perimeter-to-area ratio had a negative effect on crane presence with 95% credible intervals below zero, and wetland extent had a positive effect with 95% credible intervals above zero (Table 2.2). However, there was a slight difference in estimated effect of density of surrounding urbanised areas between the IID and AR1 models. Although density of surrounding urbanised areas was found to have a negative effect in all models, the mean effect size was estimated to be smaller, with a 95% credible interval concentrated around 0, in the binomial presence-absence and marked point process models which incorporated an AR1 temporal correlation structure, but was estimated as being more strongly negative with a 95% credible interval below 0 in those models with an IID temporal structure (Table 2.2).

Probability of presence of breeding pairs of cranes across space in 2015 was predicted using the binomial presence-absence and marked point process models with IID temporal structure. Predictions from the binomial presence-absence model (Figure 2.5 (a)) show a wider spatial range in areas of high probability of presence, compared to predictions from the marked point process model (Figure 2.5 (b)).

Table 2.2: Posterior mean and 95% credible intervals for: regression coefficients of environmental covariates (density of surrounding urbanised areas within a 10km buffer β_{UD}, wetland extent β_{WE}, and wetland perimeter:area ratio β_{PA}); scaling parameter (ζ) representing the interaction between $G(s)$ and the probability of crane presence; temporal correlation parameter ρ_t from the AR1 process; parameters of the spatial, $G(s)$, and spatio-temporal, $M(s,t)$, fields (spatial range ρ_s, and standard deviation σ). The covariate coefficients and scaling parameter values with credible intervals which do not cross zero are in bold. Model processing times (given by CPU used) and Watanabe–Akaike information criterion (WAIC) scores are also given. All values given are rounded to 2 decimal places.

	Binomial Presence-Absence		Marked Point Process	
	IID	AR1	IID	AR1
β_{UD}	**-0.58 [-1.19,-0.04]**	-0.14 [-1.15,0.72]	**-0.74 [-1.48,-0.1]**	-0.09 [-1.19,0.85]
β_{WE}	**0.08 [0.02,0.14]**	**0.12 [0.02,0.24]**	**0.1 [0.03,0.16]**	**0.1 [0,0.21]**
β_{PA}	**-3.02 [-3.92,-2.2]**	**-3.49 [-4.57,-2.53]**	**-3.02 [-3.94,-2.19]**	**-3.47 [-4.55,-2.51]**
ζ	NA	NA	**0.62 [0.11,1.16]**	**0.99 [0.04,2.05]**
$M(s,t)$ ρ_t	NA	0.99 [0.98,1]	NA	0.99 [0.98,1]
$M(s,t)$ ρ_s	346.7 [183.45,612.59]	119.95 [70.38,197.16]	238.66 [142.06,315.93]	145.15 [67.5,282.16]
$M(s,t)$ σ	1.22 [0.66,2.01]	3.03 [1.94,4.25]	0.98 [0.56,1.29]	3.34 [2.24,4.86]
$G(s)$ ρ_s	NA	NA	105.97 [88.57,185.44]	124.19 [83.17,188.41]
$G(s)$ σ	NA	NA	1.22 [1.07,1.32]	1.34 [1.01,1.83]
CPU	63.26	123.64	108.62	174.94
WAIC	464.38	425.38	28045.01	28024.94

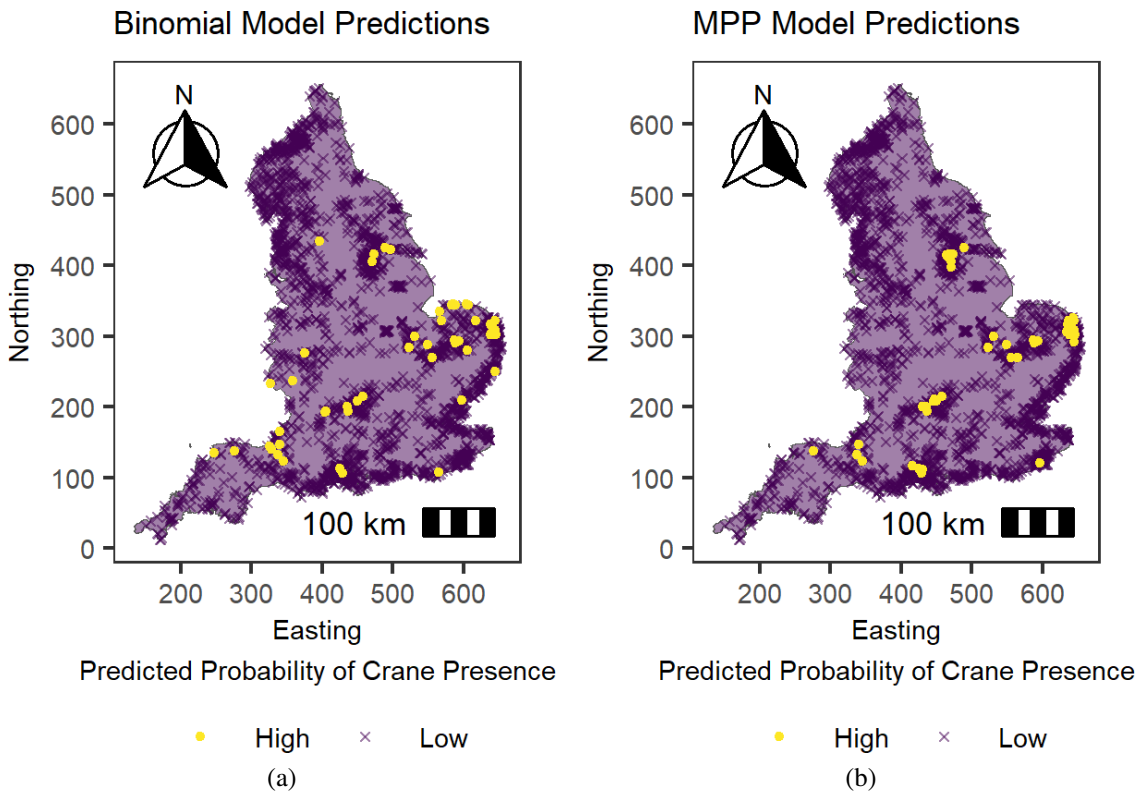

Figure 2.5: Mean predicted probability of presence of a breeding pair of cranes at each wetland location in 2015. Predictions were made using (a) the binomial presence-absence model and (b) the marked point process model, both with IID temporal structure. Colour scale is given in low-high probability as interest is in relative differences across space and not absolute values. 'Low' represents a value of mean predicted probability of crane presence less than or equal to the 99th quantile of mean predicted probabilities across all four models analysed. 'High' represents a value of mean predicted probability of crane presence greater than this cutoff point. Purple background colour is used for visual clarity, and does not represent a value on the colour scale.

2.4 Discussion

The analysis performed in this chapter contained 4 different models of varying complexity; with the simplest model being a spatio-temporal model with a single likelihood with an IID assumption between years. The following section will compare the relative benefits of the different models with regard to the ecological aim of predicting species distribution and representing relevant ecological processes in space and time.

Predictions of high probability of crane presence from the marked point process model (Figure 2.5 (b)) correspond to areas of high wetland density (Figure 2.4 (a)), provided these high density areas overlap with areas of high species intensity (Figure 2.4 (b)). Differences can be observed in the high probability of presence along the Norfolk Coast (East) predicted by the binomial presence-absence model (Figure 2.5 (a)), likely due to the presence of cranes to the South East of this area (Figure 2.1). However, this is not the case in the marked point process prediction, where it is taken into account that this area has a lower density of wetland habitat relative to the area where the existing population is observed. Additionally, the binomial presence-absence model predicts a high probability of presence at a single wetland in the North-West of England, likely due to the large extent of this wetland. Below this, several wetlands spanning the West and South-West of England are predicted to have mid-to-high probability of crane presence. This does not occur in the marked point process prediction, where spatial structure of the predictions is more constrained and dependent on wetland density.

The scaling parameter ζ represents the strength and direction of the interaction between the point field $G(s)$ and the probability of crane presence. In the marked point process model with an AR1 temporal structure, the positive effect of wetland density on probability of crane presence is of greater magnitude than that of the model with IID temporal structure (Table 2.2). This is due to the fact that the AR1 model borrows strength across years, meaning that the repeated presence of cranes in high-wetland-density areas over time indicates a stronger effect than that observed in the IID model, which considers each year of data independently.

The spatio-temporal field $M(s,t)$ in the AR1 models has a smaller posterior spatial range and larger standard deviation than that of the IID models (Table 2.2). This is due to the fact that

the AR1 models borrow strength across years, meaning that the spatial structure is influenced by the repeated occurrence of relatively isolated crane presences over time. Similarly, the standard deviation is high, as this allows sufficient variation in the field for the estimated species intensity to range from low to very high values. On the other hand, the IID models consider each year of data independently, and so are more strongly influenced by the priors, which suggest a larger spatial range and lower standard deviation, with the intensity of the species correlated across larger intervals and lowering smoothly away from areas of higher intensity. While the priors are biologically realistic, they may contrast with the trends observed in the data due to the early stage of reintroduction at which the data were collected.

In the models with AR1 temporal structure, the temporal correlation, ρ_t, is estimated to be extremely high (Table 2.2) and the spatial structure of $M(s,t)$ is predicted to be the same for each year of data (Figure 2.2). This indicates that the spatio-temporal field in these models is capturing a spatial structure in the data which is constant over time. This strong trend of a static spatial structure may be due to the early stage of reintroduction when observations were made. At this early stage, the population is small and so may not be subject to strong dispersal pressures such as habitat density dependence, meaning that movement between habitat patches may be less common than it would be in a densely populated area. The population is also only observed in a small proportion of its potential range, meaning that a large amount of the study area is taken up by consistent zero counts. Limited movement, large numbers of consistent absences, and the binary nature of presence-absence data all lead to few observed changes in the dataset between years. Therefore, the static spatial structure picked up by the model may not reflect the behaviour of the study species (for example, strong site fidelity), and instead could be a feature of the stage of the reintroduction process the population was in when the data were collected. A longer period of observation may be required to accurately capture and predict the dispersal dynamics of the species.

Since the AR1 models detect the strong trend of a static spatial structure over time, they estimate no change in the spatial representation of the spatio-temporal field $M(s,t)$ between years (Figure 2.2). This means that the spatio-temporal field must represent the most likely spatial correlation structure for all years, and so produces an average from the full dataset. This

averaging can produce misleading estimates of species distribution, particularly when the species is observed to 'appear' in a new area of the study region part-way through the study, as it can be predicted to have a high probability of presence in this area before the appearance event. For example, breeding pairs of cranes were first observed in Somerset (South West) in 2013 as the result of a successful reintroduction project. However, the spatio-temporal field from the AR1 models shows a high intensity of cranes in this area in the years prior to this event, when no breeding pairs of cranes had been observed in the area. In this example, the covariates included in the model are also stationary across the interval of observation. As such, predictions from the models with AR1 temporal structure are very similar across all years in the study period. This not only conceals fine scale inter-annual differences in spatial distribution, but also removes novel insight from future predictions. Such an effect may be avoided by including an extra, purely spatial, field in the mark likelihood and setting priors to manually restrict this to capturing the static spatial effect, separating this strong signal from the changes in spatial structure over time which could then be picked up by the spatio-temporal field. As mentioned above, the effect observed here is a result of the data structure, and so a larger dataset collected over a longer duration may provide sufficient information to avoid these issues.

The issues created by the strong, static spatial trend picked up by the spatio-temporal field in this example demonstrate that inclusion of certain types of complexity (here an effect accounting for temporal correlation) may not necessarily improve ecological insight gained from a model. The averaged predictions created by the most complex model considered here (the marked point process with AR1 temporal correlation structure) mean that it was not the most suitable model with regard to prediction of the species distribution within the observation period. It is likely that this effect was present in the R-INLA model of this data (Soriano-Redondo et al., 2019) but was interpreted as a strong temporal trend in direction of species spread, as opposed to a static effect, due to a lack of accessible plotting methods in R-INLA at the time of analysis. However, due to the accessible `predict()` function and connection with visualisation tool `ggplot2` in R-inlabru, the true nature of this effect was more easily identified. An even more complex model, containing another purely spatial field and strong priors, may improve output quality when aiming to predict future distribution of the population.

Here, a separable space-time process is used for the spatio-temporal field. However, although this type of spatio-temporal process has the most historical precedent in this style of modelling, it may not actually be the most appropriate method for representing the dynamics of interest (Lindgren et al., 2023). A non-separable model such as the diffusion-based extension of the Gaussian Matérn field (DEMF) presented by Lindgren et al. (2023) may be more appropriate here because it incorporates a diffusion process, so could capture the spread of the population. A topic of potential future research would be to investigate the outcomes of modelling population spread using space-time processes with different levels of separability.

Of the four models considered in this paper, the most complex (the marked point process model with AR1 temporal structure) had the longest running time, and the simplest (the binomial presence-absence model with IID temporal structure) had the shortest (Table 2.2). Whilst running time is an important methodological consideration, each of these models is made extremely computationally efficient through the use of the INLA approach, allowing model choice to be more strongly determined by ecological insight gained, as opposed to computational efficiency.

Watanabe–Akaike information criterion (WAIC) scores were computed for each of the four models (Table 2.2), although it is important to note that the binomial presence-absence and marked point process models cannot be compared using this criterion due to their differing likelihoods and data structures. However, within each model type, it is interesting to note that the AR1 models have a lower score than the IID models, indicating a better fit to the data. This is unsurprising when considering that the AR1 models are more strongly influenced by the data, as information is borrowed across years, whereas the IID models are more reliant on the priors. The true meaning of such criteria in the area of point process modelling is not well understood, due to the historically theoretical nature of the topic, and as demonstrated here, these criteria do not necessarily provide a definitive answer as to selecting the 'best' model for interpretation and ecological insight.

Species distribution data are often a combination of the true underlying distribution of the species, and the observation process used to collect data, creating a need to disentangle the true drivers of species distribution from sampling effects. In the early stages of a species invasion

or reintroduction, there is a time lag that means the observed distribution may not match the true potential distribution of the species once the population has been established (De Marco, Diniz-Filho, and Bini, 2008). Making observations at this initial stage could bias inference of the effects of environmental covariates, as the distribution of the species is restricted by dispersal limitations which remain unaccounted for. Including complex model components to represent spatial correlation structures, as is demonstrated here via the inclusion of $G(s)$ in the marked point process model, can account for the fact that the species distribution is limited by the early stage of its introduction to the environment, giving a more accurate prediction of the range being constrained close to where the species has been observed. Accounting for spatial correlation can also aid in avoiding Type I errors when inferring the significance of covariate effects (Dormann et al., 2007). However, caution is advised when incorporating additional structural complexity into models of this type of data, due to its zero-inflated and relatively static nature (observed here through the issues associated with inclusion of an AR1 temporal correlation structure). Accounting for the observation process, and spatially varying detection probability is a particular strength of the `R-inlabru` package, which can also be used to model subsampled and distance sampling data (Yuan et al., 2017; Jullum, Thorarinsdottir, and Bachl, 2020).

Complex model components such as spatial and spatio-temporal random fields can be used to represent population dynamics in species distribution models. In this example, density of wetland habitat patches has a positive effect on the probability of crane presence in the marked point process model, representing the habitat selection of this species. The impact of density of available habitat patches is accounted for through the use of the point random field $G(s)$ in this model. In addition, mobility restrictions (in terms of long-term dispersal) are accounted for through the mark random field $M(s,t)$ in both model types. This provides a way of estimating restrictions on availability, when little is already known about population dispersal. Through explicit understanding of the dynamics represented by each field, the benefits of increased complexity can be achieved whilst maintaining interpretability of results. However, when increasing model complexity, it is important to maintain an understanding of the effects and role of each model component, in order to determine whether it benefits the outcomes of the modelling aims.

2.5 Conclusions

This chapter explored the impacts of increasing model complexity in species distribution and habitat selection modelling. Variations on a joint likelihood spatio-temporal marked point process model were applied in the context of predicting population spread of a reintroduced population of Eurasian crane (*Grus grus*). Of the 4 fitted models, the data proved to be insufficient to support the most complex model structure (the marked point process model with an AR1 temporal structure), leading to inaccurate predictions. However, the simpler modelling framework (the binomial presence-absence models) failed to account for the density of available habitat, so provided a less realistic prediction of population spread. These results demonstrate a non-monotonic relationship between model complexity and performance (Mccrea et al., 2023). Complex model components can be used to reduce or remove sources of bias or spurious significance by accounting for dynamics which influence the process of interest. However, increased complexity can also lead to overfitting or reduced model interpretability. There is a necessity to approach complex ecological models with caution, identifying limitations in data and grounding the inclusion of complex statistical processes in ecological theory.

Chapter 3

Scale-Dependent Habitat Selection in a Domesticated Population: Gaussian Field Integrated Step Selection Analysis in `R-inlabru`

3.1 Introduction

Chapter 2 explored the use of a joint likelihood spatio-temporal point process model to estimate habitat selection at the population-level, using occupancy data. This chapter furthers the exploration joint likelihood spatio-temporal point process modelling, this time at the individual-level, fitting two types of LGCP model to fine-scale telemetry tracking data. A case study is presented with the aim of interpreting habitat selection of cattle on a Swiss Alpine farm, demonstrating a different application to habitat selection modelling than the conservation aims of Chapter 2.

3.1.1 Movement Modelling for Agriculture

As technological advancements have allowed for a reduction in the cost of tracking devices, telemetry tracking and movement modelling has become an accessible method of improving livestock management in the agricultural sector (Bailey et al., 2018). Previous studies in this area were usually conducted using data collected by human behavioural observation, which is difficult to do, time consuming, and has implications for observer influence on subject behaviour (Lomillos et al., 2017; Bailey et al., 2018). GPS tracking has enabled efficient automation of data collection and has allowed an increase in the spatial area and temporal duration of studies (Turner et al., 2000; Swain and Friend, 2013). This is particularly relevant for the management of free range or near free range grazing animals that are pastured in large or inaccessible areas, such as at high elevations, difficult topographies, or extensive rangelands (Lomillos et al., 2017; Bailey et al., 2018).

In the agricultural sector, GPS tracking and movement modelling are used to understand space-use and habitat selection, with aims of improving animal welfare, ecological impact, and economic sustainability of farming practices (Homburger et al., 2015). Particularly in cattle farming, livestock managers are often interested in improving the uniformity of pasture space use, to ensure that the full available area is utilised by the animals (Lomillos et al., 2017; Bailey et al., 2018). Spatial aggregation in movement behaviour can lead to heavy trampling, which impacts vegetation and soil structure, and has knock-on effects for wildlife (Handcock et al., 2009). Further to this, increasing uniformity of pasture space-use can also allow stocking rate

to be increased, so has implications for economic improvement (Turner et al., 2000; Bailey et al., 2018). An understanding of habitat selection in livestock can aid in informing management practices to encourage use of the full pasture, such as the placement of fencing, water, or mineral sources (Probo et al., 2013).

GPS tracking has also revolutionised livestock farming in terms of real-time data collection and transfer. Precision livestock farming utilises automated collection of location and biologging data to improve management in real time (Wathes et al., 2008). For example, Barwick et al. (2018) use GPS tracking data for the prediction of lameness in sheep; a health condition that would otherwise be difficult to detect and treat in an extensive farming system.

Movement modelling in the agricultural sector has additional applications which extend beyond the management of livestock. For example, tracking data can be analysed to assess the impact of livestock on the behaviour of wildlife, with applications in conservation, or in the reaction of domesticated animals to wild predators (Laporte et al., 2010; Bhattacharya et al., 2020). Therefore this kind of modelling has further reaching implications for disease transmission and human-wildlife conflict. Associated pasture systems for livestock also perform key ecosystem services, such as climate change mitigation and biodiversity conservation, so understanding their usage by livestock is essential to the protection of these services (Pauler et al., 2025).

3.1.2 Data Granularity in Movement Modelling

When developing a sampling strategy, the spatial scale at which data are collected is limited by a tradeoff between extent and grain; limitations in time or finances lead to a decision between sampling over a smaller extent, or collecting data at a coarser grain (Crosby and Porter, 2018). In the case of animal movement modelling, temporal scale is similarly restricted; the battery life of tracking devices dictates the duration of the study and the intervals between observations (Davis et al., 2011). Thus, the scale of analysis in ecological studies has historically been determined by feasibility of data collection for the researcher, with little consideration of the relevance of the scale to the organism or process being studied (Jackson and Fahrig, 2015; Chandler and Hepinstall-Cymerman, 2016; Mcgarigal et al., 2016).

Although temporal frequency at which tracking observations are collected is rarely driven by

ecological understanding of movement, but rather by the limitations of tracking devices, understanding of movement behaviour and mobility has been found to be influenced by the temporal frequency at which tracking observations are collected (Mills, Patterson, and Murray, 2006; Johnson and Ganskopp, 2008; Mccann et al., 2021). Similarly, the strength and direction of effects of environmental covariates have been found to vary with spatial grain (Compton, Rhymer, and Mccollough, 2002; Thompson and Mcgarigal, 2002; Mcgarigal et al., 2016; Timm et al., 2016). It is therefore of interest to investigate the impact of data granularity, in terms of both covariate spatial grain and temporal frequency of tracking data, on model fit and parameter inference in habitat selection modelling. How do estimated effects change with spatial scale and temporal frequency, and how do the two interact?

3.1.3 Case Study

This chapter explores questions of spatial, temporal, and organisational scale in relation to a case study, modelling the habitat selection of three breeds of cattle (*Bos taurus*) on a Swiss Alpine farm.

The three breeds of cattle included in this data vary in production purpose and therefore in productivity: Original Braunvieh is common for the region as a dual-purpose breed of intermediate size and productivity level; Angus-Holstein is a crossbreed consisting of a combination of a popular beef breed mixed with a popular milk breed, so therefore is of large size and high productivity level; finally, the traditional Highland Cattle breed is of smaller size and productivity level, chosen for its 'hardy' nature and adaptability to inclement conditions. The differences in size and productivity levels of the breeds has previously been found to be linked to variations in habitat selection and movement behaviour; with smaller, hardier breeds ranging more widely and grazing on varied qualities of available forage, whereas larger, high-productivity breeds are confined to areas containing high-quality forage and use less of the landscape available to them (Pauler et al., 2020a). This can cause issues such as resource depletion and trampling, if insufficient areas of high-quality forage are provided for high-productivity breeds. Part of the objective of discovering more about habitat selection and movement behaviour of cattle in this area is to inform management practices which can improve uniformity of within-pasture space-use, to

reduce environmental impact and improve animal welfare and economic stability.

Previously, evenness of space-use has been studied by aggregating observations of individual locations into a gridded count (Pauler et al., 2020a). This chapter provides a more detailed insight into habitat selection and spatial distribution in this system, by employing methods for modelling movement, at the resource-selection and step-selection levels, in continuous-space.

3.1.4 Aims

This chapter aims to demonstrate the use of point process based approaches for step- and resource-selection modelling to estimate livestock habitat preferences. It will:

1. fit 486 models using the GF-iSSA approach to jointly estimate habitat selection parameters across multiple individuals using individual-level tracking data;

2. implement a novel extension to the complex integration scheme used to account for availability in the GF-iSSA models;

3. compare the 486 GF-iSSA models to a further 486 models using a spatial point process resource-selection model to estimate habitat selection from the same tracking data, amalgamated to a different organisational scale; and

4. investigate the impact of data granularity (in terms of spatial scale of covariates and temporal frequency of tracking observations) on inference and relative model fit for all 972 models.

3.2 Methodology

3.2.1 Data Background

This chapter analyses data from an existing dataset on environmental conditions and the spatial distribution of cattle (*Bos taurus*) in heterogeneous pastures on a Swiss Alpine farm. Cattle were contained in 3 large pasture areas (Figure 3.1). Each area represented a different type and quality of forage: Area 1 consisted of a smaller area of fertile pasture; Area 2 was of intermediate size and forage quality; and Area 3 comprised a larger area of low forage quality (woodland). Each pasture

area was split into three separate paddocks, which were used to simultaneously pasture three herds of cattle of different breeds (Original Braunvieh, Angus-Holstein, and Highland Cattle). Cattle movement behaviour was observed using GPS telemetry tracking. See Pauler et al. (2020b) for a more detailed description of environmental conditions at the study site, and Pauler et al. (2020a) for a full account of the GPS and environmental data collection methods.

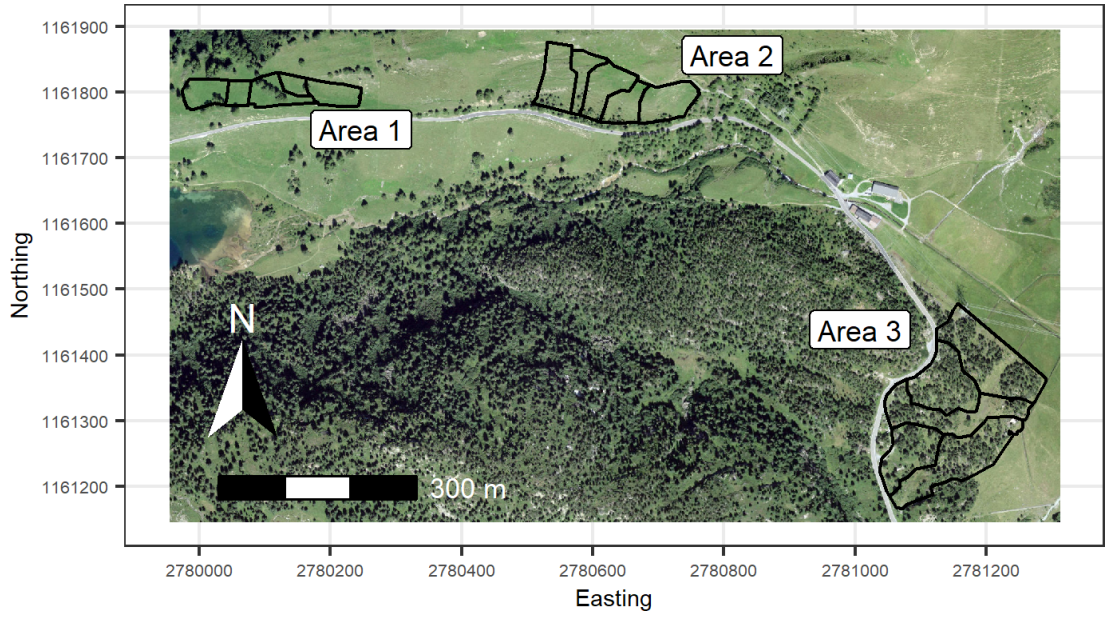

Figure 3.1: Layout of paddocks across three spatial areas of varying size and pasture quality on a Swiss Alpine farm.

Each herd of cattle contained three suckler cows and their calves (not monitored). The spatial locations of suckler cows were collected using a GPS telemetry tag attached to the bell collar of each individual. Failure of one GPS tag in the Angus-Holstein herd meant that data were only collected for two individuals from this herd. For the other two breeds, GPS location data were collected for all three individuals. Tracking data were collected at 15-/20-second intervals (with some missing observations) for a duration of 3-4 days for each of the 8 individuals (3 Highland Cattle, 3 Original Braunvieh, and 2 Angus-Holstein) in each paddock in each of the 3 pasture areas during the summer of 2018. The original data collection conducted by Pauler et al. (2020a) included a rotational system, grazing each herd in each paddock. However, in order to optimise computational efficiency and reduce mismatch in spatio-temporal resolution of covariates and tracking data, this chapter only uses the first 24 hours of tracking observations from the instances

where a herd was the first to graze a paddock. Hence, analysis is performed on a reduced dataset of 24 raw tracks with a duration of 24 hours.

Two spatial covariates were included in analysis: slope and forage quality. These were chosen based on the results of existing literature on this system having found them to be significant drivers of cattle spatial distribution (Bailey et al., 2018; Pauler et al., 2020a). Slope is a derivation of the 2m resolution topographical raster given by the swissALTI3D digital elevation model (Federal Office of Topography, Wabern). Slope was calculated using the Horn algorithm to give the steepness of elevation (Horn, 1981). Vegetation was mapped over the area, and from this forage quality was calculated using the indicator values of forage quality by Briemle, Nitsche, and Nitsche (2002). Indicator values of forage quality act as a proxy for palatability of vegetation to cattle (Pauler et al., 2020a).

3.2.2 Temporal Frequency

In order to directly understand the impact of temporal frequency on inference, analysis was performed on the same dataset, repeated with different regular temporal intervals between observations. This mimicked the real-world situation in which data are collected at different temporal intervals, but kept all other factors constant, so that the only difference between datasets was created by varying the temporal frequency. This required an initial regularisation of the raw data, using straight-line interpolation of the spatial coordinates for each track. This ensured that there were no missing observations and that observations were collected at regular intervals. The method employed for step selection analysis (GF-iSSA) is a discrete-time method of animal movement modelling. It utilises step-lengths, which are a measure of distance so require the temporal interval between observations to be regular to be comparable. Thus regularisation was a necessary step to prepare the data for modelling but did not create too many 'artificial' (i.e., interpolated) observations to be of concern.

Following regularisation, the data were then thinnned by removing interim observations to create 6 datasets with increasingly large temporal intervals: the regularised dataset with 20-second intervals between observations, and 1-minute, 5-minute, 15-minute, 30-minute, and 60-minute subsets. The temporal duration of the observation period was kept constant (24-hours)

so that the number of observations in the created subsets decreased with the increasing intervals, with the 60-minute subset being the smallest (24 observations). Figure 3.2 displays the spatial distributions for observations in the same track, with different temporal resolutions.

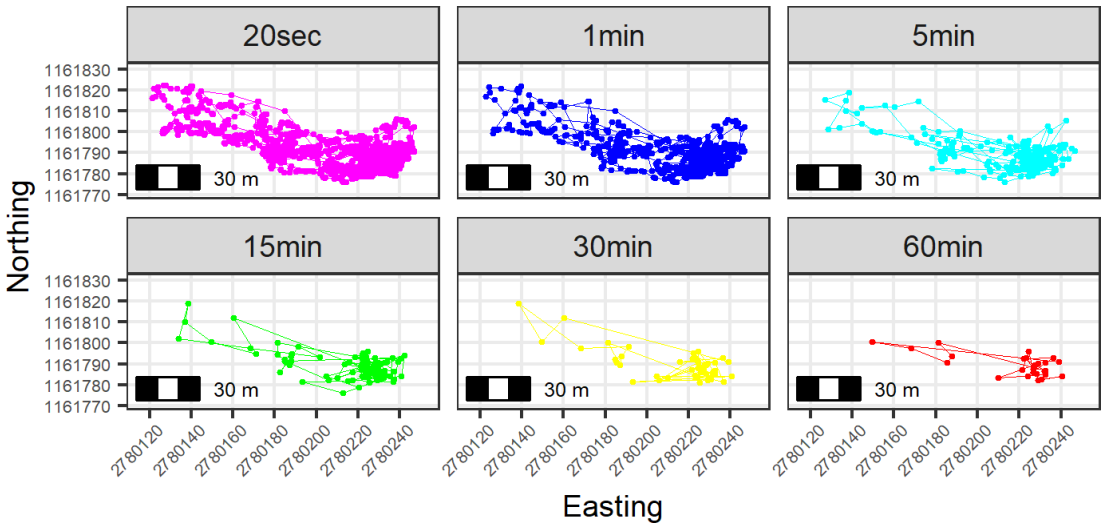

Figure 3.2: Telemetry tracking observations of one individual Angus-Holstein cross in Area 1 at six different temporal frequencies. Total sample sizes were: 20-second = 4320 observations, 1-minute = 1440 observations, 5-minute = 288 observations, 15-minute = 96 observations, 30-minute = 48 observations, 60-minute = 24 observations.

Regularisation and thinning was performed for all 24 telemetry tracks; for each of the 8 individuals in each of the 3 pasture areas. Therefore data-processing resulted in a total of 144 tracks; 6 versions of each of the 24 tracks, with observations collected at varying temporal intervals.

3.2.3 Spatial Scale

This chapter aims not only to investigate the impact of temporal frequency, but also that of spatial scale. To that end, environmental covariates were rendered at different spatial grains. The initial resolution of the slope covariate (the finest available scale for measures of elevation) was a regular $2m \times 2m$ grid. To create 2 larger scales for comparison, the values from this original raster were aggregated using the mean value to a $10m \times 10m$ grid and a $20m \times 20m$ grid. These spatial scales were determined to be suitable in reference to typical agricultural management practices (Schneider, personal communication, 2024). In order to limit the number of models compared in the analysis, both covariates were evaluated at the same scales. As such, the forage quality covariate was also rendered as a $2m^2$ resolution raster, and aggregated to $10m^2$ and $20m^2$

resolutions. Figure 3.3 shows both covariates at the three spatial resolutions.

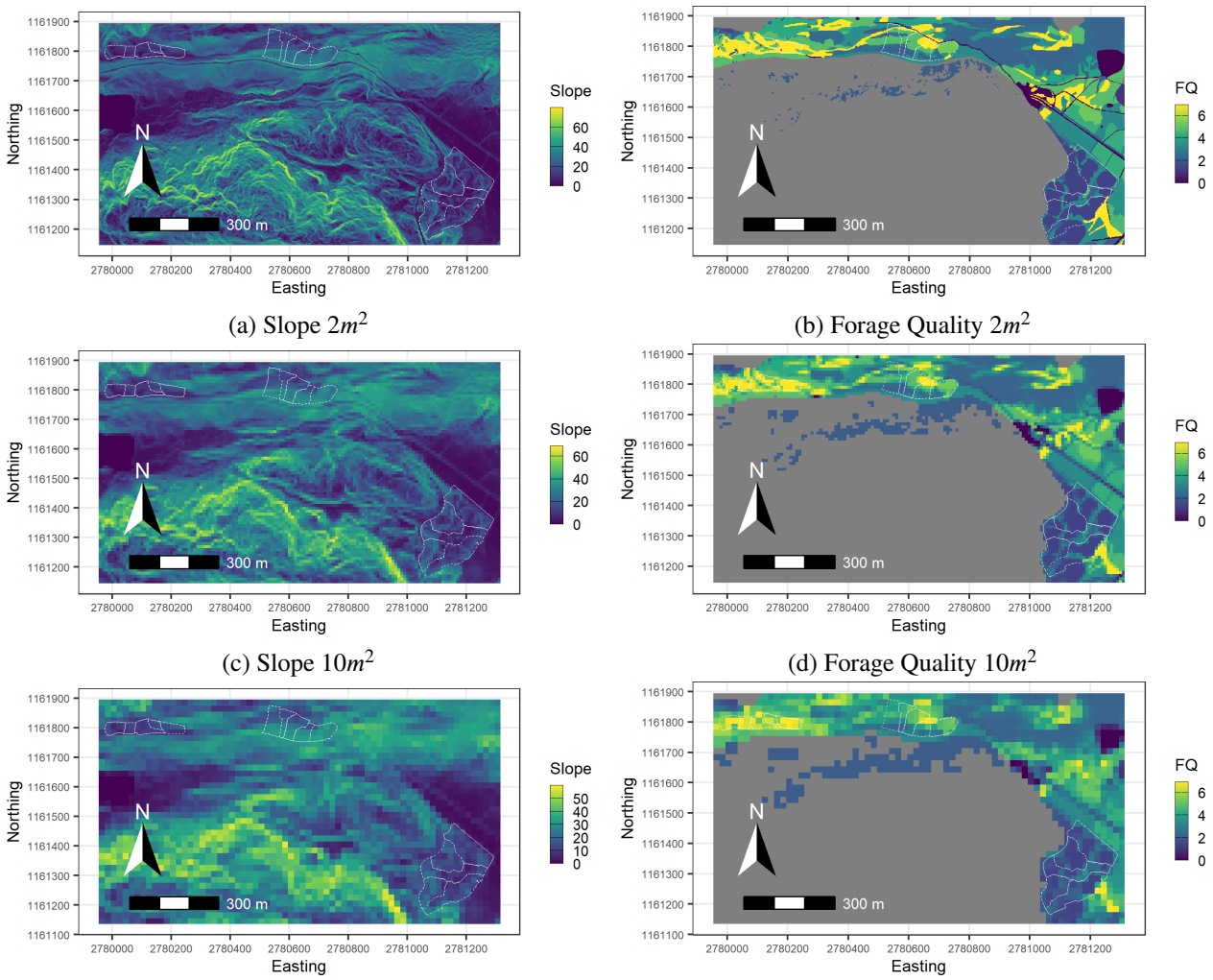

(a) Slope $2m^2$

(b) Forage Quality $2m^2$

(c) Slope $10m^2$

(d) Forage Quality $10m^2$

(e) Slope $20m^2$

(f) Forage Quality $20m^2$

Figure 3.3: Slope and Forage Quality covariates at resolutions of (a,b) $2m^2$, (c,d) $10m^2$, and (e,f) $20m^2$. Colour scale follows a gradient from low (blue) to high (yellow), indicating steepness of slope and quality of forage, respectively. Outline of paddock boundaries is given as a white, dashed line.

Both covariates were normalised using feature scaling (min-max standardisation) to ensure numerical stability in computation and keep results comparable between covariates. Feature scaling maintains an interpretable scale for the covariates as they vary from low to high positive values, whereas an alternative method such as Z-score would introduce negative values, which don't have a direct interpretation for the covariates. For example, the values for the slope covariate are levels of steepness and don't connote directionality, so a negative value would not be interpretable here.

3.2.4 Modelling Strategy

Given the variations in the temporal frequency of data and spatial scale of environmental covariates, multiple models were fitted and compared. In order to limit the overall number of models, 3 component combinations were compared: models containing only the slope covariate, only the forage quality covariate, or both covariates *at the same scale*. Telemetry tracks were grouped by herd, so that tracks from individuals occupying the same paddock at the same time were combined into a single model. These variations in data and model component combinations were analysed in two modelling frameworks: a resource selection analysis (RSA) approach, and a step selection analysis (SSA) approach. This resulted in a modelling strategy containing 972 models overall. A breakdown of these models is shown in Table 3.1.

Table 3.1: A breakdown of the 972 models fitted to Swiss cattle movement data. A different model was fitted for each combination of model feature options.

Model Feature	Feature Options
Method	RSA
	SSA
Spatial Area	Area 1
	Area 2
	Area 3
Herd	Angus-Holstein
	Highland Cattle
	Original Braunvieh
Temporal Frequency	20-second
	1-minute
	5-minute
	15-minute
	30-minute
	60-minute
Covariate Combination	Slope only
	Forage Quality only
	Slope + Forage Quality
Spatial Scale	$2m^2$
	$10m^2$
	$20m^2$

3.2.5 SSA Modelling Framework

Of the 972 herd-level models fitted to the tracking data, 486 were of the structure introduced by Arce Guillen et al. (2023), termed Gaussian field integrated step selection analysis (GF-iSSA). This method is implemented using the R package R-inlabru, and allows approximate Bayesian inference of habitat selection and movement parameters from telemetry tracking data. It is an extension of the method Integrated Step Selection Analysis (iSSA, Avgar et al., 2016), in which habitat selection and movement parameters are estimated jointly. The method is named GF-iSSA because it extends iSSA by incorporating a Gaussian Field into the resource selection function, to account for unexplained correlation structures in the data. However, due to limitations in computational efficiency, only the R-inlabru implementation of GF-iSSA is utilised here, and a Gaussian Field is not incorporated in the models. GF-iSSA differs from predecessing step selection models in the formulation of the joint likelihood as an unconditional inhomogeneous Poisson process (IPP), and in its representation of availability. For this reason, the method is still referred to as GF-iSSA throughout this chapter, despite the lack of Gaussian Field in the models, to differentiate the approach from iSSA (Avgar et al., 2016). Analagous to the 'pseudo-absence' points commonly used in step selection analysis, GF-iSSA uses a complex integration scheme to represent the area available to an individual at any one time point. The unique integration scheme utilised in the GF-iSSA approach is discussed further in Section 3.2.7. The summary given below provides an introduction to the method, as described by Arce Guillen et al. (2023).

Gaussian Field Integrated Step Selection Analysis (GF-iSSA)

Gaussian field integrated step selection snalysis (GF-iSSA) is based on the classical step selection model as defined by Forester, Im, and Rathouz (2009). Let s_t denote the spatial location of an individual at time t. Then, the spatial density of observing an individual at location s_t (given the two previous observations s_{t-1}, s_{t-2}), can be modelled as

$$f\left(s_t \mid s_{t-1}, s_{t-2}; \beta, \theta\right) = \frac{\phi\left(s_{t-2}, s_{t-1}, s_t; \theta\right) \omega\left(\mathbf{X}(s_t); \beta\right)}{\int_{q_t \in S} \phi\left(s_{t-2}, s_{t-1}, q_t; \theta\right) \omega\left(\mathbf{X}(q_t); \beta\right) dq_t}, \tag{3.1}$$

where $\mathbf{X}$ represents a set of spatial covariates describing the landscape in S, the spatial domain.

In Equation 3.1, $\phi\left(s_{t-2}, s_{t-1}, s_t; \theta\right)$ is a selection-free movement kernel (Fieberg et al., 2021); $\omega\left(\mathbf{X}(s_t); \beta\right)$ is a selection function of environmental variables; and the denominator represents a normalising constant (Forester, Im, and Rathouz, 2009; Hooten et al., 2017).

The method is termed GF-iSSA because its formulation allows for the inclusion of a Gaussian random field in the selection function, accounting for spatial correlation structures which are not explained by the fixed effects. As such, the selection function can be modelled as

$$\omega\left(\mathbf{X}(s_t); \beta\right) = \exp\left(\beta_1 X_1(s_t) + ... + \beta_p X_p(s_t) + u(s_t)\right) = \exp\left(\eta(s_t) + u(s_t)\right), \tag{3.2}$$

where $X_i, i = 1, ..., n$, are spatially structured covariates; $\eta(\cdot)$ represents the fixed effects; and $u(\cdot)$ is a Gaussian random field. Although this represents one of the benefits of this approach, it is possible to fit the model using only fixed effects, and not include the random field, as is done in this chapter.

As is common in discrete-time movement modelling, the movement kernel is parametrised by step length ϕ_{SL} and turning angle ϕ_{TA}. Although it is also possible to use other distributions, this chapter uses the Gamma distribution (with shape and rate parameters, β_{p+1} and β_{p+2}, respectively) for step length and the zero-mean von Mises distribution (with concentration parameter, β_{p+3}) for turning angle, as presented by Arce Guillen et al. (2023). Due to the special form of densities belonging to the exponential family, using the current and two previous locations, the movement kernel can be expressed as

$$\begin{aligned}
\phi\left(s_{t-2}, s_{t-1}, s_t; \theta\right) =& \phi_{SL}\left(s_{t-1}, s_t; \theta_{SL}\right) \phi_{TA}\left(s_{t-2}, s_{t-1}, s_t; \theta_{TA}\right) \\
&\propto \exp\Bigg(\beta_{p+1} \log\left(||s_t - s_{t-1}||\right) + \beta_{p+2}||s_t - s_{t-1}|| \\
&\qquad + \beta_{p+3} \cos\left(\psi_{s_{t-2}, s_{t-1}, s_t}\right)\Bigg) \\
&= \exp\left(\zeta\left(s_{t-2}, s_{t-1}, s_t\right)\right),
\end{aligned} \tag{3.3}$$

where ψ represents the turning angle, and ζ represents the joint probability model of the movement kernel. A detailed derivation of Equation 3.3 can be found in the supplementary material of Arce Guillen et al. (2023). Two factors are included in the step length definition, as a result of the transformation from polar to Euclidean coordinates.

The likelihood is then expressed as a combination of the selection function (Equation 3.2) and the movement kernel (Equation 3.3)

$$\begin{aligned} L\left(\beta, \theta \mid s_{t-2}, s_{t-1}, s_t\right) =& \frac{\exp\left(\eta(s_t) + u(s_t) + \zeta(s_{t-2}, s_{t-1}, s_t)\right)}{\int_S \exp\left(\eta(q_t) + u(q_t) + \zeta(s_{t-2}, s_{t-1}, q_t)\right) dq_t} \\ :=& \frac{\Lambda\left(s_t \mid s_{t-2}, s_{t-1}, \mathbf{X}(s_t)\right)}{\int_S \Lambda\left(q_t \mid s_{t-2}, s_{t-1}, \mathbf{X}(q_t)\right) dq_t}, \end{aligned} \tag{3.4}$$

where $u(s_t)$ represent spatial random effects, and S represents the spatial domain over which the integration scheme is defined. This is the likelihood function of a conditional inhomogeneous Poisson process (IPP), where the likelihood function is conditional on the observations at times t, $t-1$, and $t-2$. However, using equivalences demonstrated by Aarts, Fieberg, and Matthiopoulos (2012) and Muff, Signer, and Fieberg (2019), the joint log-likelihood of the model for each time point can be written as an unconditional IPP

$$\begin{aligned} \sum_{t=3}^{T} I\left(\beta, \theta \mid s_{t-2}, s_{t-1}, s_t\right) = \sum_{t=3}^{T} \Bigg(& \log\left(\Lambda\left(s_t \mid s_{t-2}, s_{t-1}, \mathbf{X}(s_t)\right) \exp(\beta_{0t})\right) \\ & - \int_S \Lambda\left(q_t \mid s_{t-2}, s_{t-1}, \mathbf{X}(q_t)\right) \exp(\beta_{0t}) dq_t \Bigg), \end{aligned} \tag{3.5}$$

for a total of $T-2$ time points, where $\beta_{0t}, t = 3, ..., T$ are time dependent intercepts. Transforming from a conditional to an unconditional IPP provides practical advantages in computation, but the slope parameters estimated by both are equivalent (Aarts, Fieberg, and Matthiopoulos, 2012; Muff, Signer, and Fieberg, 2019). When incorporating the tracks of multiple individuals into a single model, as in this chapter, a joint model with one likelihood per individual is used, and these intercepts become time *and* individual dependent (see Equation 3.8). In model fitting, the intercepts are defined as random intercepts with large fixed variance.

Model fitting is performed in `R-inlabru` using the INLA and SPDE methods. The model is fitted as an LGCP, and integration is performed at the mesh nodes which fall within the domain of availability for each observation (see Section 3.2.7). Therefore, Equation 3.5 is approximated by

$$\begin{aligned}\sum_{t=3}^{T} I\left(\beta, \theta \mid s_{t-2}, s_{t-1}, s_t\right) \approx & \sum_{t=3}^{T}\left(\log\left(\Lambda\left(s_t \mid s_{t-2}, s_{t-1}, \mathbf{X}(s_t)\right)\exp(\beta_{0t})\right)\right) \\ & - \sum_{t=3}^{T}\sum_{j=1}^{n_t} w_{t,j}\Lambda\left(q_{t,j} \mid s_{t-2}, s_{t-1}, \mathbf{X}(q_{t,j})\right)\exp(\beta_{0t}),\end{aligned} \tag{3.6}$$

for integration points $q_{t,j}$ and weights $w_{t,j}$, where n_t represents the total number of integration points at each time t. As a set of integration points is defined for each time point, it would be computationally costly to define the spatial domain S over the full area of interest. For this reason, and to act analogously to pseudo-absences in classical step selection (accounting for availability), the integration scheme is restricted to a circular domain around each observation for each time point. The radius of this domain of availability is defined by the user, and should be related to animal mobility.

SSA Models

In the presented formulation of the GF-iSSA model, the parameters estimated to describe the distributions which make up the movement kernel (the concentration parameter of the von Mises distribution and the shape and rate parameters of the Gamma distribution) are allowed to be estimated outside of their theoretical domain (i.e., with values below 0), and therefore if a user wishes to interpret the resulting distributions, restrictions need to be placed on the model to make these parameters positive-definite. This, however, adds a computational cost, which is a particular concern in this chapter, wherein a large number of models are compared. Whether or not restrictions are placed on the movement parameters does not affect the estimated coefficients in the selection function. So, in the interest of computational efficiency, these movement parameters were left unrestricted and their associated distributions are not interpreted or used to describe trends in the movement patterns of the animals.

The GF-iSSA model naturally accounts for the highly spatio-temporally correlated nature of telemetry tracking data through the model structure itself; the movement kernel has a Markovian structure wherein the current location is dependent on the two previous observations. However, this does not account for other sources of spatial autocorrelation such as missing covariates, unless a Gaussian random field is included as a component in the linear predictor. However, the

inclusion of random effects increases computational costs and can cloud model interpretability. Additionally, subject to prior specifications, including a GRF brings the risk of spatial confounding, reducing the estimated significance of fixed effects (Hodges and Reich, 2010). The aim of this chapter is to compare the estimates of fixed effects across a large number of models. A Gaussian random field is not included, to ensure a clear interpretation of fixed effects and to keep model running times to a minimum. As such, the selection function introduced in Equation 3.2 is redefined as

$$\omega\left(\mathbf{X}(s_t);\beta\right) = \exp\left(\beta_{slope}X_{slope}(s_t) + \beta_{FQ}X_{FQ}(s_t)\right) = \exp\left(\eta(s_t)\right), \tag{3.7}$$

for the models containing both covariates, where X_{slope} represents the slope covariate and X_{FQ} represents the forage quality covariate (see Table 3.1 for model variations). The two covariates theorised to have the most important influence on movement behaviour are included as fixed effects, with the assumption that any impacts from missing covariates - as would be accounted for by a Gaussian random field - are negligible.

As mentioned in the modelling strategy (Section 3.2.4), models were fitted to data from two or three individuals, to elicit shared habitat selection from the overall herd. In the GF-iSSA model structure, a different likelihood is required for each individual. So, the movement of each individual within a herd is modelled jointly, with parameter estimation shared across likelihoods. This assumes independence given the shared components, so makes the simplifying assumption that any social movement behaviour will be captured by the shared response to environmental stimuli. Individual differences are accounted for by temporally-and-individually-indexed-intercepts. Thus the joint log-likelihood described in Equation 3.5 becomes

$$\begin{aligned}\sum_{n=1}^{N}\sum_{t=3}^{T} I\left(\beta,\theta \mid s_{n,t-2}, s_{n,t-1}, s_{n,t}\right) = \sum_{n=1}^{N}\sum_{t=3}^{T}\Bigg(&\log\left(\Lambda\left(s_{n,t} \mid s_{n,t-2}, s_{n,t-1}, \mathbf{X}(s_{n,t})\right)\exp(\beta_{0nt})\right) \\ &- \int_S \Lambda\left(q_{n,t} \mid s_{n,t-2}, s_{n,t-1}, \mathbf{X}(q_{n,t})\right)\exp(\beta_{0nt})dq_{n,t}\Bigg),\end{aligned} \tag{3.8}$$

where $n = 1, ..., N$ denotes individual, and β_{0nt} are temporally-and-individually-indexed-intercepts,

and habitat selection coefficients β are jointly estimated. Total number of individuals N varied between herds, with 3 individuals in the Original Braunvieh and Highland Cattle herds and 2 individuals in the Angus-Holstein herd. Note that each individual has its own associated set of integration points, as these are defined using the observed locations. This is covered further in Section 3.2.7.

GF-iSSA is a new method and, at the time of writing, has not been used for analysis in any publication other than that in which it was introduced. Arce Guillen et al. (2023) present a case study analysing the movement of wild animals at a coarser scale and longer duration than is investigated here. This chapter presents an alternate application for the approach, in analysing fine-scale movement behaviour of domesticated animals in the agricultural sector. As such, the representation of availability in the model was altered to include physical barriers to movement. Further information on this is provided in Section 3.2.7.

3.2.6 RSA Modelling Framework

The 486 SSA models provide an insight into habitat selection at the 'step level' - movement decisions are assumed to be made at each temporal step, relative to an area surrounding the location of the observation. For comparison, the remaining 486 models are fitted to the grouped observations of the overall tracks for each herd as a spatial point pattern. In this model formulation, habitat selection is inferred from the spatial distribution of the overall pattern created by all observations from a herd, with the full paddock area assumed to be available. In this setup, the data are modelled as a spatial inhomogeneous Poisson process (IPP) in `R-inlabru` (see Equation 1.25 in Section 1.6.1). This simpler model setup (here termed the RSA models) gives a zoomed-out perspective of the overall herd distribution and provides a baseline comparison for the more complex SSA models.

In the RSA models, point pattern intensity is defined by a spatially-varying intensity function, which is an additive combination of spatially-structured covariates. It is possible - among other options - to include a Gaussian random field in the linear predictor, but this is not included for simplicity and to keep the models comparable to the SSA models. Not accounting for the highly spatio-temporally correlated nature of the tracking data would be a violation of the assumption

of independence in the IPP. A commonly used solution in RSA is to thin data to reduce the level of correlation between observations (Hooten et al., 2014). The models fitted to data at a coarser temporal frequency can be seen to use this solution. Similarly, a random effect to account for inter-individual variation is not included in the RSA models, to keep the models simple and running times short.

The point pattern of observations is modelled as independent conditional on the point process intensity $\Lambda(s)$

$$\Lambda(s) = \exp\left(\alpha + \beta_{slope} X_{slope}(s) + \beta_{FQ} X_{FQ}(s)\right), \tag{3.9}$$

for the models containing both covariates, where α represents an intercept term, X_{slope} represents the slope covariate and X_{FQ} represents the forage quality covariate (see Table 3.1 for model variations).

Each dataset is modelled using the SSA and RSA modelling approaches. Although the models are fitted to the same data, and include the same covariates, the approaches differ in selection level; SSA is performed at the individual-level, whereas RSA is performed at the population-level. Here, SSA is spatio-temporal, whereas RSA is purely spatial. Each approach also utilises a different definition of the spatial domain over which integration is performed, which has implications for ecological interpretation of how availability is represented.

3.2.7 Integration Schemes

One of the unique features of the GF-iSSA approach is the complex integration scheme used to account for availability and improve computational efficiency. The integration scheme plays an important role in both determining the running time of a model, and in how the model interprets interactions between observations and spatial covariates.

The first step in defining the integration schemes of all 972 models was to create a Delaunay mesh triangulation. The same mesh was used for all models within a spatial area, so three meshes were created in total (one for each of Area 1, 2, and 3). To maintain accurate interpretation of fixed effects, the resolution of the mesh should be at least fine enough to capture the spatial variability in covariate values (Lindgren, Rue, and Lindström, 2011). To ensure that this was

the case, the mesh resolution was matched to the smallest covariate grain: $2m \times 2m$. For the RSA models, the integration points were defined at the mesh nodes which fell within the overall paddock boundary for each herd (Figure 3.4).

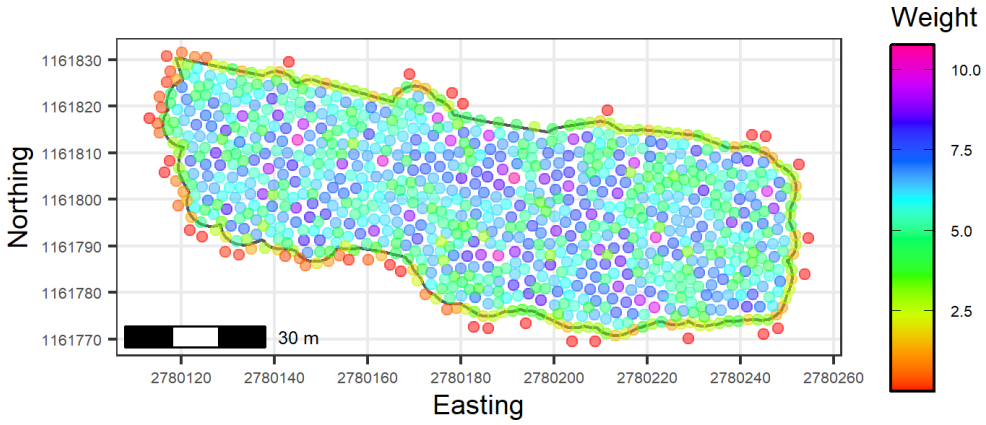

Figure 3.4: Integration scheme used in the RSA model for the Angus-Holstein herd in Area 1. Integration points are located at the mesh nodes which cover the full spatial domain available to the herd (paddock area, indicated by grey background polygon). Colour scale gives an indication of weight.

In GF-iSSA, each individual has an associated set of integration points, defined as falling within a set window around each observation in the track. To generate integration schemes for the SSA models requires a definition of this 'domain of availability': the radius of which is related to animal mobility. This was done empirically by obtaining the average maximum step length across all individuals for each temporal frequency. This resulted in a maximum step-length of 30m, 50m, 80m, 90m, 90m, and 90m for the 20-second, 1-minute, 5-minute, 15-minute, 30-minute, and 60-minute frequencies, respectively. As temporal interval increased, maximum observed step-length flattened out, meaning that the three coarsest datasets (15-minute, 30-minute, and 60-minute) were all defined to have the same radius of domain of availability. To keep models comparable the same radius was defined across all breeds. Figure 3.5 shows the domains of availability for one individual at the different temporal frequencies.

In this application, individuals are contained within a paddock and so have a physical barrier to movement as well as physiological mobility restrictions. Therefore, the domains of availability surrounding each observation were cropped to the perimeter of the paddock in which each herd was contained (see Figure 3.6 for the cropped domains of availability). This ensured that the

domain of availability gave a true representation of the area (and thus environmental conditions) available to the individual at each movement step.

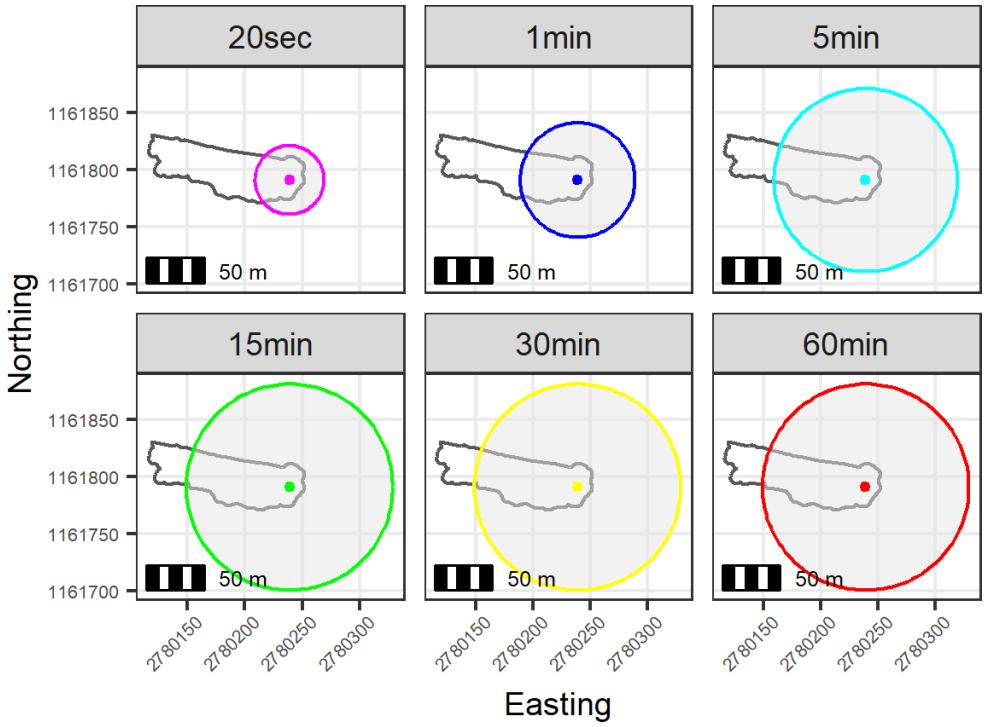

Figure 3.5: Domains of availability for the first time point at 6 different temporal frequencies for an individual Angus-Holstein cross in Area 1. Paddock area is indicated by grey background polygon. Discrete colour scale indicates temporal frequency.

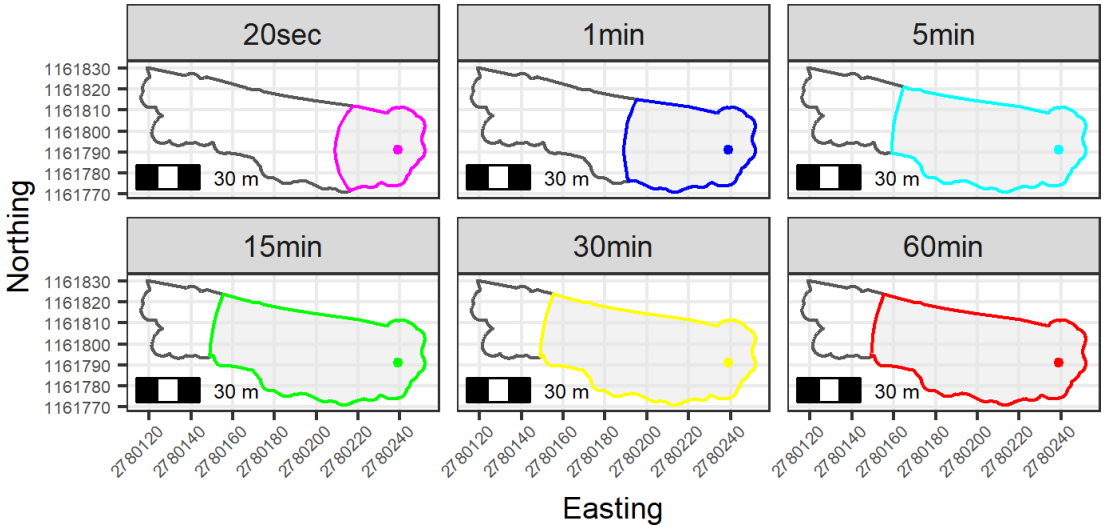

Figure 3.6: Cropped domains of availability for the first time point at 6 different temporal frequencies for an individual Angus-Holstein cross in Area 1. Paddock area is indicated by grey background polygon. Discrete colour scale indicates temporal frequency.

Finally, the integration scheme was created by distributing a set of integration points for each observation at the mesh nodes which fell within that observation's corresponding domain of availability. This was repeated for each of the 144 tracks. See Figure 3.7 for the integration points at a single time point for one individual.

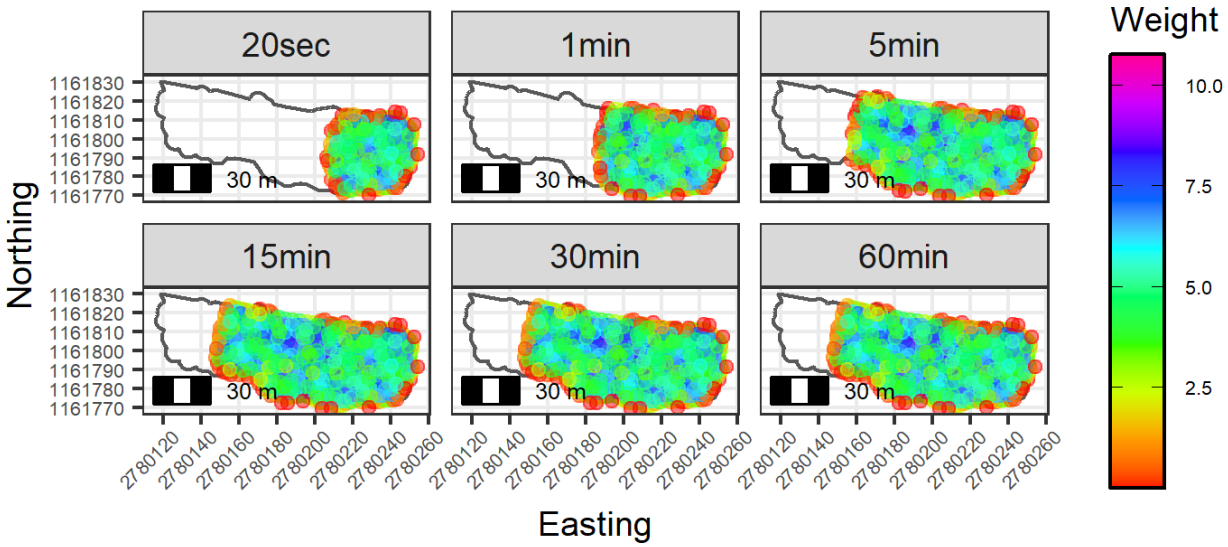

Figure 3.7: Integration points at the first time point at 6 different temporal frequencies for one individual Angus-Holstein cross in Area 1. Paddock area is indicated by grey background polygon. Colour scale gives an indication of weight.

Weights for both the SSA and RSA integration schemes were calculated using the integrals of the piecewise linear basis functions, as described in Section 1.6.1 (Lindgren, Rue, and Lindström, 2011). For the SSA integration schemes, the vertices of any triangles which did not intersect the corresponding domain of availability for that observation were given zero weights, thus integration points were only defined within the domains of availability (Arce Guillen et al., 2023).

For LGCP models fitted using `R-inlabru` (which includes both the RSA model structure and the SSA model structure), the number of integration points in the integration scheme plays an important role in determining model running time. For the more simplified RSA model, the number of integration points increases with a finer mesh, larger spatial area, or both. However, for the SSA model, each individual has a set of integration points defined around each observation, so the total number of integration points can be increased by: number of individuals; duration of study; temporal frequency of observations; radius of the domain of availability; mesh grain;

and spatial area. Therefore, with so many features of the data contributing to the number of integration points, and number of integration points contributing largely to computational cost, models can quickly become infeasibly costly. This is of particular concern in this chapter wherein a large number of models are fitted and compared, but may be less consequential in other studies where fewer models are required.

To give an idea of the difference in computational cost between the RSA and SSA methodologies, Table 3.2 contains the number of integration points, observations, and running times for a selection of the models. The number of integration points in the SSA models varies with the number of observations, and so model running time varies with temporal frequency. The SSA models are more computationally costly to run than the simpler RSA models, which contain fewer integration points. For example, the 20-second frequency SSA model has a running time of around 1.21 hours, whereas the RSA model fitted to the same data takes 1.72 seconds to run.

Table 3.2: An example of the number of integration points, observations, and running times (in seconds, rounded to 2 decimal places) for the slope-only ($2m^2$) models fitted to data from the Original Braunvieh herd in Area 3.

Model	Frequency	Integration Points	Observations	Running Time (seconds)
SSA	20-second	6 163 340	12 962	4 343.67
	1-minute	4 660 972	4 322	1 499.38
	5-minute	1 997 563	866	640.85
	15-minute	702 291	290	262.28
	30-minute	349 010	146	129.82
	60-minute	165 627	74	61.97
RSA	20-second	4 175	12 962	1.72
	1-minute	4 175	4 322	1.52
	5-minute	4 175	866	1.45
	15-minute	4 175	290	1.34
	30-minute	4 175	146	1.27
	60-minute	4 175	74	1.31

All analysis was carried out using R version 4.4.1 (R Core Team, 2025), R-INLA version 24.6.27 (Rue, Martino, and Chopin, 2009), and R-inlabru version 2.11.1 (Bachl et al., 2019) with a 2.4-3.2GHz 10C processor (384GB RAM).

3.3 Results

As analysis included a large number of models, some outputs have been omitted to provide clarity of results. Similar patterns were found across the three cattle herds, with effects being most pronounced for the Original Braunvieh herd. As inter-breed differences have been explored in previous literature (e.g., Pauler et al., 2020a), the results for only one herd are shown here. Figures 3.8-3.11 show the outputs of the 324 models fitted to location data from the Original Braunvieh herd. Outputs of the remaining 648 models can be found in Appendix B.

3.3.1 Estimation of Habitat Selection Parameters

The covariate coefficients estimated in these models can be interpreted in relation to relative use, with positive values indicating a preference for higher values of a habitat variable, and negative values indicating avoidance. For more information on interpreting parameters in habitat-selection analyses, see (Fieberg et al., 2021).

Most of the RSA models produced a posterior estimate of a negative effect with a 95% credible interval below 0 for the slope covariate on spatial distribution (Figure 3.8). Although this was not a completely uniform result, with some models producing a positive estimated effect with 95% credible intervals largely or entirely above 0. Estimated effect size and direction was broadly similar across pasture areas (i.e., Areas 1,2, and 3), particularly for models with covariates at a fine spatial grain (e.g., $2m^2$). However, decreased spatial resolution in covariates altered estimated effect size, particularly for Area 1 models, wherein the direction of the effect changed from a negative to a positive estimate with decreasing spatial grain. Inclusion of the forage quality covariate, compared to slope-only models, seemed largely to affect estimated uncertainty, with little impact on mean estimates. Estimates were largely unaffected by temporal frequency of observations, with mean values remaining largely stable across groups of models which differed only by frequency. Models fitted to data with fewer observations (i.e., coarser frequencies) produced estimates with wider credible intervals compared to those with more observations (i.e., finer frequencies).

Similarly to the RSA models, the posterior estimate for the slope effect produced by most

of the SSA models was negative with a 95% credible interval below 0 (Figure 3.9). In contrast to the RSA models (see Figure 3.8), slight differences in estimated effect size between pasture areas was most stark in the fine-grain ($2m^2$) models. Although, as was the case in the RSA models, estimated effects were broadly similar across areas. Decreasing spatial resolution did not alter the direction of the estimated effect, although for the smallest area (A1) some of the $20m^2$ multivariable models produced a 95% credible interval concentrated around 0. Increasing temporal frequency generally resulted in a smaller estimated effect size, although this trend was less pronounced in the models which included the forage quality covariate, compared to the slope-only models.

Forage quality was estimated to have a positive effect with a 95% credible interval above 0 by most of the RSA models (Figure 3.10). As with the estimated effect of slope (see Figure 3.8), the size and direction of the estimated effect of forage quality was largely similar across pasture areas, especially for fine-grain models. Spatial scale impacted estimated effect size and direction; particularly for forage-quality-only Area 1 models, and for the multivariable models of all pasture areas, wherein forage quality was estimated to have a negative effect. Again, temporal frequency had minimal influence on the estimated mean, but impacted associated uncertainty, with coarser frequencies resulting in larger credible intervals.

All SSA models estimated a negative effect for forage quality with a 95% credible interval below 0 (Figure 3.11). Area 3, the pasture area with the poorest overall forage quality, produced posterior estimates with the strongest negative effect of the three pasture areas. Increasing temporal frequency reduced estimated effect size, with finer frequency models producing a posterior effect closer to zero than coarse frequency models. This can be seen best in the univariable Area 3 models, where difference in estimated forage quality effect between temporal frequencies is most pronounced. Inclusion of the slope covariate appeared to reduce the impact of temporal frequency on effect size, particularly in the Area 3 models.

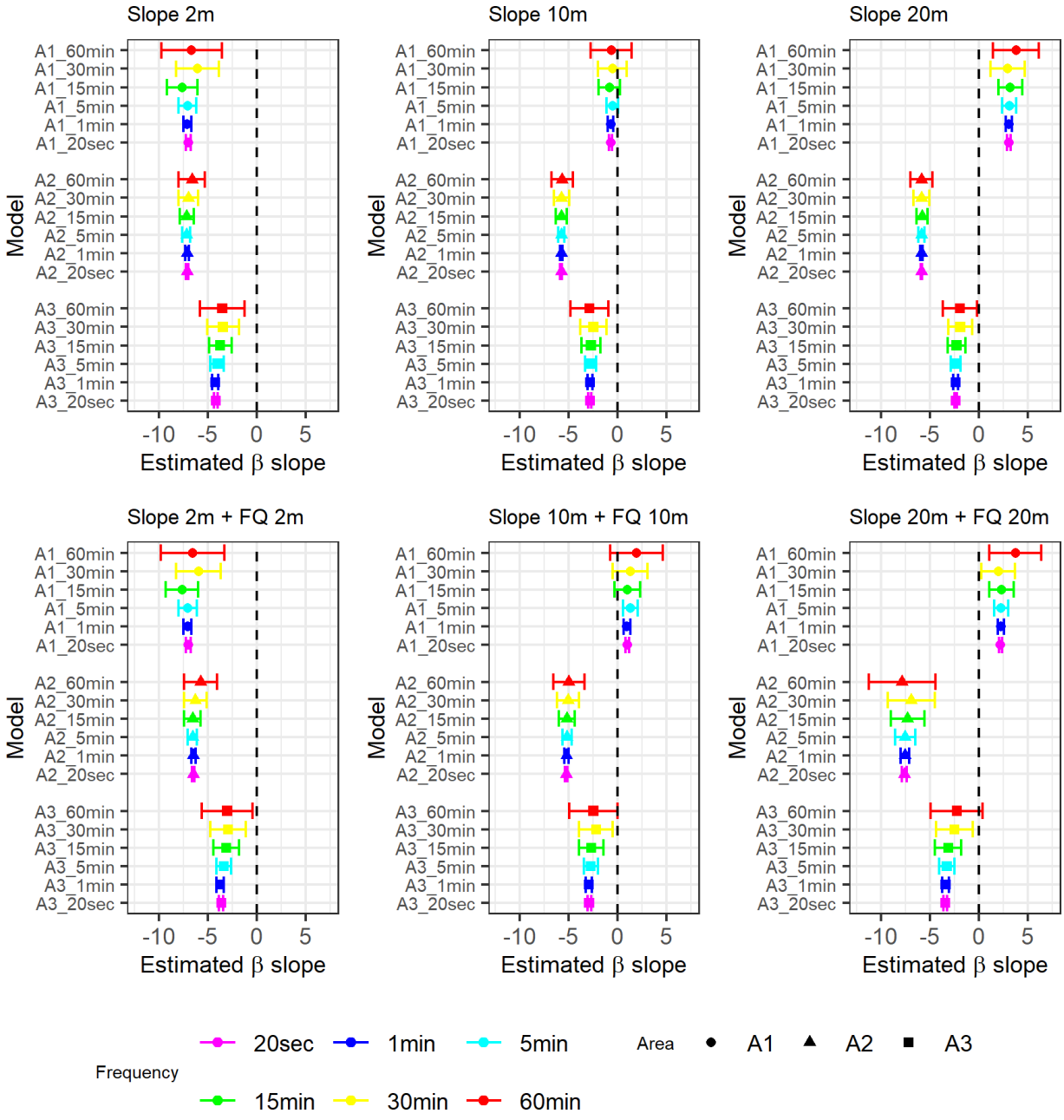

Figure 3.8: Posterior estimates for the slope covariate effect from the RSA models of the Original Braunvieh herd. Each plot represents a different spatial scale and covariate combination. Within a plot, each line on the y-axis represents a different model. Spatial area and temporal frequency are denoted by shape and colour, respectively.

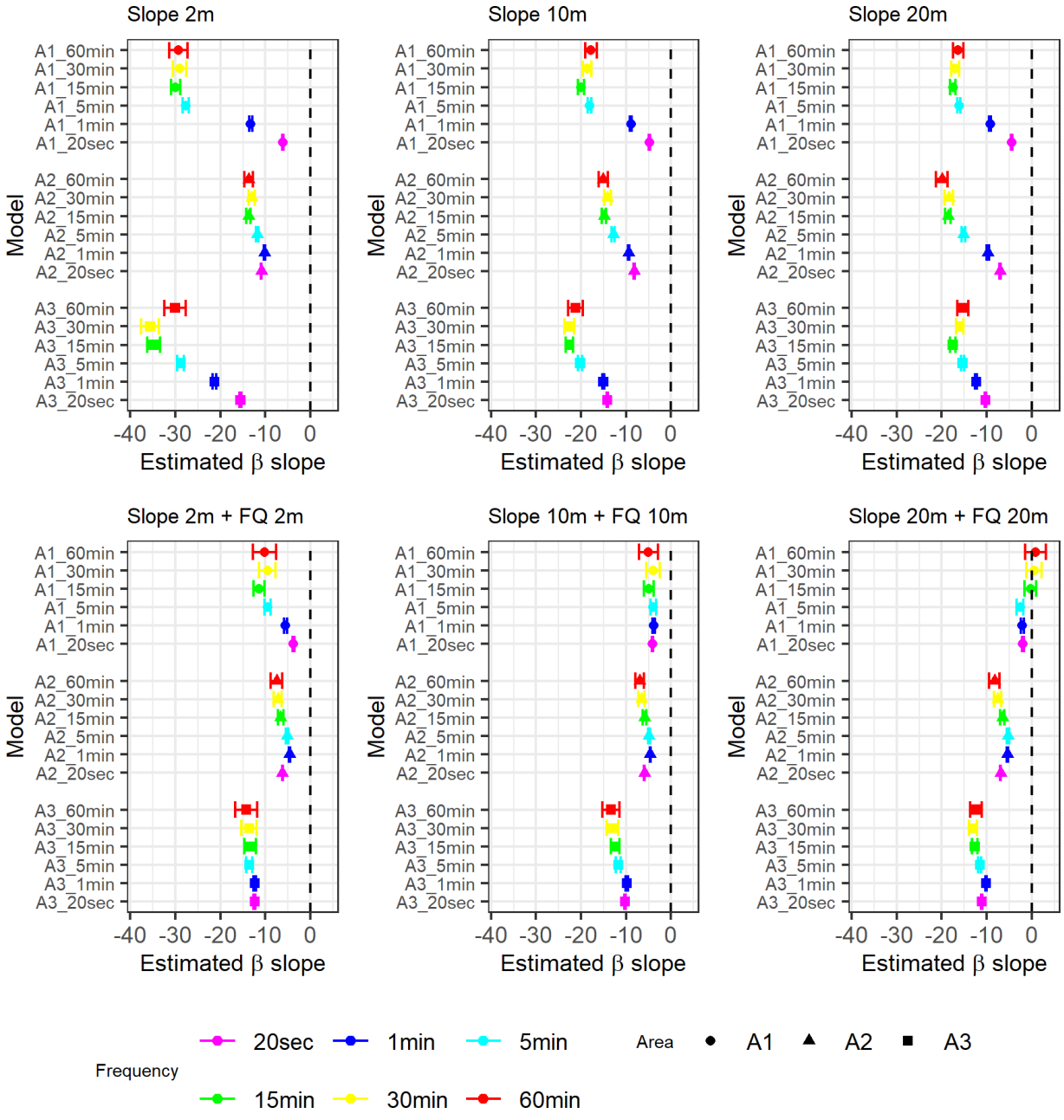

Figure 3.9: Posterior estimates for the slope covariate effect from the SSA models of the Original Braunvieh herd. Each plot represents a different spatial scale and covariate combination. Within a plot, each line on the y-axis represents a different model. Spatial area and temporal frequency are denoted by shape and colour, respectively.

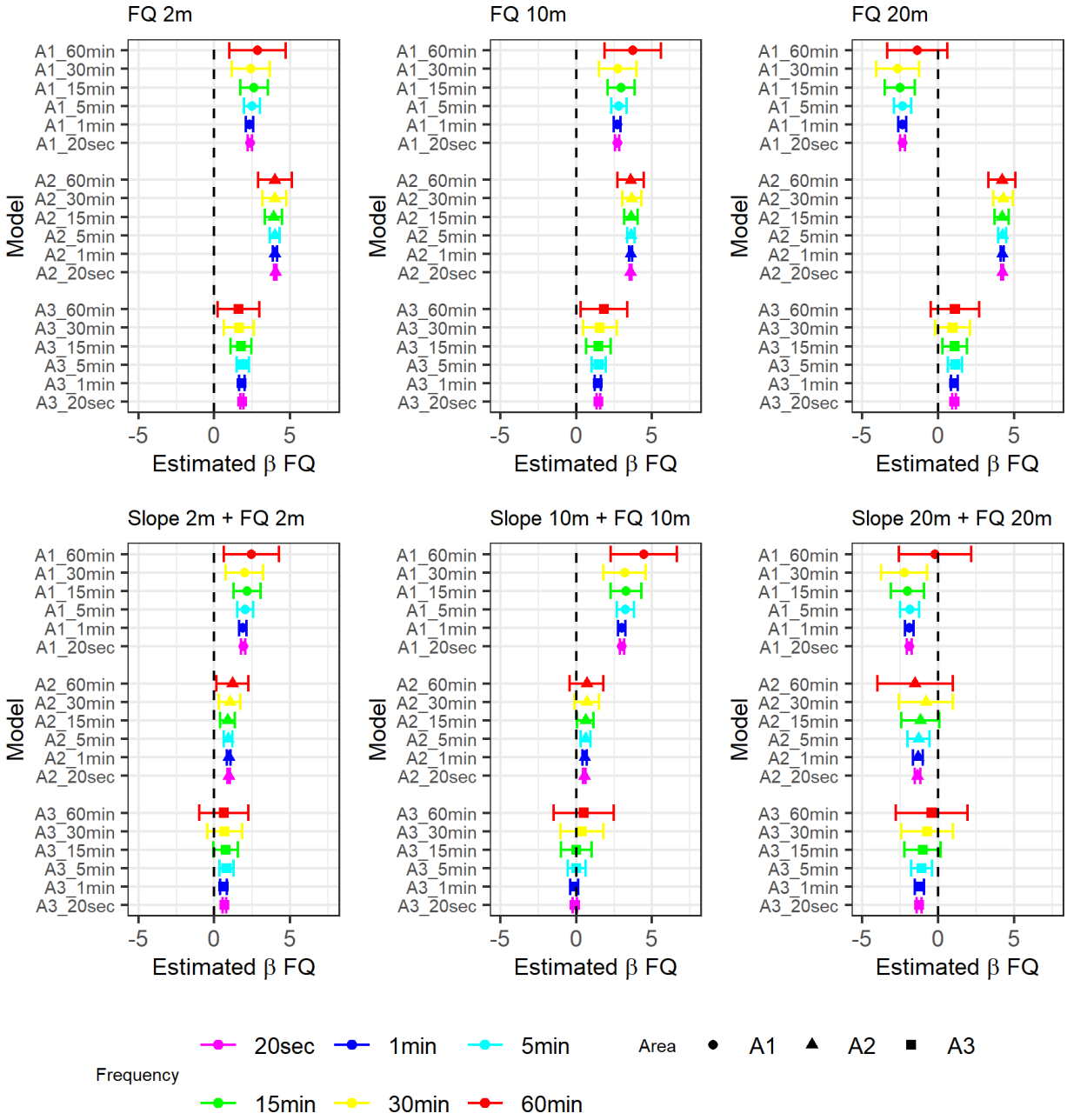

Figure 3.10: Posterior estimates for the forage quality covariate effect from the RSA models of the Original Braunvieh herd. Each plot represents a different spatial scale and covariate combination. Within a plot, each line on the y-axis represents a different model. Spatial area and temporal frequency are denoted by shape and colour, respectively.

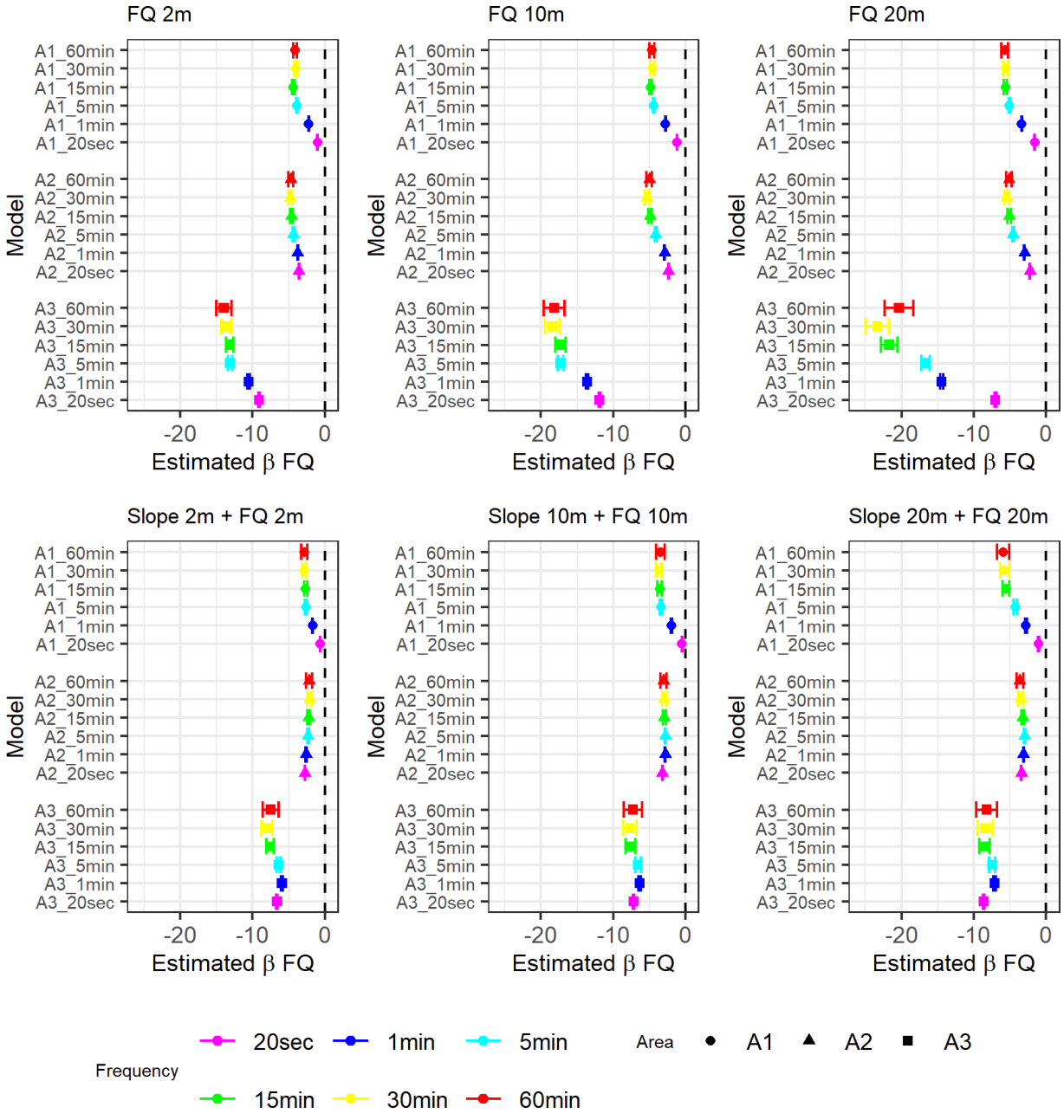

Figure 3.11: Posterior estimates for the forage quality covariate effect from the SSA models of the Original Braunvieh herd. Each plot represents a different spatial scale and covariate combination. Within a plot, each line on the y-axis represents a different model. Spatial area and temporal frequency are denoted by shape and colour, respectively.

3.3.2 Model Comparison

As recommended by Arce Guillen et al. (2023), model comparison was carried out using the deviance information criterion (DIC); a Bayesian model selection measure which balances goodness of fit with model complexity (Spiegelhalter et al., 2002). As DIC assesses goodness of fit relative to the underlying dataset, the model selection measure can only be used to compare models fitted to the same data, therefore constraining comparison to within groups of the same temporal frequency. Measure of deviance is also directly related to model likelihood, so cannot be used to compare between the RSA and SSA models. Therefore, quantitative model comparison can be conducted within 9-model groups, which share the same temporal frequency, herd, pasture area, and inferential method, and differ in covariate spatial scale and predictor composition. However, cross-group comparisons can be made about the relative rankings of these characteristics by DIC, to broaden model comparison. Thus, a 20-second model cannot be deemed a better fit than a 1-minute model, but it could be said that the model of the 9-model group that gave the worst fit was the same or different between groups.

It is also important to note that DIC provides a relative ranking, and so models are not objectively determined to be a 'good' or 'bad' fit, but can be described as a 'better' or 'worse' fit than other models in the comparison group. The objective of this model comparison is not to determine whether the models provide an overall good fit to the data, but rather to investigate how covariate spatial scale impacts model fit, and compare whether these trends are consistent between inferential methods and temporal frequencies. The trends and patterns described here were consistent across herds and spatial areas, so only DIC scores for the Original Braunvieh herd in Area 1 are presented in Figures 3.12 and 3.13. Further information for the other pasture areas is included in Tables 3.3 and 3.4.

The impact of covariate spatial scale and predictor composition on the relative DIC ranking of models within a 9-model group was largely consistent across temporal frequencies for the RSA models (Figure 3.12). However, the 60-minute models demonstrate a slight deviation from the trend by ranking models considered an intermediate fit in other temporal frequencies more poorly (e.g., $10m^2$ forage quality only and multivariable models). The model with the lowest DIC score

(best fit) and highest DIC score (worst fit) of the 9-model group was consistent across temporal frequencies within a pasture area (Table 3.3). Multivariable models were found to have the worst fit, consistently across temporal frequencies and pasture areas, whilst univariable models were found to have the best fit. However, the worst and best fitting spatial scales were found to differ between areas.

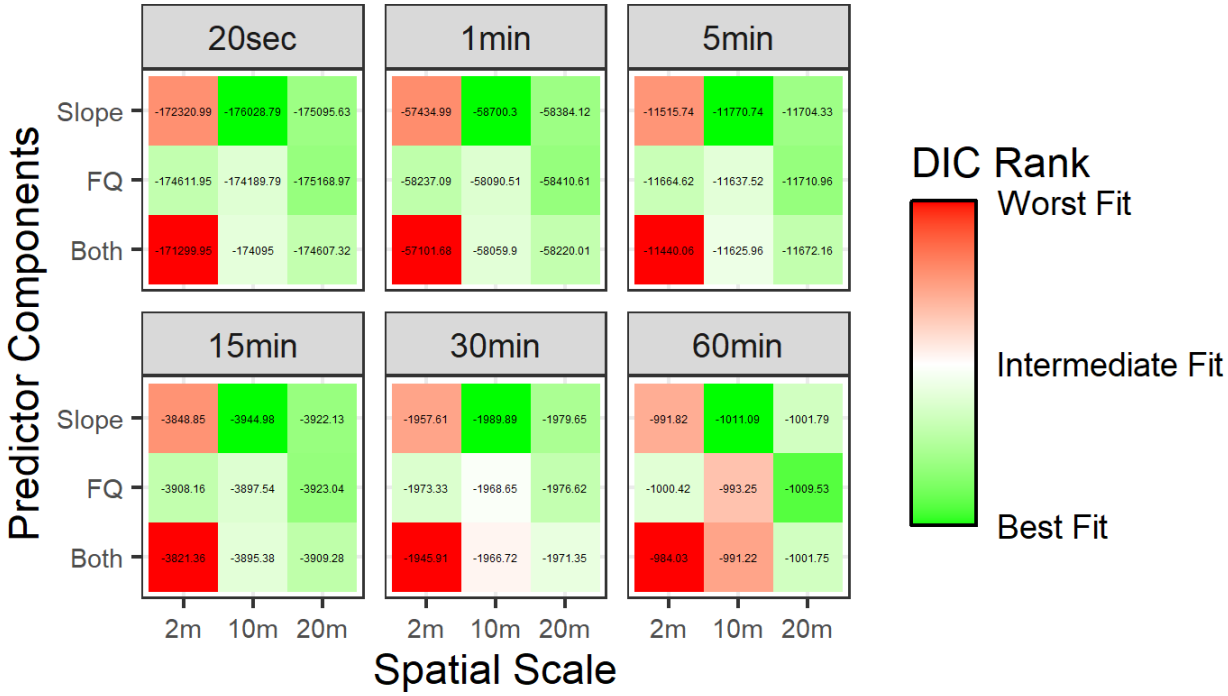

Figure 3.12: DIC scores for the RSA models of the Original Braunvieh herd in Area 1. Each plot represents a different temporal frequency group of 9 models. Within a plot, each tile represents a different spatial scale (x-axis) and covariate combination (y-axis). Numbers within a tile show the actual DIC score, whilst the tile colour represents a relative scale from worst fit (red) to best fit (green).

Table 3.3: Predictor component and scale combination with the relative highest and lowest DIC per nine model group for the RSA models fitted to data from the Original Braunvieh herd. All values given are rounded to 2 decimal places.

Area	Frequency	Lowest DIC		Highest DIC	
		Components	Scale	Components	Scale
Area 1	20-second	Slope	$10m^2$	Slope + Forage Quality	$2m^2$
	1-minute	Slope	$10m^2$	Slope + Forage Quality	$2m^2$
	5-minute	Slope	$10m^2$	Slope + Forage Quality	$2m^2$
	15-minute	Slope	$10m^2$	Slope + Forage Quality	$2m^2$
	30-minute	Slope	$10m^2$	Slope + Forage Quality	$2m^2$
	60-minute	Slope	$10m^2$	Slope + Forage Quality	$2m^2$
Area 2	20-second	Forage Quality	$2m^2$	Slope + Forage Quality	$20m^2$
	1-minute	Forage Quality	$2m^2$	Slope + Forage Quality	$20m^2$
	5-minute	Forage Quality	$2m^2$	Slope + Forage Quality	$20m^2$
	15-minute	Forage Quality	$2m^2$	Slope + Forage Quality	$20m^2$
	30-minute	Forage Quality	$2m^2$	Slope + Forage Quality	$20m^2$
	60-minute	Forage Quality	$2m^2$	Slope + Forage Quality	$20m^2$
Area 3	20-second	Forage Quality	$20m^2$	Slope + Forage Quality	$2m^2$
	1-minute	Forage Quality	$20m^2$	Slope + Forage Quality	$2m^2$
	5-minute	Forage Quality	$20m^2$	Slope + Forage Quality	$2m^2$
	15-minute	Forage Quality	$20m^2$	Slope + Forage Quality	$2m^2$
	30-minute	Forage Quality	$20m^2$	Slope + Forage Quality	$2m^2$
	60-minute	Forage Quality	$20m^2$	Slope + Forage Quality	$2m^2$

In contrast, the SSA model rankings show higher levels of variation between temporal frequency groups (Figure 3.13). For example, the $2m^2$ forage quality only model is ranked as a poorer fit for the 5-minute model group, but is placed at an intermediate level for the finer and coarser temporal frequencies (e.g., 20-second and 60-minute). Within each pasture area, the predictor components and covariate spatial scales which give the best and worst fit within a 9 model group show more inconsistency across temporal frequencies (Table 3.4), as compared to the RSA models (Table 3.3). This inconsistency suggests a stronger impact of temporal frequency on the effects of spatial scale when using the SSA method for inference, as compared to the RSA models.

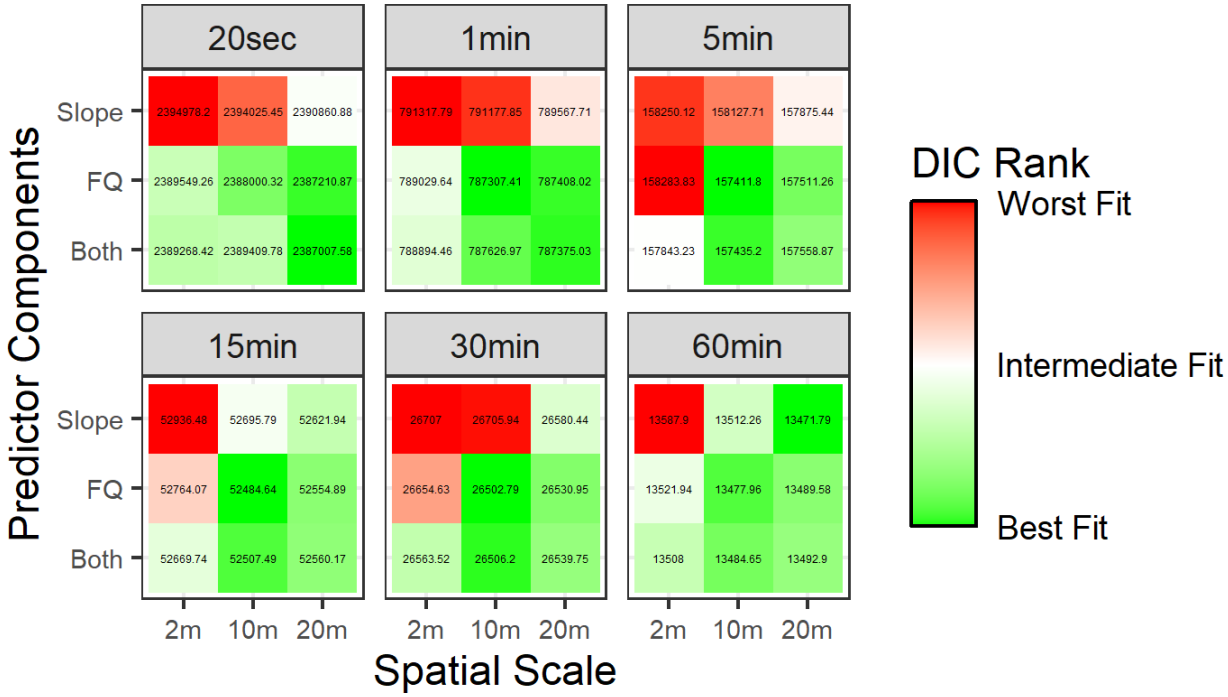

Figure 3.13: DIC scores for the SSA models of the Original Braunvieh herd in Area 1. Each plot represents a different temporal frequency group of 9 models. Within a plot, each tile represents a different spatial scale (x-axis) and covariate combination (y-axis). Numbers within a tile show the actual DIC score, whilst the tile colour represents a relative scale from worst fit (red) to best fit (green).

Table 3.4: Predictor component and scale combination with the relative highest and lowest DIC per nine model group for the SSA models fitted to data from the Original Braunvieh herd. All values given are rounded to 2 decimal places.

Area	Frequency	Lowest DIC		Highest DIC	
		Components	Scale	Components	Scale
Area 1	20-second	Slope + Forage Quality	$20m^2$	Slope	$2m^2$
	1-minute	Forage Quality	$10m^2$	Slope	$2m^2$
	5-minute	Forage Quality	$10m^2$	Forage Quality	$2m^2$
	15-minute	Forage Quality	$10m^2$	Slope	$2m^2$
	30-minute	Forage Quality	$10m^2$	Slope	$2m^2$
	60-minute	Slope	$20m^2$	Slope	$2m^2$
Area 2	20-second	Slope	$20m^2$	Slope + Forage Quality	$20m^2$
	1-minute	Slope	$2m^2$	Forage Quality	$10m^2$
	5-minute	Forage Quality	$20m^2$	Forage Quality	$10m^2$
	15-minute	Slope	$20m^2$	Forage Quality	$10m^2$
	30-minute	Slope	$20m^2$	Slope	$2m^2$
	60-minute	Slope	$2m^2$	Forage Quality	$20m^2$
Area 3	20-second	Forage Quality	$10m^2$	Slope	$2m^2$
	1-minute	Slope	$10m^2$	Slope	$2m^2$
	5-minute	Forage Quality	$10m^2$	Forage Quality	$20m^2$
	15-minute	Forage Quality	$10m^2$	Forage Quality	$20m^2$
	30-minute	Forage Quality	$10m^2$	Forage Quality	$20m^2$
	60-minute	Forage Quality	$10m^2$	Slope	$2m^2$

3.4 Discussion

This chapter centred on a case study of cattle habitat selection and space-use on a Swiss Alpine farm. Two types of IPP model, a population-level spatial RSA and an individual-level spatio-temporal SSA, were fitted to data from three breeds of cattle in three spatial areas. Estimated habitat selection parameters and model fit were compared across six temporal frequencies and three spatial scales. The following section includes a discussion of the presented results, a review of the modelling framework, and suggestions for future study.

3.4.1 Discussion of Results

Slope was found to have a negative effect according to most of the RSA and SSA models, indicating avoidance behaviour for this covariate at the macro-level of overall spatial distribution and the micro-level of movement decisions (Figures 3.8 and 3.9). This agrees with the general understanding of existing literature, that cattle tend to avoid steep slopes and prefer areas of gentler terrain (Roever et al., 2015; Bailey et al., 2018; Koczura et al., 2019). However, this result was not seen uniformly across all models, with different factors impacting both the strength and direction of the estimated covariate effect.

For the RSA models, decreasing spatial resolution of covariates had a strong impact on estimated effect size of slope (Figure 3.8). This trend was particularly prominent for models fitted to data from Area 1; the smallest of the three pasture areas. This may be due to the size of the area, relative to the size of the pixels at the coarse spatial grain, meaning that less information in covariate variation was available for the coarser grain models in this area. The slope covariate itself is also less heterogeneous for this pasture area compared to Areas 2 and 3, so decreasing covariate resolution could have resulted in a more severe homogenisation of covariate values in this area (Figure 3.3, Paton and Matthiopoulos, 2015).

Spatial scale also strongly impacted estimated effect size of forage quality by the RSA models (Figure 3.10). Again, this was seen most prominently in Area 1 for the univariable models, wherein the effect changed direction from a positive to a negative effect with decreasing spatial resolution. A preference for high-quality forage would be expected in the selection behaviour

of cattle, so the estimates from models with coarse-scale covariates tend to disagree with pre-existing understanding of cattle behaviour (Homburger et al., 2015). Area 1 contained large expanses of high-quality forage, so the reduction in spatial resolution produced a homogenised version of the covariate with little variation in values forage quality (Figure 3.3, Paton and Matthiopoulos, 2015). In comparison, univariable models fitted to data from Area 2, the pasture area with the highest level of heterogeneity in forage quality, were estimated to have the strongest positive effect. Spatial scale also seemed to have more impact on the multivariable models, suggesting that the effects of decreased spatial resolution were exacerbated when the predictor contained multiple fixed effects. This may be due to the fact that different covariates were only included at the same scale, and multi-scale covariate combinations were omitted from analysis. If the forage quality and slope covariate effects were best described at different spatial scales, then single-scale multivariable models would provide a poor model component construction. Evidence for this theory is suggested by the relative DIC rankings for the RSA models, which consistently find multivariable models to be the poorest fit (Table 3.3).

In contrast to the patterns displayed by the RSA models, spatial scale of covariates had less impact on the posterior mean estimates of the SSA models for both slope and forage quality (Figures 3.9 and 3.11). This may be due to the complex integration scheme used in GF-iSSA, which means that each observation is considered relative to a smaller available area than that in the RSA models. Within this smaller domain of availability, covariate values may be more homogeneous than those observed over the full paddock area. As such, a reduction in spatial scale may impact the variation in covariate values less in these smaller areas of availability.

Temporal frequency of observations had little impact on the posterior mean of the estimated effect of slope and forage quality in the RSA models (Figures 3.8 and 3.10). Although, models fitted to coarser frequency data estimated posteriors with a wider associated credible interval. The lack of impact of temporal frequency can also be observed in the consistency of DIC rankings across frequencies for the RSA models (Figure 3.12 and Table 3.3). This suggests that changing temporal frequency doesn't alter the relative interpretation of model component combinations or spatial scales in terms of goodness of fit. The coarser frequency datasets can be thought of as regularly thinned versions of the point pattern created by the spatial distribution of

the finer frequency data, so the same effect should be observed with higher uncertainty, as seen here. However, it is impressive that the datasets with the fewest observations (i.e., those collected at a 60-minute interval) are capable of producing a similar estimate for coefficient effect to those with the most observations (i.e., the 20-second data). This suggests that high-frequency data collection may be unnecessary when using methods to analyse overall spatial distribution, such as resource-selection functions. This is also of interest when considering that these methods typically assume independence between observations; an assumption which is violated by the highly spatio-temporally correlated nature of telemetry tracking data. Usually, when fitting models of this type to this kind of data, this assumption can be accounted for by thinning data, with the hope that this will remove any bias introduced by spatial autocorrelation (Hooten et al., 2014). Here, the same posterior mean effect is estimated by thinned data (the 60-minute dataset represents a greatly thinned version of the 20-second dataset, with only 0.56% of observations retained) as compared to correlated data. This suggests either a lack of bias in the data, or more concerningly, that the process of thinning does not remove bias.

The lack of impact of temporal frequency on estimated effects in the RSA models contrasted to the trends observed in the SSA models (Figures 3.9 and 3.11). For both slope and forage quality, increasing temporal frequency tended to lead to an estimated effect closer to 0 for the SSA models. Temporal frequency also impacted the relative interpretation of the 'best' covariate combinations and scales according to DIC ranking, which was more variable between frequencies for the SSA models (Figure 3.13 and Table 3.4) as compared to the RSA models (Figure 3.12 and Table 3.3). Temporal frequency plays a stronger role in the structure of SSA, impacting both the number of observations and the integration scheme (Table 3.2). When the temporal interval between observations is longer, the domain of availability for each step becomes larger (Figure 3.5). As temporal frequency and availability are intrinsically linked, interpretation of covariates is impacted. For highly spatio-temporally correlated data, like the 20-second dataset, observations will include steps where an animal is close to an area of preferred habitat that it has previously, or will in future, utilise, but in which it is not currently located. These areas will therefore be considered *available* but not *chosen* at these steps, potentially skewing interpretations of habitat selection as large amounts of the available area are made up of the (latently) preferable habitat.

At coarser intervals, domains of availability are larger, capturing a wider range of covariate values in the available area and so possibly providing a more balanced interpretation of the chosen step location. It is therefore difficult to disentangle the effects of changing temporal frequency from the spatial scale of the study domain, and would be of interest in future study to hold one constant while changing the other, to assess the sensitivity of model results to each feature individually. This distinction between large- and small-scale selection could be further investigated by using behavioural classification to identify movement steps which are transient, as opposed to active usage such as foraging.

This balance of use and availability may also explain the disparity in the direction of estimated effect of forage quality between the RSA and SSA models. Most RSA models estimated a positive posterior mean effect of forage quality, agreeing with existing literature on cattle habitat selection behaviour (Figure 3.10, Homburger et al., 2015). However, most SSA models produced a negative posterior mean estimate for forage quality (Figure 3.11). This was particularly prominent for models fitted to data from Area 3, which contained mostly poor quality forage (Figure 3.3). With its complex integration scheme, GF-iSSA places more weight on the surrounding available area per observation, compared to the overall summary of spatial distribution analysed with the RSA method. This disparity in covariate interpretation and estimated coefficient effect should be considered in the context of the scale of behaviour each method aims to analyse. RSA provides an overview of the overall spatial distribution, so habitat selection is performed at the population-level and should be interpreted on a large-scale. On the other hand, iSSA looks at the step-by-step movement decisions, so reveals more about the animal's short-term choices and 'realised' space-use. An analogous example to this would be the findings of Compton, Rhymer, and Mccollough (2002), who found that, at a landscape scale, wood turtles (*Clemmys insculpta*) were active in partially forested areas, showing a preference behaviour towards forest cover, but that within these areas, the turtles avoided forested sections. Therefore, the difference in direction of estimated effect for the forage quality covariate between RSA and SSA may indicate that cattle prefer high-quality forage overall, but spend a lot of time in intermediate areas.

3.4.2 Methodological Considerations and Future Research

The GF-iSSA approach used in the SSA models utilises a complex integration scheme wherein the number of integration points can be greatly increased by many features of the model or data, which has a consequential impact on model running time (Table 3.2). The number and distribution of integration points in a given spatial area is determined by the resolution of the mesh, as points are located at mesh nodes. Therefore a potential solution to improve computational efficiency would be to use a coarser mesh triangulation. However, this could negatively impact model performance (Michelot et al., 2024), and lead to incorrect covariate interpretation (Dambly et al., 2023). Therefore, other concessions to computational efficiency are made in lieu of altering the mesh resolution.

In all 972 models, inference is performed using data collected over a duration of 24 hours, and only from the instances where a herd was the first to graze a given paddock. However, an observation period of 24 hours may be considered an insufficient window to observe a representative sample of movement behaviour (Patterson et al., 2017). During the original data collection, the animals were placed in paddocks in a rotational system, with each herd occupying each paddock for a total of 3-4 days. However, the analysis contains purely spatial (not spatio-temporal) covariates, one of which being a measure of forage quality. There is potential for disparity between the static covariate information and the true state of the environment at the time of data collection, due to the covariate being subject to resource depletion (i.e., grazing, trampling). Therefore, to reduce the likelihood of such mismatch, only the instances where a herd was the first to occupy a paddock were included in analysis, and only the first 24-hours of observation were analysed. Not only does this maintain the covariate as an accurate representation of environmental conditions, it also limits the temporal duration of the observation window; a necessity to reduce computational cost, which, due to the complex integration scheme used in the SSA method for inference (GF-iSSA), is greatly increased by the number of observations.

As well as determining study duration, computational cost was a limiting factor for other modelling decisions. Despite the namesake of the method used for SSA, a Gaussian random field was not included in the selection function. This could mean that interpretation of covariate

effects is subject to spurious significance, as missing covariates are not accounted for in the SSA models (although the spatio-temporally correlated nature of the data is accounted for through the Markovian structure of the movement kernel, Arce Guillen et al., 2023). Similarly, a GRF is not included in the RSA models, to keep the predictor simple and comparable to the selection function of the SSA models. Thus the RSA models can only account for variation explained by the fixed effects. Not including a GRF avoids issues of spatial confounding (Hodges and Reich, 2010), and reduces model complexity, which improves model interpretability and running time. However, a future direction of interest for this research would be to include a Gaussian random field in the selection function of the SSA models and in the predictor of the RSA models, and assess its impact on inference. This represents one of the advantages of utilising this model framework (alongside the use of the deterministic integration scheme), as inclusion of a GRF in the models would require very little change to the current methodology.

Similarly, in order to maintain computational efficiency, restrictions were not placed on the parameters of the movement kernel, meaning that they were able to be estimated outside of their theoretical bounds. Although this did not impact inference on selection parameters, it disallowed the movement kernel to be interpreted (Arce Guillen et al., 2023). In future, it may be of interest to fit a model with restrictions on the movement parameters, in order to allow interpretation of the estimated distributions of step length and turning angle.

Although computational cost was a primary concern in modelling decisions, modelling was carried out at the herd-level, despite the associated increase in complexity of the multi-individual SSA models. This was done for a number of reasons. Firstly, it demonstrates an advantage of the GF-iSSA approach in that the movement tracks of multiple individuals can be included in the same model. This is done through joint modelling, so that each individual has its own likelihood, and parameter estimation is shared across likelihoods, meaning that habitat selection parameters can be interpreted at the herd-level. Secondly, it allows inference of the overall preferences of a herd, so provides insight into herd-level trends. This is of interest in informing management practices, which usually take the form of altering stocking rate and density (Pauler et al., 2025). Taking inference from a multi-individual model can be more interpretable and practically useful than summarising the noisier results of multiple individual-level models. For example, in rela-

tion to movement parameters used to define behavioural state, Jonsen (2016) demonstrates that estimate precision is improved when inference is made across multiple individuals. Finally, it keeps the models comparable with typical RSA approaches to modelling tracking data, which involve an amalgamation of all observations from multiple individuals (Muff, Signer, and Fieberg, 2019).

When fitting multi-individual models with GF-iSSA, each individual has its own associated set of integration points, as these are defined using the spatial locations of the observations. The mesh and domains of availability which determine the integration scheme are defined by the user, so it is possible (though computationally expensive) to create bespoke integration schemes which differ between individuals, or indeed between time points. This approach was taken here in the incorporation of paddock boundaries into the domains of availability (Figure 3.6). However the base meshes for the three pasture areas, and the radius of domain of availability for a given temporal frequency were kept constant, to maintain comparability between models. As LGCP models are defined in continuous-space, the area which is deemed available to an individual at a given step (SSA), or to the overall population (RSA), has a direct impact on estimation of the covariate effects, as not only the observations but also the background information is taken into account (Illian et al., 2013). Criticisms of the approach taken here might include: (1) the use of observations of step length to determine the radius of the domain of availability empirically for coarse data; and (2) the use of the same radius between herds. Previous research has found that decreasing the temporal frequency of tracking observations can result in reduced estimates of distance travelled, altering understanding of animal mobility (Mills, Patterson, and Murray, 2006; Johnson and Ganskopp, 2008; Davis et al., 2011; Mccann et al., 2021). This effect can be observed visually in the spatial representation of data at different temporal frequencies, wherein the coarsest dataset covers a reduced spatial area compared to data collected at finer temporal frequencies (Figure 3.2). For this analysis, the radius of domain of availability (computed using average maximum step length) remained constant for the three coarsest temporal frequency datasets. This may indicate the effect as described here, or could simply represent an upper limit to animal mobility over time. The radius was also estimated using data from, and kept constant for, all breeds of cattle. However the different cattle breeds vary in size and productivity level,

so will likely have different levels of mobility which translate to different domains of availability (Pauler et al., 2020a). Therefore, an extension to this work would be to compare differing methods to compute the radius of the domain of availability, and assess the resulting impact on inference of selection parameters.

3.5 Conclusions

This chapter explored the impact of spatial scale of covariates and temporal frequency of tracking observations on inferences about habitat selection in cattle on a Swiss Alpine farm. Two approaches modelling different levels of selection were compared. The resource selection analysis (RSA) modelled amalgamated tracking data as a spatial inhomogeneous Poisson process (IPP), using a log Gaussian Cox process (LGCP) model in `R-inlabru`. This was compared to a step selection analysis (SSA) using the spatio-temporal GF-iSSA approach, wherein individual movement tracks were modelled in a joint likelihood framework using an LGCP in `R-inlabru`. Variations in method, spatial area, cattle breed, temporal frequency of observations, covariate combination and spatial scale resulted in a modelling strategy of 972 models, which were compared in terms of selection parameter estimation and DIC.

This work represents a novel application of the GF-iSSA framework to modelling movement in an agricultural setting, and incorporates a bespoke transformation of the complex integration scheme to incorporate physical barriers to movement in the domains of availability for each step.

The results of this analysis suggest that decreasing spatial resolution of environmental covariates can alter the strength and direction of estimated effects, particularly for RSA. The impact of spatial scale may largely be determined by the heterogeneity of covariate values within the available landscape, and thus is related to the spatial area of availability. In contrast, temporal frequency of observations appears to have little impact on posterior mean estimates of selection parameters in RSA. For the SSA models, temporal frequency of observations is more influential, impacting parameter estimates and interacting with spatial scale of covariates to alter relative rankings in model comparison. Therefore, although temporal frequency of data collection is typically determined by practical restrictions (e.g., device battery life), temporal scale-dependency can impact model selection and inference in SSA.

Chapter 4

Combining Local and Global Scale Habitat Selection: Implementing the Langevin Movement Model in `R-inlabru`

4.1 Introduction

Chapter 2 explored modelling the movement of an overall population at a large spatio-temporal scale: patch-level habitat selection across a country-wide area over a number of years. Conversely, Chapter 3 examined the movement behaviours of a small group of individuals up to a very fine spatio-temporal scale: habitat selection for $2m^2$ gridded spatial covariates, with telemetry observations collected at a 20-second frequency; and compared between analyses of this data performed at different selection levels. Historically in ecology, these modelling strategies might be considered entirely separately; the former classed as a species distribution model, and the latter classed as a movement model. However, these are both examples of habitat selection models, which simply sit at either end of the spectrum of spatio-temporal scale. Habitat selection is a key element in the process which governs movement behaviour and spatial distribution (Florko et al., 2025). Modelling data at different spatial and temporal scales can offer different windows of insight into the same process; where an individual *goes* ultimately determines where it *is*, so in basic principle, movement data give a magnified perspective of species distribution data.

4.1.1 Scale and Bias in Survey and Telemetry Data

As detailed in Chapter 3, despite technological advancement in tracking apparatus, the temporal window of monitoring, and frequency of observations in telemetry tracking data are often determined by device battery life (Davis et al., 2011). This means that if the researcher wants to collect data at a fine temporal grain, the duration of the study must be relatively short. In contrast, 'one observation' of species distribution data (read: one snapshot of the overall population) is much more labour intensive to collect, and so this type of data is usually collected much more infrequently but often over a longer total duration. These two types of data are inherently linked to differences in temporal scale, which means that they give different types of insight into the same process. Telemetry data provide a detailed view into a short window of the process, giving rich insight into shorter-term behaviour. On the other hand, survey data give a general long-term overview which may be better at eliciting overall behavioural trends.

Although movement data and species distribution data arise from the same underlying pro-

cess, both are subject to different sampling methods. In order to correctly elicit information about the process of interest, data must first be separated from the biases introduced by the observation process.

Telemetry tracking data are collected by attaching a tag or collar to a number of individuals in a population, collecting observations of their spatial location (alongside additional information on environmental conditions or biometrics) at consecutive time points. For wild populations, particularly for rare or elusive species, capturing and tagging individuals is difficult and labour-intensive, which limits the number of individuals that can be tracked. In addition, there is often a fiscal limitation on resources which restricts the number of tags that can be purchased and deployed. This means that telemetry data are usually only collected for a small subset of the population (although efforts are sometimes made to determine *a priori* which individuals will provide information most indicative of group-wide behaviour). Ultimately, this means that movement data usually consist of observations of few individuals, although these individuals can be 'followed' anywhere in space.

In contrast, species distribution data theoretically have the potential to capture the locations of every individual in a population. However, restrictions in the collection of this type of data lie in the spatial distribution of the sampling method: often parts of the area of interest are inaccessible, and/or the area is too large to cover entirely with the survey method (e.g., camera trapping networks, acoustic telemetry, on-the-ground observers, aerial surveys with drones or other aircraft, or shipboard observations). As such, surveys often incorporate a sampling design which breaks down the study area into smaller windows of observation. These include subplots, line or point transects, or the areas covered by the spatial layout of stationary sampling equipment such as camera traps. Species distribution data can also be collected passively, through the records of governing bodies, agricultural sites, veterinary practices, and museums. In these instances, the observation process is not known, and may have to be reconstructed based on, for example, proximity to population centres or accessibility of reporting stations. Similarly, citizen science is becoming an increasingly important source of species distribution data with a complex and unknown observation process subject to sampling biases such as preferential sampling (where observers choose to collect data in spatial areas known to contain the species of interest). All of

these methods of data collection are also subject to imperfect detection, where some individuals may be difficult for the observer to see or identify, so their presence is not recorded.

The biases introduced by the sampling methods used to collect telemetry tracking data are often the inverse of those associated with the collection of species distribution data. Telemetry datasets contain information on few individuals, but are capable of covering a wide spatial area without restriction. In contrast, survey datasets have the potential to capture the locations of all individuals in a population, but are restricted in spatial coverage and subject to complex observation processes. Thus, the two types of data could be complementary in cancelling-out one another's biases. This complementarity has been recognised in previous studies wherein telemetry data are used to validate predictions from species distribution models (for example, Pinto et al., 2016).

As survey and telemetry data differ in organisational scale, modelling approaches fitted to these data types generally provide insight into different levels of selection behaviour. A framework which integrates survey and telemetry data into the same model provides both the advantage of offsetting the sampling biases from different types of data collection, and of giving a multi-scale insight into habitat selection. This provides a more holistic view of the underlying process than modelling either data type separately would do, as the model benefits from the detailed fine-scale perspective of a movement model, and the generalised macro-scale perspective of a species distribution model (Blackwell and Matthiopoulos, 2024).

4.1.2 Data Integration

The complementarity of different data types in cancelling out bias has provided motivation for a rapidly developing area in statistical ecology: data integration, also referred to as data fusion (Altwegg et al., 2025). This broadly refers to the integration of multiple data streams into a single joint model or multi-step modelling framework. In reference to species distribution and habitat selection, combining data from different types of survey (usually systematic and non-systematic) has been found to balance biases in detection probability and spatial coverage (Miller et al., 2019; Grabow et al., 2022; Song et al., 2025). Bringing in data on animal movement as a second data stream is also a major area of interest in spatial capture recapture literature (e.g.,

Tenan et al., 2017; Linden, Sirén, and Pekins, 2018; Hostetter et al., 2022; Badger et al., 2024). Another application of data integration exists in the estimation of population dynamics, wherein different methods of observation can provide different insights into behaviours that are difficult to observe. For example, Eisaguirre et al. (2023) combine a movement model and a survival model to estimate reproductive success.

Recounting the complementarity of telemetry and survey data in both observation bias and spatio-temporal scale, it is of interest to combine these data types. Some studies have done so through a multi-step approach (Yamamoto et al., 2015; Meehan et al., 2022; Liang et al., 2023). In some cases, multi-step modelling frameworks can, among other issues, introduce bias in parameter estimation, incur issues in uncertainty propagation, and suffer information loss (Blackwell and Matthiopoulos, 2024). Joint modelling generally avoids these disadvantages through concurrent parameter estimation, but can be more complex and computationally costly to implement. Liang et al. (2023) state that they do not use a joint modelling framework because one does not exist that *"can be implemented using readily available software and is computationally feasible for analyzing multiple tracks, presence-only observations, and environmental covariates"*. These shortcomings are precisely the aims to be addressed through the work included later in this chapter.

The construction of joint likelihood models for the integration of survey and telemetry data in habitat selection modelling is a very recent area of development. Three papers which achieve this aim are Blackwell and Matthiopoulos (2024), Buderman et al. (2025), and Lauret et al. (2025). The former two approaches use mathematical techniques to translate individual-level movement models up to population-level selection. On the other hand, Lauret et al. (2025) use a resource selection function to model telemetry data. This is a commonly used method in habitat selection modelling, but can incur issues of spurious significance when failing to account for availability or the sequential, autocorrelated nature of tracking data (Florko et al., 2025).

Buderman et al. (2025) apply this type of data integration to the area of migration ecology, developing a framework which combines gridded abundance data with telemetry tracking data to identify which proportions of a population belong to different subpopulations (e.g., resident and migratory), and where or how far those subpopulations travel. The emphasis in this approach

is on directly modelling the spatio-temporal dynamics of a population. On the other hand, the general framework presented in Blackwell and Matthiopoulos (2024) focuses on the estimation of habitat selection parameters, particularly at a spatial scale that is of most use in informing conservation and management strategies. Long-term space-use and habitat selection are estimated through the assumption that the population of interest moves according to an underlying steady-state distribution. Both approaches make use of a diffusion based movement model in the telemetry likelihood.

4.1.3 The Joint Langevin Movement Model

Blackwell and Matthiopoulos (2024) derive a joint likelihood for the integrated analysis of telemetry and spatial survey data. This is based on the statistical developments of Michelot, Blackwell, and Matthiopoulos (2019), Michelot et al. (2019), and Michelot et al. (2020). The mathematical principle of the modelling framework is based on scaling up individual-level movement to population-level estimates of spatial distribution, and was originally inspired by how an MCMC sampler uses microscopic movement to explore a parameter space and describe a macroscopic steady-state distribution. In an ecological context, this can be thought of as analogous to individual animals moving through space according to some long-term distribution described by habitat selection, which is the same underlying process which impacts the distribution of survey data (ignoring the impact of the observation process, which is accounted for separately). This framework makes the relationship between the two scales of selection mathematically tractable, and ultimately allows for joint modelling and inference from what were previously considered two very different types of data.

The Langevin movement model is a continuous-time diffusion based model which can be applied to animal movement. In ecology, the movement of individual organisms is often modelled as a diffusion process such as a random walk or stochastic process (Johnson et al., 1992). Diffusion based models of movement can be scaled up by adding correlation and drift terms to the otherwise random movement process, to emulate 'attraction' behaviours in movement such as to a central place, a landscape feature of importance, or even a moving target (Blackwell, 1997; Niu, Blackwell, and Skarin, 2016). An example commonly used in movement ecology is

the Ornstein-Uhlenbeck process, wherein a drift term is used to incorporate attraction to a given location into the diffusion process (Uhlenbeck and Ornstein, 1930; Breed, Golson, and Tinker, 2017; Eisaguirre et al., 2021). The Langevin diffusion process also incorporates a drift term, but one that can vary spatially according to a stationary distribution - the utilisation distribution $\pi(\cdot)$ which can be described through spatially structured environmental covariates (Michelot et al., 2019). It is this feature which is utilised in Blackwell and Matthiopoulos (2024) to connect small-scale movement with large-scale space-use.

The joint likelihood is not given a name by Blackwell and Matthiopoulos (2024), likely because they present a general framework for joint modelling of these types of data, and stress that movement models other than the Langevin movement model could be implemented within the framework. However, this chapter will focus on the implementation of the model largely as described in Blackwell and Matthiopoulos (2024), which uses the Langevin movement model as in Michelot et al. (2019) for the telemetry likelihood, and so hereafter in this thesis the joint modelling framework will be referred to as the 'joint Langevin movement model', with its requisite parts referred to as the 'survey model' and 'telemetry model'.

4.1.4 Statistical Modelling Framework

The following section provides a brief overview of the modelling framework for the joint Langevin movement model as presented in Blackwell and Matthiopoulos (2024). For more information, refer to Blackwell and Matthiopoulos (2024) and Michelot et al. (2019). The overall joint likelihood framework combines a telemetry likelihood and a survey likelihood.

Let $x_0, ..., x_n$ represent telemetry location data collected sequentially at times $t_0, ..., t_n$, and δ_{t_j} represent the temporal interval $t_{j+1} - t_j$. Then, each observation x_j has a Gaussian distribution that depends on the previous observation, and the overall log-likelihood of the telemetry model L_M is described as

$$L_M(\beta, \Gamma) = \sum_{j=0}^{n-1} \log \phi \left(x_{j+1} \mid x_j + \tilde{b}(x_j)\delta_{t_j}, \Gamma\delta_{t_j}\mathbf{I} \right), \tag{4.1}$$

where β are the parameters of the utilisation distribution $\pi(\cdot)$ included via the drift term $\tilde{b}(x_j)$, Γ is a diffusivity parameter controlling the speed of the process, $\mathbf{I}$ is an identity matrix, and

$\phi(x \mid \mu, \Sigma)$ denotes the density at x of the bivariate Gaussian distribution with mean μ and covariance matrix Σ. The utilisation distribution is related to the telemetry model through the approximation of the Langevin drift term

$$\tilde{b}(x) = \frac{\Gamma}{2} \int \nabla \log(\pi(z)) dG\left(z \mid x_j, \zeta\sqrt{\delta_{t_j}}\right), \tag{4.2}$$

where z denotes cells in a neighbourhood of the point x_j over which the drift term is integrated using the function $G\left(\cdot \mid x_j, \zeta\sqrt{\delta_{t_j}}\right)$ which represents a symmetric distribution centred at x_j with scale parameter $\zeta\sqrt{\delta_{t_j}}$, comparable to the distance moved in the temporal interval. The smoothing kernel $G(\cdot)$ and scale parameter ζ are expanded upon in Section 4.2. The drift term is a function of the gradient ∇. The scale parameter can be related to the distance moved in time δ_{t_j}, which allows the gradient term to match more closely with the true gradient of the process over that time interval. The reason an approximation is used is explained further in Section 4.2, and the smoothing $G(\cdot)$ and gradient ∇ transformations are discussed in more detail in Section 4.2.2. The drift term includes the utilisation distribution $\pi(\cdot)$, which can be described as the exponential of a linear predictor $\eta(\cdot)$

$$\begin{aligned} \pi(x) &\propto \exp\left(\eta(x)\right) \\ &= \exp\left(\beta_1 c_1(x) + ... + \beta_k c_k(x)\right), \end{aligned} \tag{4.3}$$

where $c_i(\cdot)$ are spatially varying covariates, and β_i are estimated habitat selection parameters. Note that if the utilisation distribution $\pi(\cdot)$ is flat, then $\tilde{b}(\cdot) \equiv 0$ and the movement process is just Brownian motion. The definition of the utilisation distribution is shared with the survey model, where it is proportional to the intensity of an inhomogeneous Poisson process (IPP)

$$\begin{aligned} \lambda(x) &\propto \pi(x) \\ &= \exp(\alpha + \eta(x)), \end{aligned} \tag{4.4}$$

where α is an intercept term related to abundance and dependent on population size, detectability, and survey effort. Letting $y_1, ...y_m$ represent observed locations in the survey dataset, the log-likelihood of the survey model L_S is described as

$$L_S(\alpha, \beta) = -\exp(\alpha) \int_A \exp(\eta(y)) dy + m\alpha + \sum_{i=1}^{m} \eta(y_i), \tag{4.5}$$

where A denotes the spatial region over which the survey took place, and the intercept term depends on the number of observed locations m.

Using the log-likelihoods defined in Equations 4.5 and 4.1, the overall log-likelihood for the joint model L can be defined as

$$\begin{aligned} L(\alpha, \beta, \gamma) = &-\exp(\alpha) \int_A \exp\left(\eta(y, \beta)\right) dy + m\alpha + \sum_{i=1}^{m} \eta(y_i, \beta) \\ &+ \sum_{j=0}^{n-1} \log \phi \left(x_{j+1} \mid x_j + \tilde{b}(x_j, \beta, \gamma)\delta_{t_j}, \exp(\gamma)\delta_{t_j} \mathbf{I} \right), \end{aligned} \tag{4.6}$$

where, for convenience, the diffusivity parameter Γ is included via $\gamma = \log(\Gamma)$.

4.1.5 Benefits of Implementation in R-inlabru

Blackwell and Matthiopoulos (2024) demonstrate the use of maximum likelihood estimation to obtain parameter estimates from the joint Langevin movement model, but mention that implementation in other inferential frameworks is possible for the joint likelihood. A Bayesian framework would allow the incorporation of prior beliefs, and could be used for more detailed inference, but likely was not used in the original paper due to the associated computational cost. INLA offers a computationally efficient alternative to traditional methods for Bayesian inference - such as MCMC - so implementation in the INLA framework would provide the benefits of Bayesian inference without the associated cost (Rue, Martino, and Chopin, 2009). The flexibility and user-friendliness of the software package R-inlabru (a wrapper around and extension to R-INLA) could provide additional improvements to different aspects of the model and end-user experience (Bachl et al., 2019). This chapter will explore implementation of the joint Langevin movement model in R-inlabru. The potential benefits are listed below.

Principally, the INLA method for approximate Bayesian inference is extremely computationally efficient, and so is a fast method for complex modelling of large spatio-temporal datasets (Rue, Martino, and Chopin, 2009). Using INLA for inference would enable more detailed analysis than has been presented previously, equivalent to MCMC, but without the additional com-

putational cost. In addition, placing the model in a Bayesian framework would allow the incorporation of prior beliefs, allowing more robust inference from complex ecological data.

An additional advantage is the combination of the INLA + SPDE methodology, which enables the inclusion of a continuously-indexed Gaussian random field in the model (Lindgren, Rue, and Lindström, 2011; Simpson, Lindgren, and Rue, 2012). This can be used to account for latent spatial or spatio-temporal structures in the data, explaining more variation than when using the covariates alone. The inclusion of a random effect in models can help to avoid spurious significance in estimation of fixed effects, and can improve accuracy of predictions. Implementing the model in `R-inlabru` improves its flexibility in this sense.

`R-inlabru` was originally developed with ecologist users in mind, and as such, one of the key principles of its development is to be user-friendly and accessible to non-statisticians (Illian and Burslem, 2017; Bachl et al., 2019). Syntax is more concise and easy to understand than in the predecessing `R-INLA` package, with a similar structure to the popular `R` function `glm` syntax. A criticism of the approach presented by Blackwell and Matthiopoulos (2024) is that it is too technically challenging to be accessible for ecologist users (Lauret et al., 2025). This is unsurprising, given that a common issue many users face with continuous-time movement modelling is accessibility (Patterson et al., 2017). By translating the approach to the `R-inlabru` framework, the models are presented in a familiar and accessible software package, wherein numerical computation is performed internally, and inference is made more interpretable through the use of inbuilt functions and visualisation tools.

Implementation of the model in `R-inlabru` also allows for various complexities to be built in to the observation process of the survey model. Many of the commonly used methods for fitting models to this macro-scale spatial data make the assumption that the full area has been observed, ignoring the complexities that usually impact data collection. For example, survey data are often collected along point or line transects, at subplots, or, in the case of citizen science or passive records, through some more complex unknown method of reporting. Ignoring the spatial structure of the data collection method during the model fitting stage means that the model will lack the crucial distinction between areas missing observations due to absence of the species, and those which have simply not been observed in the first place (and so wherein the presence/absence

of the species is unknown). R-inlabru was developed specifically to deal with incorporating complex observation processes, so is an ideal package for implementing the survey model (Yuan et al., 2017; Jullum, Thorarinsdottir, and Bachl, 2020).

In summary, implementation of the joint Langevin movement model in R-inlabru should enable computationally efficient and detailed inference from combined survey and telemetry data streams. Complex observation processes and spatial autocorrelation can be accounted for by methods already integral to the R-inlabru framework. Model fitting, prediction, and interpretation of outputs are user-friendly, making this technically challenging joint likelihood accessible to end-users.

4.1.6 Aims

This chapter aims to implement the joint Langevin movement model in R-inlabru. It will:

1. demonstrate the statistical theory behind and practical syntax of the implementation of the joint Langevin movement modelling framework in R-inlabru; see Section 4.2 and Section 4.3.2, respectively;

2. evaluate the effectiveness of the R-inlabru version of the models for habitat selection parameter estimation and prediction of spatial distribution (Section 4.3.2); and

3. investigate the benefits of the R-inlabru implementation of the framework, including: gains in computational efficiency (Section 4.3.5); inclusion of complex observation processes (Section 4.3.6); and accounting for unexplained spatial correlation through the inclusion of a Gaussian random field (Section 4.3.7).

4.2 Model Implementation

The following section describes the joint Langevin movement model, with some modifications for implementation in the R-inlabru framework. For a more in-depth description of the original model on which this is based, see Blackwell and Matthiopoulos (2024) and Michelot et al. (2019). In R-inlabru, the modelling framework is implemented as a joint model with 3 likelihoods: a Gaussian likelihood for each of the X and Y dimensions of the telemetry model, and a log

Gaussian Cox process (LGCP) likelihood for the survey model. The habitat selection parameters β are jointly estimated across the 3 likelihoods.

The survey and telemetry models are connected in their definition of the latent utilisation distribution, described using the linear predictor $\eta(x)$, which for the telemetry likelihoods is contained in the Langevin drift term $\tilde{b}(\cdot)$ (Equation 4.2). When placed in a joint modelling framework, data are integrated from the two sources to jointly estimate the habitat selection parameters β. A simplified diagrammatical representation of the model structure can be seen in Figure 4.1.

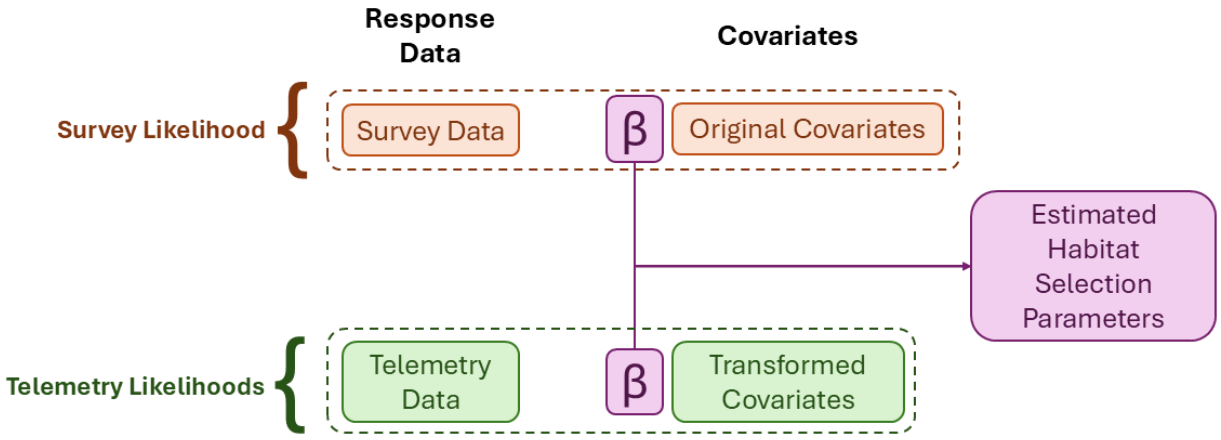

Figure 4.1: A simplified diagrammatical representation of the joint Langevin diffusion based movement model. Habitat selection parameters are jointly estimated from survey and telemetry data.

In essence, this joint model allows for the integration of two data streams at different spatio-temporal scales, and results in estimation of shared habitat selection parameters at the population-level; a macro-scale which is useful to inform conservation management strategies. Modelling is streamlined and accelerated by pre-processing: applying the gradient and smoothing transformations to the spatial covariates prior to model fitting.

4.2.1 Telemetry Model

The Langevin diffusion framework models the expected movement of an individual from its current location to the next location (in terms of X and Y coordinates) as a bivariate Gaussian distribution (see Equation 4.1). This means that the X and Y dimensions are jointly normally distributed, but are not correlated with one another, as they have the covariance structure

$$\Sigma = \begin{bmatrix} \Gamma\delta_t & 0 \\ 0 & \Gamma\delta_t \end{bmatrix}, \tag{4.7}$$

where the variance of the distribution for each dimension, $\sigma^2 = \Gamma\delta_t$, does not depend on the location of the animal.

To implement the telemetry model, the bivariate Gaussian distribution described in Equation 4.1 can be modelled as two independent univariate Gaussian distributions; one for each dimension X and Y. This formulation of the model relies on two theorems:

Theorem 1. *The marginal distributions of two random variables X and Y with bivariate normal distribution* $\phi(\mu_X, \mu_Y, \sigma_X^2, \sigma_Y^2, \rho)$ *are themselves normally distributed.*

Theorem 2. *Two uncorrelated random variables X and Y with bivariate normal distribution* $\phi(\mu_X, \mu_Y, \sigma_X^2, \sigma_Y^2, \rho)$ *are independent.*

Proofs of both Theorems 1 and 2 can be found in Section 4.7 of Bertsekas and Tsitsiklis (2002).

The joint Langevin movement model assumes no bias in the directionality of an individual track, so movement preferences are isotropic and only based on covariate values and location rather than direction. This lack of directional bias in the model means that the movement kernels in the X and Y dimensions are uncorrelated.

Being that the movement kernel follows a bivariate Gaussian distribution (Equation 4.1), the marginal distributions for the two dimensions X and Y are univariate Gaussian distributions (Theorem 1). Furthermore, since there is no bias in directionality in the model, the movement kernels for the two dimensions X and Y are uncorrelated, so are independent (Theorem 2). So, the locations in the two dimensions X and Y can be modelled as

$$\begin{aligned} X &\sim \mathrm{N}(\mu_X, \sigma_X^2) \\ Y &\sim \mathrm{N}(\mu_Y, \sigma_Y^2), \end{aligned} \tag{4.8}$$

where each one follows an independent Gaussian distribution.

In the INLA Gaussian likelihood, the mean is linked to the linear predictor through $\mu = \eta$. Therefore, the linear predictors specified in the x and y telemetry likelihoods are

$$\begin{aligned} \mu_X &= \eta(X) = X_t + \tilde{b}(X_t)\delta_t \\ \mu_Y &= \eta(Y) = Y_t + \tilde{b}(Y_t)\delta_t, \end{aligned} \tag{4.9}$$

where X_t represents the X-coordinate of the location x_{j_t}, and Y_t represents its Y-coordinate, and the definition of the mean is taken from Equation 4.1.

The diffusivity parameter Γ is fixed, as this avoids any additional complexity that would be introduced by having to estimate in the model a latent parameter which impacts both the mean and variance of the Gaussian likelihoods. This is related to animal mobility and is assumed to be equivalent to the distance moved in one unit of time. Choosing a sensible value for the Γ parameter is explored in Chapter 5. The telemetry likelihoods are therefore specified as Gaussian likelihoods with fixed precision. In INLA, the precision κ_1 of a Gaussian likelihood can be fixed by setting the value for θ_1

$$\theta_1 = \log(\kappa_1). \tag{4.10}$$

As shown in Equation 4.7, the variance of each Gaussian distribution is $\sigma^2 = \Gamma\delta_t$. Therefore the value of θ_1 is set to

$$\theta_1 = \log\left(\frac{1}{\Gamma\delta_t}\right). \tag{4.11}$$

The joint log-likelihood for the telemetry model can be described as

$$\begin{aligned} L_M(\beta) &= L_X(\beta) + L_Y(\beta) \\ &= \sum_{t=0}^{n-1} \log \mathrm{N}(X_{t+1} | X_t + \tilde{b}(X_t)\delta_t, \Gamma\delta_t) \\ &\quad + \sum_{t=0}^{n-1} \log \mathrm{N}(Y_{t+1} | Y_t + \tilde{b}(Y_t)\delta_t, \Gamma\delta_t), \end{aligned} \tag{4.12}$$

where the joint telemetry log-likelihood L_M is described using the log-likelihoods for each di-

mension L_X, and L_Y.

The telemetry likelihoods only consider locations in pairs (the current and next position of the individual). This Markov property means that incorporating multiple individuals into a single model is very straightforward because the full movement track is not taken into account. This enables the entire telemetry dataset to be modelled using just two likelihoods (one for each dimension), instead of requiring separate models for each individual, as was the case for the GF-iSSA model in Chapter 3.

4.2.2 Transformations

The mean of the bivariate Gaussian distribution described in Equation 4.1 ($\mu = x_j + \tilde{b}(x_j)\delta_{t_j}$) incorporates an approximation of the Langevin drift term $\tilde{b}(x_j)$. Note that here the x term represents information from both spatial coordinates, $x = \{X, Y\}$. This drift is what gives some estimated direction to the movement, setting it apart from random Brownian Motion. The Langevin diffusion for location x at time t satisfies the stochastic differential equation

$$dx(t) = b(x(t))dt + \frac{\Gamma}{2}d\mathbf{W}_2(t), \tag{4.13}$$

where $\mathbf{W}_2(t)$ is a 2-dimensional Brownian motion, Γ is a diffusivity parameter controlling the speed of the process (related to animal mobility), and $b(x(t))$ is the Langevin drift term. The Langevin drift term can be described using

$$b(x(t)) = \frac{\Gamma}{2}\nabla_x \log \pi(x(t)), \tag{4.14}$$

where it is related to the utilisation distribution $\pi(x)$, and $\nabla_x(\cdot)$ represents the gradient of a surface. The underlying utilisation distribution is assumed to represent the true long-term spatial distribution of the population, resulting from the cumulative effects of individuals moving according to shared habitat selection. The drift term impacting the expected movement of an individual is based on this latent distribution. Essentially, an individual's expected movement will follow the gradient of the utilisation distribution, drifting towards high-intensity areas.

The drift term described in Equation 4.14 is written in terms of continuous-time. In practice, a

time-discretisation of the process is used. This is achieved by using the standard Euler-Maruyama approach to approximate the process over a short timestep δ_t. Thus, the drift term is replaced with a discrete-time approximation as described in Equation 4.2. This introduces a smoothing kernel $G(\cdot)$. This smoothing transformation allows for a wider area of the utilisation distribution to be included in the calculation of drift - accounting for the fact that movement is taking place over a time *interval* and not just in a single instant. This avoids bias when working with the time-discretised version of the process.

In order to convert the linear predictor $\eta(\cdot)$ to the approximation of the Langevin drift term $\tilde{b}(\cdot)$, two transformations need to be applied: the gradient transformation $\nabla(\cdot)$, and the smoothing transformation $G(\cdot)$ (Equation 4.2). These transformations can be applied to the spatially-indexed covariates directly as a pre-processing step, to simplify and accelerate model fitting.

The first step in this process is a queen case gradient transformation applied to each cell in the covariate grid, as presented in Horn (1981). The gradient calculation is written using the following notation

$$\begin{matrix} Z_{-+} & Z_{0+} & Z_{++} \\ Z_{-0} & Z_{00} & Z_{+0} \\ Z_{--} & Z_{0-} & Z_{+-} \end{matrix},$$

where Z_{00} denotes the focal cell, and the signs indicate the position of the cell in relation to the focal cell, as shown. The first sign indicates a cell to the West (-) or East (+) of the focal cell, and the second sign indicates a cell to the South (-) or North (+) of the focal cell. For example, Z_{+-} indicates the cell diagonally South-East of the focal cell. Using this notation, the slope in the West-to-East direction p and the slope in the South-to-North direction q are calculated

$$\begin{aligned} p &= \frac{[(Z_{++} + 2Z_{+0} + Z_{+-}) - (Z_{-+} + 2Z_{-0} + Z_{--})]}{8\Delta x} \\ q &= \frac{[(Z_{++} + 2Z_{0+} + Z_{-+}) - (Z_{+-} + 2Z_{0-} + Z_{--})]}{8\Delta y}, \end{aligned} \tag{4.15}$$

where Δx is the grid interval in the West-to-East direction and Δy is the grid interval in the

South-to-North direction. In practice, this interval is determined by the spatial grid resolution of available covariate information. The impacts of spatial grain on habitat selection inference have been explored in a similar context in Chapter 3.

This particular type of gradient calculation was selected over the more simple rook case (including only adjacent cells and not diagonals) because the animal is assumed to be moving through continuous-space, so cells diagonally adjacent to the focal cell are still accessible and could influence movement. In this formulation, the horizontally and vertically adjacent cells have more weight in their respective calculations, but diagonal cells are also incorporated.

Following application of the gradient transformations, the resulting derivatives are smoothed according to $G(\cdot)$. This is done using a Gaussian kernel with scale parameter $\zeta\sqrt{\delta_t}$. The smoothing transformation is incorporated to avoid bias introduced by the time discretisation of the process. Thus, the scale parameter should be comparable to the distance moved in δ_t. If the diffusivity parameter Γ (related to animal mobility) is assumed to be equivalent to the distance moved in one unit of time, then the scale parameter can be set to $\zeta = \sqrt{\Gamma}$.

4.2.3 Survey Model

In R-inlabru the intensity of the IPP describing the utilisation distribution in the survey model (Equation 4.4) is modelled as a log Gaussian Cox process (LGCP). The definition of the log-likelihood matches Equation 4.5. continuous-space over the region A is approximated through the integration scheme using a Delaunay mesh triangulation.

4.2.4 Joint Model

The overall joint likelihood combines the survey likelihood (Equation 4.5) with the two telemetry likelihoods (Equation 4.12). The combined log-likelihood is

$$
\begin{aligned}
L(\alpha, \beta) &= L_S(\alpha, \beta) + L_X(\beta) + L_Y(\beta) \\
&= -\exp(\alpha) \int_A \exp(\eta(y)) dy + m\alpha + \sum_{i=1}^{m} \eta(y_i) \\
&\quad + \sum_{t=0}^{n-1} \log \mathrm{N}(X_{t+1} | X_t + \tilde{b}(X_t)\delta_t, \Gamma\delta_t) \\
&\quad + \sum_{t=0}^{n-1} \log \mathrm{N}(Y_{t+1} | Y_t + \tilde{b}(Y_t)\delta_t, \Gamma\delta_t),
\end{aligned}
\tag{4.16}
$$

which is a function of the habitat selection parameters β, and the intercept term α, related to population abundance.

4.3 Simulated Case Study

In order to demonstrate the implementation of the joint Langevin movement model in R-inlabru, a case study was carried out by fitting several models to simulated data. A number of different options and comparisons were evaluated. The remainder of this section is broken down as follows: Section 4.3.1 describes the methodology used to generate the simulated data; Section 4.3.2 compares the joint model with its requisite parts; Section 4.3.3 explores the impact of boundary conditions on generating simulated data; Section 4.3.4 explores the impact of poor quality datasets on the models; Section 4.3.5 compares the R-inlabru implementation of the model against a JAGS version to investigate computational cost; Section 4.3.6 demonstrates inclusion of complex observation processes; and finally Section 4.3.7 illustrates the inclusion of a Gaussian random field (GRF) in the linear predictor.

All analysis was carried out using R version 4.5.1 (R Core Team, 2025), R-INLA version 25.06.22-1 (Rue, Martino, and Chopin, 2009), and R-inlabru version 2.12.0.9022 (Bachl et al., 2019) with a 2.4GHz 4C processor (16GB RAM).

4.3.1 Simulation Methodology

The following subsection contains a description of the method used to simulate data for model evaluation and comparison. The simulated data were produced using Langevin diffusion based movement rules, applied to an intensity surface generated using spatial covariates and fixed habi-

tat selection parameters.

The first step needed to simulate data involved the creation of spatial covariates, to describe the 'landscape' over which the individuals would 'move'. Two spatially structured covariates were created over a 100×100 grid. These consisted of an 'environmental' covariate with fine-scale heterogeneity ($c_{env}(x)$), and an 'attraction to centre' covariate peaking at the centre of the study area and gradually decreasing towards the boundary in all directions ($c_{mid}(x)$). In comparison to a real-world application, the environmental covariate could represent a heterogeneous habitat variable such as vegetation, whereas the attraction to centre covariate might represent a behavioural influence wherein individual movement is constrained to some distance from a given centre of attraction, such as in a central place foragers or colonial populations. For the purpose of this simulation, the attraction to centre covariate also serves to keep the population of simulated individuals within the area of interest, as otherwise the directional gradient of the environmental covariate alone would lead to an unnecessary wastage of simulation time wherein individual movement may 'drift off of the page'. A boundary condition is also implemented to prevent this issue from occurring. However, parameter estimation is one of the key criteria used to evaluate the performance of the models, and a boundary condition is an influence on movement behaviour which diverges from the rules generated by the parametrised 'true intensity' (see Section 4.3.3 for an exploration of this effect). Thus, the attraction to centre covariate is included to reduce the strength of the effect of the boundary condition on influencing movement behaviour.

The values of both covariates were set to a range of 0 to 1. The smoothing and gradient transformations from Equation 4.2 were then applied to the covariates. The original and transformed covariates are displayed in Figures 4.2 and 4.3.

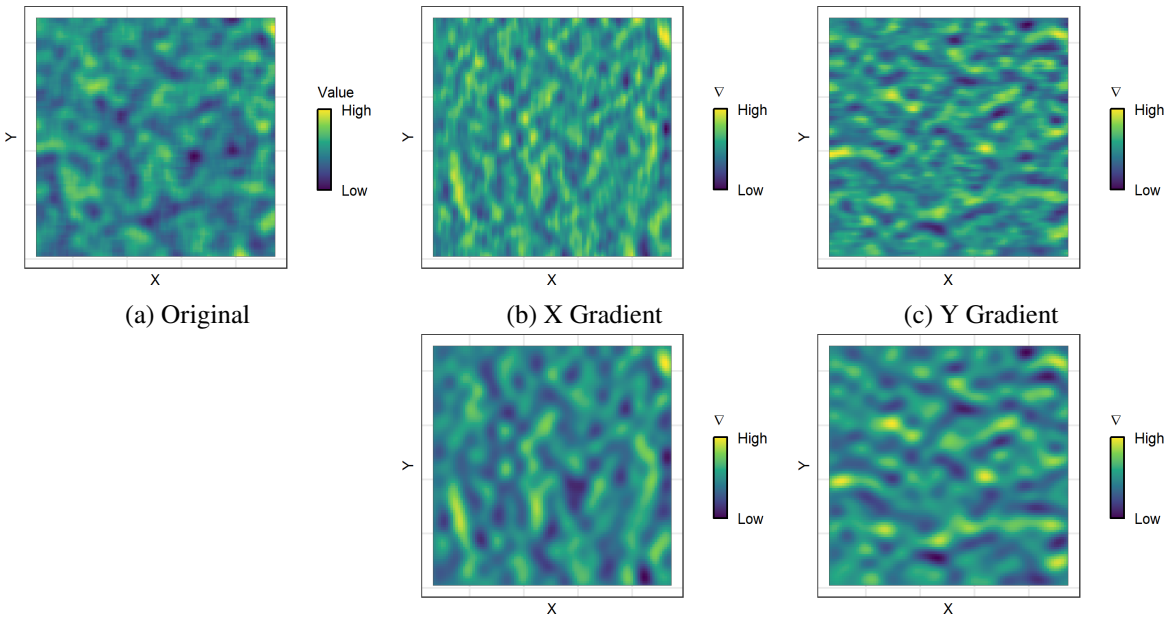

(a) Original (b) X Gradient (c) Y Gradient

(e) Smoothed X Gradient (f) Smoothed Y Gradient

Figure 4.2: The environmental covariate $c_{env}(x)$: (a) the original (non-transformed) covariate; (b) the x gradient; (c) the y gradient; (d) the smoothed x gradient; and (e) the smoothed y gradient. The colour scale of all plots follows a relative gradient from low (blue) to high (yellow).

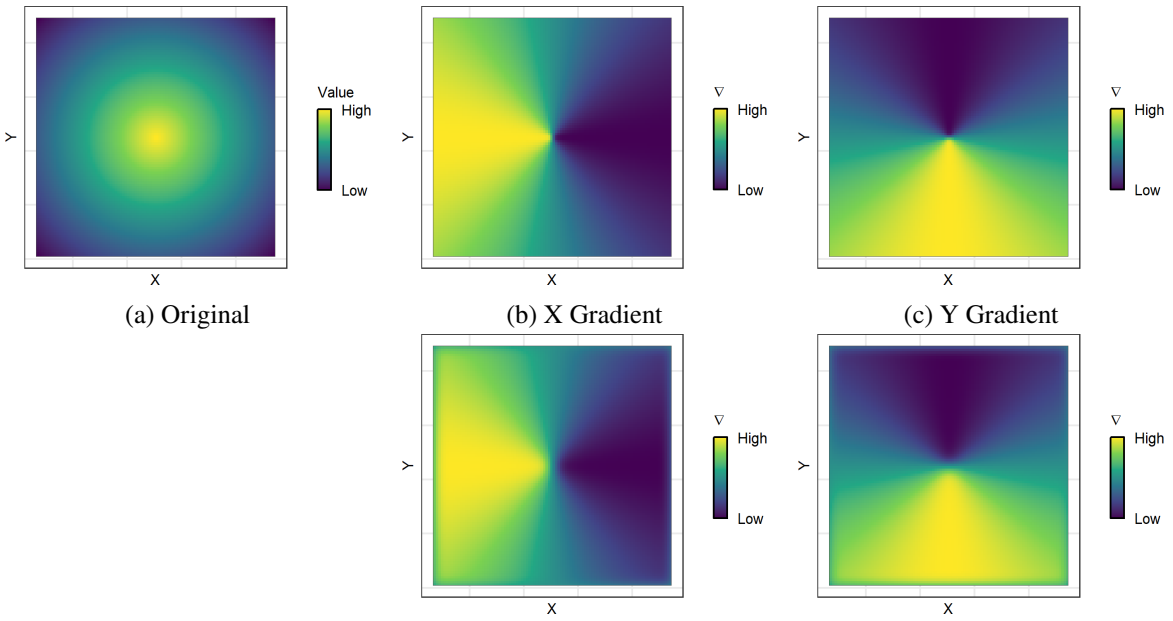

(a) Original (b) X Gradient (c) Y Gradient

(e) Smoothed X Gradient (f) Smoothed Y Gradient

Figure 4.3: The attraction to centre covariate $c_{mid}(x)$: (a) the original (non-transformed) covariate; (b) the x gradient; (c) the y gradient; (d) the smoothed x gradient; and (e) the smoothed y gradient. The colour scale of all plots follows a relative gradient from low (blue) to high (yellow).

A grid of the true intensity surface was created using the original (non-transformed) covariates (see Figure 4.4). The value of true intensity in each grid cell was defined as

$$\lambda(x) = \exp\left(\alpha + \beta_{env} \cdot c_{env}(x) + \beta_{mid} \cdot c_{mid}(x)\right), \tag{4.17}$$

where $\alpha = -7$, $\beta_{env} = 2$ and $\beta_{mid} = 3$.

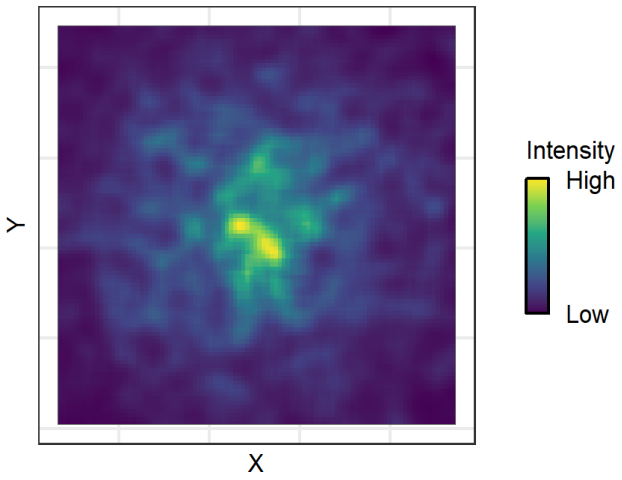

Figure 4.4: The intensity surface generated from fixed parameters and spatial covariates. The colour scale follows a gradient of relative intensity from low (blue) to high (yellow), as interest is in relative differences across space and not absolute values.

To calculate the number of individuals to include in the simulation, a value was randomly sampled from a Poisson distribution with rate parameter equal to the sum of the intensity surface λ. This resulted in a total of 114 individuals in the simulation.

The Langevin diffusion based movement rules require information on the location of an individual at the previous timestep. Therefore, the simulated tracks require a start point. The start point of each individual track was generated directly from the intensity surface. A sample was taken from the cell index of the intensity grid, with a probability proportional to the λ value for each cell. Replacement was set as TRUE so that the same cell may be used more than once.

The location of each individual at time $t + 1$ was generated using a sample (of size 1) from a bivariate Gaussian distribution with mean $\mu = x_t + \tilde{b}(x_t)$ and covariance matrix $\Sigma = \Gamma I_2$. These definitions come from Equation 4.1 but are simplified because $\delta_t = 1$ in the simulation. Γ is the diffusivity parameter controlling the speed of the process. It is related to animal mobility and

here was defined to be equivalent to the width of 1 covariate grid cell. This process was repeated so that each individual track contains 1000 observations. The output from the simulation can be seen in the form of individual tracks and an overall heatmap in Figure 4.5. The heatmap is used to identify whether the simulated data provides a good representation of the true underlying intensity surface (Figure 4.4).

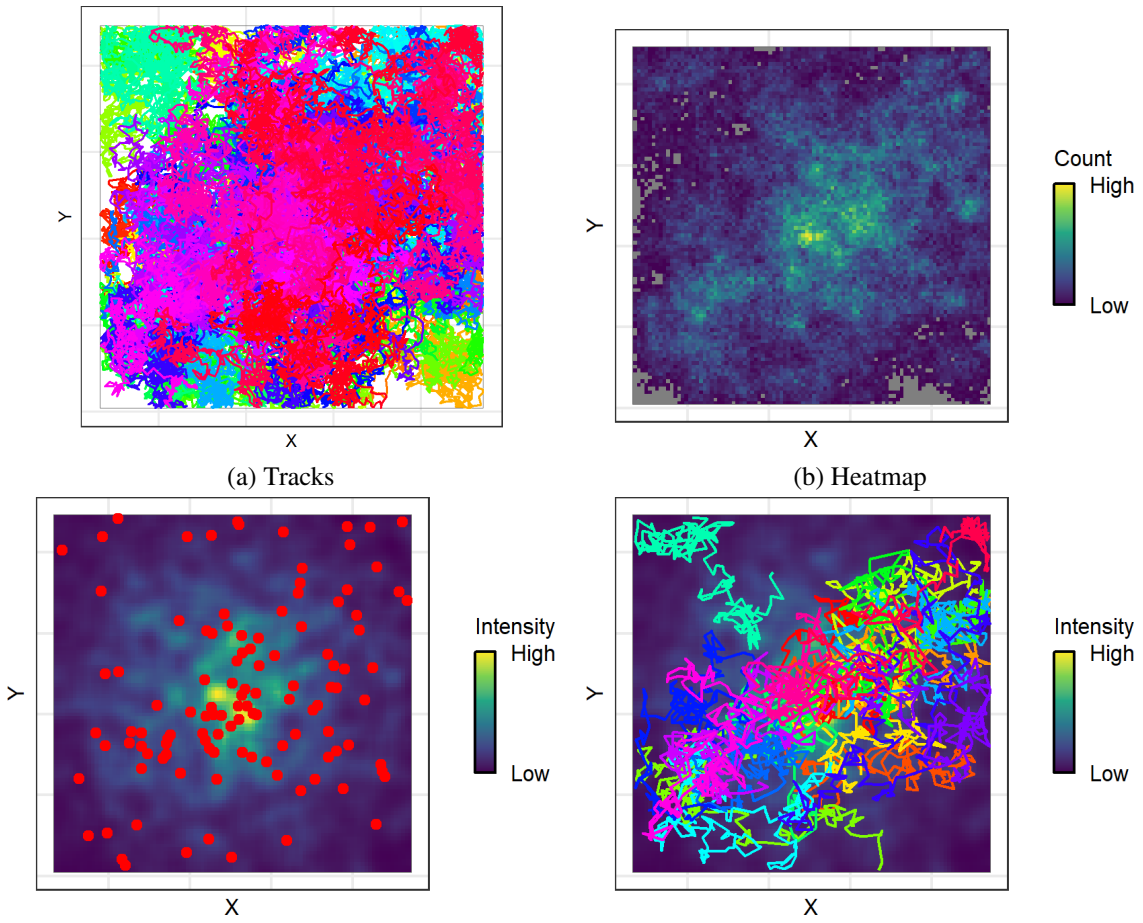

(a) Tracks (b) Heatmap

(c) Survey Data (d) Telemetry Data

Figure 4.5: (a) The simulated tracks for 114 individuals generated using Langevin diffusion based movement rules, coloured by individual. (b) A heatmap of the simulated data, generated by counting the number of observations within each cell of a fine grid. The colour scale follows a gradient of counts from low (blue) to high (yellow), as interest is in relative differences across space and not absolute values. Grey indicates a zero count. (c) Survey data points (red) consisting of the locations of all individuals in the simulation at time $t = 1000$. (d) Telemetry tracks for 20 individuals, generated from a thinned version of the simulated data. Tracks are coloured by individual. Background colour scale for (c) and (d) shows true intensity, which follows a gradient of relative intensity from low (blue) to high (yellow), as interest is in relative differences across space and not absolute values.

If the individual was estimated to move outside of the study area boundary in a given step, this

step was rejected. The step was resampled from the distribution until a step was found that fell within the boundary of the study area. This represents a hard boundary, which is the boundary condition which introduces the least bias to the movement behaviour (see Section 4.3.3 for more details).

Survey data were collected by taking a 'snapshot' of the locations of all individuals at a single time point (the final step of the simulation, $t = 1000$). Using the final step ensures that data are not counted twice in the joint modelling framework, as this step is not included in the telemetry dataset. It also ensures that the distribution of the survey data is representative of the steady-state distribution defined by the Langevin diffusion movement rules, as it has had a long burn-in period (although this is a minor concern given that the initial locations are derived directly from the true intensity). The distribution of the survey data is displayed in Figure 4.5.

Telemetry data were collected by selecting a random sample of 20 of the regular simulated tracks. The tracks were thinned so that only 1 in every 5 observations were collected. This was done to reflect the case that real telemetry data are collected on a coarser temporal scale than that at which the movement process is operating. As mentioned, the final step for each track ($t = 1000$) was removed as it is missing information needed for modelling (the location of the individual at time $t + 1$ is required, and cannot be calculated for this final step). Removing this step also ensures that the observation is not counted twice in the joint model, as it is used as survey data. The spatial distribution of the tracks can be observed in Figure 4.5.

These simulated datasets are used to fit and compare models in Sections 4.3.2, 4.3.5, and 4.3.4. The parametrisation of the true intensity (Equation 4.17) provides a yardstick against which to assess the accuracy of parameter estimation in the models, and the true intensity surface (Figure 4.4) provides a means of visually assessing predictive accuracy and the models' ability to recover a representation of the steady state distribution. Sections 4.3.3 and 4.3.7 use a similar approach to that described in this section, but with some differences in the specification of the boundary conditions, or in the component makeup of the true intensity, respectively.

4.3.2 Modelling in R-inlabru

Implementing the joint Langevin movement model in R-inlabru provides a user-friendly environment for model fitting, as well as interpreting and plotting model outputs. R-inlabru code is concise, and the software package contains existing methods for predicting from complex spatial models. This subsection demonstrates the implementation of the joint movement model, as well as its requisite parts, in the R-inlabru package. It also demonstrates the speed and accuracy of this method for inference.

Three models were fitted to the survey and telemetry data generated from the simulation: the survey model, the telemetry model, and the joint model. The survey model is the inhomogeneous Poisson process (IPP) with intensity defined in Equation 4.4, fitted as a log Gaussian Cox process (LGCP) in R-inlabru. An example of this model is shown in Code Listing 1. The model components contain the intercept term, the values of the environmental and attraction to centre covariates (derived from spatial Spatraster objects), and the covariate coefficient terms. Covariates are not included using a linear mapper, as would be typical in inlabru syntax, to allow the coefficients to be jointly estimated with the telemetry likelihoods in the Joint model (Code Listing 3), although this syntactical difference does not impact parameter estimation in the survey model. The components are combined in an additive formula. The likelihood defines the model family as LGCP, and calls to the survey data; boundary of the area of interest; and the Delaunay mesh triangulation representation of continuous-space (all previously constructed). Finally, the model is fitted by combining the components and likelihood in the bru() call.

Listing 1: Survey Model

```
## Specify survey model components
cmp_surv <- ~ Intercept(1) +
  env_val(main=env_covariate,
          main_layer="env",
          model="const") +
  mid_val(main=mid_covariate,
          main_layer="mid",
          model="const") +
  beta.env(1)+
  beta.mid(1)

## Specify survey formula
form_surv <- geometry ~ Intercept +
  (env_val*beta.env) +
  (mid_val*beta.mid)

## Specify survey likelihood
lik_surv <-
  like(formula=form_surv,
       family="cp",
       data=surv_pts,
       samplers=bnd_sf,
       domain=list(geometry=mesh))

## Fit survey model
fit_surv <- bru(cmp_surv,
                lik_surv)
```

The telemetry model is the Langevin diffusion based movement model consisting of the joint model of the X and Y dimension likelihoods, as defined in Equation 4.12 and fitted using a joint model of two Gaussian likelihoods in R-inlabru. The code for this model can be seen in Code Listing 2. The model is defined using the same structure as the survey model: components, formula, and likelihood. The formulae are separate for the x and y dimensions, each specifying the mean of an independent Gaussian distribution as defined in Equation 4.1. The smoothing and gradient transformations incorporated in the drift term (Equation 4.2) are applied during pre-processing of the covariates, as in Section 4.3.1. As such, location and environmental data are supplied directly to the formulae from columns in a data frame object. There is also a different

likelihood for each dimension, wherein the family is defined as Gaussian and the precision is fixed to the θ_1 parameter, as defined in Equation 4.11. The final `bru()` call fits a joint model, combining both likelihoods.

Listing 2: Telemetry Model

```
## Specify telemetry model components
cmp_tel <- ~ 0 + beta.env(1) + beta.mid(1)

## Specify telemetry formulae
form_tel_x <- loc_tplus1_x ~
  loc_t_x + (Gamma/2)*((envvalx*beta.env)+
                         (midvalx*beta.mid))*delta_t

form_tel_y <- loc_tplus1_y ~
  loc_t_y + (Gamma/2)*((envvaly*beta.env)+
                         (midvaly*beta.mid))*delta_t

## Specify telemetry likelihoods
lik_tel_x <-
  like(formula=form_tel_x,
       family="gaussian",
       data=tel_pts,
       control.family=list(hyper=list(prec=list(fixed=TRUE,
                                                initial=theta1))))
lik_tel_y <-
  like(formula=form_tel_y,
       family="gaussian",
       data=tel_pts,
       control.family=list(hyper=list(prec=list(fixed=TRUE,
                                                initial=theta1))))

## Fit model
fit_tel <- bru(cmp_tel,
               lik_tel_x,
               lik_tel_y)
```

Finally, the joint model is the three-likelihood joint model which combines the one survey and two telemetry likelihoods, as defined in Equation 4.16. The code for this model, as seen in Code Listing 3, simply combines the likelihoods from the survey and telemetry models defined in Code Listings 1 and 2.

Listing 3: Joint Model

```
## Fit model
fit_joint <- bru(cmp_surv,
                 lik_tel_x,
                 lik_tel_y,
                 lik_surv)
```

Implementation in the INLA framework makes the models highly computationally efficient. The running times were: 5.47 seconds, 4.31 seconds, and 5.45 seconds for the survey, telemetry, and joint models respectively when fitted with a 2.40GHz i5 processor (16GB RAM). Despite the additional complexity introduced by the joint modelling framework, the joint model actually took less time to run than the survey model (time difference: 0.02 seconds). This may be due to improved convergence times through the introduction of additional information, since the joint model integrates multiple data sources.

The models fitted to the survey data (the survey and joint models) include an intercept parameter α, the true value of which is -7. All of the models include coefficients for the two covariates, β_{env} and β_{mid} the true values of which are 2 and 3, respectively. A summary of the estimated parameter means and their 95% credible intervals is shown in Table 4.1. The survey and joint models estimated intercept terms with means close to and 95% credible intervals containing the true parameter value of -7. For each of the models, the covariates were estimated to have a positive effect, with means close to and 95% credible intervals containing the true parameter values of 2 and 3 for the environmental covariate and attraction to centre covariate coefficients, respectively.

Table 4.1: Posterior mean and 95% credible intervals for the Intercept, β_{env}, and β_{mid} parameters from the survey, telemetry, and joint models. All values given are rounded to 2 decimal places.

Model	Intercept	β_{env}	β_{mid}
Survey Model	-6.62 [-7.54,-5.70]	1.60 [0.11,3.09]	2.69 [1.81,3.58]
Telemetry Model	NA	2.09 [1.09,3.10]	2.96 [0.98,4.93]
Joint Model	-6.81 [-7.46,-6.15]	1.94 [1.11,2.78]	2.74 [1.93,3.55]

The fitted survey, telemetry, and joint models were used to predict onto a spatial grid over

the study area to provide an estimate of the utilisation distribution (see Figure 4.6). These predictions can be compared to Figure 4.4, to see that the models returned a visually comparable estimate of the spatial distribution of the true intensity surface. Spatial predictions provide a clear communicative tool for understanding animal space-use which can be used to inform management decisions in real-world applications. The `R-inlabru` `predict()` function makes spatial prediction straightforward.

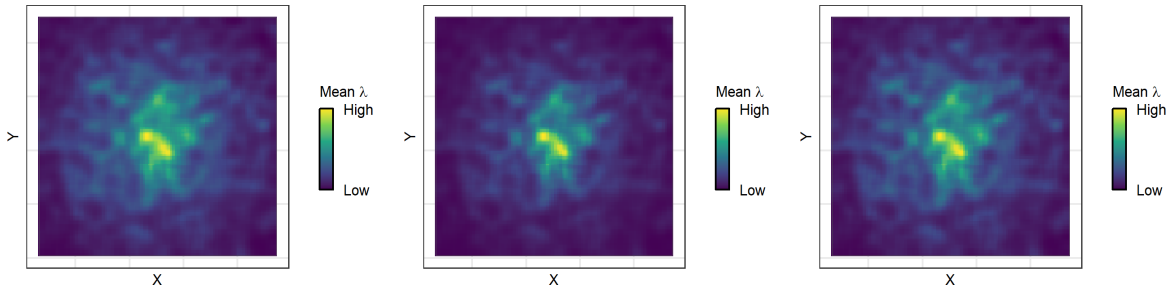

(a) Survey (b) Telemetry (c) Joint

Figure 4.6: The predictions of the spatial distribution of intensity (i.e., a spatial representation of the utilisation distribution surface) from (a) the survey model, (b) the telemetry model, and (c) the joint model. The colour scale for each plot follows a gradient of relative mean predicted intensity from low (blue) to high (yellow), as interest is in relative differences across space and not absolute values.

Abundance calculations were also carried out using predictions from the survey and joint models, giving estimates and 95% credible intervals of 113.13 [93.91, 136.41] and 113.63 [93.64, 135.81], respectively. The true number of individuals in the study was 114, so abundance was accurately returned by both models.

4.3.3 Optimisation of Boundary Conditions for Simulation

The Langevin diffusion method for modelling movement assumes convergence towards a steady-state distribution (i.e., a description of overall space-use which does not change over time). In real-world applications, this does not necessarily require the population to be closed or individuals to remain within the study area, but only that the overall behaviour of the group (in terms of its relationship with the spatially-structured covariates) remains the same. This means that this model would be inappropriate for modelling long-term shifts in population distribution, such as migration, which may be more appropriately investigated using the methodology of Buderman et al. (2025). Randomness in movement behaviour and variation at the individual-level may

permit some individuals to leave the area, but this does not negate the effect of the utilisation distribution, which describes overall group-level, long-term space-use preferences. In the joint model, the base-rate intensity of the population (i.e., the number of individuals) is captured by the intercept term of the survey likelihood (Equation 4.5) - so if the size of the group is greatly enlarged or reduced this would affect the description of the utilisation distribution, but in scale only - the relative spatial distribution of the intensity surface would remain the same. Thus, if the aim of a study is to elicit overall population habitat selection, even when some individuals may leave the area of interest, this model is appropriate. The exact number of individuals that may exit the study area without impacting the assumptions of the model has not yet been investigated, and poses an area of future research interest. Though not the focus here, estimating abundance is also possible, and accurate, but modifications would be required if abundance was to change over time as the purely spatial nature of the survey model is intrinsic to the model formulation - incorporating a temporal dependency to the intercept term used in abundance estimation would require future research to assess feasibility.

Although it is not necessary to have data on a closed population for application of the models, in a simulation context, having simulated individuals drift outside of the study area is inefficient. Once a simulated individual has left the area defined by the constructed covariates, there is no information on the gradient of the underlying distribution outside of this fixed area, meaning that the remainder of the track is lost. This is in contrast to the aim of simulation: to generate data. The attraction to centre covariate is used to encourage simulated individuals to remain within the area of interest. However, there is a level of randomness included in the simulated movement behaviour via Brownian Motion. So, individuals do not have to strictly adhere to the gradient defined by the true intensity, and may follow a path which moves outside of the defined area. To combat this, ensuring computational efficiency and data retainment, a boundary condition is imposed on the simulation.

If simulated behaviour is assumed to behave according to the Langevin diffusion movement rules, then a boundary condition is an extraneous influence outside of the parametrised utilisation distribution. This could cause biases, violating the assumptions of the models by altering the behaviour exhibited by the simulated individuals. This is particularly pertinent as the parameters

describing the true intensity surface are used to assess the accuracy of the models. Therefore, it is in the interests of this chapter to assess the impact of boundary conditions on model outputs, and determine which type of boundary condition may cause the least bias.

Here, four types of boundary condition are considered:

Hard Boundary: As described in Section 4.3.1, a hard boundary means that if a step in a track is estimated outside of the given area, this is rejected, and the step is resampled until a step within the area is estimated. In this way, the new step is still estimated from the true utilisation distribution, but with some interference.

Toroidal Boundary: The toroidal boundary condition means that if a step in a track is estimated outside of the given area, the individual immediately re-enters the area at the opposite end of the axis.

Respawning: In the respawn simulation, if a step in a track is estimated outside of the fixed area, the next step is allowed to be estimated anywhere in the study domain, with a probability of occurring in a given cell determined according to the true intensity. Essentially, the individual 'leaves' the area and is 'respawned' anywhere, according to the utilisation distribution.

No Boundary: In this version of the simulation, animals move off the edge of the study area and may or may not re-enter. This is made possible by first simulating on a larger area, and then cropping to a smaller central area to collect data for model fitting. This solves the problem of the undefined gradient outside of the study area boundary, but is also more computationally costly and wasteful compared to the other options for simulation.

Each of the four versions of the simulation was run using Langevin diffusion movement rules, with drift defined according to the same true intensity surface (as described in Equation 4.17). Figure 4.7 contains an example of a few of the simulated tracks from each simulation, to give a visual representation of the simulated movement behaviour. From a visual assessment alone, it is apparent that the toroidal boundary condition creates an unrealistic representation of movement, wherein the individual is estimated to move much farther than is expected given the diffusivity

parameter (related to animal mobility and defined here to cover a single grid-cell). The respawn condition also creates some unrealistically large steps in the movement tracks, although not as many as with the toroidal boundary condition.

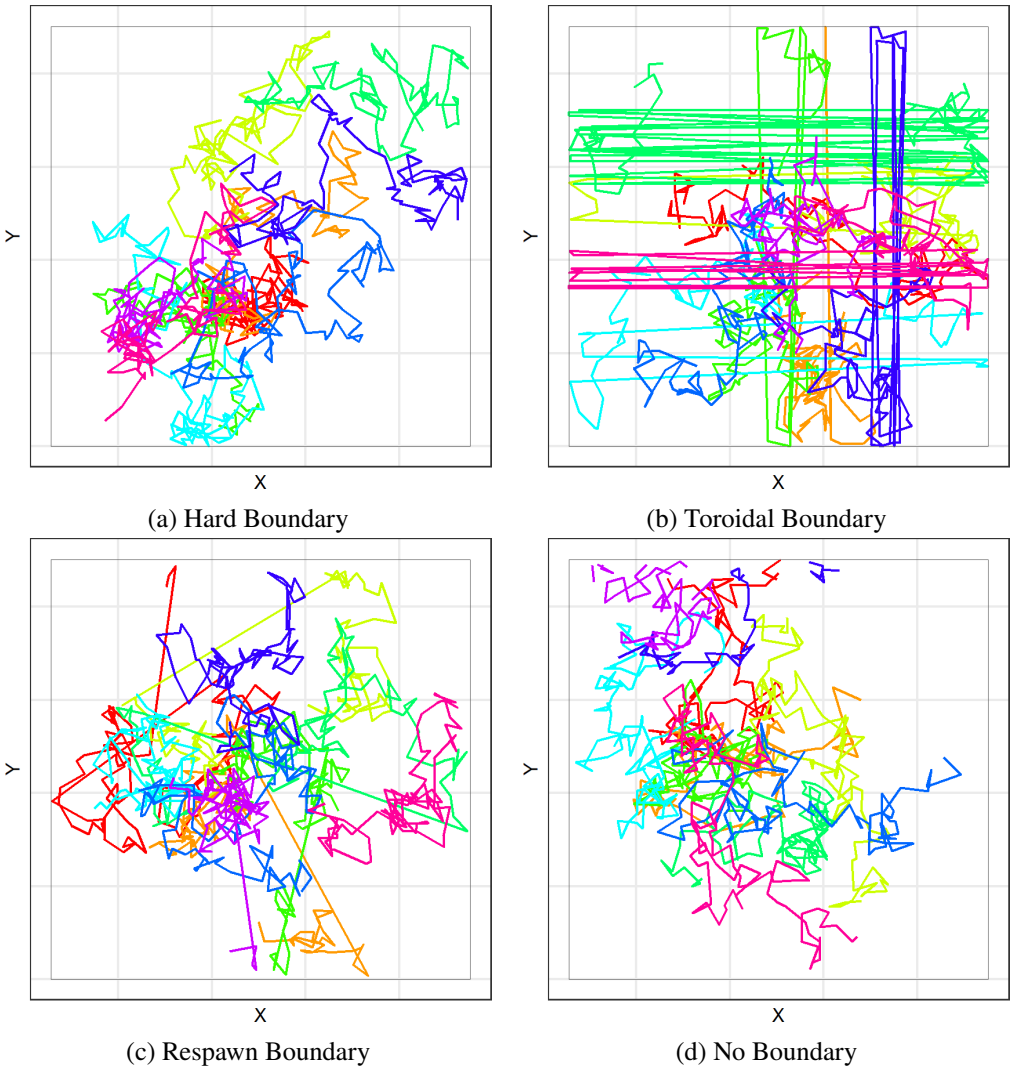

(a) Hard Boundary (b) Toroidal Boundary

(c) Respawn Boundary (d) No Boundary

Figure 4.7: Examples of 10 spatial tracks generated from simulation with (a) Hard Boundary; (b) Toroidal Boundary; (c) Respawn Boundary; and (d) No Boundary. Tracks are coloured by individual.

Figure 4.8 contains a heatmap representation of all of the observations from each simulation. This provides a visual means of assessing how well the raw simulated data can recover the spatial distribution of the true intensity surface (see Figure 4.11 for comparison). The hard boundary condition produces a simulated dataset with the most spatial coverage out of the four, although this is balanced by not capturing the highest intensity areas of the true intensity as strongly. On

the other hand, the respawn dataset captures the high intensity areas, but has the poorest spatial coverage of the four simulations.

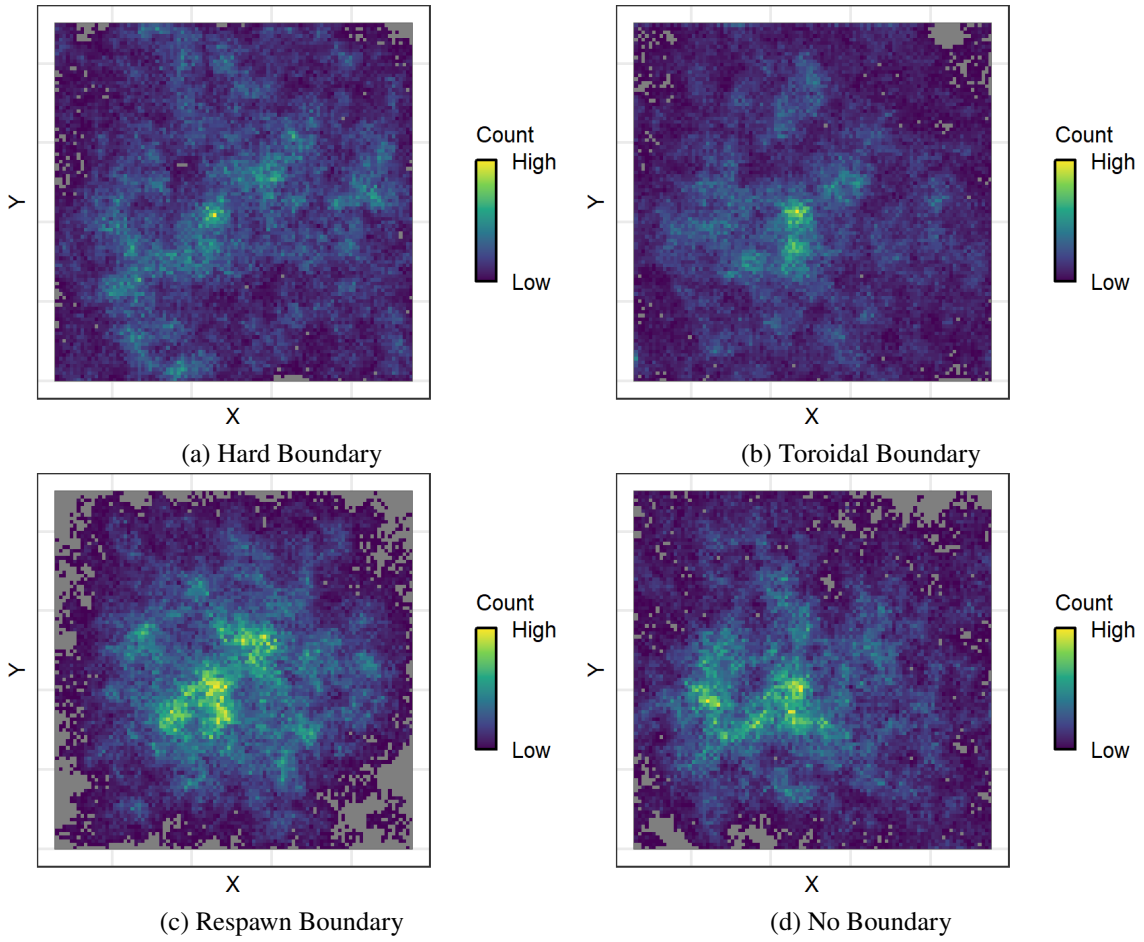

(a) Hard Boundary (b) Toroidal Boundary

(c) Respawn Boundary (d) No Boundary

Figure 4.8: Heatmaps of data generated from simulation with (a) Hard Boundary; (b) Toroidal Boundary; (c) Respawn Boundary; and (d) No Boundary. Heatmaps were generated by counting the number of observations within each cell of a fine grid. The colour scale follows a gradient of counts from low (blue) to high (yellow), as interest is in relative differences across space and not absolute values. Grey indicates a zero count.

As in Section 4.3.1, a survey dataset was produced from each simulated dataset by taking a snapshot of the overall population at the 1000th timestep. As well as the datasets taken from each of the four simulations, a dataset is generated directly from the intensity surface by taking a sample from the cell index of the intensity grid, with probability equal to the cell λ value. This represents a completely unbiased version of the survey data, for comparison against the other simulated datasets. Figure 4.9 displays the spatial distribution of the 5 survey datasets. The poor spatial coverage of the respawn simulation can again be observed here, as it translates to a bias

toward the centre in the distribution of the respawn survey data, compared to the distribution of points generated directly from the true intensity surface.

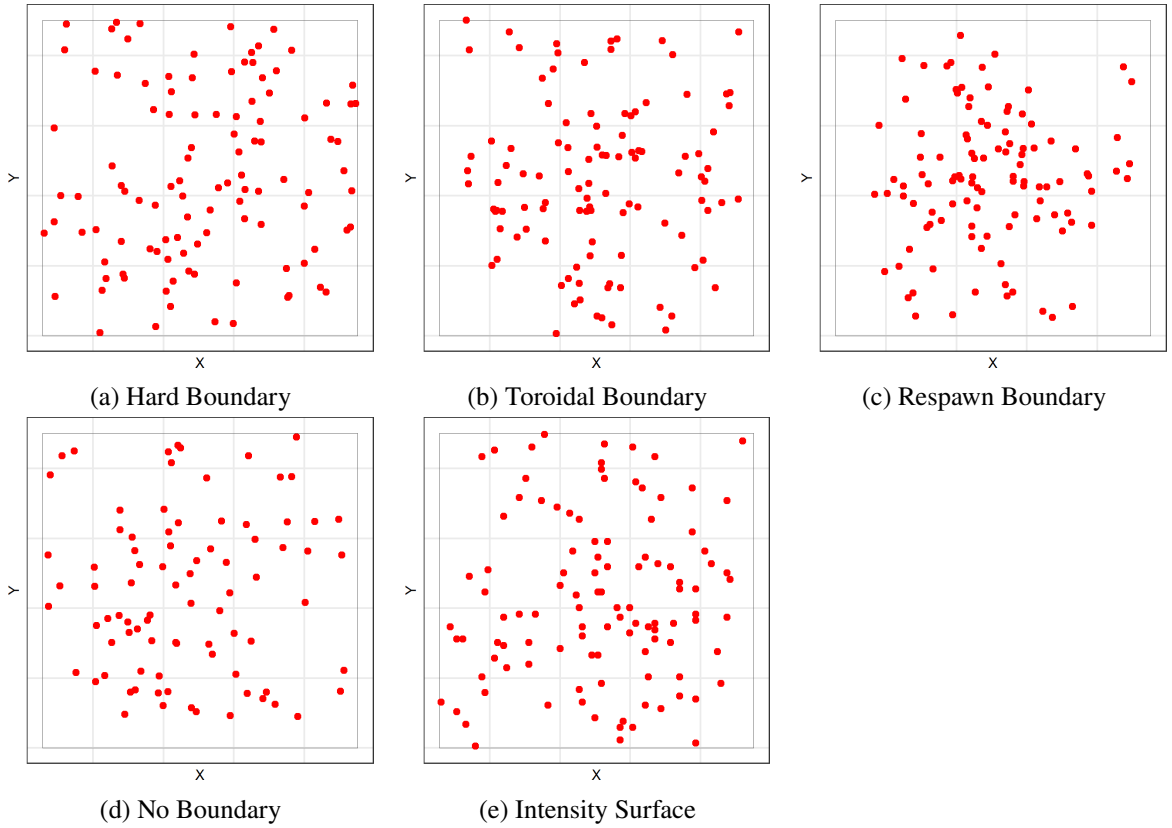

(a) Hard Boundary (b) Toroidal Boundary (c) Respawn Boundary

(d) No Boundary (e) Intensity Surface

Figure 4.9: Spatial distribution of survey data generated from simulation with (a) Hard Boundary; (b) Toroidal Boundary; (c) Respawn; (d) No Boundary; and (e) generated directly from the intensity surface.

The survey model, an inhomogeneous Poisson process (IPP) with intensity as described in Equation 4.4, was fitted to each of the five datasets using a log Gaussian Cox process (LGCP) model in R-inlabru. The predictor of the model contained an intercept term, and the two spatial covariates constructed in Section 4.3.1. The posterior estimates for the intercept, as well as the coefficients for each of the covariates estimated by each of the five models, are contained in Figure 4.10 and Table 4.2. The influence of the wide spatial coverage created by the hard boundary condition can be observed here, as the effect of the attraction to centre covariate is underestimated, and the intercept term is overestimated, to compensate, by the model fitted to these data. The model fitted to the dataset derived from the simulation with no boundary condition best matches the estimates from the model fitted to data derived directly from the true intensity.

These models, along with the toroidal model, most accurately estimate the true parameter values. The model fitted to respawn simulated data overestimates the effects of both the attraction to centre and environmental covariate, and underestimates the intercept term.

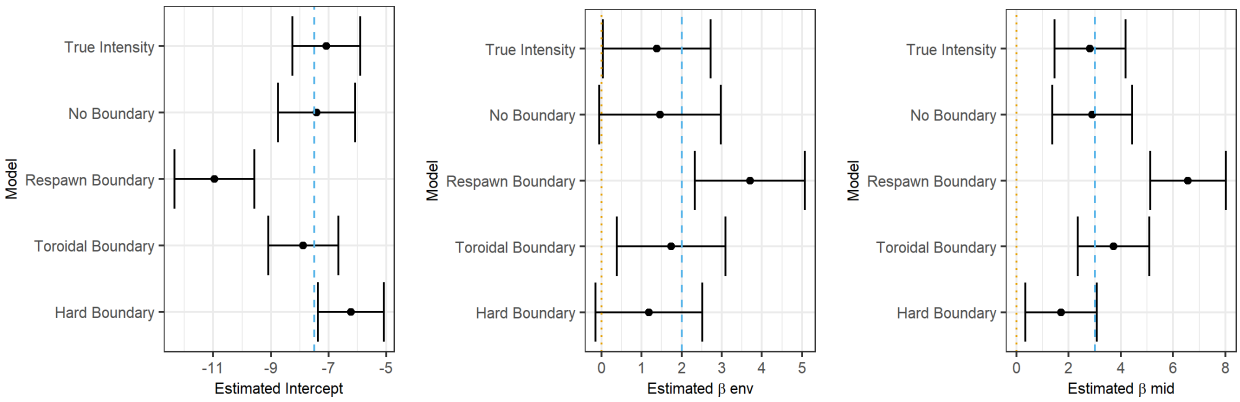

(a) Intercept (b) β_{env} (c) β_{mid}

Figure 4.10: Posterior mean and 95% credible intervals for the (a) Intercept, (b) β_{env}, and (c) β_{mid} parameters from the models fitted to the five survey datasets. True parameter values (-7.5, 2, and 3, respectively) are shown with dashed vertical lines.

Table 4.2: Posterior mean and 95% credible intervals for the Intercept, β_{env}, and β_{mid} parameters from the models fitted to the five survey datasets. All values given are rounded to 2 decimal places.

Dataset	Intercept	β_{env}	β_{mid}
Hard Boundary	-6.22 [-7.36,-5.07]	1.18 [-0.15,2.52]	1.71 [0.35,3.07]
Toroidal Boundary	-7.87 [-9.09,-6.66]	1.74 [0.39,3.09]	3.72 [2.35,5.08]
Respawn	-10.96 [-12.35,-9.58]	3.70 [2.33,5.07]	6.57 [5.12,8.02]
No Boundary	-7.41 [-8.75,-6.08]	1.46 [-0.05,2.98]	2.91 [1.38,4.44]
True Intensity	-7.07 [-8.25,-5.89]	1.38 [0.04,2.73]	2.81 [1.46,4.17]

The utilisation distribution was also predicted using each of the five models (Figure 4.11). All models predict the spatial distribution of the true intensity surface with reasonable accuracy. However, the poor spatial coverage of the respawn data can again be seen here, with a central bias in the predicted distribution of intensity.

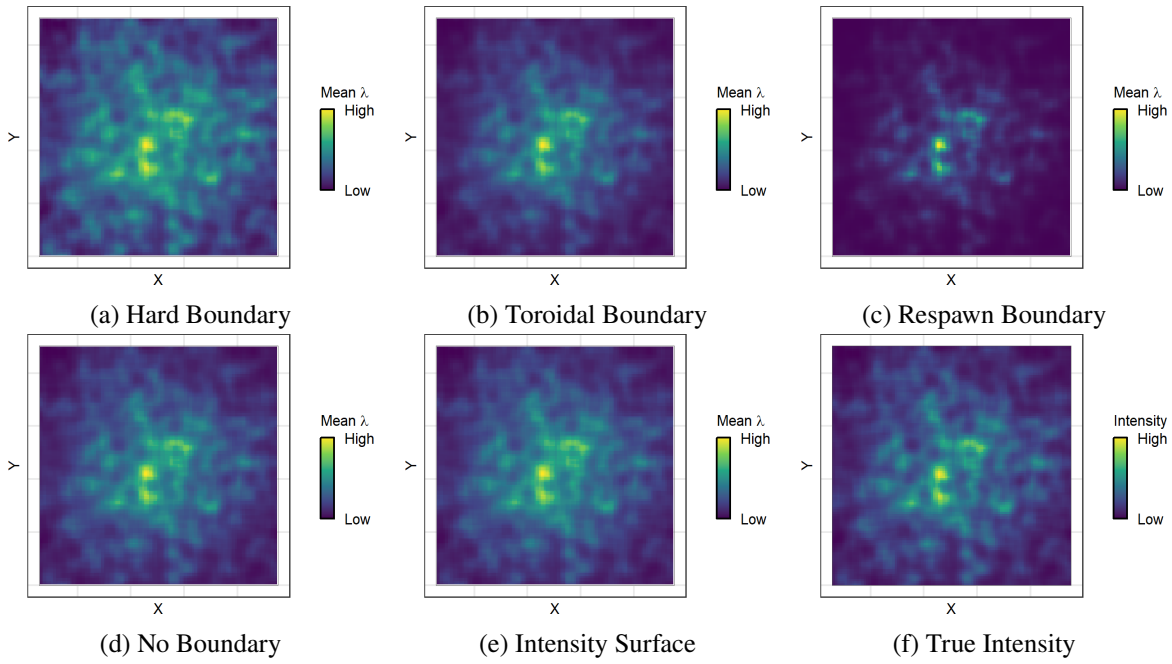

(a) Hard Boundary (b) Toroidal Boundary (c) Respawn Boundary

(d) No Boundary (e) Intensity Surface (f) True Intensity

Figure 4.11: Predictions of the utilisation distribution from the models fitted to the survey data generated from simulation with (a) Hard Boundary; (b) Toroidal Boundary; (c) Respawn; (d) No Boundary; and (e) generated directly from the intensity surface. (f) the true intensity surface. The colour scale follows a gradient of relative mean intensity from low (blue) to high (yellow), as interest is in relative differences across space and not absolute values.

Abundance was also estimated using each of the five models (Table 4.3). The true number of individuals for this set of simulations was 108, so abundance was accurately returned by all models except the one fitted to the data from the simulation with no boundary conditions. This simulation allowed individual tracks to move outside of the study area, and therefore resulted in a loss of data.

Table 4.3: Posterior mean and 95% credible intervals for estimated abundance from the models fitted to the five survey datasets. All values given are rounded to 2 decimal places.

Dataset	Abundance Estimate
Hard Boundary	108.11 [89.16,129.49]
Toroidal Boundary	107.74 [87.34,128.71]
Respawn	108.09 [88.85,129.08]
No Boundary	85.15 [69.18,103.40]
True Intensity	107.80 [89.84,129.80]

This subsection focused on the influence of boundary conditions in the simulation on the dis-

tribution of simulated data and outputs of the survey models. The toroidal boundary condition does not incur any biases in the distribution of survey data, and leads to accurate model estimates and predictions. However, it creates unrealistic movement paths, making it unsuitable for simulating telemetry data. Similarly, imposing no boundary condition on the simulation generates unbiased data, which accurately reflects the true intensity. Nevertheless, this method of simulation results in data loss as individual paths are allowed to exit the area of interest. This causes an underestimation of abundance from the survey model, and may create smaller or broken paths in the telemetry data. As such, the simulation with no boundary condition is inefficient. The simulation wherein individuals 'respawn' when hitting the boundary edge results in simulated data with a poor spatial coverage, and creates strong biases in parameter estimation and prediction in the survey model. In comparison, imposing a hard boundary condition on the simulation results in slight biases in parameter estimation, but provides the best spatial coverage, results in no data loss, creates individual paths with realistic movement behaviour, and returns an accurate representation of the true intensity surface. Therefore, the simulation with the hard boundary condition was selected as the most realistic and efficient simulation method, and was used when generating data in Section 4.3.1.

4.3.4 Borrowing Strength: Poor Quality Data

One of the advantages of the Langevin diffusion approach to movement modelling is data integration and multiscale modelling. The insights at both the large-scale population-level, and small-scale individual-level are combined to give an overall estimate of habitat selection. Section 4.3.2 demonstrated the implementation of the Langevin joint models and its requisite parts in `R-inlabru`. However, all models were fitted to robust datasets, making the joint modelling framework seem somewhat unnecessary in the aims of estimating habitat selection parameters or predicting the utilisation distribution. This subsection demonstrates the data-integration advantages of the joint modelling framework when poorer quality datasets are available. The aim of this subsection is to investigate whether parameter estimation or predictive accuracy is improved through the joint modelling approach, as compared to modelling the requisite parts of the model separately. What are the costs and benefits of this more complicated joint model?

To emulate the smaller sample sizes which may be available in an applied situation, the original simulated datasets are compared to thinned versions. This ensures that the data come from the same patterns and processes, but the models have less information because there are fewer observations. In the survey data, the overall point pattern is homogeneously thinned to leave 25% of the points (Figure 4.12). In the telemetry data, the number of individual tracks is reduced to 25% of the original (5 tracks, Figure 4.13).

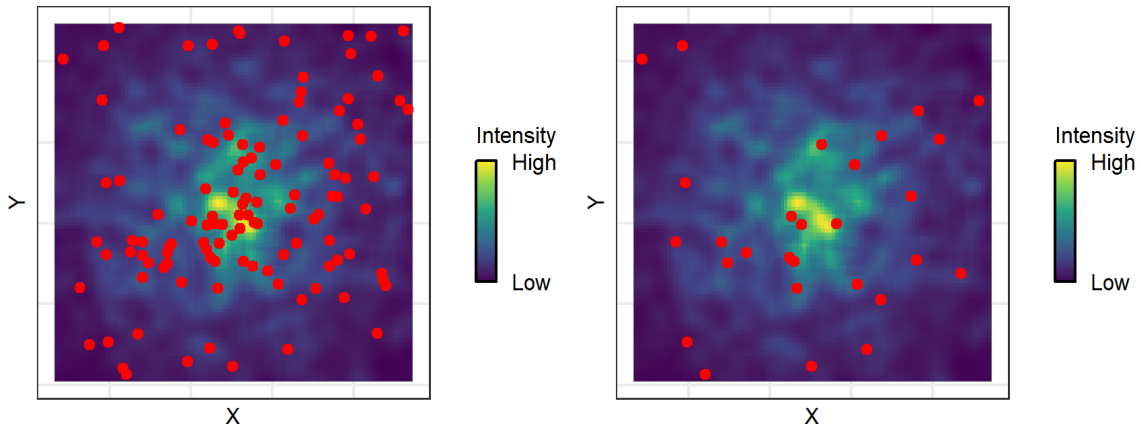

(a) Survey Data (b) Thinned Survey Data

Figure 4.12: Spatial distribution of survey data (a) containing all simulated individuals; (b) thinned homogeneously by 75%. Background colour scale shows true intensity, which follows a gradient of relative intensity from low (blue) to high (yellow), as interest is in relative differences across space and not absolute values.

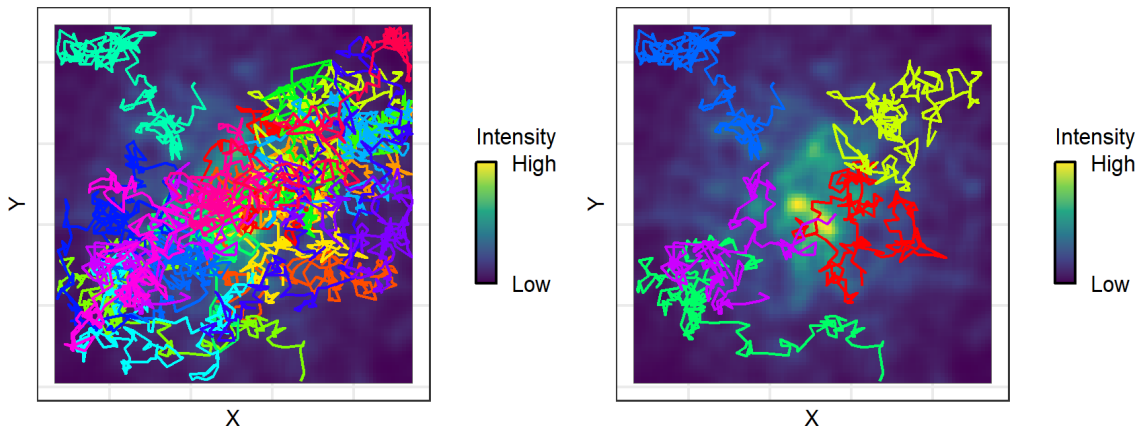

(a) Telemetry Data (b) Thinned Telemetry Data

Figure 4.13: Telemetry tracks for (a) 20 individuals; and (b) 5 individuals. Background colour scale shows true intensity, which follows a gradient of relative intensity from low (blue) to high (yellow), as interest is in relative differences across space and not absolute values.

The same survey, telemetry, and joint models as described in Section 4.3.2 were fitted to the thinned versions of the survey and telemetry data. For the joint models, combinations of the original (full) and thinned survey and telemetry datasets were fitted, resulting in three new models: thinned telemetry and full survey; full telemetry and thinned survey, and both thinned survey and telemetry. The outputs of these new models are compared to the models fitted in Section 4.3.2 in Table 4.4 and Figure 4.14. With the thinned data, the weaknesses of each model type are revealed: the macro-scale survey model estimates a 95% credible interval containing 0 for the covariate which varies at a fine scale, the environmental covariate. Conversely, the local-scale telemetry model estimates a 95% credible interval containing 0 for the covariate which varies at a coarse scale, the attraction to centre covariate. However, when the large and small scale perspectives are combined in the joint models, the weaknesses of these respective datasets offset one another, and both covariates are correctly estimated to have a positive effect with a 95% credible interval above 0.

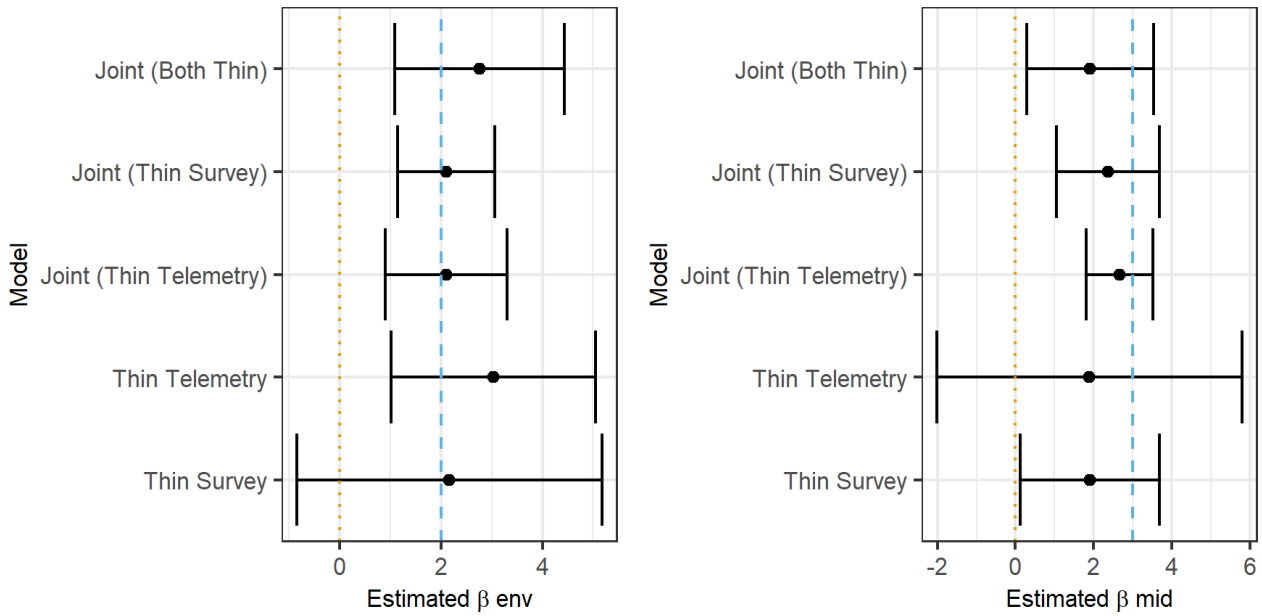

(a) β_{env} (b) β_{mid}

Figure 4.14: Posterior mean and 95% credible intervals for the (a) β_{env} and (b) β_{mid} parameters from the survey, telemetry, and joint models fitted to thinned survey and telemetry datasets. True parameter values (2, and 3, respectively) are shown with blue, dashed, vertical lines. The location of the 0 mark is shown with an orange, dotted, vertical line.

Table 4.4: Posterior mean and 95% credible intervals for the Intercept, β_{env}, and β_{mid} parameters from the survey, telemetry, and joint models fitted to full and thinned datasets. Covariate effects with an estimated 95% credible interval which contains 0 are highlighted in bold. All values given are rounded to 2 decimal places.

Model	Data	Intercept	β_{env}	β_{mid}
Survey Model	Full	-6.62 [-7.54,-5.70]	1.60 [0.11,3.09]	2.69 [1.81,3.58]
	Thin	-7.89 [-9.74,-6.04]	**2.17 [-0.84,5.17]**	1.90 [0.11,3.68]
Telemetry Model	Full	NA	2.09 [1.09,3.10]	2.96 [0.98,4.93]
	Thin	NA	3.03 [1.01,5.04]	**1.90 [-2.01,5.80]**
Joint Model	Both Full	-6.81 [-7.46,-6.15]	1.94 [1.11,2.78]	2.74 [1.93,3.55]
	Telemetry Thin	-6.85 [-7.65,-6.04]	2.10 [0.90,3.30]	2.66 [1.80,3.53]
	Survey Thin	-8.10 [-9.06,-7.14]	2.11 [1.15,3.06]	2.37 [1.05,3.69]
	Both Thin	-8.18 [-9.46,-6.89]	2.76 [1.09,4.44]	1.91 [0.30,3.53]

The five new models were also used to make spatial predictions of the utilisation distribution. These predictions, along with the true intensity surface, can be seen in Figure 4.15.

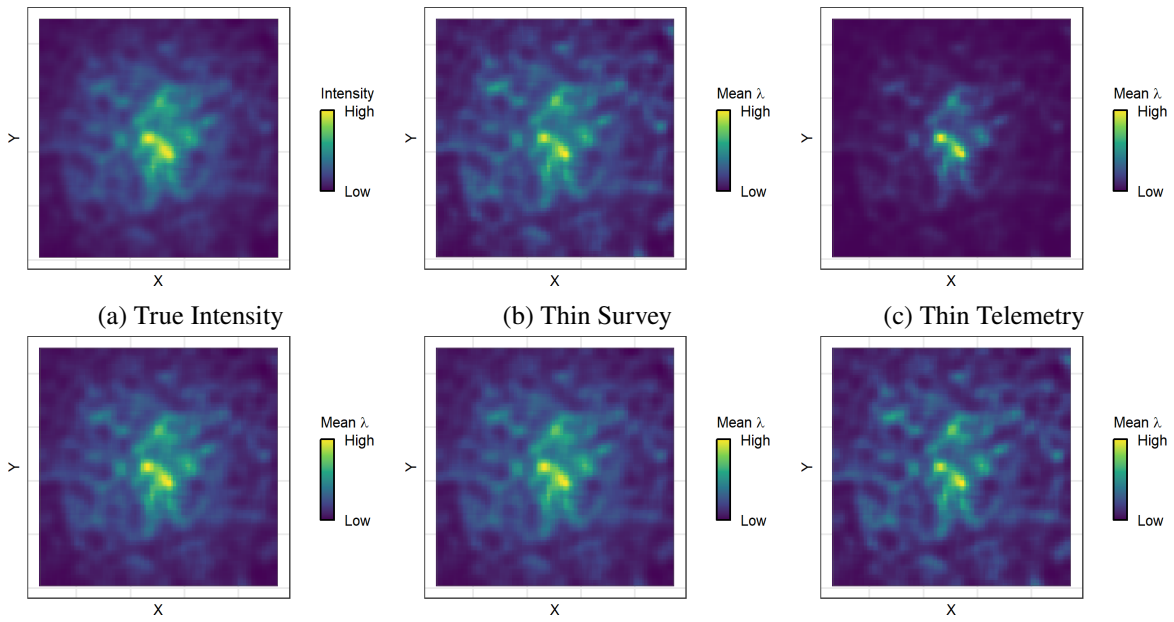

(a) True Intensity (b) Thin Survey (c) Thin Telemetry

(d) Joint (Thin Telemetry) (e) Joint (Thin Survey) (f) Joint (Both Thin)

Figure 4.15: (a) the true intensity surface; and the predictions of the spatial distribution of intensity (i.e., a spatial representation of the utilisation distribution surface) from: (b) the survey model fitted to thinned survey data; (c) the telemetry model fitted to thinned telemetry data; and the joint model fitted to (d) full survey data and thin telemetry data; (e) thin survey data and full telemetry data; and (f) thin survey data and thin telemetry data. The colour scale for each plot follows a gradient of relative mean predicted intensity from low (blue) to high (yellow), as interest is in relative differences across space and not absolute values.

4.3.5 Improving Computational Efficiency

This chapter takes an existing approach to data integration and multiscale habitat selection modelling, and implements it in a new software, R-inlabru. R-inlabru makes use of the INLA method for approximate Bayesian inference, whereas originally the Langevin diffusion based movement model was implemented using full MCMC parameter estimation in JAGS (although it could also be implemented using other software platforms for inference with MCMC, such as NIMBLE). How does the R-inlabru method compare to the original JAGS implementation? What is gained by utilising this approach, and is accuracy in parameter estimation lost by using an approximate method for inference?

Table 4.5 contains the running times for each of the models fitted in R-inlabru and JAGS. There is a vast difference in the computational cost of the models between software implementations, with the JAGS models taking far longer to run than the R-inlabru models. For example, the JAGS joint model took 42 minutes to run, compared to only a 5 second running time for the corresponding R-inlabru joint model. This is as expected when taking into account that R-inlabru uses the INLA method for approximate inference, whereas JAGS implements full MCMC exploration of the parameter space.

Table 4.5: Running times for fitting the survey, telemetry, and joint models to simulated data using R-inlabru and JAGS. All values given are in seconds and rounded to 2 decimal places.

	Model Running Time (seconds)	
	JAGS	R-inlabru
Survey Model	1082.08	5.47
Telemetry Model	1385.24	4.31
Joint Model	2502.90	5.45

Figure 4.16 and Table 4.6 contain the posterior estimates for the intercept term, and covariate coefficients from the R-inlabru and JAGS models. For each of the three model types - survey, telemetry, and joint - it is found that parameters are estimated with similar accuracy and uncertainty between the JAGS and R-inlabru implementations. Therefore, despite the fact that the R-inlabru method relies on INLA, an approximation, this does not appear to incur a cost in

terms of the accuracy of parameter estimation.

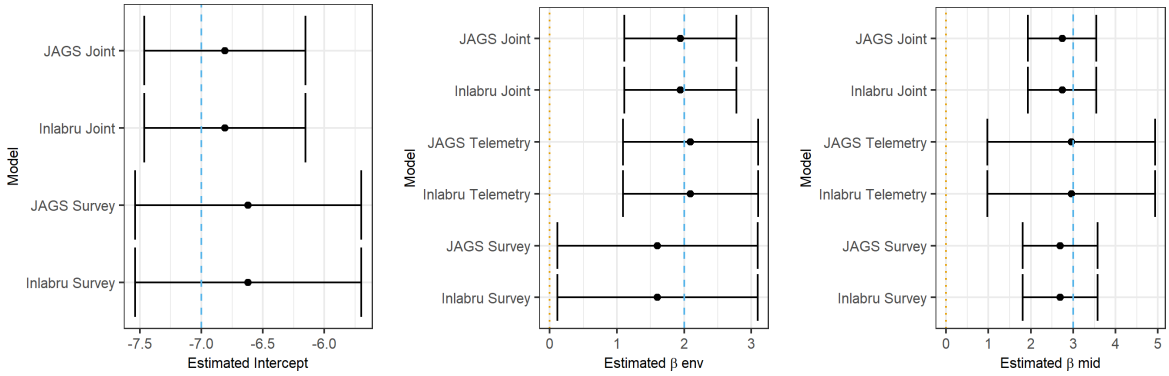

(a) Intercept (b) β_{env} (c) β_{mid}

Figure 4.16: Posterior mean and 95% credible intervals for the (a) Intercept, (b) β_{env}, and (c) β_{mid} parameters from the survey, telemetry, and joint models fitted in JAGS and `R-inlabru`. True parameter values (-7, 2, and 3, respectively) are shown with blue, dashed, vertical lines. The location of the 0 mark is shown with an orange, dotted, vertical line.

Table 4.6: Posterior mean and 95% credible intervals for the Intercept, β_{env}, and β_{mid} parameters from the survey, telemetry, and joint models fitted in JAGS and `R-inlabru`. All values given are rounded to 2 decimal places.

Model	Software	Intercept	β_{env}	β_{mid}
Survey Model	`R-inlabru`	-6.62 [-7.54,-5.70]	1.60 [0.11,3.09]	2.69 [1.81,3.58]
	JAGS	-6.62 [-7.54,-5.70]	1.60 [0.11,3.09]	2.69 [1.81,3.58]
Telemetry Model	`R-inlabru`	NA	2.09 [1.09,3.10]	2.96 [0.98,4.93]
	JAGS	NA	2.09 [1.09,3.10]	2.96 [0.98,4.93]
Joint Model	`R-inlabru`	-6.81 [-7.46,-6.15]	1.94 [1.11,2.78]	2.74 [1.93,3.55]
	JAGS	-6.81 [-7.46,-6.15]	1.94 [1.11,2.78]	2.74 [1.93,3.55]

Figure 4.17 contains predictions from the `R-inlabru` and MCMC joint models, as well as the spatial distribution of the true intensity, for comparison. Both models recover the spatial distribution of the utilisation distribution well, giving accurate predictions which match the true intensity. The predictions from both models are similar, demonstrating that despite the approximate methods used in the `R-inlabru` implementation, predictive accuracy is not diminished.

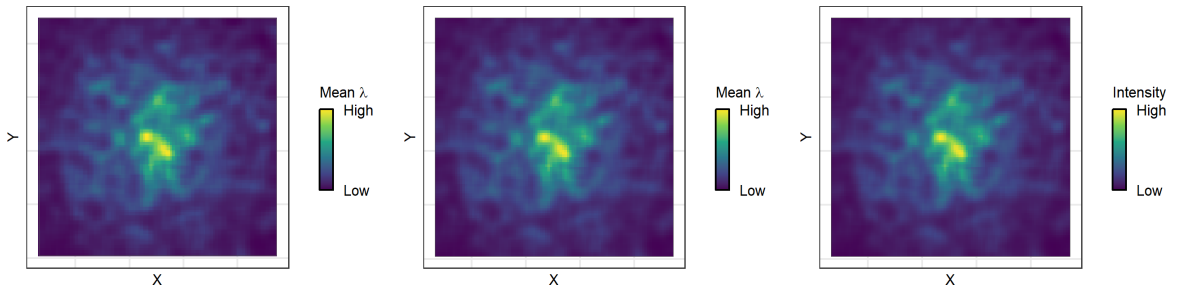

(a) R-inlabru (b) MCMC (c) True Intensity

Figure 4.17: The predictions of the spatial distribution of intensity (i.e., a spatial representation of the utilisation distribution surface) from (a) the joint R-inlabru model, and (b) the joint MCMC model. (c) shows the true intensity. The colour scale for each plot follows a gradient of relative mean predicted intensity from low (blue) to high (yellow), as interest is in relative differences across space and not absolute values.

This subsection has demonstrated that the JAGS and R-inlabru implementations of the Langevin diffusion based movement model are comparable in terms of both predictive accuracy and parameter estimation, but that the R-inlabru approach cuts computational cost considerably. In summary, R-inlabru is both a reliable and efficient software platform in which to implement the model, providing a strong improvement in terms of speed when compared to previous implementations of the approach. This is of particular relevance when considering the large and complex nature of ecological survey and telemetry tracking datasets; using R-inlabru will allow practitioners to fit the model to real data within a feasible timeframe.

4.3.6 Complex Observation Processes

As seen in Section 4.3.5, R-inlabru provides a computationally efficient framework in which to fit the Langevin diffusion based movement model. Aside from making use of the fast INLA method for inference, another advantage of R-inlabru is its ability to account for complex observation processes. One of the applied aims of the Langevin model is to improve habitat selection estimation by integrating data from multiple sources. Often, the collection of ecological survey data is subject to the restrictions of external influences such as accessibility, feasibility; fiscal limitations; and even observer effort and skill. As a result, the probability of observing an individual in the area of interest is often spatially or spatio-temporally varying, and not always in a predictable fashion. R-inlabru was first developed with the aim of accounting for complex observation processes in ecological data, and there exists a range of literature containing

R-inlabru models which incorporate complex effort surfaces to account for spatially varying detection probabilities (Yuan et al., 2017; Martino et al., 2021; Ribeiro et al., 2023; Panunzi et al., 2025b). Therefore, the R-inlabru framework also provides the advantage of containing established methods for handling complexity in the observation process associated with spatial and spatio-temporal data. This subsection explores how the model handles a more complex dataset, and demonstrates the inclusion of a complex observation process in the survey model.

Even when subplots are regularly dispersed over the area of interest, it is possible that very few points are observed. In this example, 25 $10m \times 10m$ subplots were evenly distributed over the study area, which resulted in the spatial location of only 30 of the 114 individuals being observed. The spatial distribution of the survey data can be seen in Figure 4.18.

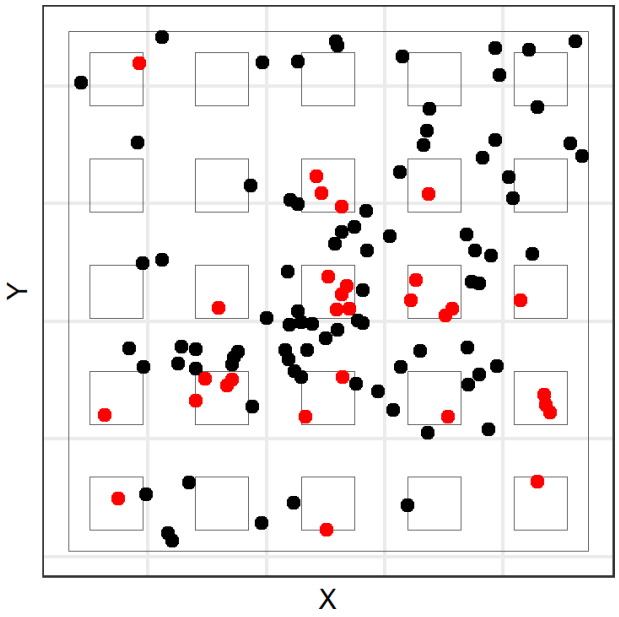

Figure 4.18: Spatial distribution of survey data (black), and points observed when using subplot observation process (red).

Four models were fitted to the subplot-thinned data: versions of the survey and joint models which did and did not include a complex observation process (wherein detection probability was defined as 1 within subplot areas and 0 outside of subplots) to account for the subplots. The mean and 95% credible intervals for the habitat selection parameters estimated from these models can be seen in Table 4.7 and Figure 4.19. The models which did not account for the sampling method underestimated the intercept term. The effect of the attraction to centre covariate was well

estimated by all four models, despite the incorrect specification of the models without subplots. There may have been insufficient data in the survey models (both with correctly and incorrectly specified observation processes) to accurately estimate the effect of the environmental covariate, as both survey models returned a 95% credible interval containing 0 for this variable. However, this was corrected through the inclusion of the telemetry data in the joint models, which both returned the true parameter value. This demonstrates the impact of data integration in correcting biases.

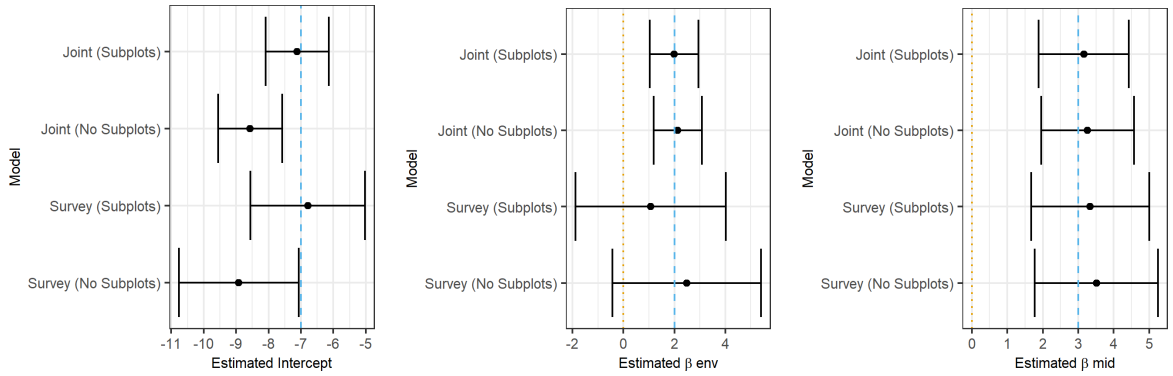

(a) Intercept (b) β_{env} (c) β_{mid}

Figure 4.19: Posterior mean and 95% credible intervals for the (a) Intercept, (b) β_{env}, and (c) β_{mid} parameters from the survey and joint models fitted to the subplot-thinned survey data, with and without a complex observation process to account for the subplots. True parameter values (-7, 2, and 3, respectively) are shown with blue, dashed, vertical lines. The location of the 0 mark is shown with an orange, dotted, vertical line.

Table 4.7: Posterior mean and 95% credible intervals for the Intercept, β_{env}, and β_{mid} parameters from the survey and joint models fitted to the subplot-thinned survey data, with and without a complex observation process to account for the subplots. All values given are rounded to 2 decimal places.

Model	Observation	Intercept	β_{env}	β_{mid}
Survey Model	Subplots	-6.79 [-8.55,-5.02]	1.07 [-1.89,4.03]	3.33 [1.67,5.00]
	No Subplots	-8.92 [-10.77,-7.07]	2.49 [-0.43,5.41]	3.51 [1.77,5.25]
Joint Model	Subplots	-7.12 [-8.09,-6.14]	1.99 [1.04,2.94]	3.15 [1.88,4.43]
	No Subplots	-8.57 [-9.55,-7.58]	2.13 [1.18,3.08]	3.26 [1.96,4.57]

The four new models were also used to make spatial predictions of the utilisation distribution, as seen in Figure 4.20. Despite the poor quality data and incorrect observation process specification in the No Subplots models, all models were able to return a reasonable prediction of the

true intensity surface.

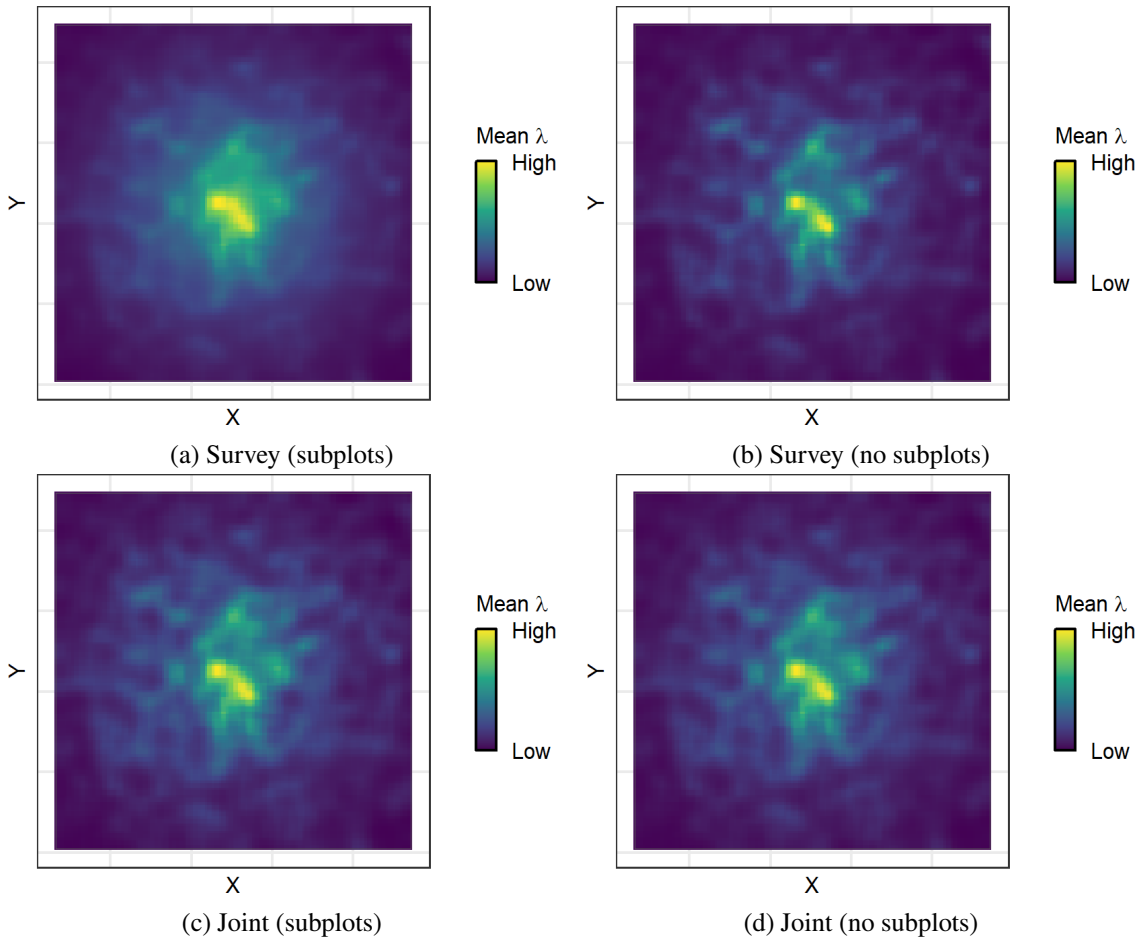

(a) Survey (subplots) (b) Survey (no subplots)

(c) Joint (subplots) (d) Joint (no subplots)

Figure 4.20: The predictions of the spatial distribution of intensity (i.e., a spatial representation of the utilisation distribution surface) from the survey model (a) accounting for subplots and (b) without accounting for subplots; and from the joint model (c) accounting for subplots and (d) without accounting for subplots. The colour scale for each plot follows a gradient of relative mean predicted intensity from low (blue) to high (yellow), as interest is in relative differences across space and not absolute values.

The four models were used to estimate abundance (Figure 4.21). The effect of incorrectly specifying the observation process can be observed here, as the No Subplots models greatly underestimate abundance. However, despite the models only containing observations of 30 individuals, accounting for the subplot sampling method allows for an estimate close to the correct number of individuals (114) from both the survey and joint models.

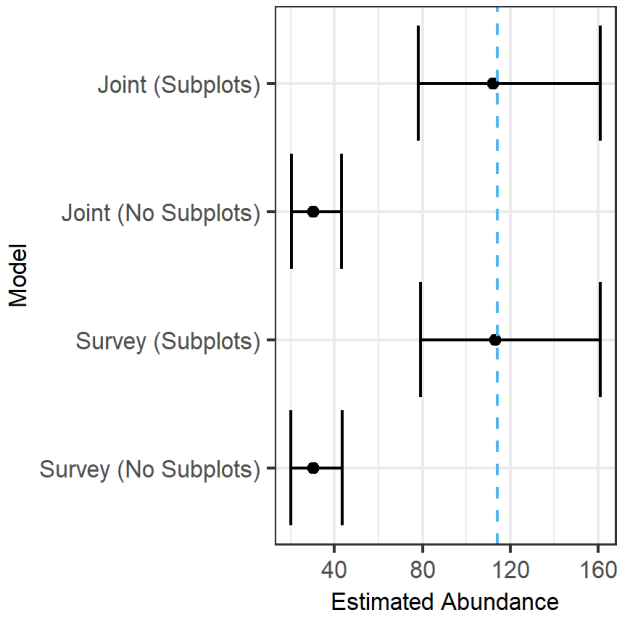

Figure 4.21: Abundance estimates from the survey and joint models fitted to the subplot-thinned survey data, with and without a complex observation process to account for the subplots. True abundance (114 individuals) is shown with a blue, dashed, vertical line.

Table 4.8: Posterior mean and 95% credible intervals for estimated abundance from the survey and joint models fitted to the subplot-thinned survey data, with and without a complex observation process to account for the subplots. All values given are rounded to 2 decimal places.

Model	Observation	Abundance Estimate
Survey Model	Subplots	113.04 [79.29,161.14]
	No Subplots	30.15 [19.96,43.66]
Joint Model	Subplots	112.07 [78.26,161.12]
	No Subplots	30.14 [20.43,43.24]

4.3.7 Accounting for Spatial Autocorrelation

In addition to gains in computational efficiency, concise syntax, and the ability to account for complex observation processes, implementing the joint Langevin movement model in `R-inlabru` allows for the inclusion of a Gaussian random field in the predictor. This means that unexplained sources of spatial correlation in the data can be accounted for, reducing the risk of spurious significance in interpretation of covariate effects and biases in prediction. This subsection demonstrates the steps required to include a Gaussian random field in the models, and shows the utility of this feature.

Building a Gaussian Random Field into the Modelling Framework

When implementing the joint Langevin movement model, the smoothing and gradient transformations of the Langevin drift term, as defined in Equation 4.2, are applied to the predictor as a pre-processing step. When the model only contains fixed effects, the transformations are applied to the spatial covariates, as demonstrated in Section 4.3.1. However, this process becomes more complicated when a spatial random effect is included in the predictor, as the effect is estimated in the model and not predefined. As a workaround, the transformations can be applied to the integration scheme, allowing the effect to be partially pre-processed and improving computational efficiency. This approach takes the following steps:

1. Weighted integration points are generated across the area of interest (note that the exact coordinate locations of these are used directly and not aggregated at the mesh vertices, so operations are more computationally expensive than typical R-inlabru models).

2. The mapping matrix, A, is extracted from the integration scheme. In spatial models, the A matrix maps continuous spatial covariates and spatial fields defined at the mesh nodes to observation locations, projecting spatial information to the response.

3. The gradient transformation for each dimension (as defined in Equation 4.15) is applied to the A matrix. The coordinates of the integration points are shifted by h (default value $h = 1e - 6$), and the A matrix for these shifted points is generated. This allows for the gradient to be calculated between the original points and a location very close to these, in order to incorporate the gradient transformation as defined in Equation 4.15. The parameter h is at the spatial scale that two points are evaluated as close to each other to calculate the gradient. The values of the original A matrix are then subtracted from the shifted A matrix and the values of the resulting matrix are divided by h. This process is repeated for each dimension.

4. The distance, $dist$, between the original (not shifted) integration points and each of the telemetry observations is calculated. These are used to define a 2-dimensional Gaussian

kernel around each telemetry observation

$$f(x) = \frac{1}{2\pi\sigma^2} \times e^{\frac{-dist^2}{2\sigma^2}}, \tag{4.18}$$

where π is the mathematical constant approximately equal to 3.14 (not to be confused with the utilisation distribution). This is used to weight the integration points (those outside of the kernel area for a given observation will have 0 weight).

5. The kernel integral is normalised by dividing the kernel by the sum of the kernel multiplied by the weights of the integration points that fall within the area of interest for the given observation. A scaled version of the kernel is used for numerical integration. This is computed by multiplying the kernel by the weights of the integration points that fall within the area of interest for the given observation.

6. The kernel weight information is incorporated into the transformed A matrices from Step 3.

7. The final A matrices are incorporated into the telemetry likelihoods, transforming the latent field as it is estimated by acting as a mapping matrix with built in smoothing and gradient transformations.

The pre-processing of the integration scheme allows the Gaussian random field to be jointly estimated across the survey and two telemetry likelihoods within the joint Langevin movement modelling framework.

Omission of the Attraction to Centre Covariate

To demonstrate the utility of this feature, survey, telemetry and joint models were fitted to the data from Section 4.3.1. The models were defined exactly as those fitted in Section 4.3.2, but a fixed effect for the attraction to centre covariate was not included. This mimics the real-world scenario in which spatial covariates which are difficult or impossible to define are not included as fixed effects in the model predictor. Each of the models was fitted with and without a Gaussian random field in the predictor. The estimated mean and 95% credible intervals for the intercept term and environmental covariate effect from each of these six models in shown in Table 4.9 and

Figure 4.22. The macro-scale survey model without a GRF estimates a 95% credible interval containing 0 for the environmental covariate. However, error is improved through the inclusion of a GRF in the model, wherein the 95% credible interval is estimated to be entirely above 0. The estimates of the environmental covariate effect from the local-scale telemetry models are unaffected by the exclusion of the attraction to centre covariate, and are accurately returned by the models with and without a GRF. The joint and survey models without a GRF overestimate the intercept term, whereas the models containing a GRF correct this bias somewhat, estimating 95% credible intervals for the intercept term which contain the true value.

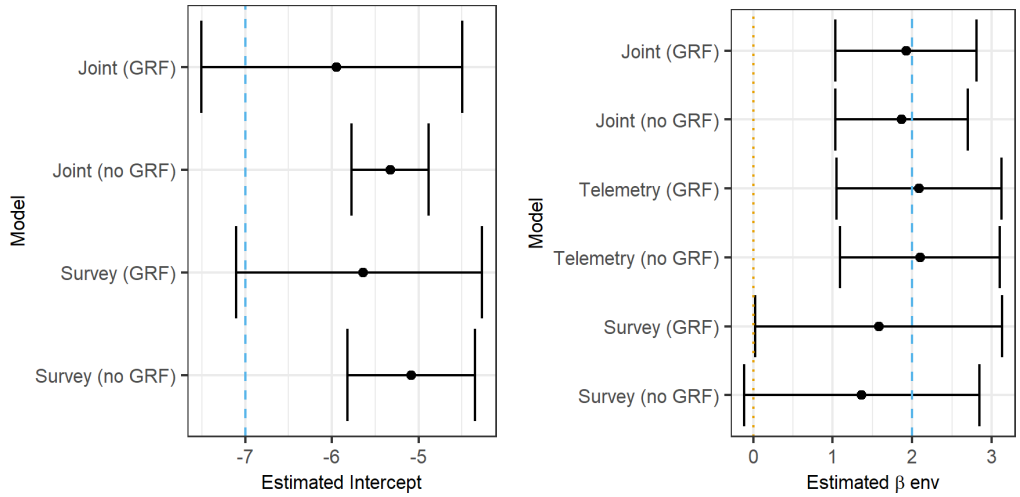

(a) Intercept (b) β_{env}

Figure 4.22: Posterior mean and 95% credible intervals for the (a) Intercept and (b) β_{env} parameters from the survey, telemetry, and joint models with and without a GRF. True parameter values (-7, 2, and 3, respectively) are shown with blue, dashed, vertical lines. The location of the 0 mark is shown with an orange, dotted, vertical line.

Table 4.9: Posterior mean and 95% credible intervals for the Intercept, β_{env}, and β_{mid} parameters from the survey, telemetry, and joint models fitted with and without a GRF. All values given are rounded to 2 decimal places.

Model	Predictor	Intercept	β_{env}
Survey Model	GRF	-5.64 [-7.10,-4.26]	1.58 [0.02,3.13]
	No GRF	-5.09 [-5.82,-4.35]	1.36 [-0.12,2.84]
Telemetry Model	GRF	NA	2.08 [1.05,3.12]
	No GRF	NA	2.10 [1.09,3.10]
Joint Model	GRF	-5.95 [-7.50,-4.50]	1.92 [1.03,2.81]
	No GRF	-5.33 [-5.77,-4.88]	1.87 [1.03,2.70]

The six models were also used to produce spatial predictions of the utilisation distribution, as seen in Figure 4.23. The models without a GRF can only predict using the estimated effect of the environmental covariate, so do not recover the true intensity surface. The inclusion of a GRF in the models recovers the effect of the missing attraction to centre covariate, providing a better prediction of the intensity surface.

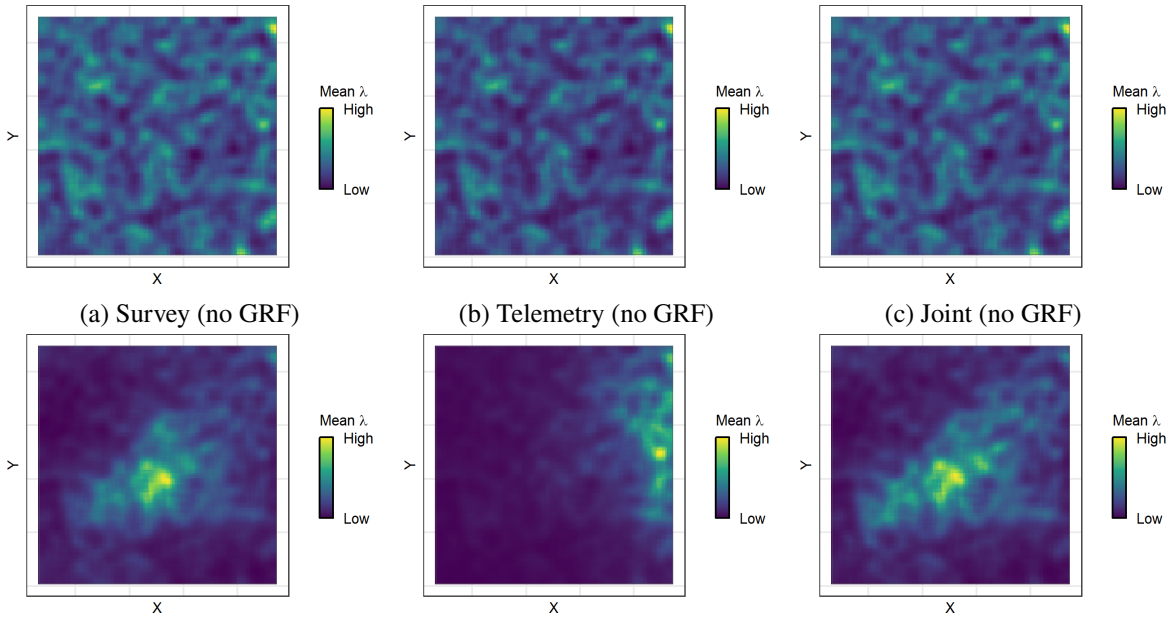

(a) Survey (no GRF) (b) Telemetry (no GRF) (c) Joint (no GRF)

(d) Survey (GRF) (e) Telemetry (GRF) (f) Joint (GRF)

Figure 4.23: The predictions of the spatial distribution of intensity (i.e., a spatial representation of the utilisation distribution surface) from (a) the survey model without a GRF, (b) the telemetry model without a GRF, and (c) the joint model without a GRF; (d) the survey model with a GRF, (e) the telemetry model with a GRF, and (f) the joint model with a GRF. The colour scale for each plot follows a gradient of relative mean predicted intensity from low (blue) to high (yellow), as interest is in relative differences across space and not absolute values.

The parameters of the estimated Gaussian random field from each of the models which contained this effect are shown in Table 4.10. The estimated range of each field corresponds to the scale of variation in the attraction to centre covariate (the length or breadth of half of the area of interest, 50). This means that the scale of the source of unexplained correlation in the data has been well estimated by the models. A spatial representation of the Gaussian random field was predicted using each of the three models. This can be seen in Figure 4.24. The survey and joint model capture the spatial distribution of the missing covariate well. There is a diagonal bias in

the field predicted by the telemetry model, which is likely due to the distribution of the points used by this model. However, this bias is largely corrected in the joint model.

Table 4.10: Posterior mean and 95% credible intervals for the estimated Gaussian random field range and standard deviation. All values given are rounded to 2 decimal places.

Model	Range ρ	Standard Deviation σ
Survey Model	60.85 [26.23,129.60]	0.80 [0.48,1.28]
Telemetry Model	71.36 [24.49,170.52]	0.80 [0.31,1.62]
Joint Model	66.92 [31.67,133.17]	0.88 [0.53,1.42]

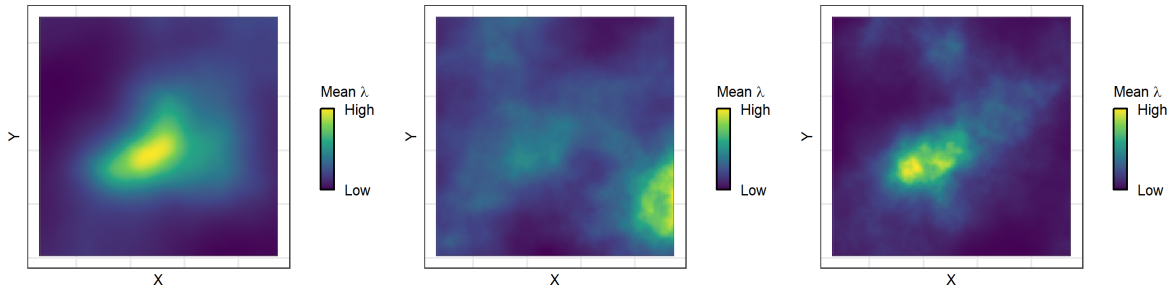

(a) Survey Model (b) Telemetry Model (c) Joint Model

Figure 4.24: The estimated Gaussian random fields from (a) survey model; (b) telemetry model; and (c) joint model. The colour scale of all plots follows a relative gradient from low (blue) to high (yellow), as interest is in relative differences across space and not absolute values.

Estimating a Local-range GRF

When attempting to recover the effect of the missing attraction to centre covariate, the telemetry model does not return an accurate spatial distribution in the estimated field (although the scale of the missing effect is well estimated). The poor recovery of the spatial distribution may be due to the scale of variation in the covariate being a poor match to this type of data, which is better suited to local scale effects. It is important to evaluate whether this may be the case, or whether there may be an underlying flaw in the construction of this model feature and the telemetry model is unable to accurately predict a spatial field.

Here, a GRF with a small-scale range is simulated and used to describe the true intensity surface on which the movement simulation is based. The simulated environmental and attraction to centre covariates were not included, so that the value of true intensity in each grid cell was defined as

$$\lambda(x) = \exp(\alpha + \psi(x)), \tag{4.19}$$

where $\alpha = -5$ and $\psi(x)$ is a spatial Gaussian random field with Matérn covariance structure. The range of the field is $\rho = 20$ and the standard deviation is $\sigma = 2$.

The Langevin movement simulation as described in Section 4.3.1 was carried out using this intensity surface, and the survey, telemetry, and joint models were fitted to the resulting datasets. The parameters of the estimated Gaussian random field from each of the models are shown in Table 4.11. The survey model estimates a field with a very wide range and low standard deviation, indicating that the model estimates the field to have little impact on the spatial distribution of survey data (see Section 1.6.3). In contrast, the telemetry model estimates a mean range and standard deviation closer to the true values, with smaller associated 95% credible intervals. The joint model provides the best estimate for the posterior mean range of the field.

Table 4.11: Posterior mean and 95% credible intervals for the estimated Gaussian random field range and standard deviation. All values given are rounded to 2 decimal places.

Model	Range ρ	Standard Deviation σ
Survey Model	556.24 [24.80,3479.65]	0.16 [0.02,0.51]
Telemetry Model	55.66 [19.57,127.21]	0.78 [0.37,1.40]
Joint Model	34.09 [10.06,97.72]	0.44 [0.23,0.70]

The spatial distribution of the predicted fields can be compared to the new true field for this example in Figure 4.25. The survey model performs poorly at recovering the spatial distribution of the field. Excepting the effects introduced by the boundary condition in the simulation, which cause an estimate of low relative intensity to be predicted at the edges of the spatial domain, the telemetry and joint models recover the relative distribution of the field in space, with high points in the lower left and upper right of the area. Overall, the models incorporating telemetry data perform better than the survey model at recovering the effects of the small scale field. This suggests that the performance of the models at recovering the spatial field is linked to the comparability in spatial scale between the field range and modelling level. However, more rigorous testing would be required to understand the full impact of this effect, including a sensitivity analysis of model parameters impacting the spatial domain (e.g., Γ).

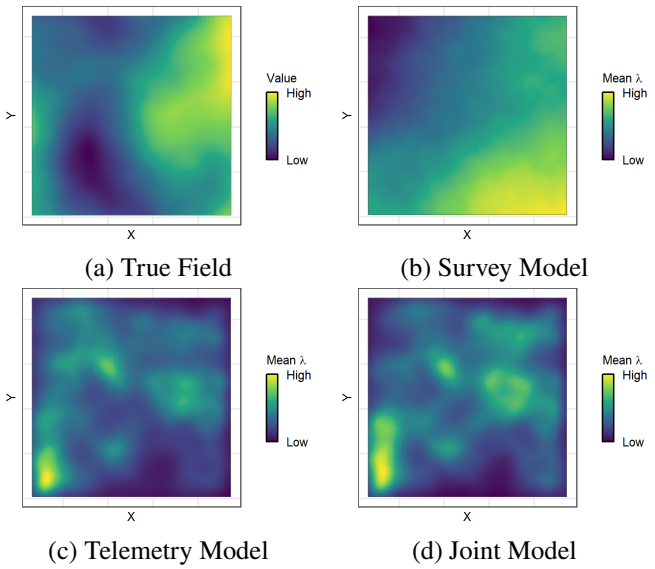

(a) True Field (b) Survey Model

(c) Telemetry Model (d) Joint Model

Figure 4.25: (a) The true Gaussian random field, and the estimated fields from (b) survey model; (c) telemetry model; and (d) joint model. The colour scale of all plots follows a relative gradient from low (blue) to high (yellow), as interest is in relative differences across space and not absolute values.

4.4 Discussion

This chapter demonstrated the translation of the joint Langevin movement model presented by Blackwell and Matthiopoulos (2024) into a version which could be implemented in the `R-inlabru` software package. The simulated case study presented use of the modelling framework for inference and prediction, and demonstrated the strengths of the `R-inlabru` approach in terms of accuracy, computational efficiency, and accounting for complex observation processes and missing covariates. Overall, the `R-inlabru` implementation of the framework provides an advantageous and accessible platform for inference using this joint modelling approach to data integration.

Although the approach presented in this chapter is similar to that introduced by Blackwell and Matthiopoulos (2024), implementation in `R-inlabru` necessitated some alterations to the method which could present limitations. In contrast to Blackwell and Matthiopoulos (2024), the movement parameter Γ is fixed instead of being estimated in the model. This was done in order to simplify the `R-inlabru` implementation of the method, as INLA would require a more complex approach to handle having an unknown parameter in both the mean and variance of the Gaussian likelihood (see Equation 4.1, noting that Γ is incorporated in the mean through the drift term as described in Equation 4.2). In Blackwell and Matthiopoulos (2024), Γ is treated

as a nuisance parameter, as the focus is on estimating habitat selection parameters β. As Γ is not a parameter of interest for interpretation, fixing Γ to a appropriate value (optimally taken from the data; such as average step-length) was deemed a reasonable limitation for the approach. However, this does contrast with what has been described in the literature as best practice, as no parameters describing movement (in terms of mobility) are estimated in the model (Avgar et al., 2016). In future, an avenue of research interest would include performing a sensitivity analysis to assess the impact of altering the value of the Γ parameter on model outputs.

A current limitation of both the approach presented by Blackwell and Matthiopoulos (2024) and its translation to `R-inlabru` here, is that further development would be required for applications which require a spherical geometry. The current construction of the functions for pre-processing the integration scheme to allow for a Gaussian random field to be incorporated into the linear predictor of the telemetry likelihood are limited to R^2 manifolds. For applications covering large enough distances so as to require the spherical nature of the Earth's geometry to be taken into account, the approach as currently implemented could not be used. However, this is simply an area requiring further development, and not a definite restriction.

The joint modelling framework holds the assumption that the individuals included in the telemetry study are randomly sampled from the same population as is observed in the survey (Blackwell and Matthiopoulos, 2024). This can be an issue if telemetry data come from a subset of the population with demographic traits that make the individuals easier to catch or tag, or if certain individuals are more likely to be observed in the survey due to physical or behavioural traits. It also assumes that the datasets are observed in the same temporal frame, such as season or time of day. If this is not the case, differences in life history strategy or activity could translate to differences in selection behaviour between the types of observation. If selection differs systematically between the data streams, then the assumption that both datasets provide information on the same selection process underlying the same utilisation distribution breaks down. The `R-inlabru` implementation of the model enables extensions to account for differences in sampling procedure, allowing the observation process to be modelled explicitly and so disentangling its influence from selection behaviour. However, care must still be taken to ensure that sampling has not created a systematic difference in the demography and life history of the sampled

individuals between data types.

In relation to differences in sampling between telemetry and survey datasets, the results here are demonstrated using a simulation study wherein telemetry and survey data have similar spatial coverage. Whilst differences in spatial coverage between datasets would not present an issue with this modelling framework (and actually constitutes an advantage of data integration), the support lent from one dataset to another is related to the spatial coverage of each. As such, it would be of interest to perform similar assessments to those presented here in a more realistic applied scenario wherein the spatial coverage of survey and telemetry data are less similar.

Another potential limitation of the overall approach as presented by Blackwell and Matthiopoulos (2024) and translated here, is that the movement model does not include directional persistence. Although proximity to the location of the previous observation (in terms of Euclidean distance) is taken into account, the direction in which the individual has been travelling is not. This is in contrast to other commonly used approaches for movement modelling, such as the GF-iSSA approach used in Chapter 3, which incorporates turning angles from previous steps into the movement kernel (Arce Guillen et al., 2023). The joint Langevin movement model only accounts for directional bias towards environmental stimuli (through the drift term), rather than the tendency for animals to maintain the direction of previous movement steps. However, directional persistence is a widespread behavioural phenomenon that has been observed in many animal groups, so it is of interest to replicate this behaviour for biological realism in movement modelling (Duffy, 2010). An area of current development aims to improve the model through the use of the underdamped Langevin process, which incorporates both drift towards the utilisation distribution and directional persistence by using velocity (Michelot, 2024). Future advancements of the `R-inlabru` implementation of the model could look to incorporating this approach.

In Blackwell and Matthiopoulos (2024) α is treated as a nuisance parameter, and its interpretation (though possible using the approach presented there) is not explored. Here, the α parameter, or intercept term, included in the survey and joint models is used in the estimation of abundance. In the common instance that not all individuals in a population are observed, but that sampling effort is accounted for through the observation process (as in Section 4.3.6), α can be used to accurately estimate population abundance. Thus, applications of the framework are not limited

solely to habitat selection estimation, and extend to other areas of interest in ecology. Implementation in the R-inlabru software package makes interpretation of this parameter simple, as methods for estimating abundance from point process models like the survey model are already established (e.g., Torney et al., 2023).

An advantage of the R-inlabru implementation of the joint Langevin movement model that has not been explored here, but could provide an area of future development, is the introduction of additional data streams. The joint likelihood construction could accommodate the integration of multiple forms of survey data, bringing in another area of interest for current research in ecology: data integration for species distribution modelling (Miller et al., 2019; Altwegg et al., 2025). This could provide the benefit of further balancing biases in detection and spatial distribution for the survey data, by combining data from multiple sources, such as combining large amounts of citizen science data with small but reliable structured survey datasets (Matthiopoulos et al., 2022). Building this additional complexity into the modelling framework would increase computational cost, and could potentially stretch the assumption that all data streams provide information on the same underlying population, but despite these limitations, provides a promising avenue of future development.

4.5 Conclusions

The joint Langevin movement model enables the integration of data from multiple sources, to improve estimates of long-term habitat selection. Telemetry tracking data from multiple individuals can be modelled simultaneously, combined with population-level survey data. This method would be of practical benefit in many applied scenarios, where it is often of interest to estimate overall population-level space use and habitat selection, as this is the scale at which conservation measures can be implemented. However, the usability of the framework was hampered by the lack of a user-friendly and computationally efficient method for detailed inference. Previous implementation of the likelihood contained no method of incorporating complex observation structures or accounting for spatial autocorrelation in the data. Implementing the model in R-inlabru places the likelihood into an accessible and computationally efficient framework for approximate Bayesian inference, which allows for the inclusion of a Gaussian random field

to account for spatial correlation, and contains multiple pre-existing methods for accounting for spatially varying detection.

Chapter 5

Habitat Selection and Distribution of a Semi-Domesticated Population: Application of the Langevin Diffusion Movement Model

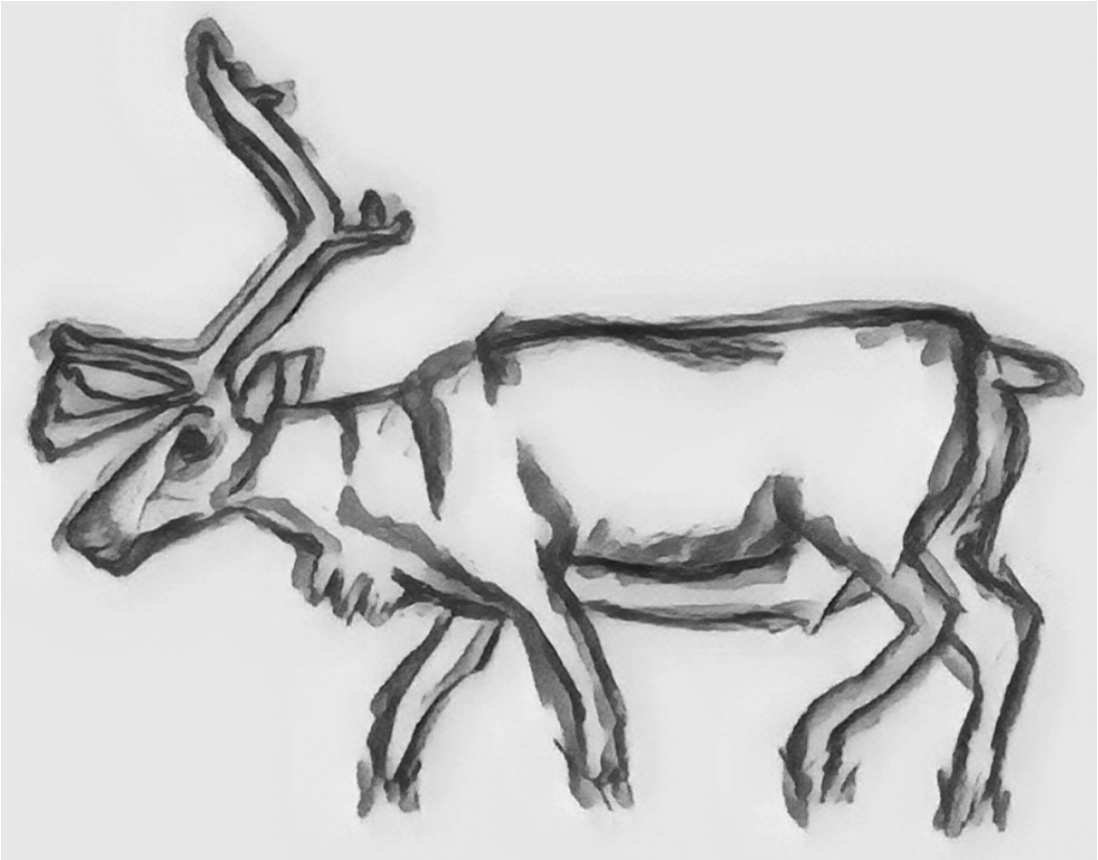

5.1 Introduction

Chapter 3 compared different approaches to habitat selection modelling using `R-inlabru` at different levels of selection: RSA and SSA. In Chapter 4, an approach was developed to integrate multiple data streams into a joint modelling framework in `R-inlabru` that combines these selection levels: the joint Langevin movement model. The following chapter focuses on a case study, wherein the modelling framework proposed in Chapter 4 is applied to real data from a population of semi-domesticated reindeer (*Rangifer tarandus tarandus*) in Northern Finland.

5.1.1 Understanding Space-Use in Semi-Domesticated Populations

For local and indigenous people in Northern Fennoscandia, reindeer husbandry is an important cultural practice and source of income (Turunen et al., 2009; Rasmus et al., 2020). Reindeer are considered to be a semi-domesticated species, and reindeer husbandry is generally characterised by less intensive management as compared to the keeping of domesticated livestock. In accordance with the Reindeer Husbandry Act (848/1990), semi-domesticated reindeer herds are allowed to free-range with access to public and private lands. This free-ranging behaviour is a necessity for the foraging requirements of semi-domesticated reindeer, but traditional husbandry practices are threatened by a large number of competing land-uses in herding districts, including predator conservation, industrial development, and forestry (Rasmus et al., 2020).

In Northern Finland, the protection and conservation of predator populations constitutes a national aim, and thus coexistence with predators is encouraged (Rasmus et al., 2020). However, this is a source of conflict, as growing predator populations have led to an increase in depredation of semi-domesticated reindeer populations, impacting rural livelihoods and well-being. Reindeer populations are often unguarded over long free-ranging periods, leaving them more susceptible to predation than more intensively managed livestock (Mattisson, Odden, and Linnell, 2014). Models of reindeer movement, space-use and habitat selection can aid in understanding depredation in both semi-domesticated and domesticated livestock populations. Mattisson, Odden, and Linnell (2014) found domesticated livestock depredation to change in relation to reindeer population densities, as semi-domesticated reindeer represent a preferential prey species for wild predators.

Opposingly, Moa et al. (2006) suggest that depredation of domesticated and semi-domesticated livestock is the result of chance encounters with predators. However, this still provides a motivation for understanding the spatial distribution of semi-domesticated reindeer populations, as changes in habitat selection behaviour and space-use could lead to increased chance-encounter rates with predators.

Although semi-domesticated reindeer are in an early phase of domestication, they have been shown to exhibit more relaxed fright and flight responses as compared to wild reindeer populations (Nieminen, 2013). Mitigation of livestock predation on semi-domesticated species requires more intensive management, the labour cost of which can prove economically infeasible to reindeer herders (Mattisson, Odden, and Linnell, 2014). In addition, research by Nieminen (2013) found evidence to suggest that the practice of supplementary feeding could cause a reduction in the flight distances of semi-domesticated reindeer. This has a knock-on effect for population response to anthropogenic disturbance or predation.

In addition to coexistence with predators, reindeer herders also face challenges posed by competition for space-use with other land-use types such as forestry, mining, wind-power development, and infrastructure (Horstkotte et al., 2023). Habitat fragmentation has led to a loss in the overall quality of reindeer herding ranges, restricting the spatial area of available grazing pastures and increasing the need for supplementary feeding practices (Lundqvist, 2007). Restrictions in the spatial area available to semi-domesticated reindeer populations can cause increased grazing pressure on remaining pastures and lead to devastating impacts on a key food source (lichen) through trampling (Pape and Löffler, 2016; Heggenes et al., 2017). Reduced movement can also exacerbate infectious pressure of parasites on grazing livestock, increasing the risk of parasitic infection in semi-domesticated reindeer populations, with implications for economic loss (Waller, 2005).

Industrial development is expanding rapidly in Northern Fennoscandia, particularly with the construction of wind turbines (Flydal et al., 2010). This has been found to alter the use of movement corridors by semi-domesticated reindeer populations, and increase movement activity and population fragmentation (Skarin et al., 2015). Demand for increased timber production in the commercial forestry industry has also been found to impact reindeer habitat selection and space-

use, as the availability of forage for reindeer is threatened by the introduction of exotic tree species (Roturier et al., 2007; Horstkotte et al., 2023).

In response to the pressures of competing land-uses and livestock depredation, reindeer herders are forced to employ more intensive management practices, such as supplementary feeding, reducing the economic stability of traditional livelihoods. Understanding impacts of different land-use types on reindeer movement, habitat selection, and space-use can aid in reducing land-use conflict and lessen reliance on supplementary feeding by mitigating direct and indirect (behavioural) loss of grazing grounds (Horstkotte et al., 2023).

5.1.2 Scale Dependent Habitat Selection in Reindeer

Semi-domesticated reindeer have been found to show variations in movement, space-use, and habitat selection behaviour over different spatial and organisational scales.

Skarin and Alam (2017) found that semi-domesticated populations of reindeer in Fennoscandia demonstrated a multi-scale response to the disturbance created by industrial development. At the regional scale, reindeer displayed an avoidance for wind farm construction sites, but at the local scale a preference behaviour was exhibited. This complex multi-scale response may be due to the overall avoidance of wind farms being excepted for the necessity of using a key migration route at the local scale. In general, it demonstrates that habitat selection in semi-domesticated reindeer can be scale-dependent.

Pape and Löffler (2016) have also linked semi-domesticated reindeer movement and space-use to scale. In particular, they examine differences in selection behaviour at different organisational scales: the individual- and population-levels. In this comparison, reindeer were found to exhibit scale-dependent selection behaviour.

Overall, the space-use of semi-domesticated reindeer populations is a balance between the influences of herders and livestock, meaning that habitat selection can best be understood in relation to movement decisions made at different spatial, temporal, and organisational scales (Horstkotte et al., 2022).

5.1.3 Case Study

This chapter explores the application of the joint Langevin movement model to real data in a case study modelling movement, space-use, and habitat selection of semi-domesticated reindeer in the Oraniemi herding district, Northern Finland. In particular, the effects of a large number of competing land-use types on reindeer habitat selection are investigated during a period of free-ranging.

5.1.4 Aims

This chapter aims to demonstrate the application of the joint Langevin movement model, which incorporates a spatial point process formulation to represent the utilisation distribution, to estimate habitat selection and space-use in a semi-domesticated population. It will:

1. fit 99 model variations using the survey, telemetry, and joint Langevin movement models as presented in Chapter 4 to estimate habitat selection parameters and predict spatial distribution of a semi-domesticated population, using tracking data at the individual- and population-levels;

2. demonstrate the use of a fixed parameter in a continuous-time movement modelling framework to account for availability at the individual-level; and,

3. using the 99 models, investigate the impact of model complexity (in terms of number of fixed and random effects, and number of data streams) on inference in terms of parameter estimation and spatial prediction.

5.2 Methodology

5.2.1 Data Background

The study site for this analysis is the $3,796 km^2$ region covered by the Oraniemi herding cooperative, which is located over the Sodankylä (60%), Pelkosenniemi (15%) and Savukoski (25%) municipalities in Northern Finland (Figure 5.1 (a)). Although the Oraniemi herding district is a specifically designated area for reindeer herding with access to public and private land in

accordance with the Reindeer Husbandry Act (848/1990), reindeer herders coexist with many other land-uses. There is mining and active ore exploration in the area, including the Kevitsa mine (visible in Figure 5.1 (b) as a grey/blue patch in the North West of the region) and the Sakatti mine project (Lassila, 2021). There is also a population centre at the Western border: the residential area of Sodankylä (Figure 5.1 (b)). Land-use is also shared with intensive forestry (Kumpula, Colpaert, and Tanskanen, 2008). Of seven reindeer herding districts in Middle Lapland, Oraniemi has been found to have the lowest proportions of lichen and arboreal lichen pasture, but the highest proportions of dwarf shrubs, leaf and grass pastures (Kumpula et al., 2006). This distribution of pasture types is likely due to impacts from the forestry industry (Kumpula et al., 2006). As well as these pasture types, the area also contains large aapa mires, indicated visually in Figure 5.1 (b) by the darker patches in the North (Koitelaiskaira) and South (Luiro River, Kumpula, Colpaert, and Tanskanen, 2008). The area is bordered to the West by the Kitinen river, as well as containing several smaller rivers and large lakes (Figure 5.1 (b)).

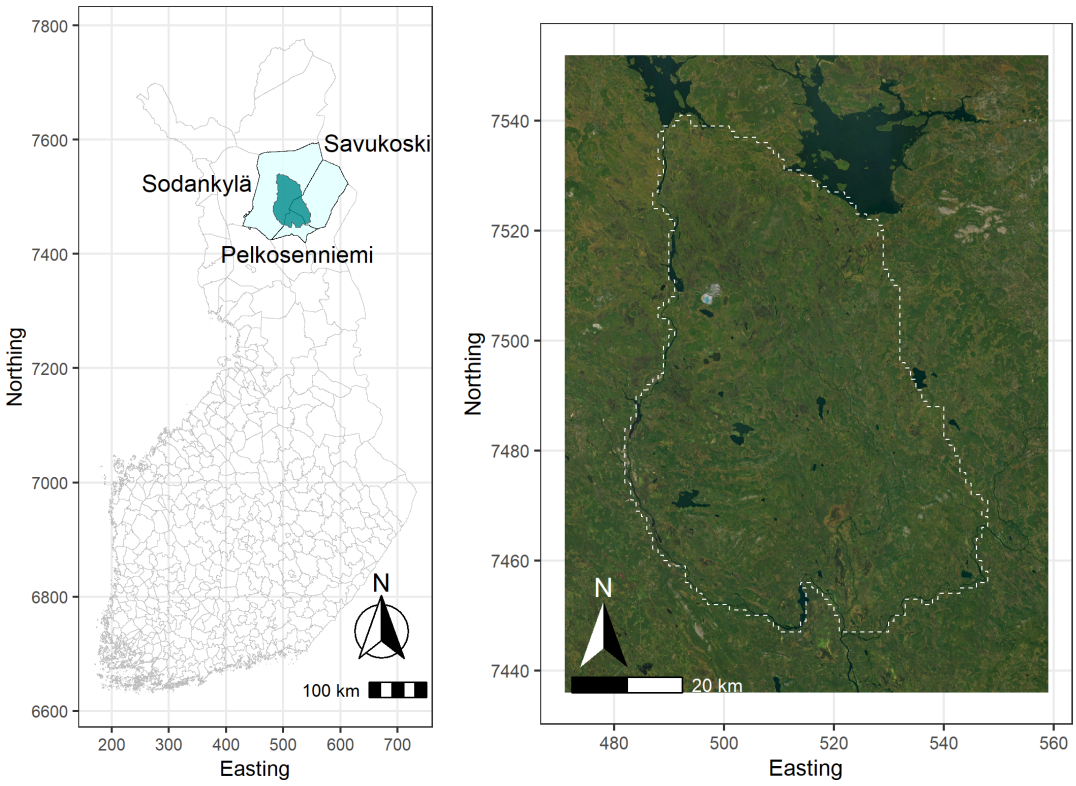

(a) Location (b) Land Uses

Figure 5.1: (a) Location of Oraniemi herding district, Northern Finland, (b) Satellite imagery of land-use in Oraniemi herding district.

Following the autumn and early winter slaughter season, the Oraniemi reindeer herding co-operative contains up to 6000 reindeer, which includes females ($\sim$ 78%), males ($\sim$ 7%), and calves ($\sim$ 15%) (Kumpula, personal communication, 2025). Reindeer husbandry in the Oraniemi district is usually conducted using a combination of corralling and supplementary feeding during winter and periods of free-ranging in summer-autumn (Kumpula, Colpaert, and Tanskanen, 2008). Over the summer-autumn free-ranging period from May-October 2019, daily location tracking data were obtained for 79 female reindeer (*Rangifer tarandus tarandus*) using GPS collars. Adult females were tracked because this demographic makes up most of the herd and should provide a representative sample of overall herd spatial distribution (Skarin et al., 2010). Data were cleaned to remove any observations during periods wherein reindeer were gathered in round corrals, leaving a total of 12 172 observations (Figure 5.2 (a)). For more details on GPS data collection, with an example for the Ivalo region, see Anttonen, Jouko, and Colpaert (2011). As reindeer have been shown to exhibit seasonal differences in habitat selection, and because reindeer movement is restricted by fencing in winter, only data collected over the summer-autumn free-ranging period was used to ensure that the study was carried out over an ecologically relevant temporal domain (Pape and Löffler, 2016).

5.2.2 Data Breakdown

Reindeer have been found to display a general synchronicity in movement behaviour, likely due to a shared response to environmental stimuli (Pape and Löffler, 2016). This supports the assumptions that (1) the sampled population of tagged individuals is spatially representative of the overall distribution of the full population; and (2) individual movement is likely to describe overall long-term preferences of the population. The joint Langevin movement model also includes the assumption that data streams provide observations of the same population (Blackwell and Matthiopoulos, 2024). Therefore, under these assumptions, GPS tracking data were broken down into 'telemetry' and 'survey' subsets, in order to take advantage of the benefit of estimating habitat preference using data 'collected' at multiple organisational scales and to provide a case study using the joint Langevin movement model for inference.

In the literature, studies modelling the movement of Arctic ungulates often use data from

around 15-25 individuals (Pape and Löffler, 2015; Eftestøl et al., 2016; Serrouya et al., 2017; Lesmerises, Johnson, and St-Laurent, 2018). Although, some use as few as 5-8 tracks (Mårell and Edenius, 2006; Beyer et al., 2016), or as many as 36-40 (Dyer et al., 2001; Kumpula, Colpaert, and Tanskanen, 2008). As part of this analysis, the number of telemetry tracks included in the models were varied to assess the impact this has on inference. To create the telemetry subsets, the GPS data were stratified by number of observations per individual, to give the most complete tracks, and then split into 5-, 10-, 20-, and 30-individual subsets. The spatial distribution of the original 79 tracks and the subsetted tracks can be seen in Figure 5.2.

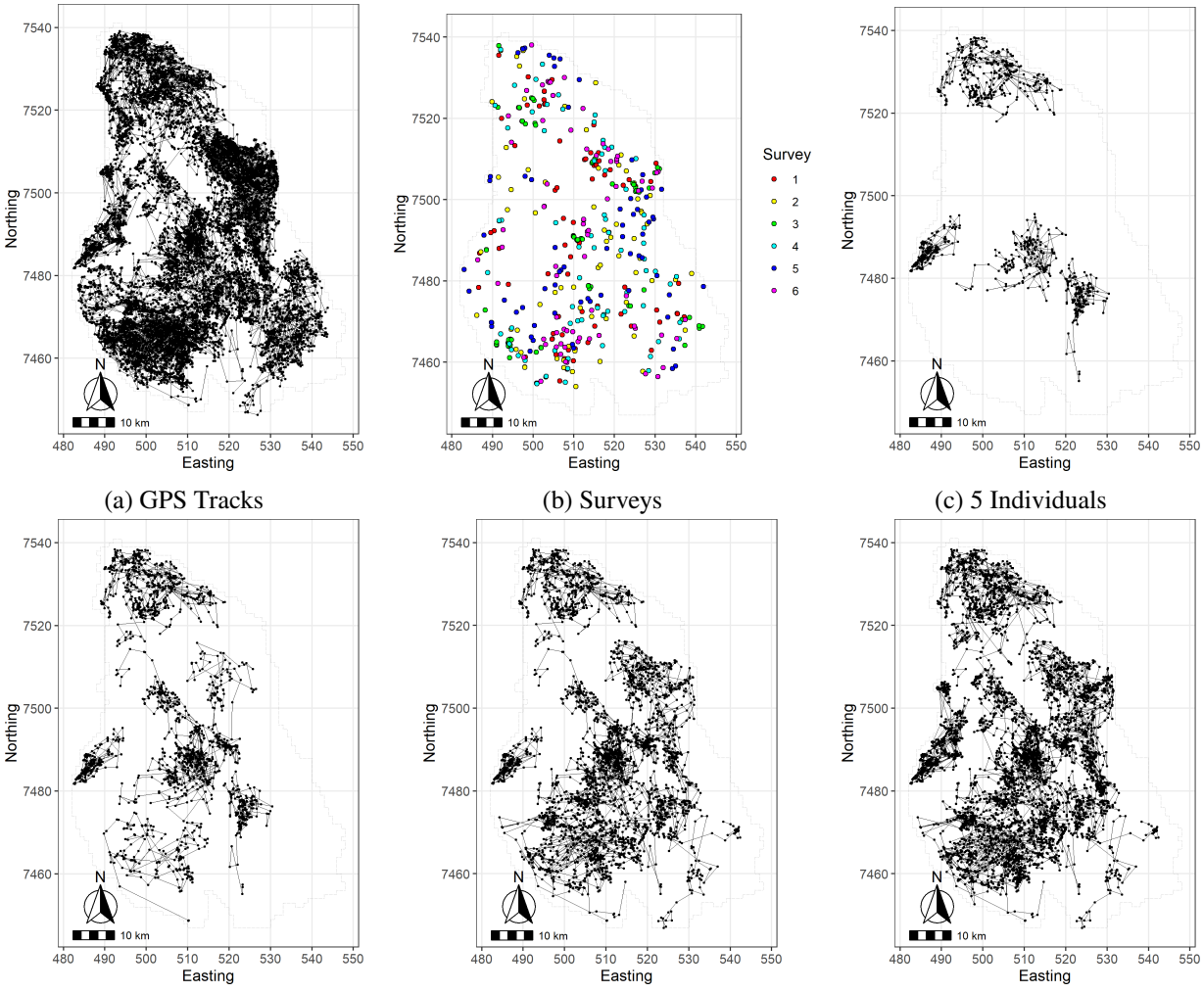

(a) GPS Tracks (b) Surveys (c) 5 Individuals

(d) 10 Individuals (e) 20 Individuals (f) 30 Individuals

Figure 5.2: Distribution of GPS tracking data throughout study site. (a) distribution of all 79 tracks in telemetry dataset, (b) constructed 'survey' data, (c) 5-track subset of telemetry data, (d) 10-track subset of telemetry data, (e) 20-track subset of telemetry data, (f) 30-track subset of telemetry data. Colour scale in (b) represents different survey dates.

In addition to the telemetry subsets, the data were also processed to create artificial surveys

of the overall distribution of the population. The tagged individuals are not assumed to represent the overall number of individuals in the population, so abundance is not estimated, but they are assumed to give an accurate representation of the population's relative spatial distribution. Thus, surveys of spatial distribution are created using an overall snapshot of the observed locations of all tagged individuals at a given time point (day). The study duration covers 6 months over the summer period, so conducting 1 survey per month gives 6 replicates with an even temporal coverage. Some tracks contained missing observations, so not all individuals are observed on all days. To ensure the most information is included in the surveys, the first day of the month with the maximum number of individuals observed that month is used as the survey day. The distribution of survey data can be seen in Figure 5.2.

The joint Langevin models combine both the survey data and one of the telemetry data subsets. Therefore, one subset of observations needs to be removed from the other to ensure data are not counted twice in the joint model. Removing the observations of the telemetry individuals from the survey dataset alters the distribution of the point pattern in the survey data and creates artificial 'absences' in the places where the telemetry individuals are (because in a point process, both points and background information are fed into the model). To avoid this issue, but still ensure the dataset is not artificially inflated by counting these observations twice, the survey days are removed from the telemetry data instead. This simply creates some gaps in the telemetry tracks (which the movement model can handle, because it is formatted in continuous-time) rather than biasing the data. It also means that the joint models are fitted to exactly the same datasets as the separate survey and telemetry models.

5.2.3 Covariates

Environmental conditions in the area are described using 9 land-use covariates. These were developed using a guided classification system applied to Landsat-7 ETM+ satellite imagery from 2001, to produce a $16m^2$ resolution gridded representation of the herding district, with pixels split into 17 land-use classes (Kumpula et al., 2006). Similar pasture classes were amalgamated to summarise the classifications into 9 land-use types, and of these, 9 $1km^2$ resolution rasters were produced, wherein each the value for each pixel was given by the proportion of $16m^2$ pixels of

a given land-use type it contained. For more information on the creation of land-use covariates, see Kumpula et al. (2006). The spatial distributions of the 9 land-use covariates are given in Figure 5.3. As the covariates are given as proportions of land-use type covering a given area, their values are bound between 0 and 1. The mining areas and population centre are contained within the Infrastructure covariate.

For the purposes of this analysis, it is assumed that the distribution of these land-use types, and the within-season habitat preferences of reindeer remain stable over time.

The smoothing and gradient transformations as described in Chapter 4 Section 4.2.2 were applied to each of the 9 land-use covariates as a pre-processing step for the telemetry models. The diffusivity parameter Γ should be related to animal mobility, and so here was calculated using the mean daily step length from the telemetry dataset with 30 individuals, which resulted in a value of $\Gamma = 2km$.

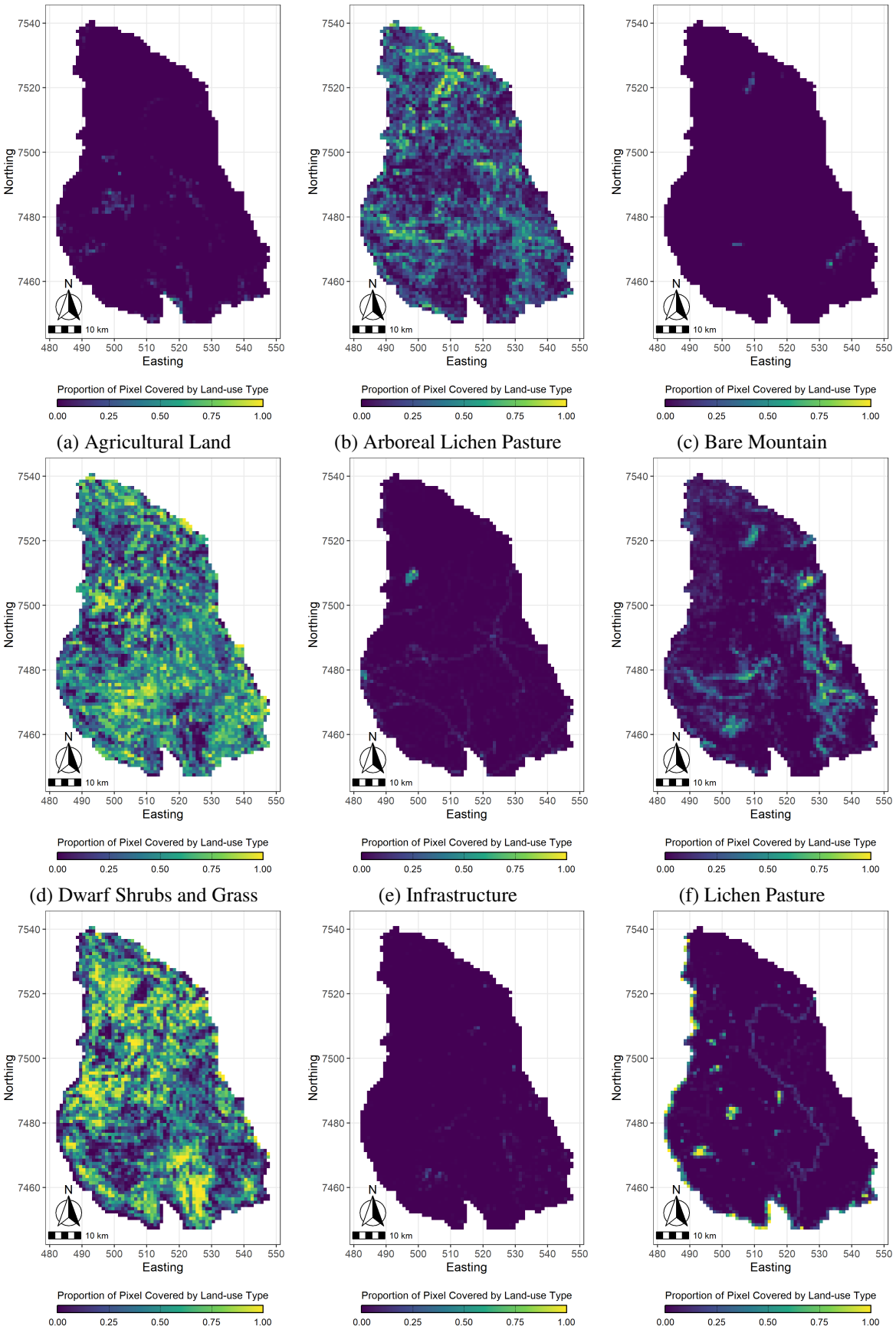

(a) Agricultural Land (b) Arboreal Lichen Pasture (c) Bare Mountain

(d) Dwarf Shrubs and Grass (e) Infrastructure (f) Lichen Pasture

(g) Mires and Fens (h) Sand and Gravel (i) Water

Figure 5.3: Spatial distribution of land-use covariates. Colour scale is on a gradient of 0 (blue) to 1 (yellow), indicating the proportion of the 1km×1km pixel covered by this land use type.

5.2.4 Modelling Strategy

The survey, telemetry and joint Langevin movement models as described in Chapter 4 were fitted to various combinations of the processed data. A telemetry and joint model were fitted to each of the subsets of the telemetry data (5-, 10-, 20-, and 30-individuals). The joint models also incorporated the survey data as an additional data stream, and a separate survey model was fitted to this data. This resulted in a set of 9 core multivariable models (4 telemetry, 1 survey, and 4 joint) of which further permutations were fitted, for comparison. As described in Chapter 4, the survey, telemetry and joint models all share the same formulation for the predictor of the utilisation distribution (and in the joint model, estimation of selection parameters is shared across likelihoods). For this initial set of 9 multivariable models, the predictor for utilisation distribution, as described in Equation 4.3, can be written as

$$\eta(x) = \sum_{k=1}^{9} \beta_k c_k(x), \tag{5.1}$$

where for $k \in \{1, ..., 9\}$, $c_k(x)$ represent each of the 9 land-use covariates, and β_k represent the estimated selection parameters.

Another set of 9 models were fitted with a Gaussian random field included in the predictor for the utilisation distribution. These 9 models share a description of the predictor which can be written as

$$\eta(x) = \psi(x) + \sum_{k=1}^{9} \beta_k c_k(x), \tag{5.2}$$

where $\psi(x)$ represents a spatially structured Gaussian random field. PC-priors were set for the parameters of the field, using $P(\rho < 5) = 0.01$ for the range parameter and $P(\sigma > 2) = 0.01$ for the standard deviation (see Section 1.6.3).

In addition to the 18 multivariable models, 81 univariable versions of the models were fitted: a set of 9 models for each of the 9 fixed effects. For each of these models, the predictor can be described as

$$\eta(x) = \beta_k c_k(x), \tag{5.3}$$

where only one of the 9 land-use covariates is included. These models were included to provide comparison against the more complex (and therefore less interpretable) multivariable models for each estimated effect.

This resulted in a total modelling strategy of 99 models, producing 27 posterior estimates for each of the 9 land-use covariates. The modelling strategy is summarised in Table 5.1, which also provides the running times for each of the 18 multivariable models and an example subset of 9 of the univariable models. Similar to Chapter 3, this chapter aims to explore the behaviour of this modelling framework under a range of conditions in an applied context, which is why such a large number of models were analysed here.

As can be seen in Table 5.1, most of the models ran in an efficient timeframe. Although, incorporation of a GRF into the predictor increased model running times; the multivariable joint model with a GRF took approximately 4.23 hours to run, whereas its equivalent without a GRF only had a running time of 53.41 seconds. For this reason, and because a GRF would replicate the effects of the missing covariates in the univariable models, the option of a GRF was only included for the 9 multivariable models, and not the 81 univariable models.

An IID random effect was also included in the survey models, to account for variations in month that survey data were collected. As this model component was not of interest for interpretation, and to improve computational efficiency, the IID random effect was set to have a fixed, high variance.

As the survey model was fitted as a log Gaussian Cox process (LGCP), it incorporated a Delaunay mesh triangulation in order to represent continuous-space. The mesh resolution should be at least fine enough to capture variation in covariate values over space, so the mesh was specified with a resolution which matched the covariate grain of $1km \times 1km$ (Lindgren, Rue, and Lindström, 2011).

All analysis was carried out using `R` version 4.5.1 (R Core Team, 2025), `R-INLA` version 25.06.22-1 (Rue, Martino, and Chopin, 2009), and `R-inlabru` version 2.12.0.9022 (Bachl et al.,

2019) with a 2.4-3.2GHz 10C processor (384GB RAM).

Table 5.1: The running times (in seconds, rounded to 2 decimal places) for each of the 18 multivariable models, and one set of 9 of the 81 univariable models (Lichen Pasture covariate).

Model	Predictor	Individuals	Running Time (seconds)
Multivariable Survey Model	GRF		8847.22
	No GRF		21.44
Multivariable Telemetry Model	GRF	5	168.10
		10	232.30
		20	342.75
		30	430.28
	No GRF	5	11.40
		10	14.50
		20	17.71
		30	18.39
Multivariable Joint Model	GRF	5	10297.15
		10	4525.85
		20	33541.38
		30	15233.31
	No GRF	5	49.67
		10	41.08
		20	103.41
		30	53.41
Univariable Survey Model	No GRF		38.02
Univariable Telemetry Model	No GRF	5	11.27
		10	9.84
		20	11.29
		30	26.92
Univariable Joint Model	No GRF	5	53.17
		10	33.19
		20	39.32
		30	117.69

5.3 Results

The estimated posterior mean effects of the 9 land-use variables can be interpreted as habitat selection parameters, wherein a positive effect indicates preference for a given habitat type and a negative effect indicates avoidance. Here, results are presented visually in Figures 5.4, 5.5, and 5.6. Numeric values associated with these figures can be found in Appendix C.

The estimated posterior mean effects of reindeer habitat selection of 9 land-use variables are compared across the 9 multivariable models which did not contain a random field in Figure 5.4, with values provided in Table C.1. For all land-use types, the strength and direction of estimated effect contrasted between survey and telemetry models. Models fitted to the survey data alone estimated a negative mean effect of arboreal lichen pasture, dwarf shrubs and grass, infrastructure, mires and fens, and water. Conversely, the 4 models fitted to varying subsets of the telemetry data alone estimated a positive mean effect of agricultural land, dwarf shrubs and grass, lichen pasture, mires and fens, sand and gravel, and water.

Number of individuals included in the telemetry dataset also impacted estimation of habitat selection parameters. In the case of bare mountain and infrastructure, a positive mean effect was only estimated by the telemetry models fitted to data from a larger number of individuals, with models fitted to data from fewer individuals estimating a 95% credible interval which contained 0 (Figure 5.4).

The direction of posterior mean estimates for habitat selection parameters from the joint models containing both data streams were varied, concurring with the survey data for agricultural land and lichen pasture with a 95% credible interval containing 0, and a negative effect of water (Figure 5.4). In the case of arboreal lichen pasture, dwarf shrubs and grass, infrastructure, mires and fens, and sand and gravel, the significance of the estimated effect from the joint models varied with number of individuals included in the telemetry dataset.

The most unusual result appears for the bare mountain covariate, wherein the joint models estimate a negative effect, but the survey and telemetry models estimate a positive effect or a 95% credible interval concentrated around 0 (Figure 5.4).

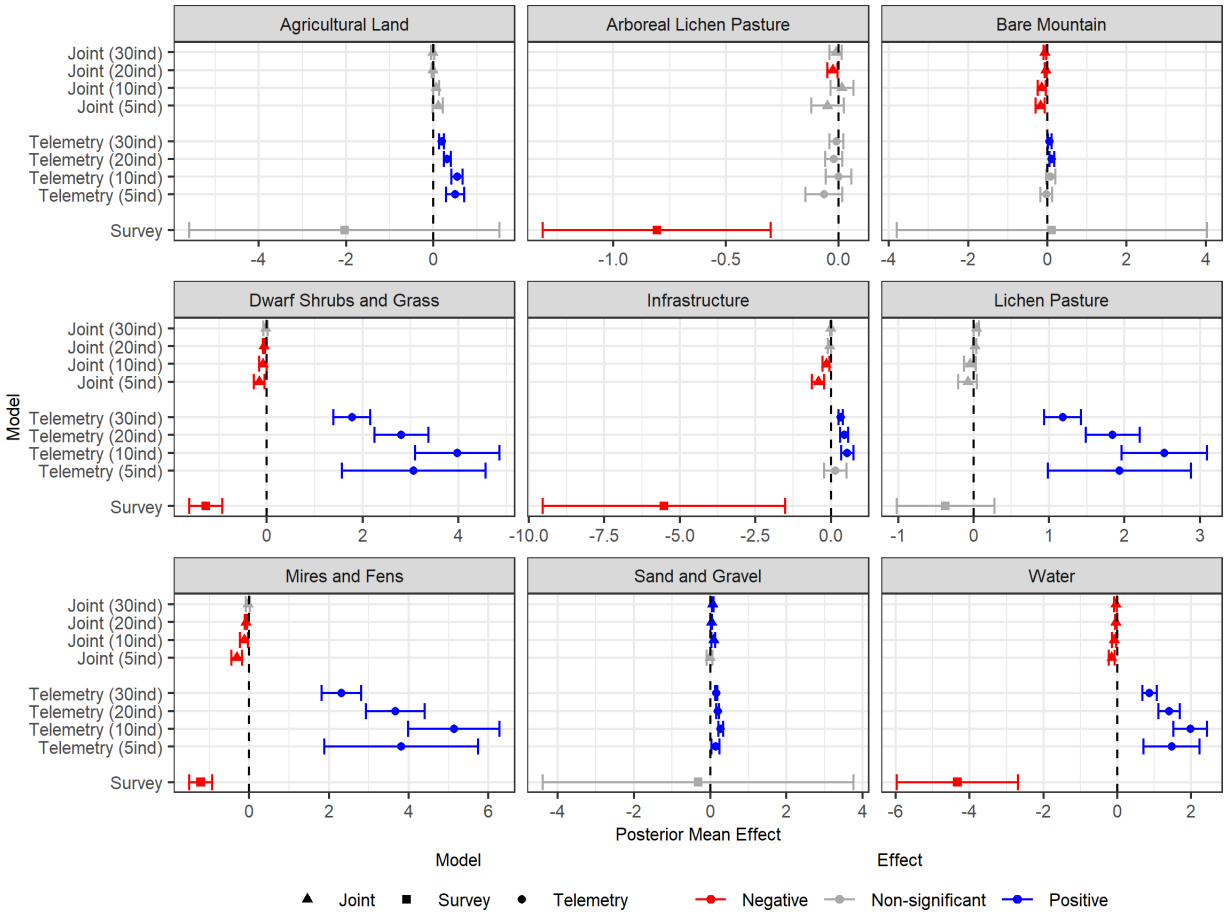

Figure 5.4: Estimated posterior mean and 95% credible intervals for effects of each of the 9 land-use covariates from the 9 multivariable models (without a GRF). Zero is indicated by a dashed, vertical line. Colour scale indicates the contents of the 95% credible interval: red = 95% CI entirely below 0, grey = 95% CI contains 0, and blue = 95% CI entirely above 0. Shape indicates the modelling framework: triangle = survey, circle = telemetry, and square = joint.

Figure 5.5 provides a visual representation of posterior mean estimates of the effect of land-use variables from the 81 univariable models (see Table C.2 for values).

Posterior mean estimates of habitat selection parameters from the 81 univariable models often differed in effect size and direction to the estimates made by their corresponding multivariable models, particularly in the case of the models fitted to telemetry data only. For example, most multivariable telemetry models estimated a positive effect of infrastructure (Figure 5.4), but corresponding univariable models estimated a negative effect.

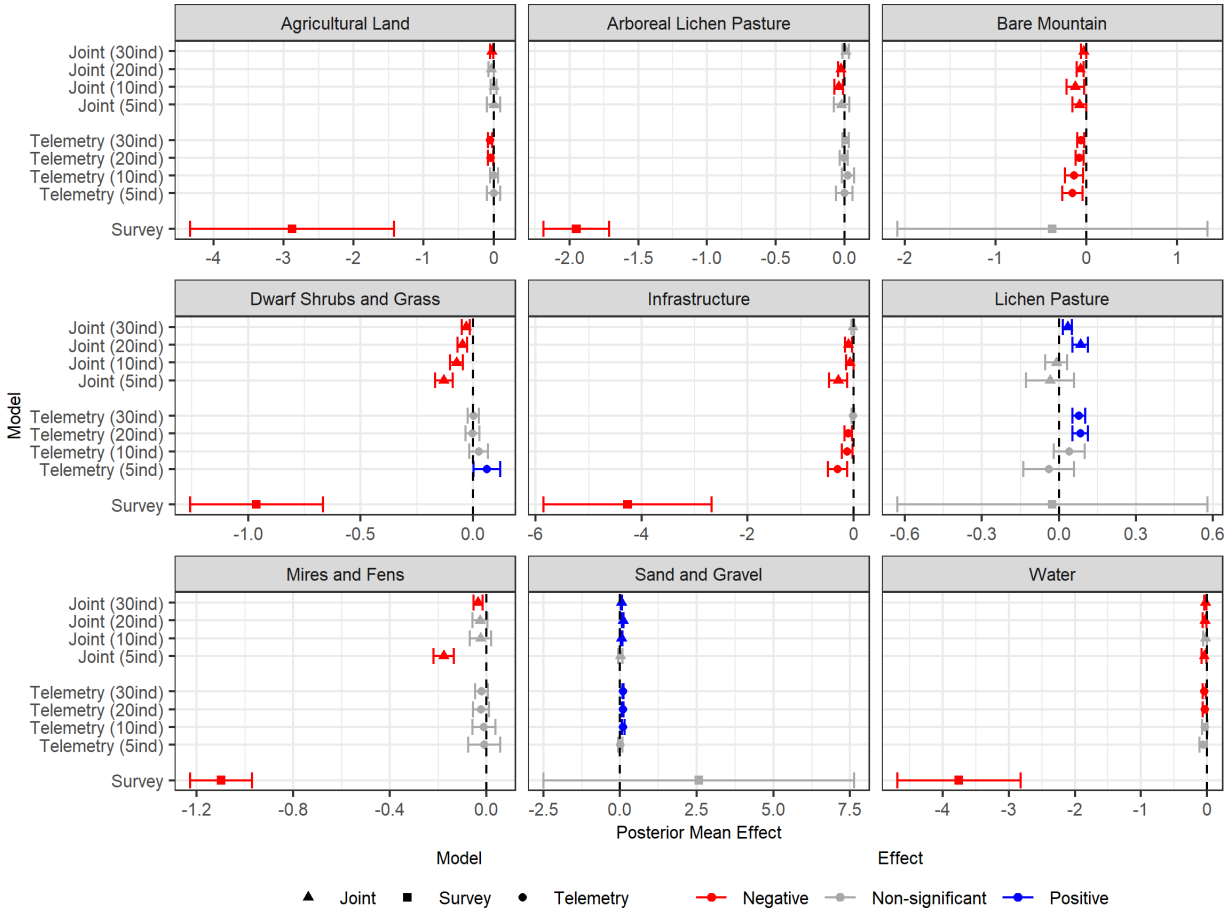

Figure 5.5: Estimated posterior mean and 95% credible intervals for effects of each of the 9 land-use covariates from the 81 univariable models. Zero is indicated by a dashed, vertical line. Colour scale indicates the contents of the 95% credible interval: red = 95% CI entirely below 0, grey = 95% CI contains 0, and blue = 95% CI entirely above 0. Shape indicates the modelling framework: triangle = survey, circle = telemetry, and square = joint.

For some models, the 95% credible interval for a land-use variable was estimated to contain 0 by the multivariable models, but was estimated to be entirely above or below 0 by the univariable models. For example, the multivariable survey model produced a 95% credible interval containing 0 for agricultural land, but the corresponding univariable model estimated this variable to have a negative effect with a 95% credible interval entirely below 0 (Figures 5.4 and 5.5).

The impact of number of individuals in the telemetry data on posterior mean estimates from the telemetry and joint models was less regular for the univariable models compared to the multivariable models. For example, in the case of dwarf shrubs and grass and infrastructure, increasing the number of individuals in the telemetry data resulted in a loss of significance in the posterior mean estimate from the telemetry models (Figure 5.5). Alternatively, in the case of arboreal lichen pasture, a negative effect with 95% credible interval below 0 was only estimated for the joint models fitted to the 10- and 20-individual telemetry data subsets, and the 95% credible interval contained 0 for those fitted to the 5- and 30-individual data.

For the group of univariable models, each joint model always estimated an effect direction which concurred with either the estimate of the survey-only model, or its corresponding telemetry model. In the univariable models, the bare mountain covariate was estimated to have a negative effect in the telemetry and joint models, whereas in the survey model the 95% credible interval contained 0 (Figure 5.5).

Posterior mean estimates of habitat selection parameters from the multivariable models containing a Gaussian random field (GRF) in the linear predictor are plotted in Figure 5.6. Values can be read in Table C.3.

In several cases, incorporation of a GRF in the linear predictor resulted in a loss of significance for estimated habitat selection parameters. For example, the effect of arboreal lichen pasture was estimated to be negative in the multivariable and univariable survey models without a GRF (Figures 5.4 and 5.5) but the 95% credible interval contained 0 in the corresponding model that contained a GRF (Figure 5.6). Contrastingly, the joint model fitted to telemetry data from 10 individuals estimated a positive effect with 95% credible interval above 0 for agricultural land (Figure 5.6), whereas the corresponding model without a GRF produced a 95% credible interval which contained 0 (Figure 5.4).

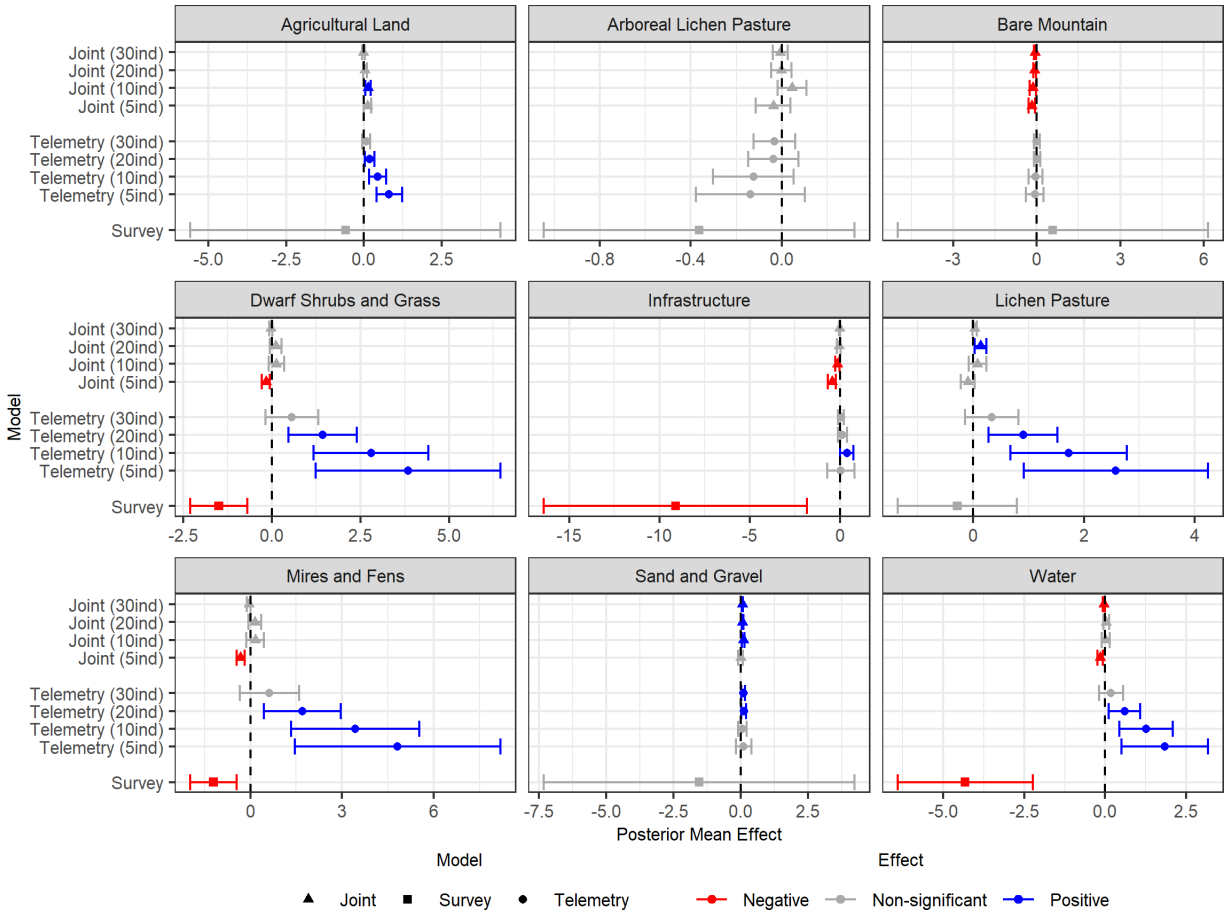

Figure 5.6: Estimated posterior mean and 95% credible intervals for effects of each of the 9 land-use covariates from the 9 multivariable models containing a GRF. Zero is indicated by a dashed, vertical line. Colour scale indicates the contents of the 95% credible interval: red = 95% CI entirely below 0, grey = 95% CI contains 0, and blue = 95% CI entirely above 0. Shape indicates the modelling framework: triangle = survey, circle = telemetry, and square = joint.

Table 5.2 contains the posterior estimated mean values for the range and standard deviation parameters of the GRF. The survey model, joint models, and the telemetry model fitted to data from 5 individuals all produced an estimated range of around 4km, whereas the telemetry models fitted to data from more individuals estimated a GRF with a smaller range. Despite strong priors, the telemetry models estimated a GRF with a high standard deviation. The GRF produced by the survey and joint models had a comparatively lower standard deviation. This may be an indication of similar issues to estimating the random field as discussed in Chapter 4. The relationship between parameter values (such as the fixed Γ parameter), spatial scale of fixed and random effects, and the performance of the model in terms of predicting the spatial distribution of the random field constitutes an area of interest for future research.

Table 5.2: Posterior mean and 95% credible intervals for the estimated Gaussian random field range and standard deviation predicted from the 10 multivariable models with a GRF. All values given are rounded to 2 decimal places.

Model	Individuals	Range ρ	Standard Deviation σ
Survey		3.71	0.65
		[3.71,3.71]	[0.65,0.65]
Telemetry	5	4.1	6.01
		[2.52,6.45]	[4.93,7.21]
	10	1.92	8.7
		[1.2,2.88]	[6.52,11.47]
	20	1.35	7.48
		[1.23,1.48]	[6.8,8.23]
	30	1.43	6.4
		[0.79,2.41]	[3.89,9.92]
Joint	5	4.02	0.77
		[4.02,4.02]	[0.77,0.77]
	10	4.3	0.95
		[3.67,5.02]	[0.83,1.07]
	20	4.37	1.05
		[4.36,4.37]	[1.05,1.05]
	30	4.47	1.19
		[4.47,4.47]	[1.19,1.19]

The spatial distribution of the predicted fields from the survey model and the telemetry and joint models fitted to data from 30 individuals are shown in Figure 5.7. The survey model estimates a relatively smooth field, whereas the telemetry model estimates clustering at a much finer scale. The estimated GRF from the joint model represents a balance of the two.

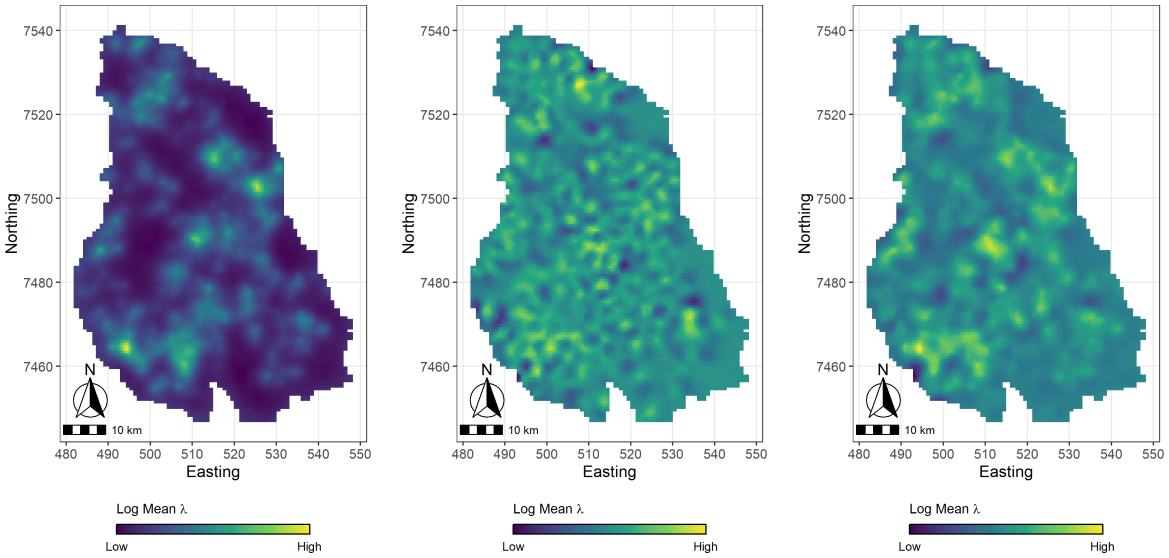

(a) Survey (b) Telemetry (c) Joint

Figure 5.7: Posterior estimated Gaussian random fields from the multivariable (a) survey model, (b) telemetry model with 30 individuals, and (c) joint model with 30 individuals. Colour scale follows a relative gradient of log mean intensity from low (blue) to high (yellow), as interest is in relative differences across space and not absolute values.

Figure 5.8 demonstrates a spatial representation of the utilisation distribution from the multivariable survey, 30-individual telemetry, and 30-individual joint models with and without a GRF. For the telemetry and joint models which contain a GRF, this is highly influential in predicting space-use (as visible by the comparison of spatial predictions to the spatial representation of the field in Figure 5.7). On the other hand, the survey model which contains a GRF predicts a utilisation distribution which is balanced in the influence of the GRF and fixed effects. For the models which did not contain a GRF, the prediction from the joint model mirrors influences from both the survey and telemetry predictions.

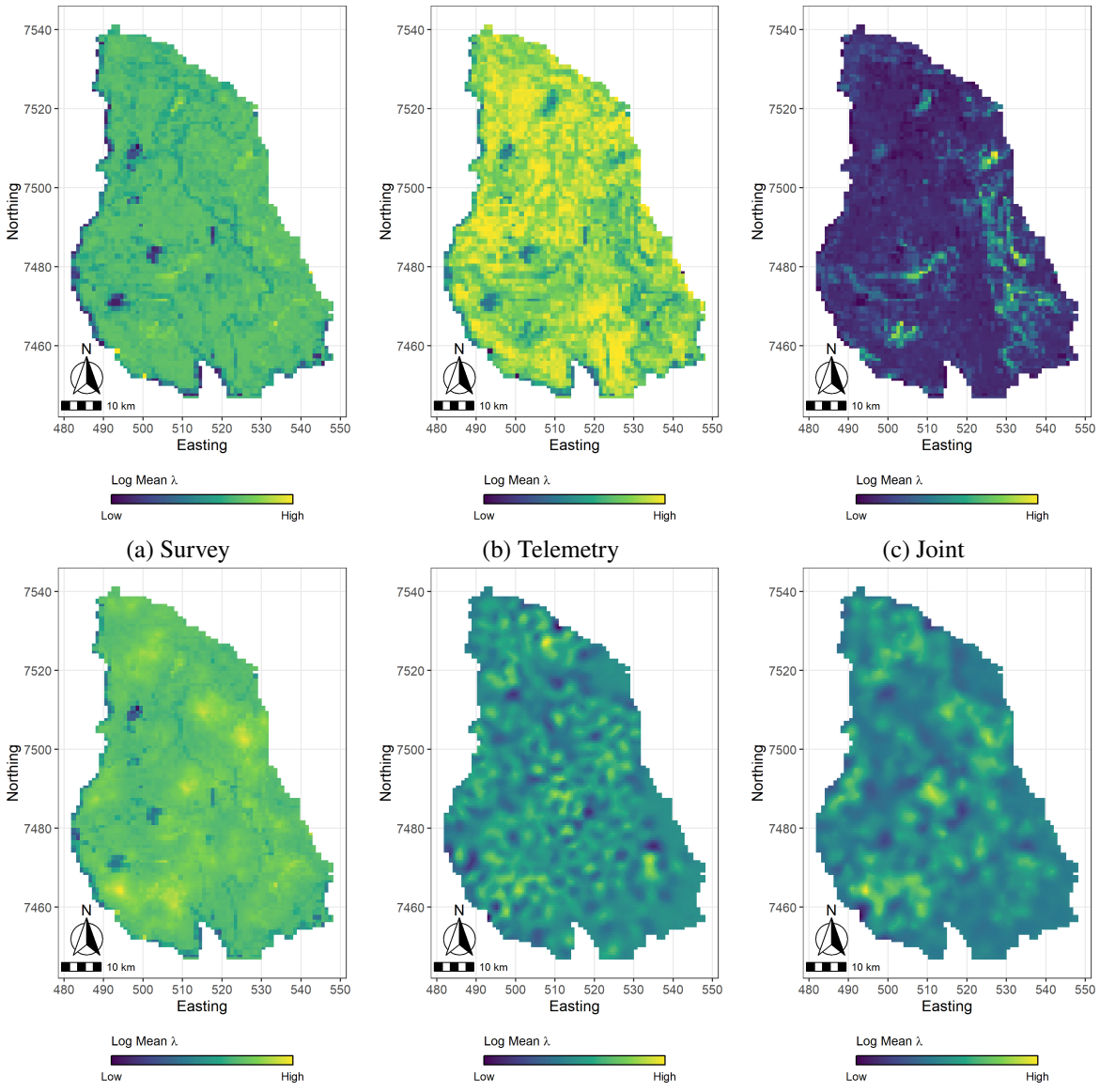

(a) Survey (b) Telemetry (c) Joint

(d) Survey (GRF) (e) Telemetry (GRF) (f) Joint (GRF)

Figure 5.8: Posterior predicted spatial distribution of the utilisation distribution from the multi-variable (a,d) survey models, (b,e) telemetry models with 30 individuals, and (c,f) joint models with 30 individuals. Predictions in the first row (a-c) were produced from models which did not contain a GRF, and predictions in the second row (d-f) were produced from models which did contain a GRF. Colour scale follows a relative gradient of log mean intensity from low (blue) to high (yellow), as interest is in relative differences across space and not absolute values.

5.4 Discussion

The way in which data were subsetted resulted in windows of insight into habitat selection at different organisational scales (Figure 5.2). The survey data contained the locations of all individuals as a representative sample of the overall population distribution. Contrastingly, the telemetry data subsets contained fewer individuals, so gave a more fine-scale insight into local habitat selection.

Heterogeneity in covariate values occurs at very different spatial scales for the different land-use covariates (Figure 5.3). Most of the land-uses which represent available forage for reindeer (arboreal lichen pasture, dwarf shrubs and grass, and mires and fens) occur throughout the study domain with fine-scale heterogeneity. However, other land-use types (agricultural land, bare mountain, and sand and gravel) follow a different spatial structure characterised by large areas of homogeneity where the land use type is absent (i.e., a 0 value on the covariate scale). The remaining land-uses (infrastructure, lichen pasture, and water) follow a spatial structure that falls somewhere between these extremes. The impact of this unusual spatial structure on the survey models can be observed in the estimated 95% credible intervals, which are much wider for agricultural land, bare mountain, infrastructure, and sand and gravel, indicating a higher level of uncertainty in these estimated effects (Figure 5.4). The spatial scale of covariate structure is likely to influence inference differently for the models analysed at different organisational scales. Survey models aim to infer large-scale trends in overall spatial distribution, whereas telemetry models investigate habitat variables as a function of small-scale local movement.

In the multivariable models, there is a clear difference in the estimated direction of effect between the survey and telemetry models for covariates with small- and intermediate-scale heterogeneous structures (dwarf shrubs and grass, infrastructure, mires and fens, and water, Figures 5.4 and 5.6). For all of these covariates, the survey model estimates a negative effect, indicating habitat avoidance, whereas the telemetry models estimate a positive effect, indicating habitat preference. This may be due to the difference in organisational-scale at which the models evaluate habitat selection; the individual-level telemetry models indicate a preference for these land-uses at the local scale, but the survey models find a negative relationship between these covariates

and the overall spatial distribution of the population. This disparity between the individual- and population-level models can also be explained when considering that reindeer space use is subject to different restrictions at macro- and micro-scales: reindeer herders are likely to have more influence on selection of regional areas, whereas fine-scale movement decisions are more likely to be influenced by reindeer foraging behaviour (Horstkotte et al., 2022).

Estimated effect strength and direction often differed for the same land-use covariate between the multivariable and univariable models. This result demonstrates that the inclusion of a large number of covariates in habitat selection models can reduce model interpretability, as estimates of the strength and direction of covariates are influenced by the presence of other fixed effects. Existing literature has found reindeer movement to be subject to the effect of complex interactions between variables, which were difficult to detect when examining responses independently (Valente et al., 2020). This may explain strange results inferred from the joint multivariable models when compared to the survey and telemetry models. In particular, in the multivariable model (Figure 5.4) the bare mountain covariate is estimated to have a negative effect by the joint models, but this estimated habitat avoidance is not reflected in the telemetry or survey model estimates. This is not the case in the corresponding univariable models (Figure 5.5), where the joint models also estimate a negative effect, but this estimated habitat avoidance is reflected in the estimates of the telemetry models. Generally, the joint models tended to provide a more consistent estimate of the strength and direction of effects between the multivariable and univariable models, as compared to the survey and telemetry models which often estimated a different result dependent on the number of fixed effects in the models. This represents an advantage of the joint modelling approach, in that it can borrow strength across datastreams to produce more consistent estimates as compared to models carried out at a single organisational scale. However, it also presents a disadvantage, in that when many fixed effects are evaluated, some interpretability is lost in this complex model structure.

Due to the nature of the land-use covariates used in this analysis, the model suffers from perfect multicollinearity, introducing identifiability issues and potentially unstable estimates. Future research could involve reformulation of the predictor, such as removing one of the spatial covariates, to eliminate this issue.

In the joint Langevin movement model, a diffusivity parameter is used to represent availability restrictions (Chapter 4). This was defined using empirical measures of step-length, in a similar fashion to Chapter 3. This resulted in a value for this parameter (2km) which was close to the spatial resolution of the environmental variables and the Delaunay mesh triangulation ($1km^2$), and so may account for the highly localised effect of the estimated Gaussian random field in the telemetry model (Figure 5.7). Existing literature has found reindeer movement rates to be dynamic, changing in response to external stimuli, and potentially more wide-ranging than is considered here (Skarin et al., 2010). It has also been found that using step-lengths generated from coarse-frequency tracking data can lead to an underestimation of mobility (Mills, Patterson, and Murray, 2006; Johnson and Ganskopp, 2008; Davis et al., 2011; Mccann et al., 2021). The representation of availability in the telemetry models may therefore be overly constrained, or oversimplified given the 6-month duration of the observational period and the dynamic nature of reindeer movement behaviour. A potential avenue for future research would be to investigate the impact of changing the value assigned to the diffusivity parameter on habitat selection inference in this framework.

Inclusion of a Gaussian random field in the models caused a loss of significance for many of the estimated effects of land-use covariates (Figure 5.6). This may have been due to spatial confounding, as the spatial scale of the random field was estimated to be small in all of the models (Table 5.2), so may have accounted for the small-scale variation in spatial structure that would otherwise have been explained by the heterogeneous fixed effects (Illian et al., 2014). This also resulted in reduced interpretability in predictions of overall reindeer spatial distribution from these models (Figure 5.8). Existing literature has found the main drivers of reindeer habitat selection to be elevation; vegetation; insect harassment; and anthropogenic disturbance, which are respectively accounted for through the bare mountain; arboreal lichen pasture, dwarf shrubs and grass, lichen pasture, and mires and fens; sand and gravel; and infrastructure land-use covariates included here (Skarin et al., 2010; Pape and Löffler, 2016). A possible effect not accounted for via fixed effects here is the impact of predator species, which have been found to have a strong influence on reindeer movement behaviour via depredation (Sunde et al., 2000; Moa et al., 2006; Mattisson, Odden, and Linnell, 2014; Rivrud et al., 2018; Rasmus et al., 2020). It may not be

possible to account for this effect via a spatial random field if its spatial scale is similar to that of the other fixed effects, as is seen here. However, an avenue of future research could be to investigate the incorporation of a larger scale effect, or to account for predator densities through an additional data stream (as in joint species distribution modelling, Sadykova et al., 2017).

For the models which did not contain a Gaussian random field, and therefore predicted the utilisation distribution using only fixed effects, overall predictions of spatial distribution differed between models fitted to different data streams (Figure 5.8). Negative effects of water and infrastructure are visually evident in the prediction from the survey model characterised by large dark spots in the West of the region, related to large lakes and the Kevitsa mining area (see Figures 5.3 and 5.1). The telemetry prediction is strongly characterised by the effect of variables representing available forage such as mires and fens and dwarf shrubs and grass. This aligns with existing literature which suggests small-scale reindeer habitat selection is determined by foraging behaviour (Horstkotte et al., 2022). Although infrastructure and water are predicted to have a positive effect in the telemetry models (Figure 5.4), the spatial prediction provides an interpretation of these estimates in relation to other estimated effects, so large lakes and the Kevitsa mining area are still estimated to be areas of lower relative mean intensity overall. The prediction from the joint model estimates a lower relative mean intensity for areas with high proportions of water, but is largely characterised by influence of the lichen pasture covariate. This is initially surprising given that the 95% credible interval for the effect of lichen pasture contained 0 in this model, but is more interpretable when the effect is viewed in relation to the other covariates. The only 95% credible intervals which did not contain 0 estimated in this model were for those covariates with an unusual spatial structure where higher proportions of the land-use type are found in very small areas in a few locations in the district. Since this makes the effect of these covariates difficult to detect visually in the prediction map, the lichen pasture effect seems more apparent. These differences between predictions made from the joint model and its requisite parts suggest that integrating multiple data streams in multivariable model is not simply a combination of the estimated effects from each organisational scale, but provides an alternative viewpoint supported by a larger amount of data. Spatial predictions and habitat selection estimates need to be combined and considered in relation to all fixed effects included in the model, to gain a full understanding

of model outputs.

5.5 Conclusions

This chapter demonstrated the application of the joint Langevin movement modelling framework in `R-inlabru` that was developed in Chapter 4 to real data. The survey, telemetry, and joint models were fitted to tracking data of semi-domesticated reindeer, to provide an understanding of habitat selection in a multi-use landscape. Variations in model type, number of individuals, and model components resulted in a modelling strategy of 99 models, which were compared in terms of selection parameter estimation. Models were also used to generate predicted spatial distributions for the overall reindeer population, and the effects of including a Gaussian random field in the linear predictor were investigated.

This work represents the first application of the `R-inlabru` formulation of the joint Langevin movement model to real data, and so is the first time individual-level habitat selection has been modelled in a continuous-time framework which uses INLA for inference.

The scale of spatial heterogeneity in environmental covariates influenced the significance of estimated effects differently between the survey and telemetry models, suggesting that the performance of models formulated for different organisational scales is likely related to the spatial structure of environmental covariates. Including a Gaussian random field in models to account for unexplained spatial structures in the data appeared to incur issues with overfitting or spatial confounding, and led to less interpretable predictions of species distribution. These effects were also likely linked to the spatial scale of heterogeneity in habitat variables, and may have been dependent on the representation of availability in the models. This chapter also demonstrated the benefit of joint modelling in borrowing strength across data streams to provide stable habitat selection parameter estimates, but that behaviour of complex joint models can be difficult to interpret when a large number of fixed effects are included in the predictor. Overall these results suggest that interpretability in complex models can depend on the spatial structure of fixed effects, and their scale in relation to model and random effect parameters.

Chapter 6

Conclusions

The main aim of this thesis was to explore the use of joint likelihood spatio-temporal point process models in the study of animal movement and habitat selection. This was motivated by the definition of point process models as a unifying framework in habitat selection and species distribution modelling (Miller et al., 2019; Matthiopoulos et al., 2022), the emergence of joint likelihood methods as a central theme in quantitative ecology (Altwegg et al., 2025), and the need to demonstrate usage and applications of fitting these complex models to ecological data (Illian and Burslem, 2017). Throughout the thesis, the central method of joint likelihood spatio-temporal point process modelling was investigated at varying spatial, temporal, and organisational scales; using different data types and model formulations; and with applications in different areas of ecology, such as reintroduction biology, agriculture, and management of semi-domesticated species. Key themes of availability, model complexity, and spatio-temporal scale were explored throughout.

In Chapter 2, models of varying complexity were used to evaluate a spatio-temporal marked point process approach to predicting population spread of a reintroduced population of Eurasian crane (*Grus grus*). Presence-absence (occupancy) data collected using a preferential sampling framework at a coarse temporal scale were analysed. The joint structure of the model allowed for the simultaneous modelling of underlying distribution of habitat patch locations, alongside occupancy data in a marked point process framework. Ecological processes impacting data distribution were accounted for through the inclusion of spatial and spatio-temporal random effects.

In Chapter 3, a spatio-temporal step-selection framework utilising point process methodology (GF-iSSA, Arce Guillen et al., 2023) was compared to a spatial point process resource selection model. Analysis was performed using presence-only tracking data of three breeds of cattle (*Bos taurus*) on a Swiss Alpine farm. A bespoke integration scheme was created, in order to account for additional restrictions in habitat availability imposed by this new application of GF-iSSA. Joint modelling was incorporated in the step-selection models, wherein the joint likelihood enabled shared parameter estimation from the tracks of multiple individuals. Comparisons were made between covariate spatial scales and tracking data temporal frequencies, to investigate the impact of data granularity on inference of habitat selection parameters and model fit.

Chapter 4 introduced a new method for performing inference using the joint likelihood ap-

proach for modelling tracking and survey data, the joint Langevin movement model (Blackwell and Matthiopoulos, 2024). The model was translated for implementation in the `R-inlabru` framework, using the INLA method for inference (Rue, Martino, and Chopin, 2009; Bachl et al., 2019; Van Niekerk et al., 2023). Varying advantages of this were demonstrated, including: incorporation of spatially varying detection probabilities in the survey likelihood; computationally efficient estimation of parameter values and spatial predictions; and accounting for spatial autocorrelation through the inclusion of a Gaussian random field in the predictor. The joint model demonstrated here combines multiple data streams at different organisational, spatial, and temporal scales. The utilisation distribution connecting the different likelihoods was modelled using spatial point process methodology.

Finally, Chapter 5 demonstrated the application of the approach developed in Chapter 4 to real data, modelling habitat selection of a semi-domesticated population of reindeer (*Rangifer tarandus tarandus*). Here, comparisons were made between models with multiple data streams and models with a single data stream; datasets of varying size; and different predictor component combinations. The use of a spatial random effect to account for unknown sources of spatial autocorrelation was investigated.

All of the analysis performed in this thesis (except for the JAGS comparison in Section 4.3.5) was carried out using the INLA method for inference (Rue, Martino, and Chopin, 2009). Models were fitted in the accessible software package `R-inlabru`. Utilisation of these frameworks for modelling and inference allowed the analyses demonstrated here to be relatively computationally efficient, and accessible for use in applied ecological contexts (Illian and Burslem, 2017). The case studies presented in this thesis therefore provide a demonstrative review of the applied usage of joint likelihood spatio-temporal point process models in understanding animal space-use and habitat selection. The remainder of this chapter contains a discussion of the methods and results, in the context of the key themes of availability, model complexity, and scale; suggestions for future research; and final closing remarks.

6.1 Discussion of Methods and Results

6.1.1 Availability

One of the aims of this thesis was to explore different ways to define availability in models of habitat selection. This was achieved by using different methods relevant to the modelling approaches presented in each chapter. These methods, and their varying impact on results, are discussed further here.

In Chapter 2, availability was defined through the incorporation of spatial and spatio-temporal random effects in a marked point process modelling structure. Formulating the model as a marked point process enabled any underlying spatial correlation structures in the distribution of habitat (wetlands) to be accounted for through a spatial random field ($G(s)$), allowing the distribution of crane presence, independent of wetland distribution, to be modelled and interpreted. In addition, restrictions in population dispersal ability were estimated using a spatio-temporal random field ($M(s,t)$). This model structure resulted in more realistic predictions of population spatial distribution that incorporated restrictions in dispersal ability, and the density of available habitat patches (Figure 2.5). The spatial distribution of the random fields as seen in Figure 2.4 demonstrates their role in restricting spatial predictions: had these random effects not been incorporated, estimates of species distribution would have likely extended beyond the population's current range. However, the data, which were characterised by a relatively stable distribution with a high proportion of absences, as is typical of early reintroduction data, proved to be insufficient in supporting the estimation of a complex component which modelled correlations in spatial distribution over time. This therefore demonstrates the limitation of using complex random effects to account for underlying ecological processes impacting availability.

Chapter 3 investigated description of availability at a different organisational scale, the individual-level of selection. In this approach, availability was accounted for through the creation of a bespoke integration scheme, which accounted for both animal mobility and physical barriers to movement. Animal mobility was defined using the average maximum distance from the empirical distribution of step-lengths, which was then used as the radius for the circular domain of availability. Domains of availability at each timestep were then cropped to paddock boundaries,

so also incorporated geographical inaccessibility. Using this approach, empirical estimations of step-length plateaued at coarser temporal resolutions, which may be indicative of a phenomenon wherein animal mobility is underestimated when temporal frequency is reduced (Mills, Patterson, and Murray, 2006; Johnson and Ganskopp, 2008). Results showed that posterior estimates of habitat selection parameters from SSA models were more highly influenced by temporal frequency as compared to the relatively impervious (though simplistic) RSA approach, which defined only physical restrictions on availability (paddock boundaries) and not animal mobility (Figures 3.8-3.11). This suggests that inferences are likely to be dependent on the definition of availability, which is intrinsically linked to temporal frequency, and as has been found in existing literature (Matthiopoulos et al., 2020). It would be of interest to investigate further how different variations of radius of domain of availability impact inference given a constant temporal frequency, in order to disentangle this effect.

In the joint Langevin movement model presented in Chapter 4, availability is incorporated through the definition of a diffusivity parameter (Γ), related to animal mobility. This is included directly in the model formulation, and in relation to the scaling parameter of the Gaussian smoothing kernel used in covariate transformations. In the original framework proposed by Blackwell and Matthiopoulos (2024) this parameter is estimated in the model, although treated as a nuisance parameter. In order to implement the model in `R-inlabru`, a simplification requiring this parameter to be fixed was used. This misaligns with existing guidance on best practice, as movement parameters are not estimated in the model (Avgar et al., 2016). However, the role of the diffusivity parameter in this framework is twofold: (1) as a necessary inclusion in the smoothing kernel due to the use of the Euler-Maruyama approach to approximate the process in discrete-time; and (2) as a biological representation of availability. Therefore, if the parameter were to be estimated in the model, its interpretation would be difficult, as these separate roles would need to be disentangled. Future development of this model could incorporate adjustments to allow the estimation and interpretation of this parameter.

In Chapter 5, the `R-inlabru` formulation of the joint Langevin movement model is applied to real data. In this chapter, the diffusivity parameter was defined using empirical measures of step-length, in a similar fashion to Chapter 3. This resulted in a value for this parameter (2km) which

was close to the spatial resolution of the environmental variables ($1km^2$), and so may account for the highly localised effect of the estimated Gaussian random field in the telemetry model (Figure 5.7). In this chapter, estimates of habitat selection parameters were found to generally differ in strength and direction between the survey and telemetry models (Figure 5.4). Representing differences in availability via this framework may be of benefit in disentangling movement drivers at different spatio-temporal scales. However, it would also be of interest to examine the impact of changing values of the diffusivity parameter on inference of habitat selection parameters - an area of potential future research.

6.1.2 Model Complexity

Another key theme of this thesis was the evaluation of model complexity and its impact on model interpretability and computational efficiency. This is summarised in relation to each chapter here.

Chapter 2 compared across four models with differing levels of complexity. The most complex (and computationally costly) model (the marked point process model with AR1 temporal structure) incorporated components that the data were insufficient to support, resulting in unrealistic predictions of population spatial distribution. On the other hand, a model of intermediate complexity (the marked point process model with IID temporal structure) performed better than simpler models (the binomial presence-absence models) in terms of predicting a more realistic spatial distribution for the population (Figure 2.5). Therefore, the results of this chapter demonstrate a non-monotonic relationship between model complexity and performance. The utility of complex model components in representing intricate ecological processes is demonstrated, but caution is advised in their usage.

In Chapter 3 a simpler RSA model construction was compared to the more complex SSA models. The unique integration scheme used in the SSA models was found to greatly increase computational cost, limiting the usage of this modelling framework dependent on different data factors (such as number of individuals, study duration, observation temporal frequency, radius of the domain of availability, mesh grain, and overall spatial area, Table 3.2). The RSA and SSA approaches were also differently impacted by variations in spatio-temporal scale of data, although RSA models were found to perform well even with low numbers of observations Figures 3.8-3.11.

The results of this chapter suggest that simple and complex frameworks for modelling can both be of use in understanding animal space-use and habitat selection, and that the selection of a method should be considered in relation to modelling aims, spatio-temporal scale, and computational restrictions.

Chapter 4 demonstrates the advantage of a complex joint modelling framework in comparison to models with a single data stream. In Section 4.3.2, the simpler survey and telemetry models perform similarly well to the joint model in estimating habitat selection parameters and predicting spatial distribution. However, when fitted to poorer-quality data, as in Section 4.3.4, the more complex joint model outperforms the simpler models by borrowing strength across both data streams. This demonstrates the advantage of complex joint modelling, particularly for messy ecological data.

Finally in Chapter 5, comparisons were made across multivariable and univariable models, and the impact of incorporating a random effect in the predictor was investigated. The inclusion of a high number of fixed effects in the multivariable models led to some behaviour in the joint models that was difficult to interpret, in comparison to the corresponding univariable models (Figures 5.4 and 5.5). Including a Gaussian random field also led to less interpretable predictions of spatial distribution, potentially due to spatial confounding with covariates (Figure 5.8). Overall these results suggest that part of the relationship between model complexity and interpretability is dependent on the spatial structure of environmental variables, in terms of heterogeneity, collinearity, and scale in relation to model parameterisation.

Overall, these results show that the relationship between model complexity, performance, and interpretability is intricate and varied. Complexity can improve model performance but increase computational cost and reduce interpretability. Incorporation of complex model components and use of complex model structures should depend on inferential aims, the scale of analysis, and features of the data and system. Assessing the level of complexity needed should involve comparison of models at different levels of complexity, with reference not just to model performance, but to interpretability and computational efficiency.

6.1.3 Spatial, Temporal, and Organisational Scale

A final theme investigated in this thesis was the impact of spatial, temporal, and organisational scale (in terms of individual- versus population-level) on habitat selection inference. This was a particular focus in Chapter 3, but is also discussed here in relation to Chapters 4 and 5.

Chapter 3 investigated the effects of differences in data granularity (in terms of spatial scale of covariates and temporal frequency of tracking data) on habitat selection models at different organisational scales. The results of this chapter demonstrate that decreasing covariate spatial resolution can alter the strength and direction of estimated effects, particularly for the population-level RSA model (Figure 3.8). However, this approach seems to be resilient to reductions in the temporal frequency of tracking data (Figure 3.12). Contrastingly, observation temporal frequency was found to have a strong impact on habitat selection parameter inference in the individual-level SSA models, and also interacted with spatial scale, impacting relative model assessment rankings (Figure 3.13). These results demonstrate that changing the spatio-temporal scale of data can drastically alter inference, but that this effect is variable between modelling approaches carried out at different organisational scales.

The relationship between the spatial scale of covariate heterogeneity and the performance of models at different organisational scales also emerged as a result of Chapters 4 and 5. In Chapter 4 Section 4.3.4 the population-level survey model was found to perform more poorly at recovering the parameter value for a covariate with fine-scale heterogeneity (c_{env}), and performed better when estimating the effect of a more smooth covariate (c_{mid}, Table 4.4). In contrast, the individual-level telemetry model demonstrated an inverse performance, better estimating c_{env} and associating more uncertainty with the estimate of c_{mid}. A similar effect can be seen in the case study application of the models in Chapter 5, wherein the level of spatial heterogeneity in environmental covariates influenced the significance of estimated effects differently between the survey and telemetry models. These results suggest that the performance of models formulated for different organisational scales is likely related to the spatial structure of environmental covariates.

6.2 Potential Future Work

The methods and applications presented in this thesis demonstrate the flexibility and range of joint likelihood spatio-temporal point process methods for modelling animal movement, space-use, and habitat distribution. Some suggestions for potential future work have already been mentioned in this chapter. Further suggestions are detailed below.

In Chapter 2 a separable space-time process is used in the construction of the spatio-temporal field. Since this analysis was performed, the development of new methods for spatio-temporal modelling, such as the `R-INLAspacetime` package, have made spatio-temporal processes with different levels of separability more accessible for applied use (Lindgren et al., 2023). One such model, the diffusion-based extension of the Gaussian Matérn field (DEMF), may provide a more appropriate representation of population spread through the incorporation of a diffusion process. Therefore, a potential topic for future research would be to incorporate DEMF into the modelling framework presented here.

Computational efficiency posed a limitation to the model variations compared in Chapter 3. Future study could include extensions to the models investigated here. For example, multivariable models were generally found to perform most poorly in the 9-model group comparisons (Table 3.3). This may be due to the fact that these models incorporate both covariates at the same spatial scale. Further extensions to this work could include construction and comparison of multiscale models, where slope and forage quality covariates are included in the same model at different spatial resolutions.

In Chapter 4, an advantage of the implementation of the joint Langevin movement model in the `R-inlabru` framework is demonstrated in the proficiency of this software package for handling complex observation processes (Section 4.3.6). This benefit could be utilised in an extension of the approach where another data stream for the population-level part of the model is integrated into the joint likelihood. This forms the subject of an area of current research interest in ecology, where data integration is used to borrow strength across species distribution datasets (Miller et al., 2019).

Another potential area of development for the approach presented in Chapter 4 would be

to enable the incorporation of directional persistence in the movement model. This has been demonstrated for the underdamped Langevin process, by formulating the model in terms of velocity rather than speed (Michelot, 2024). An area of future research could include investigating the potential implementation of this approach in the `R-inlabru` framework.

Finally, the work presented in Chapter 5 is the first application of the `R-inlabru` joint Langevin movement model to real data. Future work could include variations of spatio-temporal scale of environmental covariates and tracking data and comparison across different values for the diffusivity parameter. In addition, future research could involve the application of this modelling framework to different species and systems.

6.3 Final Remarks

In summary, this thesis has provided an exploration of joint likelihood spatio-temporal point process methods for modelling animal movement, space-use, and habitat selection. This base framework has been shown to provide a versatile approach to modelling at different spatio-temporal and organisational scales, with a range of applications in reintroduction biology, agriculture, and management of semi-domesticated species. This included additional development of the complex integration scheme used in the GF-iSSA approach to discrete-time movement modelling in `R-inlabru` for its first ever application in modelling livestock movement; as well as the implementation of the first individual-level continuous-time habitat selection model in `R-inlabru`: the joint Langevin movement model. Throughout the thesis, key themes of accounting for availability; spatio-temporal and organisational scale; and model complexity have been addressed. Results have demonstrated the impacts of using different methods to account for animal mobility, habitat availability, and physical constraints on accessibility; the scale-dependency of inference related to data granularity and selection level; and the non-monotonic relationship between model complexity and performance.

Appendix A

Supplementary Material for Chapter 2

The figures included in this appendix provide further information about the structure of the estimated fields and the predictions made by the models fitted in Chapter 2. The estimated mark random fields $M(s,t)$ from the single likelihood models have a comparative structure to those from the joint likelihood models mentioned in the main text. Note that in the models with AR1 temporal structure, estimates of the mark random field $M(s,t)$ (Figure A.1) are estimated to be the same across all years, whereas the models with IID temporal structure estimate a different distribution each year (Figure A.2). The point random field $G(s)$ estimated from the marked point process model with AR1 temporal structure is similar to that of the IID model, mentioned in the main text (Figure A.3).

Predictions of probability of crane presence made using the AR1 models are very similar for all years (Figures A.4 and A.5), whereas the IID models show more variation across years (Figures A.6 and A.7). There is also a difference in the spatial spread of predictions made using the binomial presence absence models (Figures A.5 and A.7) compared to those made using the marked point process models (Figures A.4 and A.6).

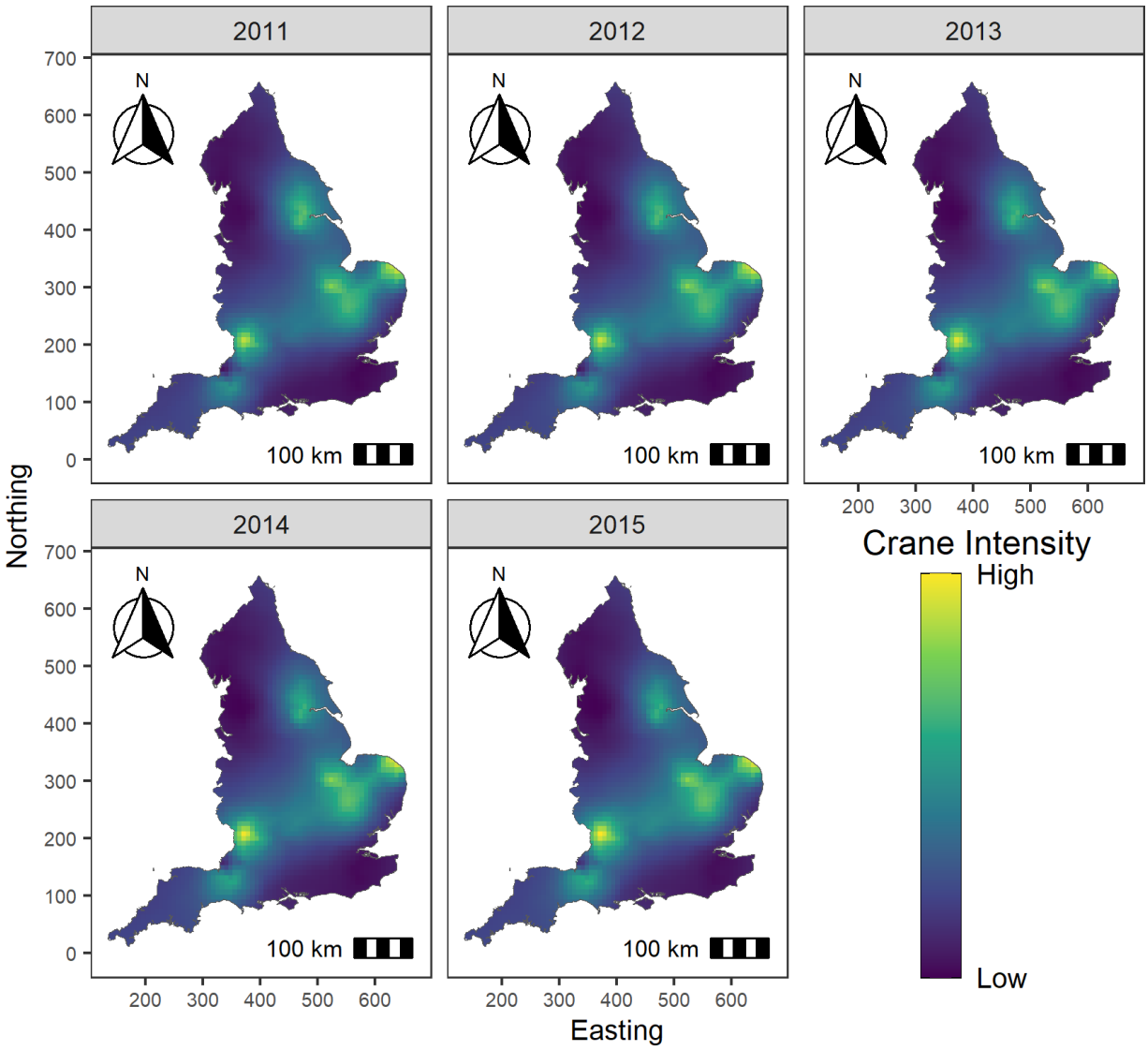

Figure A.1: Estimated mark random field ($M(s,t)$) for 2011-2015 from the binomial presence/absence with AR1 temporal structure. Colour scale is given in low-high intensity as interest is in relative differences across space and not absolute values.

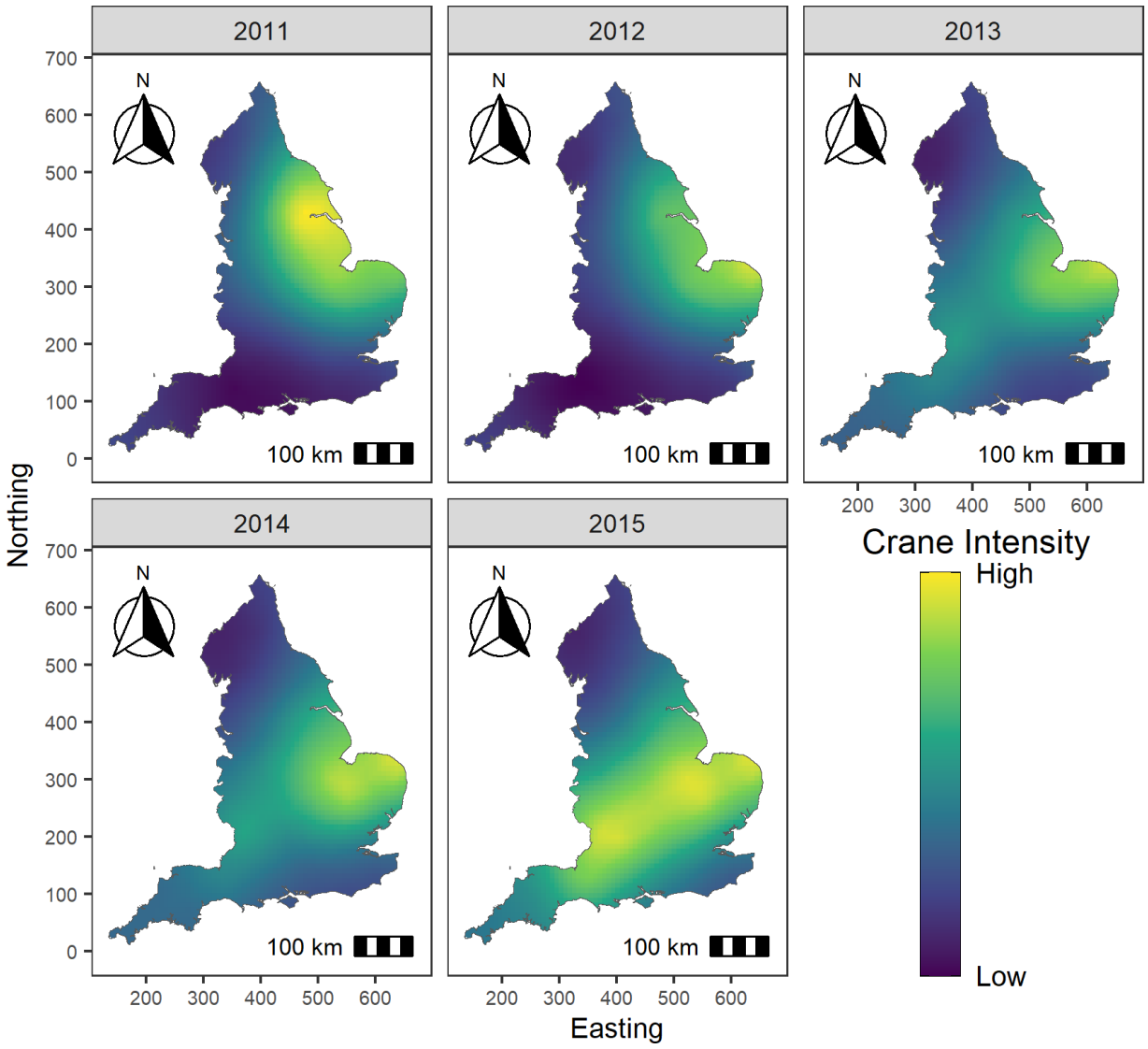

Figure A.2: Estimated mark random field ($M(s,t)$) for 2011-2015 from the binomial presence/absence with IID temporal structure. Colour scale is given in low-high intensity as interest is in relative differences across space and not absolute values.

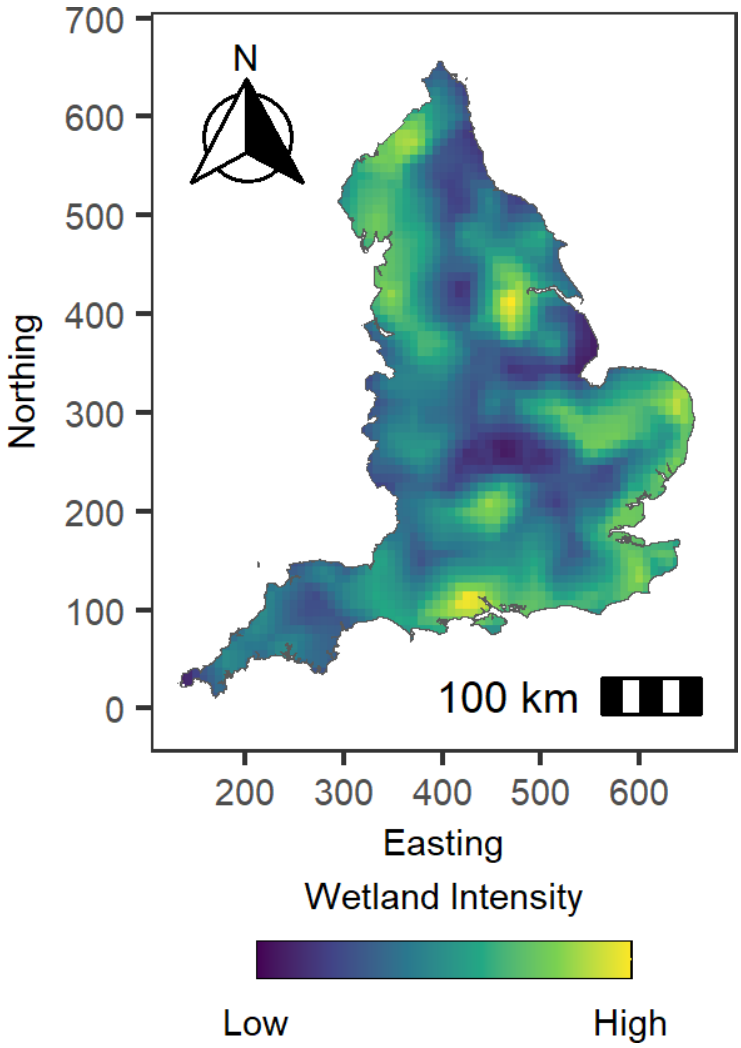

Figure A.3: Estimated point random field ($G(s)$) from the marked point process model with AR1 temporal structure. Colour scale is given in low-high intensity as interest is in relative differences across space and not absolute values.

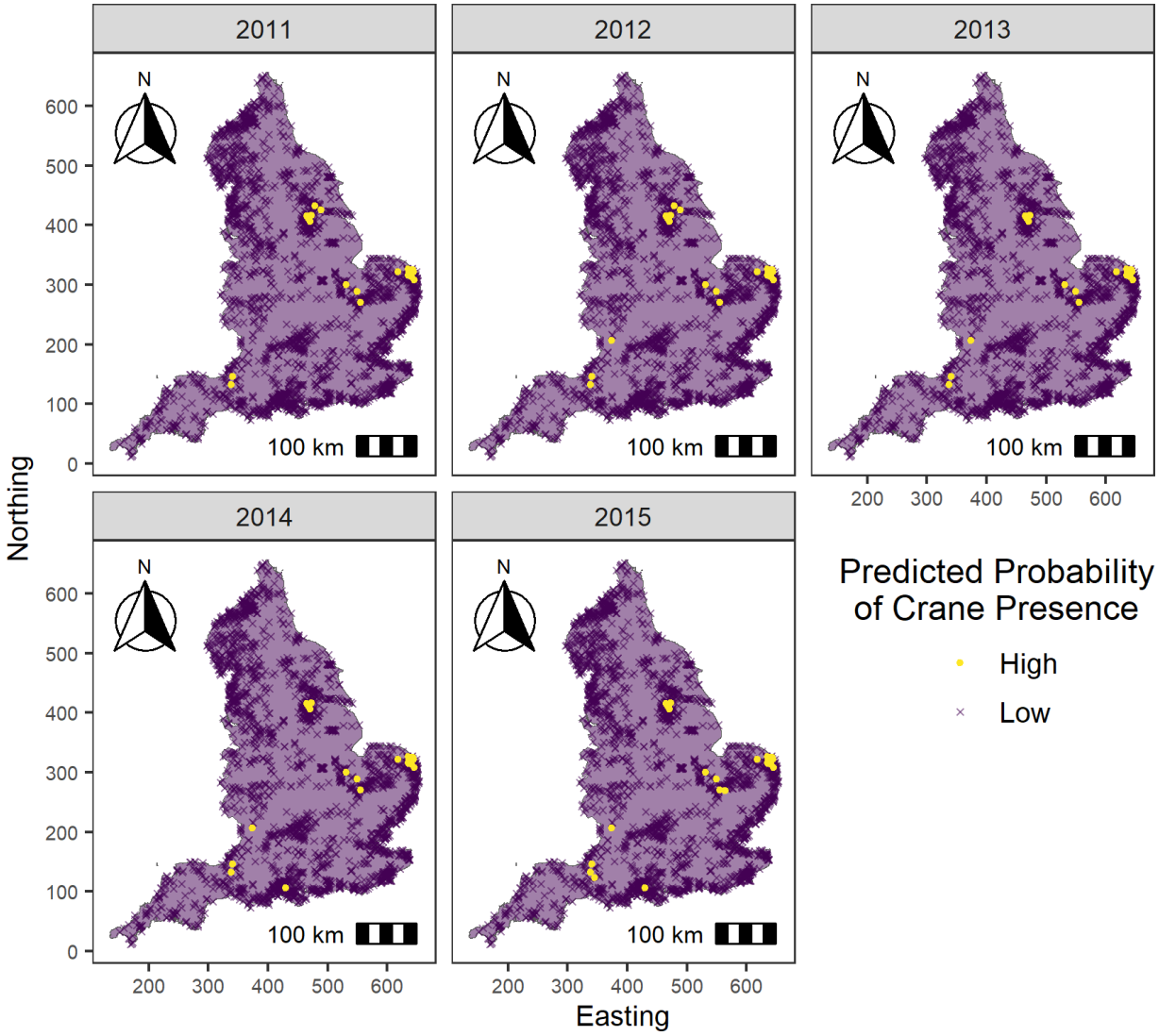

Figure A.4: Mean predicted probability of presence of a breeding pair of cranes at each wetland location for 2011-2015. Predictions were made using the marked point process model with AR1 temporal structure. Colour scale is given in low-high probability as interest is in relative differences across space and not absolute values. 'Low' represents a value of mean predicted probability of crane presence less than or equal to the 99th quantile of mean predicted probabilities across all four models analysed. 'High' represents a value of mean predicted probability of crane presence greater than this cutoff point. Purple background colour is used for visual clarity, and does not represent a value on the colour scale.

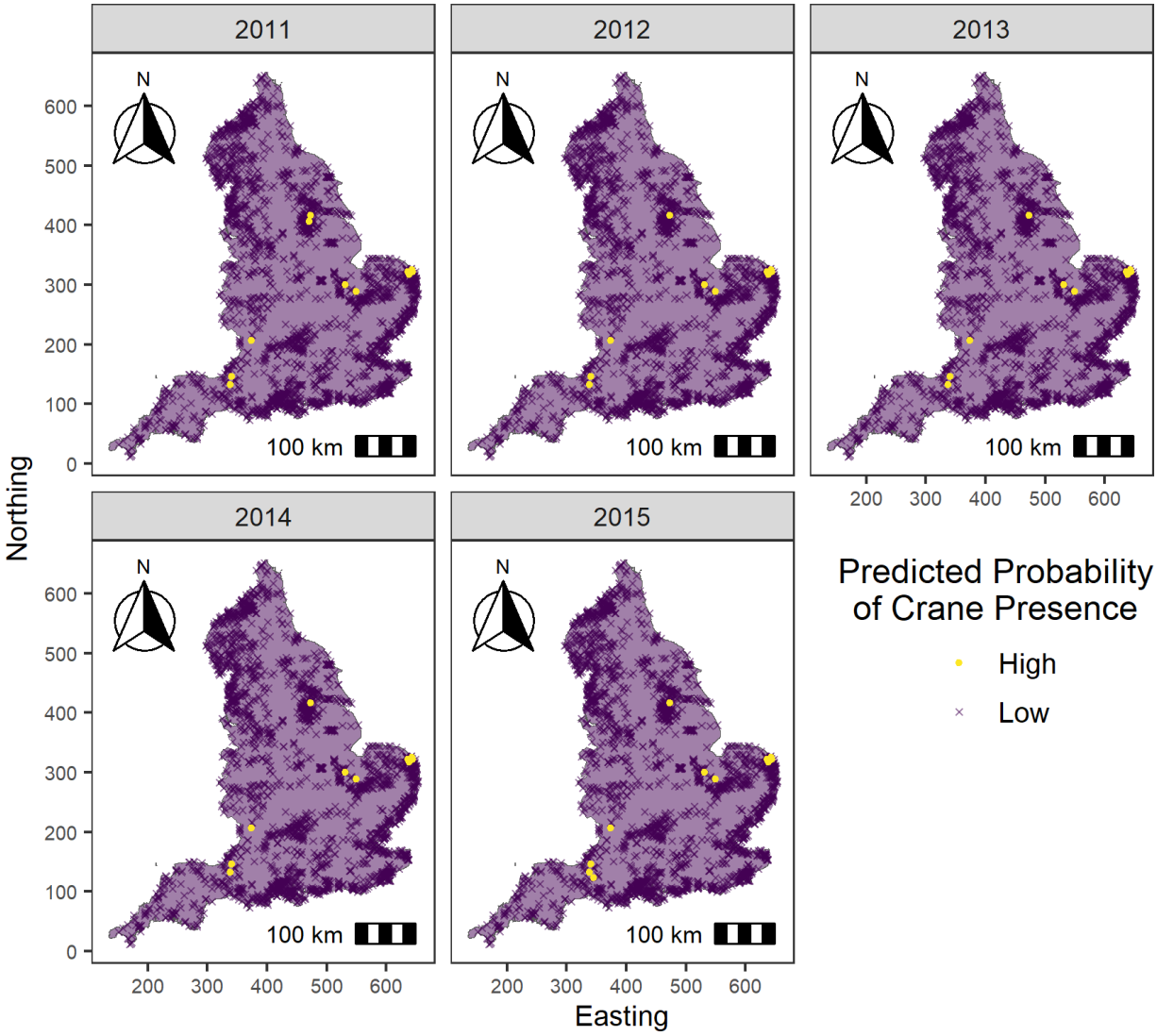

Figure A.5: Mean predicted probability of presence of a breeding pair of cranes at each wetland location for 2011-2015. Predictions were made using the binomial presence/absence model with AR1 temporal structure. Colour scale is given in low-high probability as interest is in relative differences across space and not absolute values. 'Low' represents a value of mean predicted probability of crane presence less than or equal to the 99th quantile of mean predicted probabilities across all four models analysed. 'High' represents a value of mean predicted probability of crane presence greater than this cutoff point. Purple background colour is used for visual clarity, and does not represent a value on the colour scale.

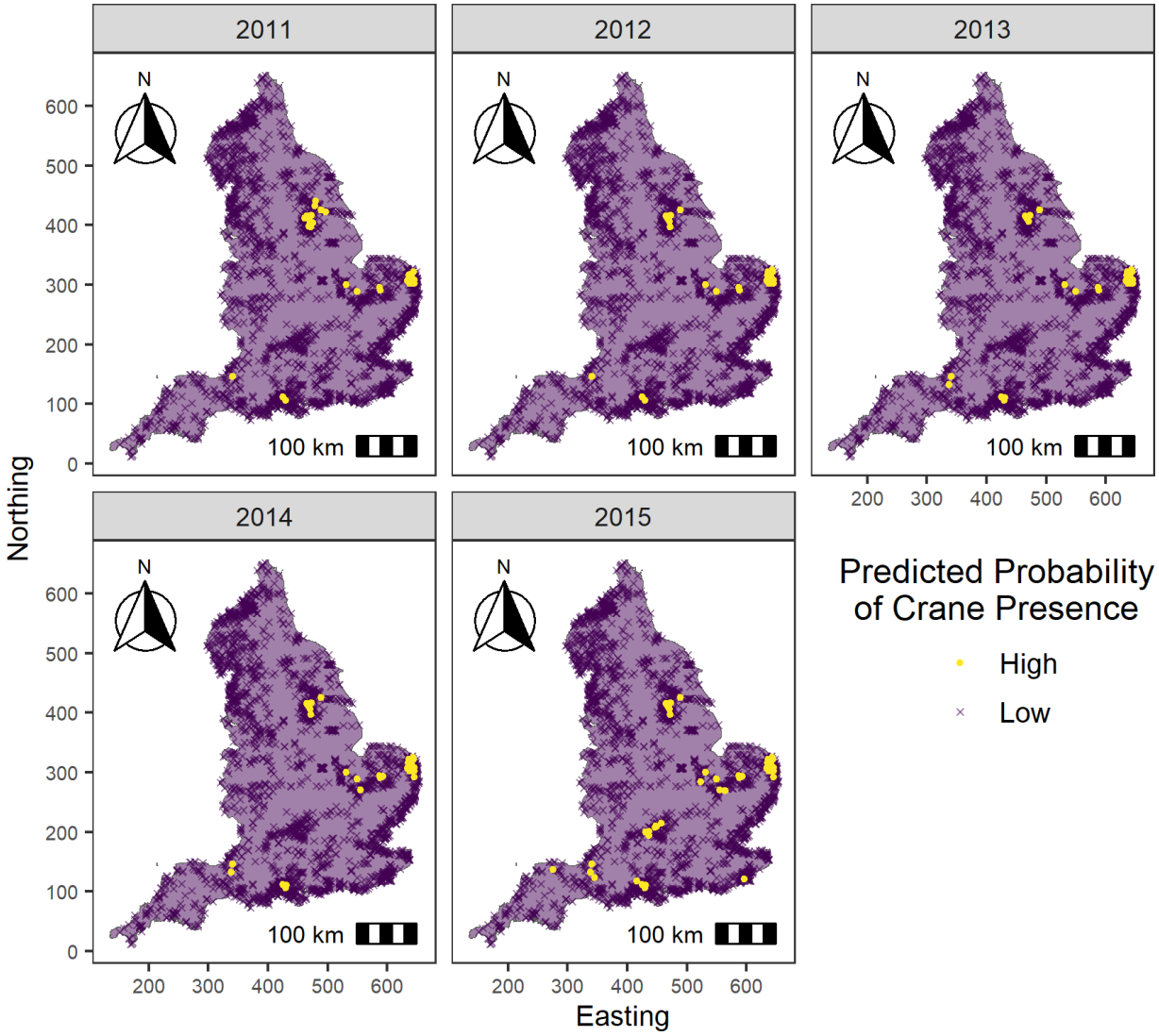

Figure A.6: Mean predicted probability of presence of a breeding pair of cranes at each wetland location for 2011-2015. Predictions were made using the marked point process model with IID temporal structure. Colour scale is given in low-high probability as interest is in relative differences across space and not absolute values. 'Low' represents a value of mean predicted probability of crane presence less than or equal to the 99th quantile of mean predicted probabilities across all four models analysed. 'High' represents a value of mean predicted probability of crane presence greater than this cutoff point. Purple background colour is used for visual clarity, and does not represent a value on the colour scale.

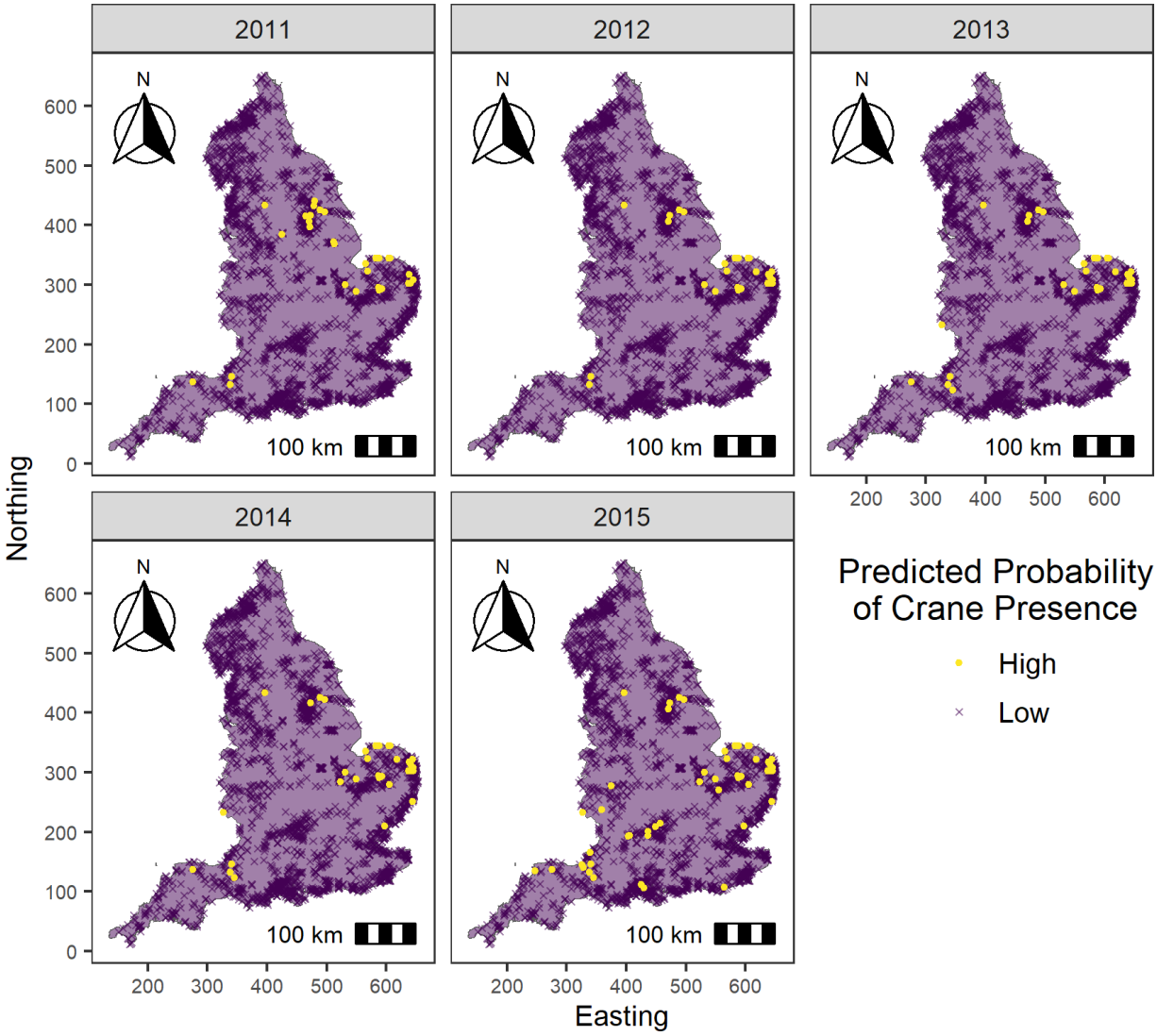

Figure A.7: Mean predicted probability of presence of a breeding pair of cranes at each wetland location for 2011-2015. Predictions were made using the binomial presence/absence model with IID temporal structure. Colour scale is given in low-high probability as interest is in relative differences across space and not absolute values. 'Low' represents a value of mean predicted probability of crane presence less than or equal to the 99th quantile of mean predicted probabilities across all four models analysed. 'High' represents a value of mean predicted probability of crane presence greater than this cutoff point. Purple background colour is used for visual clarity, and does not represent a value on the colour scale.

Appendix B

Supplementary Material for Chapter 3

The tables in this appendix contain the posterior mean and 95% credible intervals for the habitat selection parameters estimated using all 972 models fitted to the Swiss cattle movement data in Chapter 3. The patterns described in Chapter 3 were similar across the three cattle herds, with effects being most pronounced for the Original Braunvieh herd.

The estimates for the slope parameter from the RSA models fitted to data from the Original Braunvieh, Angus Holstein, and Highland Cattle herds are found in Tables B.1, B.2, and B.3, respectively. The estimates for the slope parameter from the SSA models fitted to data from the Original Braunvieh, Angus Holstein, and Highland Cattle herds are found in Tables B.4, B.5, and B.6, respectively.

The estimates for the forage quality parameter from the RSA models fitted to data from the Original Braunvieh, Angus Holstein, and Highland Cattle herds are found in Tables B.7, B.8, and B.9, respectively. The estimates for the forage quality parameter from the SSA models fitted to data from the Original Braunvieh, Angus Holstein, and Highland Cattle herds are found in Tables B.10, B.11, and B.12, respectively.

Table B.1: Posterior mean and 95% credible intervals for the β_{slope} parameter for the RSA models fitted to data from the Original Braunvieh herd. All values given are rounded to 2 decimal places.

		Slope			Slope + Forage Quality		
Area	Freq	$2m^2$	$10m^2$	$20m^2$	$2m^2$	$10m^2$	$20m^2$
1	20-sec	-7.01 [-7.24,-6.77]	-0.72 [-0.88,-0.56]	3.09 [2.91,3.27]	-6.98 [-7.23,-6.74]	0.96 [0.77,1.16]	2.24 [2.06,2.43]
	1-min	-7.1 [-7.51,-6.69]	-0.73 [-1.01,-0.45]	3.11 [2.8,3.43]	-7.08 [-7.51,-6.66]	0.95 [0.61,1.28]	2.26 [1.94,2.59]
	5-min	-7.09 [-8,-6.18]	-0.55 [-1.16,0.06]	3.12 [2.41,3.83]	-7.07 [-8.02,-6.11]	1.3 [0.56,2.05]	2.28 [1.56,3]
	15-min	-7.62 [-9.21,-6.04]	-0.85 [-1.93,0.23]	3.23 [2.01,4.45]	-7.65 [-9.31,-5.99]	0.98 [-0.33,2.29]	2.33 [1.1,3.56]
	30-min	-6.07 [-8.24,-3.9]	-0.54 [-2.02,0.93]	2.96 [1.22,4.7]	-5.94 [-8.22,-3.66]	1.27 [-0.53,3.07]	2.02 [0.3,3.74]
	60-min	-6.66 [-9.74,-3.57]	-0.65 [-2.74,1.44]	3.82 [1.47,6.16]	-6.57 [-9.82,-3.32]	1.93 [-0.73,4.58]	3.75 [1.11,6.4]
2	20-sec	-7.12 [-7.23,-7.02]	-5.78 [-5.87,-5.7]	-5.85 [-5.94,-5.77]	-6.47 [-6.6,-6.35]	-5.25 [-5.37,-5.13]	-7.59 [-7.85,-7.33]
	1-min	-7.12 [-7.31,-6.94]	-5.78 [-5.92,-5.63]	-5.85 [-5.99,-5.7]	-6.48 [-6.7,-6.27]	-5.24 [-5.44,-5.03]	-7.54 [-7.99,-7.09]
	5-min	-7.19 [-7.61,-6.78]	-5.77 [-6.09,-5.44]	-5.85 [-6.18,-5.53]	-6.57 [-7.06,-6.09]	-5.19 [-5.65,-4.72]	-7.51 [-8.51,-6.51]
	15-min	-7.16 [-7.88,-6.45]	-5.78 [-6.35,-5.22]	-5.78 [-6.34,-5.22]	-6.58 [-7.4,-5.75]	-5.2 [-6,-4.4]	-7.27 [-8.98,-5.56]
	30-min	-6.99 [-7.98,-6]	-5.75 [-6.54,-4.96]	-5.85 [-6.64,-5.06]	-6.28 [-7.45,-5.1]	-5.06 [-6.2,-3.93]	-6.89 [-9.28,-4.49]
	60-min	-6.65 [-8.02,-5.28]	-5.68 [-6.78,-4.58]	-5.85 [-6.95,-4.74]	-5.74 [-7.41,-4.07]	-5 [-6.58,-3.42]	-7.83 [-11.25,-4.41]
3	20-sec	-4.18 [-4.36,-4]	-2.84 [-2.99,-2.7]	-2.36 [-2.49,-2.23]	-3.64 [-3.84,-3.44]	-2.92 [-3.1,-2.73]	-3.42 [-3.63,-3.22]
	1-min	-4.24 [-4.55,-3.93]	-2.84 [-3.09,-2.59]	-2.34 [-2.57,-2.11]	-3.74 [-4.09,-3.39]	-2.94 [-3.26,-2.61]	-3.39 [-3.74,-3.04]
	5-min	-4.03 [-4.72,-3.35]	-2.77 [-3.33,-2.21]	-2.33 [-2.84,-1.82]	-3.37 [-4.14,-2.6]	-2.75 [-3.47,-2.03]	-3.26 [-4.04,-2.48]
	15-min	-3.73 [-4.89,-2.56]	-2.73 [-3.7,-1.77]	-2.26 [-3.14,-1.37]	-3.13 [-4.44,-1.81]	-2.72 [-3.96,-1.48]	-3.11 [-4.45,-1.77]
	30-min	-3.46 [-5.08,-1.84]	-2.49 [-3.85,-1.13]	-1.88 [-3.13,-0.63]	-2.93 [-4.76,-1.1]	-2.21 [-3.93,-0.49]	-2.48 [-4.36,-0.61]
	60-min	-3.53 [-5.81,-1.24]	-2.88 [-4.81,-0.95]	-1.91 [-3.66,-0.15]	-3.03 [-5.6,-0.45]	-2.48 [-4.93,-0.02]	-2.24 [-4.88,0.39]

Table B.2: Posterior mean and 95% credible intervals for the β_{slope} parameter for the RSA models fitted to data from the Angus Holstein herd. All values given are rounded to 2 decimal places.

		Slope			Slope + Forage Quality		
Area	Freq	$2m^2$	$10m^2$	$20m^2$	$2m^2$	$10m^2$	$20m^2$
1	20-sec	-11.38 [-11.69,-11.07]	-10.85 [-11.12,-10.59]	-7.97 [-8.2,-7.73]	-11.37 [-11.68,-11.05]	-12.03 [-12.32,-11.73]	-12.13 [-12.46,-11.79]
	1-min	-11.37 [-11.91,-10.83]	-10.87 [-11.33,-10.41]	-7.98 [-8.39,-7.58]	-11.35 [-11.9,-10.81]	-12.05 [-12.56,-11.54]	-12.12 [-12.7,-11.55]
	5-min	-11.29 [-12.5,-10.09]	-10.92 [-11.95,-9.9]	-8.01 [-8.91,-7.1]	-11.28 [-12.49,-10.07]	-12.11 [-13.25,-10.96]	-12.12 [-13.4,-10.84]
	15-min	-11.26 [-13.34,-9.18]	-11.08 [-12.85,-9.31]	-7.99 [-9.55,-6.43]	-11.16 [-13.24,-9.07]	-12.43 [-14.43,-10.43]	-12.18 [-14.4,-9.96]
	30-min	-10.26 [-13.09,-7.43]	-10.81 [-13.29,-8.34]	-7.7 [-9.88,-5.52]	-10.14 [-12.97,-7.31]	-12.15 [-14.94,-9.36]	-11.32 [-14.32,-8.31]
	60-min	-10.16 [-14.1,-6.22]	-11.29 [-14.79,-7.79]	-8.17 [-11.24,-5.09]	-9.98 [-13.9,-6.06]	-12.42 [-16.32,-8.52]	-11.99 [-16.26,-7.72]
2	20-sec	-6.46 [-6.63,-6.29]	-5.15 [-5.3,-5.01]	-3.58 [-3.7,-3.46]	-5.87 [-6.05,-5.69]	-4.73 [-4.89,-4.57]	-4.12 [-4.3,-3.93]
	1-min	-6.45 [-6.74,-6.16]	-5.11 [-5.37,-4.86]	-3.56 [-3.77,-3.34]	-5.86 [-6.18,-5.54]	-4.68 [-4.96,-4.4]	-4.06 [-4.38,-3.74]
	5-min	-6.41 [-7.07,-5.75]	-5.08 [-5.65,-4.51]	-3.54 [-4.02,-3.06]	-5.77 [-6.48,-5.06]	-4.54 [-5.17,-3.91]	-4.04 [-4.76,-3.33]
	15-min	-6.21 [-7.34,-5.09]	-5 [-5.98,-4.03]	-3.47 [-4.28,-2.66]	-5.71 [-6.91,-4.5]	-4.56 [-5.63,-3.49]	-4.06 [-5.28,-2.83]
	30-min	-6.37 [-7.96,-4.79]	-4.44 [-5.75,-3.14]	-3.03 [-4.12,-1.94]	-5.92 [-7.61,-4.23]	-4.07 [-5.51,-2.62]	-3.45 [-5.14,-1.76]
	60-min	-5.52 [-7.64,-3.4]	-3.63 [-5.31,-1.94]	-2.3 [-3.7,-0.9]	-4.05 [-6.51,-1.6]	-2.51 [-4.57,-0.46]	-2.55 [-4.84,-0.26]
3	20-sec	-7.66 [-7.9,-7.41]	-7 [-7.21,-6.78]	-6.05 [-6.24,-5.87]	-8.08 [-8.34,-7.82]	-7.47 [-7.7,-7.23]	-6.65 [-6.86,-6.45]
	1-min	-7.58 [-8,-7.16]	-6.97 [-7.35,-6.6]	-6.03 [-6.35,-5.71]	-7.98 [-8.43,-7.53]	-7.43 [-7.85,-7.02]	-6.63 [-6.99,-6.27]
	5-min	-7.88 [-8.83,-6.92]	-7.29 [-8.14,-6.44]	-6.1 [-6.82,-5.38]	-8.2 [-9.22,-7.18]	-7.73 [-8.66,-6.8]	-6.75 [-7.55,-5.95]
	15-min	-8.33 [-10.01,-6.64]	-7.88 [-9.4,-6.37]	-6.45 [-7.72,-5.19]	-8.81 [-10.61,-7.01]	-8.48 [-10.15,-6.81]	-7.39 [-8.79,-6]
	30-min	-8.51 [-10.9,-6.12]	-7.69 [-9.8,-5.58]	-6.5 [-8.28,-4.72]	-8.87 [-11.41,-6.32]	-7.85 [-10.15,-5.55]	-6.83 [-8.81,-4.85]
	60-min	-9.79 [-13.35,-6.22]	-8.13 [-11.14,-5.11]	-5.88 [-8.27,-3.49]	-10.65 [-14.45,-6.84]	-8.69 [-12,-5.38]	-6.52 [-9.19,-3.86]

Table B.3: Posterior mean and 95% credible intervals for the β_{slope} parameter for the RSA models fitted to data from the Highland Cattle herd. All values given are rounded to 2 decimal places.

		Slope			Slope + Forage Quality		
Area	Freq	$2m^2$	$10m^2$	$20m^2$	$2m^2$	$10m^2$	$20m^2$
1	20-sec	-6.37 [-6.58,-6.16]	-5.16 [-5.32,-5]	-4.99 [-5.15,-4.83]	-5.98 [-6.2,-5.76]	-4.79 [-4.97,-4.62]	-4.76 [-4.94,-4.58]
	1-min	-6.38 [-6.74,-6.02]	-5.13 [-5.41,-4.85]	-4.99 [-5.27,-4.72]	-5.99 [-6.37,-5.62]	-4.78 [-5.08,-4.48]	-4.78 [-5.09,-4.47]
	5-min	-6.36 [-7.16,-5.56]	-5.02 [-5.64,-4.39]	-4.94 [-5.55,-4.32]	-5.99 [-6.83,-5.15]	-4.66 [-5.33,-3.99]	-4.79 [-5.48,-4.1]
	15-min	-6 [-7.37,-4.64]	-4.74 [-5.8,-3.68]	-5.17 [-6.24,-4.1]	-5.77 [-7.18,-4.36]	-4.4 [-5.54,-3.26]	-5.13 [-6.33,-3.93]
	30-min	-5.36 [-7.24,-3.49]	-4.45 [-5.91,-2.98]	-5.28 [-6.8,-3.77]	-4.97 [-6.93,-3]	-3.91 [-5.52,-2.29]	-4.9 [-6.62,-3.17]
	60-min	-4.71 [-7.26,-2.16]	-4.29 [-6.31,-2.26]	-5.49 [-7.63,-3.35]	-4.09 [-6.82,-1.36]	-4.12 [-6.26,-1.99]	-4.98 [-7.42,-2.53]
2	20-sec	-2.16 [-2.25,-2.07]	-1.36 [-1.44,-1.29]	-1.17 [-1.24,-1.1]	-2.5 [-2.59,-2.41]	-2.77 [-2.85,-2.68]	-3.98 [-4.09,-3.86]
	1-min	-2.14 [-2.3,-1.98]	-1.36 [-1.49,-1.23]	-1.17 [-1.29,-1.04]	-2.48 [-2.64,-2.33]	-2.77 [-2.92,-2.62]	-3.96 [-4.16,-3.76]
	5-min	-2.13 [-2.49,-1.77]	-1.35 [-1.64,-1.06]	-1.15 [-1.43,-0.87]	-2.47 [-2.82,-2.13]	-2.77 [-3.11,-2.44]	-3.91 [-4.35,-3.47]
	15-min	-2.2 [-2.82,-1.58]	-1.28 [-1.78,-0.78]	-1.13 [-1.61,-0.65]	-2.53 [-3.13,-1.93]	-2.6 [-3.17,-2.02]	-3.8 [-4.56,-3.04]
	30-min	-1.89 [-2.75,-1.02]	-1.11 [-1.81,-0.41]	-0.96 [-1.64,-0.28]	-2.22 [-3.06,-1.38]	-2.44 [-3.26,-1.62]	-3.56 [-4.62,-2.5]
	60-min	-2.04 [-3.25,-0.83]	-0.93 [-1.91,0.04]	-0.82 [-1.76,0.12]	-2.31 [-3.51,-1.12]	-1.99 [-3.14,-0.83]	-3.13 [-4.59,-1.66]
3	20-sec	-3.16 [-3.33,-2.98]	-2.91 [-3.06,-2.76]	-2.59 [-2.72,-2.46]	-4.07 [-4.26,-3.89]	-4.22 [-4.39,-4.05]	-3.56 [-3.71,-3.41]
	1-min	-3.14 [-3.44,-2.84]	-2.88 [-3.14,-2.63]	-2.57 [-2.8,-2.35]	-4.05 [-4.38,-3.73]	-4.18 [-4.48,-3.89]	-3.53 [-3.79,-3.28]
	5-min	-3.02 [-3.69,-2.35]	-2.74 [-3.3,-2.17]	-2.43 [-2.92,-1.93]	-3.92 [-4.64,-3.2]	-4.09 [-4.74,-3.43]	-3.38 [-3.94,-2.81]
	15-min	-3.04 [-4.19,-1.88]	-2.76 [-3.74,-1.78]	-2.16 [-3,-1.32]	-3.91 [-5.16,-2.66]	-4 [-5.12,-2.87]	-3 [-3.96,-2.05]
	30-min	-3.1 [-4.73,-1.47]	-2.77 [-4.15,-1.39]	-2.22 [-3.4,-1.03]	-3.77 [-5.53,-2.01]	-3.83 [-5.41,-2.25]	-2.85 [-4.18,-1.51]
	60-min	-2.43 [-4.64,-0.23]	-1.9 [-3.72,-0.08]	-1.68 [-3.26,-0.09]	-3.34 [-5.73,-0.94]	-2.88 [-4.96,-0.8]	-2.27 [-4.05,-0.49]

Table B.4: Posterior mean and 95% credible intervals for the β_{slope} parameter for the SSA models fitted to data from the Original Braunvieh herd. All values given are rounded to 2 decimal places.

		Slope			Slope + Forage Quality		
Area	Freq	$2m^2$	$10m^2$	$20m^2$	$2m^2$	$10m^2$	$20m^2$
1	20-sec	-6.11 [-6.3,-5.92]	-4.83 [-4.95,-4.7]	-4.41 [-4.53,-4.28]	-3.79 [-4,-3.58]	-4.09 [-4.25,-3.93]	-1.94 [-2.14,-1.74]
	1-min	-13.25 [-13.62,-12.89]	-8.95 [-9.15,-8.74]	-9.23 [-9.43,-9.02]	-5.52 [-5.87,-5.18]	-3.82 [-4.1,-3.54]	-2.09 [-2.46,-1.71]
	5-min	-27.73 [-28.41,-27.05]	-18.1 [-18.55,-17.66]	-16.18 [-16.54,-15.83]	-9.5 [-10.22,-8.79]	-3.97 [-4.6,-3.34]	-2.61 [-3.35,-1.87]
	15-min	-29.95 [-31.02,-28.88]	-19.96 [-20.65,-19.26]	-17.53 [-18.12,-16.93]	-11.45 [-12.7,-10.2]	-4.95 [-6.01,-3.9]	-0.27 [-1.56,1.03]
	30-min	-29.08 [-30.54,-27.61]	-18.69 [-19.65,-17.73]	-17.03 [-17.91,-16.15]	-9.56 [-11.35,-7.77]	-4 [-5.45,-2.55]	0.55 [-1.15,2.24]
	60-min	-29.31 [-31.39,-27.24]	-17.81 [-19.08,-16.54]	-16.33 [-17.49,-15.16]	-10.23 [-12.81,-7.65]	-5.05 [-7.15,-2.95]	0.79 [-1.51,3.1]
2	20-sec	-10.92 [-11.03,-10.82]	-8.2 [-8.31,-8.08]	-7.03 [-7.12,-6.94]	-6.23 [-6.3,-6.15]	-5.93 [-5.99,-5.87]	-6.92 [-7,-6.85]
	1-min	-10.19 [-10.34,-10.04]	-9.43 [-9.61,-9.26]	-9.76 [-10,-9.52]	-4.62 [-4.73,-4.51]	-4.62 [-4.71,-4.53]	-5.4 [-5.5,-5.3]
	5-min	-11.82 [-12.09,-11.55]	-12.84 [-13.17,-12.51]	-15.21 [-15.64,-14.78]	-5.2 [-5.5,-4.9]	-4.88 [-5.1,-4.66]	-5.29 [-5.52,-5.06]
	15-min	-13.74 [-14.22,-13.25]	-14.9 [-15.43,-14.38]	-18.61 [-19.26,-17.96]	-6.62 [-7.22,-6.01]	-5.91 [-6.35,-5.46]	-6.51 [-7,-6.01]
	30-min	-13.07 [-13.77,-12.37]	-14.15 [-14.88,-13.42]	-18.45 [-19.38,-17.53]	-7.25 [-8.11,-6.39]	-6.55 [-7.19,-5.9]	-7.58 [-8.38,-6.79]
	60-min	-13.67 [-14.62,-12.71]	-15.07 [-16.09,-14.05]	-19.96 [-21.26,-18.66]	-7.54 [-8.79,-6.3]	-6.96 [-7.89,-6.03]	-8.3 [-9.45,-7.14]
3	20-sec	-15.53 [-15.75,-15.32]	-14.19 [-14.35,-14.02]	-10.31 [-10.42,-10.19]	-12.4 [-12.59,-12.22]	-10.21 [-10.36,-10.06]	-11.12 [-11.22,-11.01]
	1-min	-21.33 [-21.68,-20.98]	-15.04 [-15.23,-14.86]	-12.36 [-12.54,-12.18]	-12.36 [-12.65,-12.06]	-9.82 [-10.05,-9.6]	-10.12 [-10.27,-9.96]
	5-min	-28.82 [-29.56,-28.09]	-20.21 [-20.67,-19.75]	-15.39 [-15.75,-15.03]	-13.56 [-14.24,-12.89]	-11.75 [-12.26,-11.24]	-11.51 [-11.84,-11.18]
	15-min	-34.84 [-36.22,-33.46]	-22.54 [-23.36,-21.71]	-17.53 [-18.2,-16.87]	-13.38 [-14.61,-12.14]	-12.41 [-13.38,-11.45]	-12.65 [-13.31,-11.98]
	30-min	-35.63 [-37.55,-33.72]	-22.56 [-23.69,-21.44]	-15.95 [-16.77,-15.13]	-13.61 [-15.34,-11.89]	-13.03 [-14.36,-11.71]	-13.1 [-13.99,-12.22]
	60-min	-30.08 [-32.41,-27.76]	-21.21 [-22.82,-19.59]	-15.31 [-16.52,-14.11]	-14.25 [-16.64,-11.85]	-13.35 [-15.21,-11.5]	-12.4 [-13.69,-11.1]

Table B.5: Posterior mean and 95% credible intervals for the β_{slope} parameter for the SSA models fitted to data from the Angus Holstein herd. All values given are rounded to 2 decimal places.

		Slope			Slope + Forage Quality		
Area	Freq	$2m^2$	$10m^2$	$20m^2$	$2m^2$	$10m^2$	$20m^2$
1	20-sec	-4.01 [-4.2,-3.82]	-3.84 [-4.01,-3.67]	-1.96 [-2.09,-1.82]	-4.27 [-4.56,-3.98]	-4.7 [-4.94,-4.45]	-1.09 [-1.26,-0.93]
	1-min	-9.81 [-10.2,-9.41]	-17.2 [-17.45,-16.94]	-5.83 [-6.1,-5.55]	-2.55 [-3.08,-2.01]	-0.28 [-0.73,0.17]	1.3 [0.94,1.67]
	5-min	-24.29 [-25.02,-23.56]	-23.23 [-24.03,-22.43]	-20.99 [-21.9,-20.08]	-9.83 [-11,-8.66]	-3.09 [-4.09,-2.08]	-0.95 [-1.66,-0.23]
	15-min	-25.51 [-26.8,-24.22]	-25.28 [-26.59,-23.97]	-24.77 [-26.22,-23.31]	-11.87 [-13.74,-9.99]	-4.52 [-6.26,-2.77]	-1.82 [-3.02,-0.62]
	30-min	-25.19 [-27.03,-23.36]	-25.15 [-27,-23.31]	-24.54 [-26.44,-22.64]	-9.63 [-12.26,-7.01]	-5.16 [-7.55,-2.77]	-2.25 [-3.93,-0.57]
	60-min	-26.55 [-29.19,-23.91]	-26.72 [-29.43,-24.01]	-26.34 [-29.1,-23.57]	-9.94 [-13.68,-6.2]	-5.21 [-8.55,-1.87]	-2.56 [-4.91,-0.22]
2	20-sec	-14.67 [-14.85,-14.48]	-9.4 [-9.52,-9.28]	-10.48 [-10.63,-10.34]	-8.81 [-8.99,-8.63]	-7.59 [-7.77,-7.41]	-5.68 [-5.79,-5.57]
	1-min	-11.99 [-12.22,-11.76]	-11.36 [-11.6,-11.12]	-10.27 [-10.57,-9.97]	-9.41 [-9.68,-9.13]	-8.64 [-8.88,-8.39]	-6.13 [-6.34,-5.92]
	5-min	-13.64 [-14.06,-13.23]	-15.2 [-15.7,-14.71]	-15.88 [-16.62,-15.13]	-7.58 [-8.22,-6.95]	-8.1 [-8.76,-7.44]	-3.14 [-3.57,-2.71]
	15-min	-15.41 [-16.13,-14.7]	-16.73 [-17.51,-15.94]	-21.43 [-22.54,-20.32]	-9.36 [-10.47,-8.25]	-9.02 [-10.14,-7.9]	-4.42 [-5.24,-3.61]
	30-min	-15.16 [-16.19,-14.12]	-16.1 [-17.21,-14.99]	-19.93 [-21.37,-18.5]	-9.86 [-11.39,-8.34]	-9.17 [-10.69,-7.65]	-4.53 [-5.6,-3.45]
	60-min	-15.32 [-16.76,-13.87]	-16.22 [-17.71,-14.73]	-19.47 [-21.32,-17.62]	-10.11 [-12.26,-7.95]	-8.95 [-10.96,-6.93]	-4.81 [-6.37,-3.26]
3	20-sec	-12.12 [-12.39,-11.84]	-9.56 [-9.77,-9.34]	-10.25 [-10.37,-10.13]	-8.34 [-8.58,-8.11]	-6.72 [-6.89,-6.54]	-7.07 [-7.2,-6.94]
	1-min	-20.77 [-21.14,-20.4]	-14.2 [-14.58,-13.82]	-12.44 [-12.72,-12.16]	-7.41 [-7.78,-7.04]	-6.19 [-6.45,-5.92]	-7.63 [-7.84,-7.41]
	5-min	-33.35 [-34.52,-32.18]	-25.45 [-26.24,-24.65]	-17.92 [-18.47,-17.37]	-10.77 [-11.71,-9.83]	-9.5 [-10.2,-8.8]	-9.99 [-10.5,-9.49]
	15-min	-36.62 [-38.45,-34.79]	-25.9 [-27.26,-24.53]	-18.7 [-19.67,-17.73]	-12.33 [-13.99,-10.68]	-10.45 [-11.76,-9.14]	-11 [-11.96,-10.04]
	30-min	-40.6 [-43.15,-38.05]	-31.78 [-33.77,-29.8]	-23.43 [-24.94,-21.91]	-12.62 [-15.07,-10.16]	-10.59 [-12.55,-8.64]	-11.38 [-12.94,-9.83]
	60-min	-40.11 [-43.75,-36.46]	-30.32 [-33.09,-27.56]	-23.3 [-25.39,-21.22]	-14 [-17.52,-10.47]	-11.04 [-13.87,-8.22]	-11.06 [-13.26,-8.86]

Table B.6: Posterior mean and 95% credible intervals for the β_{slope} parameter for the SSA models fitted to data from the Highland Cattle herd. All values given are rounded to 2 decimal places.

		Slope			Slope + Forage Quality		
Area	Freq	$2m^2$	$10m^2$	$20m^2$	$2m^2$	$10m^2$	$20m^2$
1	20-sec	-15.29 [-15.45,-15.13]	-9.14 [-9.34,-8.95]	-5.18 [-5.33,-5.03]	-5.47 [-5.71,-5.24]	-4.9 [-5.07,-4.73]	-3.95 [-4.08,-3.81]
	1-min	-16.82 [-17.2,-16.45]	-11.03 [-11.36,-10.7]	-7.46 [-7.72,-7.19]	-4.93 [-5.29,-4.58]	-4.75 [-5.01,-4.5]	-4.18 [-4.4,-3.96]
	5-min	-24.05 [-24.75,-23.35]	-19.76 [-20.46,-19.05]	-13.72 [-14.35,-13.09]	-6.93 [-7.69,-6.17]	-6.17 [-6.71,-5.64]	-5.09 [-5.56,-4.62]
	15-min	-27.46 [-28.58,-26.33]	-26.03 [-27.2,-24.86]	-20.48 [-21.67,-19.29]	-8.44 [-9.71,-7.17]	-6.87 [-7.88,-5.86]	-5.65 [-6.62,-4.68]
	30-min	-27.72 [-29.22,-26.21]	-26.76 [-28.26,-25.25]	-26.75 [-28.6,-24.91]	-9.61 [-11.35,-7.86]	-7.74 [-9.19,-6.29]	-6.74 [-8.21,-5.27]
	60-min	-26.97 [-29.06,-24.87]	-26.49 [-28.59,-24.39]	-26.16 [-28.29,-24.02]	-9.04 [-11.34,-6.73]	-8.1 [-10.1,-6.1]	-7.57 [-9.7,-5.44]
2	20-sec	-6.22 [-6.28,-6.15]	-3.47 [-3.54,-3.4]	-2.4 [-2.46,-2.34]	-4.04 [-4.1,-3.98]	-5.5 [-5.55,-5.44]	-4.77 [-4.83,-4.72]
	1-min	-6.44 [-6.6,-6.27]	-6.66 [-6.77,-6.56]	-3.26 [-3.38,-3.15]	-3.34 [-3.44,-3.23]	-4.29 [-4.37,-4.21]	-4.22 [-4.3,-4.13]
	5-min	-10.11 [-10.44,-9.77]	-7.94 [-8.27,-7.61]	-6.81 [-7.16,-6.47]	-3.58 [-3.81,-3.35]	-4.37 [-4.55,-4.2]	-4.26 [-4.44,-4.08]
	15-min	-12.19 [-12.73,-11.65]	-10.69 [-11.24,-10.15]	-10.71 [-11.36,-10.07]	-4.11 [-4.53,-3.69]	-4.75 [-5.05,-4.45]	-4.74 [-5.07,-4.42]
	30-min	-12.72 [-13.48,-11.97]	-11.5 [-12.26,-10.73]	-11.63 [-12.51,-10.75]	-4 [-4.6,-3.4]	-4.83 [-5.28,-4.39]	-4.94 [-5.44,-4.44]
	60-min	-13.05 [-14.1,-12]	-11.77 [-12.78,-10.76]	-12.97 [-14.15,-11.78]	-4.04 [-4.91,-3.17]	-4.79 [-5.41,-4.16]	-4.95 [-5.69,-4.22]
3	20-sec	-11.91 [-12.11,-11.71]	-10.76 [-10.86,-10.65]	-7.99 [-8.11,-7.86]	-11.19 [-11.39,-10.98]	-9.76 [-9.93,-9.59]	-7.44 [-7.56,-7.32]
	1-min	-14.98 [-15.28,-14.68]	-12.97 [-13.2,-12.73]	-9.88 [-10,-9.75]	-11.83 [-12.14,-11.53]	-10.26 [-10.49,-10.03]	-9.35 [-9.53,-9.17]
	5-min	-22.81 [-23.42,-22.2]	-17.2 [-17.61,-16.78]	-13.54 [-13.87,-13.21]	-13.76 [-14.5,-13.03]	-13.37 [-13.87,-12.86]	-12.22 [-12.58,-11.87]
	15-min	-26 [-27.08,-24.92]	-18.71 [-19.47,-17.95]	-14.62 [-15.21,-14.03]	-14.53 [-15.88,-13.18]	-14.57 [-15.51,-13.62]	-13.05 [-13.71,-12.39]
	30-min	-28.39 [-29.99,-26.8]	-19.85 [-20.97,-18.73]	-15.1 [-15.97,-14.23]	-15.09 [-17.03,-13.14]	-15.37 [-16.74,-13.99]	-13.57 [-14.54,-12.59]
	60-min	-25.06 [-27.09,-23.02]	-18.7 [-20.23,-17.17]	-14.6 [-15.8,-13.4]	-13.42 [-16.06,-10.79]	-14.44 [-16.37,-12.52]	-13.36 [-14.75,-11.96]

Table B.7: Posterior mean and 95% credible intervals for the β_{FQ} parameter for the RSA models fitted to data from the Original Braunvieh herd. All values given are rounded to 2 decimal places.

		Forage Quality			Slope + Forage Quality		
Area	Freq	$2m^2$	$10m^2$	$20m^2$	$2m^2$	$10m^2$	$20m^2$
1	20-sec	2.35 [2.21,2.48]	2.71 [2.58,2.84]	-2.36 [-2.51,-2.21]	1.91 [1.78,2.04]	3.01 [2.87,3.16]	-1.89 [-2.05,-1.73]
	1-min	2.32 [2.09,2.55]	2.7 [2.47,2.92]	-2.37 [-2.63,-2.11]	1.88 [1.66,2.11]	3 [2.75,3.26]	-1.9 [-2.18,-1.62]
	5-min	2.49 [1.97,3.01]	2.81 [2.3,3.32]	-2.36 [-2.94,-1.78]	2.04 [1.53,2.56]	3.24 [2.66,3.82]	-1.87 [-2.51,-1.24]
	15-min	2.62 [1.7,3.54]	2.97 [2.08,3.86]	-2.53 [-3.53,-1.53]	2.17 [1.27,3.07]	3.29 [2.29,4.3]	-2.03 [-3.12,-0.94]
	30-min	2.41 [1.16,3.66]	2.74 [1.51,3.97]	-2.67 [-4.07,-1.27]	1.99 [0.77,3.22]	3.18 [1.78,4.58]	-2.25 [-3.76,-0.74]
	60-min	2.86 [1.01,4.72]	3.73 [1.85,5.6]	-1.38 [-3.37,0.62]	2.44 [0.62,4.25]	4.46 [2.29,6.64]	-0.21 [-2.59,2.17]
2	20-sec	4.02 [3.94,4.11]	3.58 [3.52,3.65]	4.22 [4.15,4.29]	0.96 [0.88,1.03]	0.54 [0.46,0.63]	-1.36 [-1.55,-1.17]
	1-min	4 [3.85,4.14]	3.59 [3.47,3.7]	4.22 [4.1,4.34]	0.94 [0.81,1.07]	0.55 [0.41,0.7]	-1.33 [-1.66,-1]
	5-min	4 [3.68,4.33]	3.61 [3.35,3.86]	4.23 [3.97,4.49]	0.92 [0.64,1.21]	0.6 [0.27,0.92]	-1.3 [-2.03,-0.57]
	15-min	3.91 [3.35,4.46]	3.61 [3.17,4.06]	4.19 [3.73,4.64]	0.87 [0.38,1.36]	0.6 [0.04,1.16]	-1.17 [-2.42,0.08]
	30-min	3.98 [3.2,4.77]	3.65 [3.03,4.28]	4.29 [3.65,4.93]	1.02 [0.3,1.73]	0.7 [-0.09,1.5]	-0.81 [-2.57,0.96]
	60-min	3.99 [2.89,5.1]	3.59 [2.72,4.46]	4.19 [3.3,5.08]	1.21 [0.16,2.26]	0.69 [-0.42,1.8]	-1.53 [-4.01,0.95]
3	20-sec	1.83 [1.73,1.93]	1.45 [1.33,1.57]	1.06 [0.94,1.19]	0.66 [0.54,0.78]	-0.1 [-0.25,0.06]	-1.26 [-1.44,-1.08]
	1-min	1.81 [1.63,1.99]	1.43 [1.23,1.64]	1.06 [0.85,1.27]	0.61 [0.4,0.82]	-0.13 [-0.39,0.14]	-1.24 [-1.55,-0.93]
	5-min	1.9 [1.5,2.3]	1.48 [1.03,1.94]	1.12 [0.65,1.59]	0.81 [0.35,1.28]	0.02 [-0.57,0.61]	-1.1 [-1.79,-0.41]
	15-min	1.76 [1.07,2.46]	1.46 [0.67,2.25]	1.09 [0.28,1.91]	0.75 [-0.06,1.56]	0.01 [-1,1.03]	-1.02 [-2.21,0.17]
	30-min	1.63 [0.64,2.62]	1.55 [0.43,2.66]	0.95 [-0.21,2.11]	0.68 [-0.46,1.83]	0.37 [-1.06,1.79]	-0.75 [-2.44,0.95]
	60-min	1.6 [0.21,2.99]	1.81 [0.28,3.35]	1.1 [-0.51,2.72]	0.63 [-0.98,2.24]	0.5 [-1.49,2.49]	-0.43 [-2.8,1.95]

Table B.8: Posterior mean and 95% credible intervals for the β_{FQ} parameter for the RSA models fitted to data from the Angus Holstein herd. All values given are rounded to 2 decimal places.

		Forage Quality			Slope + Forage Quality		
Area	Freq	$2m^2$	$10m^2$	$20m^2$	$2m^2$	$10m^2$	$20m^2$
1	20-sec	-0.27 [-0.39,-0.15]	1.31 [1.15,1.47]	2.9 [2.71,3.09]	-0.04 [-0.16,0.07]	2.07 [1.92,2.22]	6.39 [6.13,6.65]
	1-min	-0.29 [-0.49,-0.08]	1.32 [1.04,1.59]	2.88 [2.55,3.21]	-0.06 [-0.26,0.14]	2.08 [1.82,2.33]	6.36 [5.91,6.82]
	5-min	-0.27 [-0.73,0.19]	1.3 [0.68,1.91]	2.84 [2.11,3.58]	-0.04 [-0.48,0.4]	2.07 [1.5,2.64]	6.33 [5.32,7.34]
	15-min	-0.59 [-1.33,0.15]	1.59 [0.51,2.67]	2.91 [1.64,4.18]	-0.34 [-1.04,0.37]	2.35 [1.35,3.34]	6.43 [4.68,8.18]
	30-min	-0.65 [-1.67,0.38]	1.77 [0.23,3.31]	2.71 [0.92,4.49]	-0.42 [-1.39,0.56]	2.46 [1.04,3.87]	5.79 [3.4,8.17]
	60-min	-0.82 [-2.18,0.55]	1.05 [-0.97,3.08]	2.53 [0.04,5.02]	-0.57 [-1.87,0.72]	1.92 [0.02,3.82]	5.93 [2.55,9.31]
2	20-sec	2.76 [2.67,2.86]	2.6 [2.51,2.7]	3.32 [3.17,3.47]	1.03 [0.93,1.12]	0.82 [0.72,0.93]	-0.93 [-1.17,-0.69]
	1-min	2.76 [2.6,2.92]	2.61 [2.45,2.77]	3.32 [3.07,3.58]	1.03 [0.87,1.19]	0.84 [0.67,1.02]	-0.88 [-1.29,-0.46]
	5-min	2.82 [2.46,3.18]	2.76 [2.4,3.13]	3.31 [2.75,3.88]	1.1 [0.74,1.46]	1.04 [0.64,1.44]	-0.87 [-1.78,0.05]
	15-min	2.55 [1.94,3.17]	2.56 [1.95,3.18]	3.19 [2.22,4.16]	0.88 [0.26,1.49]	0.82 [0.14,1.51]	-1.01 [-2.59,0.57]
	30-min	2.48 [1.62,3.35]	2.29 [1.44,3.15]	2.93 [1.58,4.27]	0.79 [-0.06,1.64]	0.66 [-0.3,1.62]	-0.71 [-2.92,1.5]
	60-min	3.48 [2.24,4.72]	2.78 [1.55,4.02]	2.35 [0.53,4.16]	2.13 [0.75,3.51]	1.68 [0.22,3.15]	-0.41 [-3.48,2.66]
3	20-sec	1.38 [1.24,1.52]	2.43 [2.27,2.6]	3.37 [3.16,3.58]	-0.76 [-0.92,-0.6]	-0.98 [-1.18,-0.78]	-1.61 [-1.86,-1.36]
	1-min	1.4 [1.16,1.63]	2.44 [2.15,2.73]	3.36 [2.99,3.72]	-0.72 [-1,-0.44]	-0.96 [-1.31,-0.61]	-1.61 [-2.04,-1.18]
	5-min	1.54 [1.03,2.06]	2.56 [1.91,3.2]	3.28 [2.46,4.1]	-0.57 [-1.19,0.05]	-0.91 [-1.69,-0.13]	-1.75 [-2.72,-0.79]
	15-min	1.41 [0.5,2.31]	2.51 [1.39,3.62]	2.82 [1.4,4.24]	-0.86 [-1.94,0.23]	-1.2 [-2.55,0.14]	-2.58 [-4.23,-0.92]
	30-min	1.58 [0.34,2.82]	3.04 [1.51,4.56]	4.04 [2.08,6]	-0.63 [-2.13,0.87]	-0.34 [-2.18,1.49]	-0.9 [-3.22,1.42]
	60-min	1.12 [-0.7,2.94]	2.55 [0.36,4.73]	3.07 [0.29,5.86]	-1.52 [-3.7,0.67]	-1.18 [-3.82,1.46]	-1.79 [-5.07,1.49]

Table B.9: Posterior mean and 95% credible intervals for the β_{FQ} parameter for the RSA models fitted to data from the Highland Cattle herd. All values given are rounded to 2 decimal places.

		Forage Quality			Slope + Forage Quality		
Area	Freq	$2m^2$	$10m^2$	$20m^2$	$2m^2$	$10m^2$	$20m^2$
1	20-sec	1.95 [1.84,2.06]	2.05 [1.95,2.15]	2.55 [2.42,2.67]	1.1 [0.99,1.2]	0.73 [0.64,0.83]	0.33 [0.2,0.45]
	1-min	1.94 [1.75,2.13]	2.01 [1.83,2.18]	2.53 [2.31,2.74]	1.09 [0.91,1.27]	0.7 [0.54,0.87]	0.31 [0.1,0.51]
	5-min	1.88 [1.46,2.3]	1.97 [1.58,2.36]	2.4 [1.92,2.87]	1.04 [0.65,1.44]	0.69 [0.33,1.06]	0.21 [-0.25,0.67]
	15-min	1.36 [0.71,2]	1.82 [1.17,2.47]	2.31 [1.5,3.12]	0.61 [0.01,1.22]	0.62 [0.01,1.23]	0.05 [-0.72,0.82]
	30-min	1.65 [0.69,2.61]	2.08 [1.13,3.04]	2.86 [1.66,4.05]	0.94 [0.02,1.86]	0.94 [0.01,1.88]	0.53 [-0.63,1.7]
	60-min	2.02 [0.58,3.46]	1.29 [0.14,2.44]	3.08 [1.38,4.78]	1.38 [-0.02,2.78]	0.27 [-0.81,1.35]	0.69 [-0.96,2.35]
2	20-sec	-0.52 [-0.58,-0.45]	-0.59 [-0.65,-0.52]	-0.48 [-0.54,-0.41]	-1.04 [-1.11,-0.98]	-2.26 [-2.35,-2.17]	-3.91 [-4.05,-3.78]
	1-min	-0.52 [-0.63,-0.4]	-0.59 [-0.69,-0.48]	-0.48 [-0.59,-0.36]	-1.04 [-1.15,-0.93]	-2.26 [-2.42,-2.11]	-3.9 [-4.13,-3.67]
	5-min	-0.53 [-0.79,-0.27]	-0.6 [-0.84,-0.37]	-0.47 [-0.73,-0.21]	-1.05 [-1.29,-0.81]	-2.29 [-2.64,-1.94]	-3.84 [-4.36,-3.33]
	15-min	-0.49 [-0.94,-0.04]	-0.54 [-0.95,-0.13]	-0.45 [-0.89,-0.01]	-1.02 [-1.43,-0.61]	-2.09 [-2.68,-1.5]	-3.71 [-4.59,-2.83]
	30-min	-0.46 [-1.09,0.18]	-0.6 [-1.17,-0.02]	-0.51 [-1.14,0.11]	-0.95 [-1.54,-0.35]	-2.06 [-2.89,-1.24]	-3.56 [-4.79,-2.34]
	60-min	-0.3 [-1.19,0.6]	-0.43 [-1.24,0.37]	-0.48 [-1.35,0.4]	-0.82 [-1.65,0.02]	-1.58 [-2.7,-0.47]	-3.11 [-4.77,-1.46]
3	20-sec	-0.43 [-0.5,-0.35]	-0.67 [-0.76,-0.59]	-0.53 [-0.61,-0.44]	-1.05 [-1.13,-0.97]	-1.61 [-1.7,-1.52]	-1.45 [-1.54,-1.35]
	1-min	-0.42 [-0.55,-0.3]	-0.68 [-0.82,-0.53]	-0.53 [-0.68,-0.39]	-1.05 [-1.18,-0.91]	-1.61 [-1.77,-1.45]	-1.45 [-1.61,-1.28]
	5-min	-0.44 [-0.73,-0.15]	-0.8 [-1.14,-0.46]	-0.58 [-0.92,-0.25]	-1.05 [-1.36,-0.74]	-1.72 [-2.08,-1.35]	-1.46 [-1.83,-1.09]
	15-min	-0.41 [-0.9,0.08]	-0.65 [-1.22,-0.09]	-0.56 [-1.12,0.01]	-1.01 [-1.55,-0.48]	-1.55 [-2.16,-0.93]	-1.34 [-1.98,-0.71]
	30-min	-0.19 [-0.85,0.47]	-0.46 [-1.22,0.3]	-0.24 [-0.99,0.51]	-0.76 [-1.48,-0.05]	-1.31 [-2.15,-0.47]	-0.97 [-1.81,-0.14]
	60-min	-0.64 [-1.65,0.38]	-0.74 [-1.86,0.38]	-0.42 [-1.51,0.66]	-1.16 [-2.25,-0.07]	-1.39 [-2.61,-0.18]	-1.02 [-2.22,0.17]

Table B.10: Posterior mean and 95% credible intervals for the β_{FQ} parameter for the SSA models fitted to data from the Original Braunvieh herd. All values given are rounded to 2 decimal places.

		Forage Quality			Slope + Forage Quality		
Area	Freq	$2m^2$	$10m^2$	$20m^2$	$2m^2$	$10m^2$	$20m^2$
1	20-sec	-1.03 [-1.06,-1]	-1.19 [-1.22,-1.15]	-1.57 [-1.61,-1.53]	-0.65 [-0.69,-0.61]	-0.49 [-0.54,-0.45]	-1.05 [-1.12,-0.99]
	1-min	-2.23 [-2.28,-2.18]	-2.76 [-2.82,-2.7]	-3.39 [-3.46,-3.32]	-1.69 [-1.74,-1.63]	-1.96 [-2.04,-1.88]	-2.8 [-2.92,-2.67]
	5-min	-3.83 [-3.92,-3.75]	-4.38 [-4.47,-4.29]	-5.08 [-5.19,-4.98]	-2.62 [-2.73,-2.51]	-3.42 [-3.59,-3.26]	-4.23 [-4.48,-3.99]
	15-min	-4.36 [-4.5,-4.21]	-4.8 [-4.96,-4.63]	-5.63 [-5.84,-5.43]	-2.65 [-2.83,-2.46]	-3.6 [-3.87,-3.32]	-5.55 [-6,-5.09]
	30-min	-4 [-4.2,-3.81]	-4.58 [-4.82,-4.33]	-5.58 [-5.91,-5.24]	-2.86 [-3.13,-2.59]	-3.67 [-4.07,-3.28]	-5.75 [-6.36,-5.13]
	60-min	-4.11 [-4.4,-3.83]	-4.63 [-4.99,-4.28]	-5.73 [-6.23,-5.24]	-2.85 [-3.24,-2.47]	-3.44 [-4.03,-2.86]	-5.98 [-6.84,-5.12]
2	20-sec	-3.6 [-3.64,-3.56]	-2.34 [-2.38,-2.31]	-2.26 [-2.3,-2.23]	-2.77 [-2.81,-2.74]	-3.18 [-3.21,-3.15]	-3.45 [-3.49,-3.42]
	1-min	-3.75 [-3.8,-3.7]	-2.9 [-2.95,-2.85]	-3.01 [-3.06,-2.95]	-2.59 [-2.64,-2.54]	-2.81 [-2.86,-2.76]	-3.15 [-3.2,-3.1]
	5-min	-4.34 [-4.44,-4.23]	-4.11 [-4.23,-3.99]	-4.57 [-4.68,-4.45]	-2.32 [-2.43,-2.2]	-2.79 [-2.9,-2.69]	-3.02 [-3.11,-2.92]
	15-min	-4.62 [-4.8,-4.45]	-4.93 [-5.15,-4.71]	-5.1 [-5.34,-4.86]	-2.27 [-2.47,-2.08]	-2.93 [-3.11,-2.75]	-3.26 [-3.45,-3.08]
	30-min	-4.82 [-5.07,-4.57]	-5.31 [-5.63,-4.98]	-5.47 [-5.82,-5.12]	-2.11 [-2.4,-1.82]	-2.95 [-3.24,-2.66]	-3.49 [-3.81,-3.16]
	60-min	-4.72 [-5.06,-4.39]	-5.01 [-5.4,-4.62]	-5.15 [-5.55,-4.75]	-2.18 [-2.58,-1.77]	-3.06 [-3.46,-2.66]	-3.65 [-4.12,-3.19]
3	20-sec	-9.1 [-9.2,-8.99]	-11.9 [-12.04,-11.76]	-7.03 [-7.16,-6.89]	-6.62 [-6.7,-6.54]	-7.18 [-7.28,-7.07]	-8.65 [-8.77,-8.53]
	1-min	-10.55 [-10.71,-10.4]	-13.61 [-13.81,-13.4]	-14.46 [-14.67,-14.25]	-5.94 [-6.07,-5.81]	-6.34 [-6.5,-6.17]	-7.13 [-7.32,-6.94]
	5-min	-13.11 [-13.4,-12.81]	-17.27 [-17.67,-16.87]	-16.68 [-17.28,-16.09]	-6.4 [-6.69,-6.11]	-6.58 [-6.95,-6.22]	-7.45 [-7.85,-7.04]
	15-min	-13.17 [-13.68,-12.65]	-17.29 [-17.98,-16.6]	-21.71 [-22.82,-20.59]	-7.57 [-8.09,-7.06]	-7.63 [-8.28,-6.97]	-8.52 [-9.23,-7.8]
	30-min	-13.63 [-14.38,-12.89]	-18.41 [-19.41,-17.42]	-23.37 [-24.99,-21.74]	-7.98 [-8.73,-7.23]	-7.72 [-8.64,-6.8]	-8.44 [-9.48,-7.4]
	60-min	-13.96 [-15.03,-12.9]	-18.18 [-19.61,-16.75]	-20.35 [-22.31,-18.39]	-7.5 [-8.62,-6.38]	-7.26 [-8.54,-5.99]	-8.23 [-9.65,-6.82]

Table B.11: Posterior mean and 95% credible intervals for the β_{FQ} parameter for the SSA models fitted to data from the Angus Holstein herd. All values given are rounded to 2 decimal places.

		Forage Quality			Slope + Forage Quality		
Area	Freq	$2m^2$	$10m^2$	$20m^2$	$2m^2$	$10m^2$	$20m^2$
1	20-sec	-0.59 [-0.63,-0.55]	-0.57 [-0.62,-0.53]	-0.65 [-0.69,-0.6]	0.13 [0.07,0.19]	0.36 [0.3,0.42]	-0.37 [-0.43,-0.32]
	1-min	-1.97 [-2.04,-1.91]	-2.08 [-2.15,-2.01]	-2.23 [-2.3,-2.16]	-1.6 [-1.7,-1.5]	-2.01 [-2.11,-1.9]	-2.5 [-2.61,-2.39]
	5-min	-3.89 [-4,-3.77]	-4.11 [-4.22,-3.99]	-4.2 [-4.32,-4.08]	-2.49 [-2.68,-2.29]	-3.6 [-3.8,-3.4]	-4.04 [-4.21,-3.87]
	15-min	-4.16 [-4.36,-3.96]	-4.36 [-4.58,-4.13]	-4.47 [-4.7,-4.23]	-2.44 [-2.78,-2.11]	-3.61 [-3.97,-3.25]	-4.17 [-4.48,-3.86]
	30-min	-4.03 [-4.3,-3.75]	-4.4 [-4.75,-4.05]	-4.62 [-5.01,-4.22]	-2.81 [-3.24,-2.37]	-3.62 [-4.12,-3.12]	-4.28 [-4.75,-3.81]
	60-min	-4.21 [-4.6,-3.82]	-4.75 [-5.31,-4.19]	-4.94 [-5.57,-4.32]	-3.02 [-3.63,-2.41]	-3.97 [-4.71,-3.24]	-4.58 [-5.3,-3.86]
2	20-sec	-4.36 [-4.41,-4.31]	-5.09 [-5.17,-5.01]	-9.05 [-9.15,-8.95]	-3.17 [-3.23,-3.11]	-4.34 [-4.43,-4.25]	-9.46 [-9.57,-9.35]
	1-min	-3.38 [-3.46,-3.29]	-3.68 [-3.79,-3.57]	-6.84 [-6.99,-6.7]	-1.21 [-1.31,-1.12]	-2.31 [-2.43,-2.19]	-6.17 [-6.31,-6.03]
	5-min	-4.62 [-4.77,-4.47]	-5.8 [-6.01,-5.59]	-7.99 [-8.22,-7.76]	-2.33 [-2.56,-2.11]	-3.16 [-3.43,-2.88]	-6.78 [-7.04,-6.53]
	15-min	-5.12 [-5.37,-4.87]	-6.91 [-7.26,-6.57]	-8.46 [-8.85,-8.07]	-2.31 [-2.68,-1.94]	-3.4 [-3.85,-2.95]	-7.18 [-7.65,-6.71]
	30-min	-5.07 [-5.4,-4.73]	-7.04 [-7.54,-6.54]	-8.59 [-9.15,-8.02]	-2.16 [-2.67,-1.64]	-3.37 [-4.03,-2.72]	-7.21 [-7.92,-6.5]
	60-min	-5.01 [-5.46,-4.56]	-7.13 [-7.81,-6.44]	-9.2 [-10.1,-8.29]	-2.09 [-2.78,-1.39]	-3.64 [-4.53,-2.74]	-7.91 [-8.99,-6.82]
3	20-sec	-10.31 [-10.45,-10.17]	-9.49 [-9.6,-9.39]	-12.86 [-12.99,-12.72]	-8.3 [-8.43,-8.18]	-8.84 [-8.97,-8.7]	-12.5 [-12.71,-12.29]
	1-min	-11.09 [-11.28,-10.9]	-13.41 [-13.64,-13.18]	-14.45 [-14.69,-14.22]	-8.39 [-8.59,-8.2]	-10.08 [-10.31,-9.86]	-13.19 [-13.54,-12.85]
	5-min	-12.87 [-13.23,-12.5]	-15.69 [-16.16,-15.22]	-18.41 [-19.06,-17.76]	-8.79 [-9.2,-8.38]	-9.53 [-10.02,-9.04]	-12.02 [-12.69,-11.34]
	15-min	-13.02 [-13.66,-12.38]	-16.05 [-16.85,-15.24]	-19.84 [-20.94,-18.74]	-8.29 [-8.98,-7.59]	-9.2 [-10.05,-8.36]	-11.07 [-12.22,-9.92]
	30-min	-12.9 [-13.77,-12.04]	-14.87 [-15.9,-13.85]	-23.01 [-24.48,-21.53]	-9.06 [-10.03,-8.09]	-10.1 [-11.21,-8.98]	-12.85 [-14.38,-11.32]
	60-min	-12.55 [-13.81,-11.29]	-14.38 [-15.82,-12.94]	-21.29 [-23.27,-19.3]	-8.89 [-10.28,-7.5]	-10.02 [-11.64,-8.4]	-13.41 [-15.58,-11.24]

Table B.12: Posterior mean and 95% credible intervals for the β_{FQ} parameter for the SSA models fitted to data from the Highland Cattle herd. All values given are rounded to 2 decimal places.

		Forage Quality			Slope + Forage Quality		
Area	Freq	$2m^2$	$10m^2$	$20m^2$	$2m^2$	$10m^2$	$20m^2$
1	20-sec	-3.24 [-3.27,-3.2]	-2.5 [-2.53,-2.47]	-3.98 [-4.02,-3.94]	-2.7 [-2.74,-2.66]	-2.16 [-2.19,-2.12]	-3.98 [-4.03,-3.94]
	1-min	-3.21 [-3.26,-3.16]	-2.86 [-2.91,-2.81]	-3.61 [-3.66,-3.55]	-2.63 [-2.7,-2.57]	-2.42 [-2.47,-2.37]	-3.35 [-3.4,-3.29]
	5-min	-3.68 [-3.77,-3.59]	-3.53 [-3.62,-3.44]	-4.03 [-4.13,-3.93]	-2.78 [-2.91,-2.66]	-2.83 [-2.93,-2.73]	-3.51 [-3.62,-3.4]
	15-min	-4.07 [-4.23,-3.92]	-4 [-4.15,-3.85]	-4.46 [-4.63,-4.3]	-2.92 [-3.13,-2.71]	-3.04 [-3.22,-2.86]	-3.95 [-4.16,-3.74]
	30-min	-4.4 [-4.63,-4.17]	-4.27 [-4.48,-4.06]	-4.69 [-4.93,-4.46]	-3 [-3.3,-2.69]	-3.09 [-3.35,-2.84]	-4.16 [-4.48,-3.85]
	60-min	-4.32 [-4.63,-4]	-4.31 [-4.61,-4]	-4.72 [-5.06,-4.38]	-2.95 [-3.36,-2.54]	-3.03 [-3.39,-2.67]	-3.98 [-4.46,-3.51]
2	20-sec	-5.46 [-5.52,-5.41]	-3.28 [-3.33,-3.23]	-3.86 [-3.91,-3.8]	-5.09 [-5.14,-5.04]	-6.34 [-6.4,-6.28]	-6.63 [-6.69,-6.57]
	1-min	-5.54 [-5.63,-5.46]	-3.84 [-3.93,-3.76]	-4.49 [-4.59,-4.4]	-4.4 [-4.48,-4.32]	-5.23 [-5.32,-5.14]	-5.63 [-5.72,-5.55]
	5-min	-5.69 [-5.84,-5.55]	-5.39 [-5.58,-5.19]	-6.2 [-6.41,-5.98]	-3.79 [-3.94,-3.65]	-4.83 [-4.99,-4.67]	-5.26 [-5.42,-5.1]
	15-min	-6.3 [-6.54,-6.06]	-6.87 [-7.24,-6.49]	-7.94 [-8.35,-7.53]	-3.88 [-4.13,-3.63]	-5.34 [-5.64,-5.04]	-5.78 [-6.08,-5.48]
	30-min	-6.17 [-6.5,-5.84]	-7.35 [-7.87,-6.83]	-8.23 [-8.77,-7.69]	-4.01 [-4.35,-3.66]	-5.63 [-6.09,-5.18]	-6.2 [-6.67,-5.73]
	60-min	-6.17 [-6.63,-5.71]	-7.23 [-7.92,-6.53]	-8.23 [-8.96,-7.5]	-4.03 [-4.51,-3.55]	-5.67 [-6.31,-5.02]	-6.4 [-7.1,-5.7]
3	20-sec	-7.63 [-7.7,-7.55]	-9.06 [-9.15,-8.97]	-3.14 [-3.23,-3.05]	-2.97 [-3.05,-2.89]	-3.09 [-3.18,-2.99]	-2.82 [-2.91,-2.72]
	1-min	-9.1 [-9.22,-8.98]	-10.73 [-10.89,-10.58]	-3.85 [-4.01,-3.7]	-3.5 [-3.63,-3.36]	-3.26 [-3.41,-3.11]	-2.94 [-3.09,-2.78]
	5-min	-12.71 [-13.03,-12.39]	-16.12 [-16.55,-15.68]	-10.75 [-11.15,-10.35]	-5.07 [-5.45,-4.7]	-3.42 [-3.77,-3.06]	-2.73 [-3.1,-2.36]
	15-min	-14.11 [-14.66,-13.57]	-17.51 [-18.22,-16.8]	-12.1 [-12.81,-11.39]	-6.14 [-6.85,-5.42]	-3.99 [-4.63,-3.34]	-3.54 [-4.21,-2.87]
	30-min	-13.86 [-14.64,-13.09]	-17.42 [-18.44,-16.4]	-14.94 [-16.07,-13.81]	-6.66 [-7.64,-5.68]	-4.26 [-5.14,-3.37]	-3.53 [-4.42,-2.64]
	60-min	-14.54 [-15.77,-13.32]	-17.67 [-19.23,-16.12]	-15.15 [-16.66,-13.64]	-7.5 [-9.08,-5.92]	-4.92 [-6.3,-3.54]	-3.78 [-5.08,-2.48]

Appendix C

Supplementary Material for Chapter 5

The tables in this appendix contain the posterior mean and 95% credible intervals for the habitat selection parameters estimated using all 99 models fitted to the reindeer movement data in Chapter 5.

The estimated values from the 9 multivariable models without a Gaussian random field are found in Table C.1. This provides the numeric values associated with Figure 5.4 found in the main body of the text.

The estimated values from the 81 univariable models are found in Table C.2. This provides the numeric values associated with Figure 5.5 found in the main body of the text.

The estimated values from the 9 multivariable models with a Gaussian random field are found in Table C.3. This provides the numeric values associated with Figure 5.6 found in the main body of the text.

Table C.1: Posterior mean and 95% credible intervals for the habitat selection parameters from the 10 multivariable models fitted without a GRF to variations of the reindeer tracking data. All values given are rounded to 2 decimal places.

Model	β_A	β_B	β_C	β_D	β_E	β_F	β_G	β_H	β_I
Survey	-0.37 [-1.02,0.28]	-1.28 [-1.62,-0.93]	-0.81 [-1.31,-0.3]	-0.32 [-4.38,3.75]	-5.53 [-9.53,-1.53]	-4.33 [-5.98,-2.68]	-2.04 [-5.59,1.52]	-1.22 [-1.5,-0.93]	0.11 [-3.81,4.03]
Telemetry (5ind)	1.93 [0.99,2.88]	3.07 [1.57,4.57]	-0.06 [-0.15,0.02]	0.14 [0.03,0.25]	0.14 [-0.23,0.52]	1.48 [0.71,2.24]	0.5 [0.29,0.71]	3.81 [1.88,5.74]	-0.02 [-0.17,0.13]
Telemetry (10ind)	2.53 [1.96,3.09]	3.98 [3.1,4.86]	0 [-0.06,0.06]	0.28 [0.22,0.34]	0.54 [0.34,0.73]	1.98 [1.53,2.44]	0.54 [0.42,0.67]	5.14 [4,6.28]	0.08 [-0.03,0.2]
Telemetry (20ind)	1.84 [1.48,2.2]	2.81 [2.25,3.38]	-0.02 [-0.06,0.02]	0.2 [0.16,0.24]	0.44 [0.3,0.57]	1.41 [1.12,1.7]	0.32 [0.24,0.4]	3.66 [2.92,4.4]	0.11 [0.05,0.17]
Telemetry (30ind)	1.18 [0.94,1.42]	1.78 [1.4,2.16]	-0.01 [-0.04,0.02]	0.16 [0.13,0.19]	0.31 [0.24,0.39]	0.88 [0.68,1.07]	0.19 [0.13,0.25]	2.32 [1.82,2.82]	0.05 [0.01,0.1]
Telemetry (79ind)	0.73 [0.59,0.86]	1.06 [0.85,1.26]	-0.04 [-0.06,-0.02]	0.09 [0.08,0.1]	0.18 [0.14,0.22]	0.46 [0.35,0.57]	0.11 [0.08,0.15]	1.39 [1.12,1.66]	0.1 [0.08,0.12]
Joint (5ind)	-0.08 [-0.2,0.04]	-0.16 [-0.27,-0.05]	-0.05 [-0.12,0.02]	-0.01 [-0.09,0.06]	-0.43 [-0.64,-0.22]	-0.15 [-0.23,-0.07]	0.11 [-0.01,0.22]	-0.31 [-0.45,-0.18]	-0.18 [-0.29,-0.06]
Joint (10ind)	-0.05 [-0.13,0.03]	-0.09 [-0.16,-0.01]	0.01 [-0.04,0.07]	0.08 [0.04,0.13]	-0.17 [-0.28,-0.06]	-0.08 [-0.14,-0.03]	0.06 [-0.01,0.13]	-0.13 [-0.23,-0.03]	-0.14 [-0.24,-0.04]
Joint (20ind)	0.01 [-0.01,0.04]	-0.06 [-0.08,-0.04]	-0.03 [-0.05,0]	0.04 [0.02,0.05]	-0.05 [-0.1,0]	-0.03 [-0.06,-0.01]	-0.01 [-0.04,0.02]	-0.08 [-0.11,-0.05]	-0.04 [-0.07,-0.01]
Joint (30ind)	0.04 [0,0.07]	-0.03 [-0.08,0.02]	-0.01 [-0.04,0.02]	0.07 [0.05,0.09]	-0.01 [-0.03,0.01]	-0.04 [-0.07,-0.01]	-0.01 [-0.05,0.02]	-0.03 [-0.09,0.03]	-0.06 [-0.1,-0.02]

Table C.2: Posterior mean and 95% credible intervals for the habitat selection parameters from the 81 univariable models fitted to variations of the reindeer tracking data. All values given are rounded to 2 decimal places.

Survey	-0.03 [-0.63,0.58]	-0.96 [-1.26,-0.67]	-1.95 [-2.19,-1.71]	2.57 [-2.49,7.63]	-4.27 [-5.85,-2.68]	-3.76 [-4.69,-2.82]	-2.88 [-4.33,-1.42]	-1.1 [-1.23,-0.97]	-0.38 [-2.09,1.33]
Telemetry (5ind)	-0.04 [-0.14,0.06]	0.06 [0,0.12]	0 [-0.06,0.06]	0.01 [-0.06,0.09]	-0.3 [-0.48,-0.12]	-0.05 [-0.11,0]	0 [-0.1,0.1]	-0.01 [-0.07,0.06]	-0.16 [-0.27,-0.04]
Telemetry (10ind)	0.04 [-0.02,0.1]	0.03 [-0.02,0.07]	0.02 [-0.02,0.07]	0.1 [0.06,0.14]	-0.12 [-0.22,-0.02]	-0.03 [-0.07,0.01]	0 [-0.05,0.06]	-0.01 [-0.06,0.04]	-0.14 [-0.24,-0.04]
Telemetry (20ind)	0.08 [0.05,0.11]	0 [-0.03,0.03]	-0.01 [-0.04,0.02]	0.09 [0.07,0.12]	-0.1 [-0.17,-0.03]	-0.03 [-0.07,0]	-0.04 [-0.08,0]	-0.02 [-0.05,0.01]	-0.08 [-0.12,-0.03]
Telemetry (30ind)	0.08 [0.05,0.1]	0 [-0.02,0.03]	0.01 [-0.02,0.03]	0.09 [0.07,0.11]	-0.01 [-0.03,0.01]	-0.04 [-0.06,-0.01]	-0.05 [-0.08,-0.02]	-0.02 [-0.05,0.01]	-0.06 [-0.1,-0.02]
Joint (5ind)	-0.04 [-0.13,0.06]	-0.13 [-0.17,-0.09]	-0.02 [-0.08,0.03]	0.01 [-0.06,0.08]	-0.29 [-0.47,-0.12]	-0.04 [-0.08,0]	0 [-0.09,0.1]	-0.18 [-0.22,-0.13]	-0.08 [-0.16,0]
Joint (10ind)	-0.01 [-0.05,0.03]	-0.07 [-0.1,-0.04]	-0.04 [-0.07,-0.01]	0.05 [0.02,0.08]	-0.07 [-0.14,0]	-0.03 [-0.05,0]	0 [-0.04,0.04]	-0.02 [-0.07,0.02]	-0.12 [-0.22,-0.03]
Joint (20ind)	0.08 [0.05,0.11]	-0.05 [-0.07,-0.03]	-0.03 [-0.05,-0.01]	0.09 [0.07,0.12]	-0.1 [-0.16,-0.03]	-0.03 [-0.06,0]	-0.04 [-0.07,0]	-0.03 [-0.06,0]	-0.07 [-0.11,-0.03]
Joint (30ind)	0.03 [0.02,0.05]	-0.03 [-0.05,-0.01]	0.01 [-0.02,0.03]	0.05 [0.03,0.06]	-0.01 [-0.03,0.01]	-0.02 [-0.04,0]	-0.03 [-0.05,0]	-0.03 [-0.05,-0.02]	-0.03 [-0.06,0]

Table C.3: Posterior mean and 95% credible intervals for the habitat selection parameters from the 10 multivariable models fitted with a GRF to variations of the reindeer tracking data. All values given are rounded to 2 decimal places.

Model	β_A	β_B	β_C	β_D	β_E	β_F	β_G	β_H	β_I
Survey	-0.28 [-1.36,0.79]	-1.5 [-2.31,-0.69]	-0.36 [-1.05,0.32]	-1.55 [-7.31,4.21]	-9.11 [-16.4,-1.81]	-4.32 [-6.41,-2.24]	-0.6 [-5.58,4.39]	-1.21 [-1.97,-0.45]	0.58 [-5,6.15]
Telemetry (5ind)	2.57 [0.91,4.24]	3.84 [1.24,6.46]	-0.14 [-0.38,0.1]	0.1 [-0.18,0.39]	0.05 [-0.69,0.8]	1.84 [0.51,3.17]	0.81 [0.4,1.22]	4.82 [1.46,8.19]	-0.07 [-0.38,0.24]
Telemetry (10ind)	1.73 [0.67,2.77]	2.8 [1.17,4.42]	-0.12 [-0.3,0.05]	0.06 [-0.1,0.21]	0.38 [0.02,0.75]	1.27 [0.45,2.09]	0.44 [0.17,0.71]	3.43 [1.34,5.52]	-0.04 [-0.29,0.2]
Telemetry (20ind)	0.9 [0.28,1.52]	1.43 [0.46,2.4]	-0.04 [-0.15,0.07]	0.11 [0.02,0.2]	0.14 [-0.1,0.39]	0.6 [0.1,1.09]	0.18 [0.02,0.34]	1.71 [0.45,2.97]	0.01 [-0.11,0.13]
Telemetry (30ind)	0.34 [-0.14,0.82]	0.56 [-0.19,1.3]	-0.03 [-0.12,0.06]	0.09 [0.02,0.16]	0.06 [-0.09,0.22]	0.18 [-0.2,0.56]	0.07 [-0.05,0.2]	0.63 [-0.34,1.59]	0.01 [-0.09,0.11]
Telemetry (79ind)	0.11 [-0.2,0.43]	0.05 [-0.43,0.54]	-0.01 [-0.08,0.06]	0.07 [0.02,0.12]	0 [-0.11,0.11]	-0.02 [-0.27,0.23]	-0.07 [-0.17,0.02]	0.05 [-0.57,0.68]	0.03 [-0.04,0.09]
Joint (5ind)	-0.09 [-0.21,0.04]	-0.17 [-0.28,-0.06]	-0.04 [-0.11,0.04]	-0.01 [-0.09,0.07]	-0.44 [-0.66,-0.22]	-0.15 [-0.23,-0.07]	0.11 [-0.01,0.23]	-0.32 [-0.45,-0.18]	-0.18 [-0.29,-0.06]
Joint (10ind)	0.08 [-0.08,0.24]	0.13 [-0.1,0.35]	0.05 [-0.02,0.11]	0.09 [0.04,0.14]	-0.13 [-0.26,0]	0.01 [-0.11,0.14]	0.13 [0.04,0.22]	0.16 [-0.13,0.44]	-0.14 [-0.24,-0.03]
Joint (20ind)	0.14 [0.03,0.25]	0.11 [-0.06,0.27]	0 [-0.05,0.04]	0.06 [0.03,0.1]	-0.06 [-0.16,0.05]	0.03 [-0.06,0.12]	0.03 [-0.03,0.09]	0.14 [-0.07,0.35]	-0.07 [-0.12,-0.02]
Joint (30ind)	0.03 [0,0.07]	-0.04 [-0.08,0.01]	-0.01 [-0.04,0.03]	0.06 [0.03,0.08]	-0.01 [-0.04,0.01]	-0.04 [-0.08,-0.01]	-0.02 [-0.06,0.02]	-0.05 [-0.11,0.01]	-0.06 [-0.1,-0.01]

Bibliography

Aarts, G., J. Fieberg, and J. Matthiopoulos (2012). "Comparative interpretation of count, presence-absence and point methods for species distribution models". In: *Methods in Ecology and Evolution* 3.1, pp. 177–187. ISSN: 2041-210X. DOI: 10.1111/j.2041-210x.2011.00141.x.

Addicott, J., J. Aho, M. Antolin, D. Padilla, J. Richardson, and D. Soluk (1987). "Ecological Neighborhoods: Scaling Environmental Patterns". In: *Oikos* 49.3, p. 340. ISSN: 0030-1299. DOI: 10.2307/3565770.

Albery, G., A. Morris, S. Morris, J. Pemberton, T. Clutton-Brock, D. Nussey, and J. Firth (2021). "Multiple spatial behaviours govern social network positions in a wild ungulate." In: *Ecology Letters* Early View. DOI: https://doi.org/10.1111/ele.13684.

Allee, W. C. (1938). *The social life of animals*. New York: W.W. Norton & Company, inc. DOI: 10.5962/bhl.title.7226.

Altwegg, R., S. Salau, F. Abadi, F. Cervantes, A. Clark, G. Distiller, O. Gimenez, D. Henry, A. Johnston, R. Joo, and et al. (2025). "Emerging Topics and New Directions in Statistical Ecology". In: *Journal of Statistical Theory and Practice* 19.3. ISSN: 1559-8608. DOI: 10.1007/s42519-025-00460-4.

Anttonen, M., K. Jouko, and A. Colpaert (2011). "Range Selection by Semi-Domesticated Reindeer (Rangifer tarandus tarandus) in Relation to Infrastructure and Human Activity in the Boreal Forest Environment, Northern Finland". In: *arctic* 64, pp. 1–14. DOI: 10.14430/arctic4075.

Arce Guillen, R., F. Lindgren, S. Muff, T. W. Glass, G. A. Breed, and U. E. Schlägel (2023). "Accounting for unobserved spatial variation in step selection analyses of animal movement via spatial random effects". In: *Methods in Ecology and Evolution* 14.10, pp. 2639–2653. ISSN: 2041-210X. DOI: 10.1111/2041-210x.14208.

Armstrong, D. P. and P. J. Seddon (2008). "Directions in reintroduction biology". In: *Trends in Ecology & Evolution* 23.1, pp. 20–25. ISSN: 0169-5347. DOI: https://doi.org/10.1016/j.tree.2007.10.003. URL: https://www.sciencedirect.com/science/article/pii/S0169534707003345.

Avgar, T., J. R. Potts, M. A. Lewis, and M. S. Boyce (2016). "Integrated step selection analysis: bridging the gap between resource selection and animal movement". In: *Methods in Ecology and Evolution* 7.5, pp. 619–630. ISSN: 2041-210X. DOI: 10.1111/2041-210x.12528.

Bachl, F., F. Lindgren, D. Borchers, and J. Illian (2019). "inlabru: an R package for Bayesian spatial modelling from ecological survey data". In: *Methods in Ecology and Evolution* 10.6, pp. 760–766. ISSN: 2041-210X. DOI: 10.1111/2041-210x.13168.

Badger, J. J., D. S. Johnson, R. W. Baird, A. L. Bradford, M. A. Kratofil, S. D. Mahaffy, and E. M. Oleson (2024). "Incorporating telemetry information into capture-recapture analyses improves precision and accuracy of abundance estimates given spatiotemporally biased recapture effort". In: *Methods in Ecology and Evolution* 15.10, pp. 1847–1858. ISSN: 2041-210X. DOI: 10.1111/2041-210x.14408.

Bailey, D. W., M. G. Trotter, C. W. Knight, and M. G. Thomas (2018). "Use of GPS tracking collars and accelerometers for rangeland livestock production research1". In: *Translational Animal Science* 2.1, pp. 81–88. ISSN: 2573-2102. DOI: 10.1093/tas/txx006. URL: https://dx.doi.org/10.1093/tas/txx006.

Barbet-Massin, M., F. Jiguet, C. H. Albert, and W. Thuiller (2012). "Selecting pseudo-absences for species distribution models: how, where and how many?" In: *Methods in Ecology and Evolution* 3.2, pp. 327–338. ISSN: 2041-210X. DOI: 10.1111/j.2041-210x.2011.00172.x.

Barwick, J., D. Lamb, R. Dobos, D. Schneider, M. Welch, and M. Trotter (2018). "Predicting Lameness in Sheep Activity Using Tri-Axial Acceleration Signals". In: *Animals* 8.1, p. 12. ISSN: 2076-2615. DOI: 10.3390/ani8010012. URL: https://dx.doi.org/10.3390/ani8010012.

Bayes, T. (1763). "LII. An essay towards solving a problem in the doctrine of chances. By the late Rev. Mr. Bayes, F. R. S. communicated by Mr. Price, in a letter to John Canton, A. M. F. R. S". In: *Philosophical Transactions of the Royal Society of London* 53.0, pp. 370–418. ISSN: 0261-0523. DOI: 10.1098/rstl.1763.0053.

Belmont, J., S. Martino, J. Illian, and H. Rue (2024). "Spatio-temporal occupancy models with INLA". In: *Methods in Ecology and Evolution* 15.11, pp. 2087–2100. ISSN: 2041-210X. DOI: 10.1111/2041-210x.14422.

Bertsekas, D. and J. Tsitsiklis (2002). *Introduction to Probability*. Athena Scientific books. Athena Scientific. ISBN: 9781886529403. URL: https://books.google.co.uk/books?id=bcHaAAAAMAAJ.

Beyer, H. L., E. Gurarie, L. Börger, M. Panzacchi, M. Basille, I. Herfindal, B. Van Moorter, S. R. Lele, and J. Matthiopoulos (2016). "You shall not pass!: quantifying barrier permeability and proximity avoidance by animals". In: *Journal of Animal Ecology* 85.1, pp. 43–53. ISSN: 0021-8790. DOI: 10.1111/1365-2656.12275. URL: https://dx.doi.org/10.1111/1365-2656.12275.

Beyer, H. L., D. T. Haydon, J. M. Morales, J. L. Frair, M. Hebblewhite, M. Mitchell, and J. Matthiopoulos (2010). "The interpretation of habitat preference metrics under use–availability designs". In: *Philosophical Transactions of the Royal Society B: Biological Sciences* 365.1550,

pp. 2245–2254. ISSN: 0962-8436. DOI: 10.1098/rstb.2010.0083. URL: https://dx.doi.org/10.1098/rstb.2010.0083.

Bhattacharya, A., N. Chatterjee, G. S. Rawat, and B. Habib (2020). "Blue Sheep Resource Selection in Alpine Grasslands of a Western Himalayan Landscape - A Point Process Approach". In: *ZOOLOGICAL STUDIES* 59. ISSN: 1021-5506. DOI: 10.6620/ZS.2020.59-11.

Blackwell, P. G. (1997). "Random diffusion models for animal movement". In: *Ecological Modelling* 100.1-3, pp. 87–102. ISSN: 0304-3800. DOI: 10.1016/s0304-3800(97)00153-1.

Blackwell, P. G. and J. Matthiopoulos (2024). "Joint inference for telemetry and spatial survey data". In: *Ecology* 105.12. ISSN: 0012-9658. DOI: 10.1002/ecy.4457.

Blangiardo, M., M. Cameletti, G. Baio, and H. Rue (2013). "Spatial and spatio-temporal models with R-INLA". In: *Spatial and Spatio-temporal Epidemiology* 4, pp. 33–49. ISSN: 1877-5845. DOI: 10.1016/j.sste.2012.12.001. URL: https://dx.doi.org/10.1016/j.sste.2012.12.001.

Bleisch, A., B. Keller, T. Bonnot, L. Hansen, and J. Millspaugh (2017). "Initial Movements of Re- introduced Elk in the Missouri Ozarks". In: *The American Midland Naturalist* 178, pp. 1–16. DOI: 10.1674/0003-0031-178.1.1.

Bolker, B. (2009). "Learning hierarchical models: advice for the rest of us". In: *Ecological Applications* 19.3, pp. 588–592. ISSN: 1051-0761. DOI: 10.1890/08-0639.1.

Breed, G. A., E. A. Golson, and M. T. Tinker (2017). "Predicting animal home-range structure and transitions using a multistate Ornstein-Uhlenbeck biased random walk". In: *Ecology* 98.1, pp. 32–47. ISSN: 0012-9658. DOI: 10.1002/ecy.1615. URL: https://dx.doi.org/10.1002/ecy.1615.

Briemle, G., S. Nitsche, and L. Nitsche (2002). "Nutzungswertzahlen für Gefäßpflanzen des Grünlandes". In: *Schriftenreihe Für Veg* 23, pp. 203–25.

Buckley, L. B., S. A. Waaser, H. J. MacLean, and R. Fox (2011). "Does including physiology improve species distribution model predictions of responses to recent climate change?" In: *Ecology* 92.12, pp. 2214–2221.

Buderman, F. E., E. M. Hanks, V. Ruiz-Gutierrez, M. Shull, R. K. Murphy, and D. A. W. Miller (2025). "Integrated movement models for individual tracking and species distribution data". In: *Methods in Ecology and Evolution* 16.2, pp. 345–361. ISSN: 2041-210X. DOI: 10.1111/2041-210x.14482.

Carpenter, B., A. Gelman, M. D. Hoffman, D. Lee, B. Goodrich, M. Betancourt, M. Brubaker, J. Guo, P. Li, and A. Riddell (2017). "Stan: A Probabilistic Programming Language". In: *Journal of Statistical Software* 76.1, pp. 1–32. DOI: 10.18637/jss.v076.i01. URL: https://www.jstatsoft.org/index.php/jss/article/view/v076i01.

Carson, S. and J. Flemming (2014). "Seal encounters at sea: A contemporary spatial approach using R-INLA". In: *Ecological Modelling* 291, pp. 175–181. DOI: https://doi.org/10.1016/j.ecolmodel.2014.07.022.

Chadwick, F. J., D. T. Haydon, D. Husmeier, O. Ovaskainen, and J. Matthiopoulos (2024). "LIES of omission: complex observation processes in ecology". In: *Trends in Ecology & Evolution* 39.4, pp. 368–380. ISSN: 0169-5347. DOI: 10.1016/j.tree.2023.10.009.

Chandler, R. and J. Hepinstall-Cymerman (2016). "Estimating the spatial scales of landscape effects on abundance". In: *Landscape Ecology* 31.6, pp. 1383–1394. ISSN: 0921-2973. DOI: 10.1007/s10980-016-0380-z.

Chase, J. M. and M. A. Leibold (2002). "Spatial scale dictates the productivity–biodiversity relationship". In: *Nature* 416.6879, pp. 427–430. ISSN: 0028-0836. DOI: 10.1038/416427a.

Compton, B. W., J. M. Rhymer, and M. Mccollough (2002). "Habitat Selection by Wood Turtles (Clemmys insculpta): An Application of Paired Logistic Regression". In: *Ecology* 83.3, p. 833. ISSN: 0012-9658. DOI: 10.2307/3071885.

Cox, D. R. and V. Isham (1980). *Point processes*. Vol. 12. CRC Press.

Crosby, A. D. and W. F. Porter (2018). "A spatially explicit, multi-scale occupancy model for large-scale population monitoring". In: *The Journal of Wildlife Management* 82.6, pp. 1300–1310. ISSN: 0022-541X. DOI: 10.1002/jwmg.21466. URL: https://dx.doi.org/10.1002/jwmg.21466.

Dambly, L. I., N. J. B. Isaac, K. E. Jones, K. L. Boughey, and R. B. O'Hara (2023). "Integrated species distribution models fitted in INLA are sensitive to mesh parameterisation". In: *Ecography* 2023.7. ISSN: 0906-7590. DOI: 10.1111/ecog.06391.

Davis, J., M. Darr, H. Xin, J. Harmon, and J. Russell (2011). "Development of a GPS Herd Activity and Well- Being Kit (GPS HAWK) to Monitor Cattle Behavior and the Effect of Sample Interval on Travel Distance". In: *Applied Engineering in Agriculture* 27. DOI: 10.13031/2013.36224.

De Marco, P., J. A. F. Diniz-Filho, and L. M. Bini (2008). "Spatial analysis improves species distribution modelling during range expansion". In: *Biology Letters* 4.5, pp. 577–580. ISSN: 1744-9561. DOI: 10.1098/rsbl.2008.0210. URL: https://dx.doi.org/10.1098/rsbl.2008.0210.

De Valpine, P., D. Turek, C. J. Paciorek, C. Anderson-Bergman, D. T. Lang, and R. Bodik (2017). "Programming With Models: Writing Statistical Algorithms for General Model Structures With NIMBLE". In: *Journal of Computational and Graphical Statistics* 26.2, pp. 403–413. ISSN: 1061-8600. DOI: 10.1080/10618600.2016.1172487. URL: https://dx.doi.org/10.1080/10618600.2016.1172487.

Decesare, N. J., M. Hebblewhite, F. Schmiegelow, D. Hervieux, G. J. Mcdermid, L. Neufeld, M. Bradley, J. Whittington, K. G. Smith, L. E. Morgantini, and et al. (2012). "Transcending scale dependence in identifying habitat with resource selection functions". In: *Ecological Applications* 22.4, pp. 1068–1083. ISSN: 1051-0761. DOI: 10.1890/11-1610.1. URL: https://dx.doi.org/10.1890/11-1610.1.

Diggle, P. J., R. Menezes, and T.-L. Su (2010). "Geostatistical inference under preferential sampling". In: *Journal of the Royal Statistical Society: Series C (Applied Statistics)* 59.2, pp. 191–232. ISSN: 0035-9254. DOI: 10.1111/j.1467-9876.2009.00701.x.

Dormann, C. F. (2007). "Effects of incorporating spatial autocorrelation into the analysis of species distribution data". In: *Global Ecology and Biogeography* 16.2, pp. 129–138. ISSN: 1466-822X. DOI: 10.1111/j.1466-8238.2006.00279.x. URL: https://dx.doi.org/10.1111/j.1466-8238.2006.00279.x.

Dormann, C. F., J. M. McPherson, M. B. Araújo, R. Bivand, J. Bolliger, G. Carl, R. G. Davies, A. Hirzel, W. Jetz, D. W. Kissling, et al. (2007). "Methods to account for spatial autocorrelation in the analysis of species distributional data: a review". In: *Ecography* 30.5, pp. 609–628.

Duffy, K. (2010). "Why do many animals move with a predominance of roughly forward directions?" In: *Nature Precedings* 5. DOI: 10.1038/npre.2010.5156.1.

Dyer, S. J., J. P. O'Neill, S. M. Wasel, and S. Boutin (2001). "Avoidance of Industrial Development by Woodland Caribou". In: *The Journal of Wildlife Management* 65.3, pp. 531–542. ISSN: 0022541X, 19372817. URL: http://www.jstor.org/stable/3803106 (visited on 09/05/2025).

Eftestøl, S., D. Tsegaye, K. Flydal, and J. E. Colman (2016). "From high voltage (300 kV) to higher voltage (420 kV) power lines: reindeer avoid construction activities". In: *Polar Biology* 39.4, pp. 689–699. ISSN: 0722-4060. DOI: 10.1007/s00300-015-1825-6.

Eisaguirre, J. M., T. L. Booms, C. P. Barger, S. D. Goddard, and G. A. Breed (2021). "Multistate Ornstein–Uhlenbeck approach for practical estimation of movement and resource selection around central places". In: *Methods in Ecology and Evolution* 12.3, pp. 507–519. ISSN: 2041-210X. DOI: 10.1111/2041-210x.13538.

Eisaguirre, J. M., P. J. Williams, J. C. Brockman, S. B. Lewis, C. P. Barger, G. A. Breed, and T. L. Booms (2023). "A hierarchical modelling framework for estimating individual- and population-level reproductive success from movement data". In: *Methods in Ecology and Evolution* 14.8, pp. 2110–2122. ISSN: 2041-210X. DOI: 10.1111/2041-210x.14159.

Elith, J. and J. R. Leathwick (2009). "Species distribution models: ecological explanation and prediction across space and time". In: *Annual review of ecology, evolution, and systematics* 40, pp. 677–697.

Ellison, A. M. (2004). "Bayesian inference in ecology". In: *Ecology Letters* 7.6, pp. 509–520. ISSN: 1461-023X. DOI: 10.1111/j.1461-0248.2004.00603.x. URL: https://dx.doi.org/10.1111/j.1461-0248.2004.00603.x.

Ferrari, L. and M. Ventrucci (2024). "A standardization procedure to incorporate variance partitioning-based priors in latent Gaussian models". In: *Scandinavian Journal of Statistics* n/a.n/a. DOI: https://doi.org/10.1111/sjos.70042. eprint: https://onlinelibrary.wiley.com/doi/pdf/10.1111/sjos.70042. URL: https://onlinelibrary.wiley.com/doi/abs/10.1111/sjos.70042.

Fieberg, J., J. Signer, B. Smith, and T. Avgar (2021). "A 'How to' guide for interpreting parameters in habitat-selection analyses". In: *Journal of Animal Ecology* 90.5, pp. 1027–1043. ISSN: 0021-8790. DOI: 10.1111/1365-2656.13441.

Florko, K. R. N., R. R. Togunov, R. Gryba, E. Sidrow, S. H. Ferguson, D. J. Yurkowski, and M. Auger-Méthé (2025). "An introduction to statistical models used to characterize species-habitat associations with animal movement data". In: *Movement Ecology* 13.1. ISSN: 2051-3933. DOI: 10.1186/s40462-025-00549-2.

Flydal, K., S. Eftestøl, E. Reimers, and J. Colman (2010). "Effects of wind turbines on area use and behaviour of semi-domestic reindeer in enclosures". In: *Rangifer* 24. DOI: 10.7557/2.24.2.301.

Forester, J. D., H. K. Im, and P. J. Rathouz (2009). "Accounting for animal movement in estimation of resource selection functions: sampling and data analysis". In: *Ecology* 90.12, pp. 3554–3565. DOI: https://doi.org/10.1890/08-0874.1. eprint: https://esajournals.onlinelibrary.wiley.com/doi/pdf/10.1890/08-0874.1. URL: https://esajournals.onlinelibrary.wiley.com/doi/abs/10.1890/08-0874.1.

Fortin, D., H. Beyer, M. Boyce, D. Smith, T. Duchesne, and J. Mao (2005). "Wolves Influence Elk Movements: behavior Shapes a Trophic Cascade in Yellowstone National Park". In: *Ecology* 86, pp. 1320–1330. DOI: 10.1890/04-0953.

Gelman, A., J. B. Carlin, H. S. Stern, D. B. Dunson, A. Vehtari, and D. B. Rubin (2015). *Bayesian Data Analysis. Third edition.* New York: Chapman and Hall/CRC.

Gelman, A., J. Hwang, and A. Vehtari (2014). "Understanding predictive information criteria for Bayesian models". In: *Statistics and Computing* 24.6, pp. 997–1016. ISSN: 0960-3174. DOI: 10.1007/s11222-013-9416-2. URL: https://dx.doi.org/10.1007/s11222-013-9416-2.

Geman, S. and D. Geman (1984). "Stochastic Relaxation, Gibbs Distributions, and the Bayesian Restoration of Images". In: *IEEE Transactions on Pattern Analysis and Machine Intelligence* PAMI-6.6, pp. 721–741. ISSN: 0162-8828. DOI: 10.1109/tpami.1984.4767596.

Grabow, M., J. L. P. Louvrier, A. Planillo, S. Kiefer, S. Drenske, K. Börner, M. Stillfried, R. Hagen, S. Kimmig, T. M. Straka, and et al. (2022). "Data-integration of opportunistic species observations into hierarchical modeling frameworks improves spatial predictions for urban red squirrels". In: *Frontiers in Ecology and Evolution* 10. ISSN: 2296-701X. DOI: 10.3389/fevo.2022.881247.

Graf, R. F., K. Bollmann, W. Suter, and H. Bugmann (2005). "The Importance of Spatial Scale in Habitat Models: Capercaillie in the Swiss Alps". In: *Landscape Ecology* 20.6, pp. 703–717. ISSN: 0921-2973. DOI: 10.1007/s10980-005-0063-7. URL: https://dx.doi.org/10.1007/s10980-005-0063-7.

Griffin, L., J. Finn, C. Diez, and A. Danylchuk (2019). "Movements, connectivity, and space use of immature green turtles within coastal habitats of the Culebra Archipelago, Puerto Rico:

implications for conservation". In: *Endangered Species Research* 40, pp. 75–90. DOI: https://doi.org/10.3354/esr00976.

Gutowsky, L., J. Romine, N. Heredia, P. Bigelow, M. Parsley, P. Sandstrom, C. Suski, A. Danylchuk, S. Cooke, and R. Gresswell (2020). "Revealing migration and reproductive habitat of invasive fish under an active population suppression program". In: *Conservation Science and Practice* 2(3), e119. DOI: https://doi.org/10.1111/csp2.119.

Hald-Mortensen, C. (2023). "The Main Drivers of Biodiversity Loss: A Brief Overview". In: *Journal of Ecology & Natural Resources* 7. DOI: 10.23880/jenr-16000346.

Handcock, R. N., D. L. Swain, G. J. Bishop-Hurley, K. P. Patison, T. Wark, P. Valencia, P. Corke, and C. J. O'Neill (2009). "Monitoring Animal Behaviour and Environmental Interactions Using Wireless Sensor Networks, GPS Collars and Satellite Remote Sensing". In: *Sensors* 9.5, pp. 3586–3603. ISSN: 1424-8220. DOI: 10.3390/s90503586. URL: https://dx.doi.org/10.3390/s90503586.

Haydon, D., J. Morales, A. Yott, D. Jenkins, R. Rosatte, and J. Fryxell (2008). "Socially informed random walks: Incorporating group dynamics into models of population spread and growth". In: *Proceedings. Biological sciences / The Royal Society* 275, pp. 1101–9. DOI: 10.1098/rspb.2007.1688.

Hazen, E. L., B. Abrahms, S. Brodie, G. Carroll, H. Welch, and S. J. Bograd (2021). "Where did they not go? Considerations for generating pseudo-absences for telemetry-based habitat models". In: *Movement Ecology* 9.1. ISSN: 2051-3933. DOI: 10.1186/s40462-021-00240-2.

Heggenes, J., A. Odland, T. Chevalier, J. Ahlberg, A. Berg, H. Larsson, and D. K. Bjerketvedt (2017). "Herbivore grazing—or trampling? Trampling effects by a large ungulate in cold high-latitude ecosystems". In: *Ecology and Evolution* 7.16, pp. 6423–6431. ISSN: 2045-7758. DOI: 10.1002/ece3.3130. URL: https://dx.doi.org/10.1002/ece3.3130.

Hodges, J. S. and B. J. Reich (2010). "Adding Spatially-Correlated Errors Can Mess Up the Fixed Effect You Love". In: *The American Statistician* 64.4, pp. 325–334. ISSN: 0003-1305. DOI: 10.1198/tast.2010.10052.

Homburger, H., A. Lüscher, M. Scherer-Lorenzen, and M. K. Schneider (2015). "Patterns of livestock activity on heterogeneous subalpine pastures reveal distinct responses to spatial autocorrelation, environment and management". In: *Movement Ecology* 3.1. ISSN: 2051-3933. DOI: 10.1186/s40462-015-0053-6. URL: https://dx.doi.org/10.1186/s40462-015-0053-6.

Hooten, M., E. Hanks, D. Johnson, and M. Alldredge (2014). "Temporal Variation and Scale in Movement-Based Resource Selection Functions". In: *Statistical Methodology* 17, pp. 82–98. DOI: 10.1016/j.stamet.2012.12.001.

Hooten, M. B., D. S. Johnson, B. T. Mcclintock, and J. M. Morales (2017). *Animal Movement*. Boca Raton: CRC Press. DOI: 10.1201/9781315117744.

Horn, B. (1981). "Hill shading and the reflectance map". In: *Proceedings of the IEEE* 69.1, pp. 14–47. ISSN: 0018-9219. DOI: 10.1109/proc.1981.11918.

Horstkotte, T., O. Holand, K. Jouko, and J. Moen (2022). *Reindeer Husbandry and Global Environmental Change*. London: Routledge. ISBN: 9781003118565. DOI: 10.4324/9781003118565.

Horstkotte, T., P. Sandström, W. Neumann, A. Skarin, S. Adler, U. Roos, and J. Sjögren (2023). "Semi-domesticated reindeer avoid winter habitats with exotic tree species Pinus contorta". In: *Forest Ecology and Management* 540, p. 121062. ISSN: 0378-1127. DOI: https://doi.org/10.1016/j.foreco.2023.121062. URL: https://www.sciencedirect.com/science/article/pii/S0378112723002967.

Hostetter, N. J., E. V. Regehr, R. R. Wilson, J. A. Royle, and S. J. Converse (2022). "Modeling spatiotemporal abundance and movement dynamics using an integrated spatial capture–recapture movement model". In: *Ecology* 103.10. ISSN: 0012-9658. DOI: 10.1002/ecy.3772.

Hume, C. (2008). *Wetland Vision Technical Document: overview and reporting of project philosophy and technical approach*. Tech. rep. 80. The Wetland Vision Partnership.

Illian, J. and D. Burslem (2017). "Improving the usability of spatial point process methodology: an interdisciplinary dialogue between statistics and ecology". In: *AStA Advances in Statistical Analysis* 101.4, pp. 495–520. ISSN: 1863-8171. DOI: 10.1007/s10182-017-0301-8. URL: https://dx.doi.org/10.1007/s10182-017-0301-8.

Illian, J., S. Martino, S. Sørbye, J. Gallego-Fernández, M. Zunzunegui, M. Esquivias, and J. M. Travis (2013). "Fitting complex ecological point process models with integrated nested Laplace approximation". In: *Methods in Ecology and Evolution* 4.4, pp. 305–315. ISSN: 2041-210X. DOI: 10.1111/2041-210x.12017. URL: https://dx.doi.org/10.1111/2041-210x.12017.

Illian, J., S. Sørbye, H. Rue, and D. Hendrichsen (2014). "Using INLA To Fit A Complex Point Process Model With Temporally Varying Effects – A Case Study". In: *Journal of Environmental Statistics* 3, pp. 1–29.

Illian, J., S. Sørbye, and H. Rue (2012). "A toolbox for fitting complex spatial point process models using integrated nested Laplace approximation (INLA)". In: *The Annals of Applied Statistics* 6.4, pp. 1499–1530. ISSN: 1932-6157. DOI: 10.1214/11-aoas530.

Iverson, L. R., M. W. Schwartz, and A. M. Prasad (2004). "How fast and far might tree species migrate in the eastern United States due to climate change?" In: *Global Ecology and Biogeography* 13.3, pp. 209–219.

Jackson, H. B. and L. Fahrig (2015). "Are ecologists conducting research at the optimal scale?" In: *Global Ecology and Biogeography* 24.1, pp. 52–63. ISSN: 1466-822X. DOI: 10.1111/geb.12233.

Johnsgard, P. A. (1983). *Cranes of the World*. Cambridge University Press.

Johnson, A. R., J. A. Wiens, B. T. Milne, and T. O. Crist (1992). "Animal movements and population dynamics in heterogeneous landscapes". In: *Landscape Ecology* 7.1, pp. 63–75. ISSN: 0921-2973. DOI: 10.1007/bf02573958.

Johnson, D. S., J. M. London, and C. E. Kuhn (2011). "Bayesian Inference for Animal Space Use and Other Movement Metrics". In: *Journal of Agricultural, Biological and Environmental Statistics* 16.3, pp. 357–370. ISSN: 1085-7117. DOI: 10.1007/s13253-011-0056-8.

Johnson, D. S., J. M. London, M.-A. Lea, and J. W. Durban (2008). "CONTINUOUS-TIME CORRELATED RANDOM WALK MODEL FOR ANIMAL TELEMETRY DATA". In: *Ecology* 89.5, pp. 1208–1215. ISSN: 0012-9658. DOI: 10.1890/07-1032.1.

Johnson, D. D. and D. C. Ganskopp (2008). "GPS Collar Sampling Frequency: Effects on Measures of Resource Use". In: *Rangeland Ecology & Management* 61.2, pp. 226–231. ISSN: 1550-7424. DOI: 10.2111/07-044.1.

Jonsen, I. (2016). "Joint estimation over multiple individuals improves behavioural state inference from animal movement data". In: *Scientific Reports* 6.1, p. 20625. ISSN: 2045-2322. DOI: 10.1038/srep20625. URL: https://dx.doi.org/10.1038/srep20625.

Jullum, M., T. Thorarinsdottir, and F. E. Bachl (2020). "Estimating seal pup production in the Greenland Sea by using Bayesian hierarchical modelling". In: *Journal of the Royal Statistical Society: Series C (Applied Statistics)* 69.2, pp. 327–352. ISSN: 0035-9254. DOI: 10.1111/rssc.12397.

Klaassen, B. and F. Broekhuis (2018). "Living on the edge: Multiscale habitat selection by cheetahs in a human-wildlife landscape". In: *Ecology and Evolution* 8.15, pp. 7611–7623. ISSN: 2045-7758. DOI: 10.1002/ece3.4269. URL: https://dx.doi.org/10.1002/ece3.4269.

Kneib, T., J. Müller, and T. Hothorn (2008). "Spatial smoothing techniques for the assessment of habitat suitability". In: *Environmental and Ecological Statistics* 15.3, pp. 343–364.

Koczura, M., B. Martin, M. Bouchon, G. Turille, J. Berard, A. Farruggia, M. Kreuzer, and M. Coppa (2019). "Grazing behaviour of dairy cows on biodiverse mountain pastures is more influenced by slope than cow breed". In: *Animal* 13.11, pp. 2594–2602. ISSN: 1751-7311. DOI: https://doi.org/10.1017/S175173111900079X. URL: https://www.sciencedirect.com/science/article/pii/S175173111900079X.

Kühn, I. (2006). "Incorporating spatial autocorrelation may invert observed patterns". In: *Diversity and Distributions* 0.0, p. 061117052025001. ISSN: 1366-9516. DOI: 10.1111/j.1472-4642.2006.00293.x.

Kumpula, J., A. Colpaert, and A. Tanskanen (2008). "Porojen laidunten valinta muuttuneessa metsä- ja maisemarakenteessa Keski-Lapissa". In: *Suomen Riista* 54, pp. 69–82.

Kumpula, J., A. Colpaert, A. Tanskanen, M. Anttonen, H. Törmänen, and J. Siitari (2006). *Development of reindeer pasture inventory – Pasture inventory of Central Lapland herding communities in 2005–2006*. Tech. rep. Finnish Game and Fisheries Research Institute.

Laporte, I., T. B. Muhly, J. A. Pitt, M. Alexander, and M. Musiani (2010). "Effects of Wolves on Elk and Cattle Behaviors: Implications for Livestock Production and Wolf Conservation". In: *PLOS One* 5.8, e11954. ISSN: 1932-6203. DOI: 10.1371/journal.pone.0011954. URL: https://dx.doi.org/10.1371/journal.pone.0011954.

Lassila, M. (2021). "The Arctic mineral resource rush and the ontological struggle for the Viiankiaapa peatland in Sodankylä, Finland". In: *Globalizations* 18.4, pp. 635–649. ISSN: 1474-7731. DOI: 10.1080/14747731.2020.1831818.

Lauret, V., N. Courbin, O. Scher, and A. Besnard (2025). "Integrating individual tracking data and spatial surveys to improve estimation of animal spatial distribution". In: *Ecosphere* 16.5. ISSN: 2150-8925. DOI: 10.1002/ecs2.70283.

Lavender, E., D. Aleynik, J. Dodd, J. Illian, M. James, P. J. Wright, S. Smout, and J. Thorburn (2022). "Movement patterns of a Critically Endangered elasmobranch (Dipturus intermedius) in a Marine Protected Area". In: *Aquatic Conservation: Marine and Freshwater Ecosystems* 32.2, pp. 348–365. ISSN: 1052-7613. DOI: 10.1002/aqc.3753.

Laxton, M. R., G. Nightingale, F. Lindgren, A. Sivakumaran, and R. Othieno (2023a). "Extending the R number by applying hyperparameters of Log Gaussian Cox process models in an epidemiological context to provide insights into COVID-19 positivity in the City of Edinburgh and in students residing at Edinburgh University". In: *PLOS ONE* 18.11, e0291348. ISSN: 1932-6203. DOI: 10.1371/journal.pone.0291348.

Laxton, M. R., Ó. Rodríguez De Rivera, A. Soriano-Redondo, and J. B. Illian (2023b). "Balancing structural complexity with ecological insight in spatio-temporal species distribution models". In: *Methods in Ecology and Evolution* 14.1, pp. 162–172. ISSN: 2041-210X. DOI: 10.1111/2041-210x.13957.

Laxton, M. R., Ó. Rodríguez de Rivera, A. Soriano-Redondo, and J. B. Illian (2022a). *Code from: Balancing structural complexity with ecological insight in spatio-temporal species distribution models*. DOI: https://doi.org/10.5281/zenodo.6907553.

— (2022b). *Transformed crane data from: Balancing structural complexity with ecological insight in spatio-temporal species distribution models*. DOI: https://doi.org/10.5061/dryad.2z34tmpps.

Lele, S. R. and J. L. Keim (2006). "Weighted distributions and estimation of resource selection probability functions." In: *Ecology* 87 12, pp. 3021–8. URL: https://api.semanticscholar.org/CorpusID:13615931.

Lesmerises, F., C. J. Johnson, and M.-H. St-Laurent (2018). "Landscape knowledge is an important driver of the fission dynamics of an alpine ungulate". In: *Animal Behaviour* 140, pp. 39–47. ISSN: 0003-3472. DOI: https://doi.org/10.1016/j.anbehav.2018.03.014. URL: https://www.sciencedirect.com/science/article/pii/S0003347218301039.

Levin, S. A. (1992). "The Problem of Pattern and Scale in Ecology: The Robert H. MacArthur Award Lecture". In: *Ecology* 73.6, pp. 1943–1967. ISSN: 0012-9658. DOI: 10.2307/1941447.

Li, J., Y. Zhang, L. Zhao, W. Deng, F. Qian, and K. Ma (2021). "Scale and Landscape Features Matter for Understanding Waterbird Habitat Selection". In: *Remote Sensing* 13.21, p. 4397. ISSN: 2072-4292. DOI: 10.3390/rs13214397.

Liang, D., H. Bailey, A. L. Hoover, S. Eckert, P. Zarate, J. Alfaro-Shigueto, J. C. Mangel, N. De Paz Campos, J. Q. Davila, D. S. Barturen, and et al. (2023). "Integrating telemetry and point observations to inform management and conservation of migratory marine species". In: *Ecosphere* 14.1. ISSN: 2150-8925. DOI: 10.1002/ecs2.4375.

Lichstein, J. W., T. R. Simons, S. A. Shriner, and K. E. Franzreb (2002). "SPATIAL AUTOCORRELATION AND AUTOREGRESSIVE MODELS IN ECOLOGY". In: *Ecological Monographs* 72.3, pp. 445–463. ISSN: 0012-9615.

Linden, D. W., A. P. K. Sirén, and P. J. Pekins (2018). "Integrating telemetry data into spatial capture–recapture modifies inferences on multi-scale resource selection". In: *Ecosphere* 9.4. ISSN: 2150-8925. DOI: 10.1002/ecs2.2203.

Lindgren, F., H. Bakka, D. Bolin, E. Krainski, and H. Rue (2023). "A diffusion-based spatio-temporal extension of Gaussian Matern fields". In.

Lindgren, F., H. Rue, and J. Lindström (2011). "An explicit link between Gaussian fields and Gaussian Markov random fields: the stochastic partial differential equation approach". In: *Journal of the Royal Statistical Society: Series B (Statistical Methodology)* 73.4, pp. 423–498. ISSN: 1369-7412. DOI: 10.1111/j.1467-9868.2011.00777.x. URL: https://doi.org/10.1111/j.1467-9868.2011.00777.x.

Lindgren, F., F. Bachl, J. Illian, M. H. Suen, H. Rue, and A. E. Seaton (2024). *inlabru: software for fitting latent Gaussian models with non-linear predictors*. arXiv: 2407.00791 [stat.ME]. URL: https://arxiv.org/abs/2407.00791.

Liu, Y., J. Zidek, A. Trites, and B. Battaile (2016). "BAYESIAN DATA FUSION APPROACHES TO PREDICTING SPATIAL TRACKS: APPLICATION TO MARINE MAMMALS". In: *The Annals of Applied Statistics* 10(3), pp. 1517–1546. URL: https://www.jstor.org/stable/43956891.

Lomillos, J., M. Alonso, J. García, and V. Lacasa (2017). "Monitoring lidia cattle with GPS-GPRS technology; a study on grazing behaviour and spatial distribution". In: *Veterinaria México OA* 4. DOI: 10.21753/vmoa.4.4.405.

Lundqvist, H. (2007). "Ecological Cost-Benefit Modelling of Herbivore Habitat Quality Degradation due to Range Fragmentation". In: *Transactions in GIS* 11.5, pp. 745–763. DOI: https://doi.org/10.1111/j.1467-9671.2007.01070.x. eprint: https://onlinelibrary.wiley.com/doi/pdf/10.1111/j.1467-9671.2007.01070.x. URL: https://onlinelibrary.wiley.com/doi/abs/10.1111/j.1467-9671.2007.01070.x.

Mårell, A. and L. Edenius (2006). "Spatial Heterogeneity and Hierarchical Feeding Habitat Selection by Reindeer". In: *Arctic Antarctic and Alpine Research - ARCT ANTARCT ALP RES* 38, pp. 413–420. DOI: 10.1657/1523-0430(2006)38[413:SHAHFH]2.0.CO;2.

Martino, S., D. Pace, S. Moro, E. Casoli, D. Ventura, A. Frachea, M. Silvestri, A. Arcangeli, G. Giacomini, G. Ardizzone, and G. Jona Lasinio (2021). "Integration of presence-only data from several sources: a case study on dolphins' spatial distribution". In: *Ecography* 44. DOI: 10.1111/ecog.05843.

Matthiopoulos, J., E. Wakefield, J. W. E. Jeglinski, R. W. Furness, M. Trinder, G. Tyler, A. Mccluskie, S. Allen, J. Braithwaite, and T. Evans (2022). "Integrated modelling of seabird-habitat associations from multi-platform data: A review". In: *Journal of Applied Ecology* 59.4, pp. 909–920. ISSN: 0021-8901. DOI: 10.1111/1365-2664.14114.

Matthiopoulos, J., J. Fieberg, G. Aarts, F. Barraquand, and B. E. Kendall (2020). "Within Reach? Habitat Availability as a Function of Individual Mobility and Spatial Structuring". In: *The American Naturalist* 195.6, pp. 1009–1026. ISSN: 0003-0147. DOI: 10.1086/708519.

Mattisson, J., J. Odden, and J. Linnell (2014). "A catch-22 conflict: Access to semi-domestic reindeer modulates Eurasian lynx depredation on domestic sheep". In: *Biological Conservation* 179, pp. 116–122. ISSN: 0006-3207. DOI: https://doi.org/10.1016/j.biocon.2014.09.004. URL: https://www.sciencedirect.com/science/article/pii/S0006320714003139.

Mayor, S., D. Schneider, J. Schaefer, and S. Mahoney (2009). "Habitat Selection at Multiple Scales". In: *Ecoscience* 16, pp. 238–247. DOI: 10.2980/16-2-3238.

Mccann, R., A. M. Bracken, C. Christensen, I. Fürtbauer, and A. J. King (2021). "The Relationship Between GPS Sampling Interval and Estimated Daily Travel Distances in Chacma Baboons (Papio ursinus)". In: *International Journal of Primatology*. ISSN: 0164-0291. DOI: 10.1007/s10764-021-00220-8.

Mcclintock, B. T., D. S. Johnson, M. B. Hooten, J. M. Ver Hoef, and J. M. Morales (2014). "When to be discrete: the importance of time formulation in understanding animal movement". In: *Movement Ecology* 2.1. ISSN: 2051-3933. DOI: 10.1186/s40462-014-0021-6. URL: https://dx.doi.org/10.1186/s40462-014-0021-6.

Mccrea, R., R. King, L. Graham, and L. Börger (2023). "Realising the promise of large data and complex models". In: *Methods in Ecology and Evolution* 14.1, pp. 4–11. ISSN: 2041-210X. DOI: 10.1111/2041-210x.14050.

Mcgarigal, K., H. Y. Wan, K. A. Zeller, B. C. Timm, and S. A. Cushman (2016). "Multi-scale habitat selection modeling: a review and outlook". In: *Landscape Ecology* 31.6, pp. 1161–1175. ISSN: 0921-2973. DOI: 10.1007/s10980-016-0374-x.

Meehan, T. D., S. P. Saunders, W. V. Deluca, N. L. Michel, J. Grand, J. L. Deppe, M. F. Jimenez, E. J. Knight, N. E. Seavy, M. A. Smith, and et al. (2022). "Integrating data types to estimate spatial patterns of avian migration across the Western Hemisphere". In: *Ecological Applications* 32.7. ISSN: 1051-0761. DOI: 10.1002/eap.2679.

Michelot, T. (2024). "Multiscale modelling of animal movementwith persistent dynamics". arXiv: 2406.15195 [stat.AP]. URL: https://arxiv.org/abs/2406.15195.

Michelot, T. and P. G. Blackwell (2019). "State-switching continuous-time correlated random walks". In: *Methods in Ecology and Evolution* 10.5, pp. 637–649. ISSN: 2041-210X. DOI: 10.1111/2041-210x.13154.

Michelot, T., P. G. Blackwell, S. Chamaillé-Jammes, and J. Matthiopoulos (2020). "Inference in MCMC step selection models". In: *Biometrics* 76.2, pp. 438–447. ISSN: 0006-341X. DOI: 10.1111/biom.13170.

Michelot, T., P. G. Blackwell, and J. Matthiopoulos (2019). "Linking resource selection and step selection models for habitat preferences in animals". In: *Ecology* 100.1. ISSN: 0012-9658. DOI: 10.1002/ecy.2452. URL: https://dx.doi.org/10.1002/ecy.2452.

Michelot, T., P. Gloaguen, P. G. Blackwell, and M.-P. Étienne (2019). "The Langevin diffusion as a continuous-time model of animal movement and habitat selection". In: *Methods in Ecology and Evolution* 10.11, pp. 1894–1907. ISSN: 2041-210X. DOI: 10.1111/2041-210x.13275.

Michelot, T., N. J. Klappstein, J. R. Potts, and J. Fieberg (2024). "Understanding step selection analysis through numerical integration". In: *Methods in Ecology and Evolution* 15.1, pp. 24–35. ISSN: 2041-210X. DOI: 10.1111/2041-210x.14248.

Miller, D. A. W., K. Pacifici, J. S. Sanderlin, and B. J. Reich (2019). "The recent past and promising future for data integration methods to estimate species' distributions". In: *Methods in Ecology and Evolution* 10.1, pp. 22–37. ISSN: 2041-210X. DOI: 10.1111/2041-210x.13110.

Miller, D. L., R. Glennie, and A. E. Seaton (2020). "Understanding the Stochastic Partial Differential Equation Approach to Smoothing". In: *Journal of Agricultural, Biological and Environmental Statistics* 25.1, pp. 1–16. ISSN: 1085-7117. DOI: 10.1007/s13253-019-00377-z.

Miller, J. A. (2012). "Species distribution models". In: *Progress in Physical Geography: Earth and Environment* 36.5, pp. 681–692. ISSN: 0309-1333. DOI: 10.1177/0309133312442522.

Mills, K., B. Patterson, and D. Murray (2006). "Effects of Variable Sampling Frequencies on GPS Transmitter Efficiency and Estimated Wolf Home Range Size and Movement Distance". In: *Wildlife Society Bulletin* 34, pp. 1463–1469. DOI: 10.2193/0091-7648(2006)34%5B1463:EOVSFO%5D2.0.CO;2.

Moa, P. F., I. Herfindal, J. D. C. Linnell, K. Overskaug, T. Kvam, and R. Andersen (2006). "Does the spatiotemporal distribution of livestock influence forage patch selection in Eurasian lynx Lynx lynx?" In: *Wildlife Biology* 12.1, pp. 63–70. DOI: 10.2981/0909-6396(2006)12[63:DTSDOL]2.0.CO;2. URL: https://doi.org/10.2981/0909-6396(2006)12%5B63:DTSDOL%5D2.0.CO;2.

Møller, J. and R. Waagepetersen (2004). "Modern Statistics for Spatial Point Processes". In: *Scandinavian Journal of Statistics* 34, pp. 643–684. DOI: 10.1111/j.1467-9469.2007.00569.x.

Møller, J., A. R. Syversveen, and R. P. Waagepetersen (1998). "Log Gaussian Cox Processes". In: *Scandinavian Journal of Statistics* 25.3, pp. 451–482. ISSN: 0303-6898. DOI: 10.1111/1467-9469.00115.

Morera-Pujol, V., P. S. Mostert, K. J. Murphy, T. Burkitt, B. Coad, B. J. Mcmahon, M. Nieuwenhuis, K. Morelle, A. I. Ward, and S. Ciuti (2023). "Bayesian species distribution models integrate presence-only and presence-absence data to predict deer distribution and relative abundance". In: *Ecography* 2023.2. ISSN: 0906-7590. DOI: 10.1111/ecog.06451.

Morton, D., C. Rowland, C. Wood, L. Meek, C. Marston, G. Smith, R. Wadsworth, and I. C. Simpson (2011). *Final Report for LCM2007-the new UK land cover map*. Tech. rep. 11/07. Countryside Survey Technical Report.

Muff, S., J. Signer, and J. Fieberg (2019). "Accounting for individual-specific variation in habitat-selection studies: Efficient estimation of mixed-effects models using Bayesian or frequentist computation". In: *Journal of Animal Ecology* 89(1), pp. 80–92. DOI: https://doi.org/10.1111/1365-2656.13087.

Murphy, J. (2020). "Climate change, interspecific competition, and poleward vs. depth distribution shifts: Spatial analyses of the eastern Bering Sea snow and Tanner crab (Chionoecetes opilio and C. bairdi)". In: *Fisheries Research* 223, Article 105417. DOI: https://doi.org/10.1016/j.fishres.2019.105417.

Nieminen, M. (2013). "Response distances of wild forest reindeer (Rangifer tarandus fennicus Lönnb.) and semi-domestic reindeer (R. t. tarandus L.) to direct provocation by a human on foot/snowshoes". In: *Rangifer* 33, p. 1. DOI: 10.7557/2.33.1.2614.

Niu, M., P. G. Blackwell, and A. Skarin (2016). "Modeling interdependent animal movement in continuous time". In: *Biometrics* 72.2, pp. 315–324. ISSN: 0006-341X. DOI: 10.1111/biom.12454. URL: https://dx.doi.org/10.1111/biom.12454.

Pagel, J. and F. M. Schurr (2012). "Forecasting species ranges by statistical estimation of ecological niches and spatial population dynamics". In: *Global Ecology and Biogeography* 21.2, pp. 293–304.

Panunzi, G., J. Belmont, J. Illian, and S. Martino (2025a). "Species Distribution Modeling Approach for Biased Citizen Science Data". In: *Italian Statistical Society Series on Advances in Statistics*. Italian Statistical Society Series on Advances in Statistics, pp. 379–385. DOI: 10.1007/978-3-031-64447-4_64.

Panunzi, G., S. Moro, I. Marques, S. Martino, F. Colloca, F. Ferretti, and G. Jona Lasinio (2025b). "Estimating the spatial distribution of the white shark in the Mediterranean Sea via an integrated species distribution model accounting for physical barriers". In: *Environmetrics* 36.1. ISSN: 1180-4009. DOI: 10.1002/env.2876.

Pape, R. and J. Löffler (2015). "Seasonality of habitat selection shown to buffer alpine reindeer pastoralism against climate variability". In: *Ecosphere* 6.12, pp. 1–9. ISSN: 2150-8925. DOI: 10.1890/es15-00169.1.

Pape, R. and J. Löffler (2016). "Towards a process-based biogeography of reindeer—scaling space, time, and organizational levels of space use". In: *Norsk Geografisk Tidsskrift - Norwegian Journal of Geography* 70.4, pp. 230–246. DOI: 10.1080/00291951.2016.1203018.

eprint: https://doi.org/10.1080/00291951.2016.1203018. URL: https://doi.org/10.1080/00291951.2016.1203018.

Paradinas, I., D. Conesa, M. G. Pennino, F. Muñoz, A. M. Fernández, A. López-Quílez, and J. M. Bellido (2015). "Bayesian spatio-temporal approach to identifying fish nurseries by validating persistence areas". In: *Marine Ecology Progress Series* 528, pp. 245–255.

Paradinas, I., J. B. Illian, A. Alonso-Fernändez, M. G. Pennino, and S. Smout (2023). "Combining fishery data through integrated species distribution models". In: *ICES Journal of Marine Science* 80.10, pp. 2579–2590. ISSN: 1054-3139. DOI: 10.1093/icesjms/fsad069.

Paton, R. S. and J. Matthiopoulos (2015). "Defining the scale of habitat availability for models of habitat selection". In: *Ecology*. ISSN: 0012-9658. DOI: 10.1890/14-2241.1. URL: https://dx.doi.org/10.1890/14-2241.1.

Patterson, T. A., A. Parton, R. Langrock, P. G. Blackwell, L. Thomas, and R. King (2017). "Statistical modelling of individual animal movement: an overview of key methods and a discussion of practical challenges". In: *AStA Advances in Statistical Analysis* 101.4, pp. 399–438. ISSN: 1863-8171. DOI: 10.1007/s10182-017-0302-7. URL: https://dx.doi.org/10.1007/s10182-017-0302-7.

Pauler, C. M., H. Homburger, A. Lüscher, M. Scherer-Lorenzen, and M. K. Schneider (2025). "Ecosystem services in mountain pastures: A complex network of site conditions, climate and management". In: *Agriculture, Ecosystems & Environment* 377, p. 109272. ISSN: 0167-8809. DOI: https://doi.org/10.1016/j.agee.2024.109272. URL: https://www.sciencedirect.com/science/article/pii/S0167880924003906.

Pauler, C. M., J. Isselstein, J. Berard, T. Braunbeck, and M. K. Schneider (2020a). "Grazing Allometry: Anatomy, Movement, and Foraging Behavior of Three Cattle Breeds of Different Productivity". In: *Frontiers in Veterinary Science* 7. ISSN: 2297-1769. DOI: 10.3389/fvets.2020.00494.

Pauler, C. M., J. Isselstein, M. Suter, J. Berard, T. Braunbeck, and M. K. Schneider (2020b). "Choosy grazers: Influence of plant traits on forage selection by three cattle breeds". In: *Functional Ecology* 34.5, pp. 980–992. ISSN: 0269-8463. DOI: 10.1111/1365-2435.13542.

Pekarsky, S., I. Schiffner, Y. Markin, and R. Nathan (2021). "Using movement ecology to evaluate the effectiveness of multiple human-wildlife conflict management practices". In: *Biological Conservation* 262, p. 109306. ISSN: 0006-3207. DOI: https://doi.org/10.1016/j.biocon.2021.109306. URL: https://www.sciencedirect.com/science/article/pii/S000632072100358X.

Pennino, M. G., I. Paradinas, J. B. Illian, F. Muñoz, J. M. Bellido, A. López-Quílez, and D. Conesa (2019). "Accounting for preferential sampling in species distribution models". In: *Ecology and Evolution* 9.1, pp. 653–663. ISSN: 2045-7758. DOI: 10.1002/ece3.4789. URL: https://dx.doi.org/10.1002/ece3.4789.

Pepin, K., C. Leach, C. Marques-Toledo, K. Laass, K. Paixao, A. Luis, D. Hayman, N. Johnson, M. Buhnerkempe, S. Carver, D. Grear, K. Tsao, A. Eiras, and C. Webb (2015). "Utility of mosquito surveillance data for spatial prioritization of vector control against dengue viruses in three Brazilian cities". In: *Parasites and Vectors* 8, Article 98. DOI: 10.1186/s13071-015-0659-y.

Phillips, S. J., M. Dudík, J. Elith, C. H. Graham, A. Lehmann, J. Leathwick, and S. Ferrier (2009). "Sample selection bias and presence-only distribution models: implications for background and pseudo-absence data". In: *Ecological Applications* 19.1, pp. 181–197. ISSN: 1051-0761. DOI: 10.1890/07-2153.1.

Pinto, C., J. A. Thorburn, F. Neat, P. J. Wright, S. Wright, B. E. Scott, T. Cornulier, and J. M. J. Travis (2016). "Using individual tracking data to validate the predictions of species distribution models". In: *Diversity and Distributions* 22.6, pp. 682–693. ISSN: 1366-9516. DOI: 10.1111/ddi.12437. URL: https://dx.doi.org/10.1111/ddi.12437.

Planillo, A., M. Wenzler-Meya, I. Reinhardt, G. Kluth, F.-U. F. Michler, N. Stier, J. Louvrier, K. Steyer, B. Gillich, S. Rieger, F. Knauer, T. Kuemmerle, and S. Kramer-Schadt (2023). "Understanding habitat selection of range-expanding populations of large carnivores: 20 years of grey wolves (Canis lupus) recolonizing Germany". In: *Diversity and Distributions* 30, n/a–n/a. DOI: 10.1111/ddi.13789.

Plummer, M. (2012). "JAGS: Just Another Gibbs Sampler". In: *Astrophysics Source Code Library*.

Poggiato, G., T. Münkemüller, D. Bystrova, J. Arbel, J. S. Clark, and W. Thuiller (2021). "On the Interpretations of Joint Modeling in Community Ecology". In: *Trends in Ecology & Evolution* 36.5, pp. 391–401. ISSN: 0169-5347. DOI: 10.1016/j.tree.2021.01.002.

Pollock, L. J., R. Tingley, W. K. Morris, N. Golding, R. B. O'Hara, K. M. Parris, P. A. Vesk, and M. A. Mccarthy (2014). "Understanding co-occurrence by modelling species simultaneously with a Joint Species Distribution Model (JSDM)". In: *Methods in Ecology and Evolution* 5.5, pp. 397–406. ISSN: 2041-210X. DOI: 10.1111/2041-210x.12180.

Pritchard, D. J., J. Fa, S. Oldfield, and S. Harrop (2011). "Bring the Captive Closer to the Wild: Redefining the Role of Ex Situ Conservation". In: *Oryx* 45. DOI: 10.1017/S0030605310001766.

Probo, M., A. Massolo, M. Lonati, D. Bailey, A. Gorlier, L. Maurino, and G. Lombardi (2013). "Use of mineral mix supplements to modify the grazing patterns by cattle for the restoration of sub-alpine and alpine shrub-encroached grasslands". In: *The Rangeland Journal* 35, pp. 85–93. DOI: 10.1071/RJ12108.

R Core Team (2021). *R: A Language and Environment for Statistical Computing*. R Foundation for Statistical Computing. Vienna, Austria.

— (2025). *R: A Language and Environment for Statistical Computing*. R Foundation for Statistical Computing. Vienna, Austria. URL: https://www.R-project.org/.

Rabin, L. A. (2003). "Maintaining Behavioural Diversity in Captivity for Conservation: Natural Behaviour Management". In: *Animal Welfare* 12.1, pp. 85–94. DOI: 10.1017/S0962728600025409.

Rasmus, S., I. Kojola, M. Turunen, H. Norberg, J. Kumpula, and T. Ollila (2020). "Mission impossible? Pursuing the co-existence of viable predator populations and sustainable reindeer husbandry in Finland". In: *Journal of Rural Studies* 80, pp. 135–148. ISSN: 0743-0167. DOI: https://doi.org/10.1016/j.jrurstud.2020.08.017. URL: https://www.sciencedirect.com/science/article/pii/S0743016719306539.

Rhodes, E. C., H. L. Perotto-Baldivieso, M. C. Reeves, and L. A. Gonzalez (2022). "Perspectives on the Special Issue for Applications of Remote Sensing for Livestock and Grazingland Management". In: *Remote Sensing* 14.8, p. 1882. ISSN: 2072-4292. DOI: 10.3390/rs14081882.

Ribeiro, R., J. Matthiopoulos, F. Lindgren, C. Tello, C. M. Zariquiey, W. Valderrama, T. E. Rocke, and D. G. Streicker (2023). "Incorporating environmental heterogeneity and observation effort to predict host distribution and viral spillover from a bat reservoir". In: *Proceedings of the Royal Society B: Biological Sciences* 290.2011. ISSN: 0962-8452. DOI: 10.1098/rspb.2023.1739.

Rivrud, I. M., T. R. Sivertsen, A. Mysterud, B. Åhman, O.-G. Støen, and A. Skarin (2018). "Reindeer green-wave surfing constrained by predators". In: *Ecosphere* 9.5, e02210. ISSN: 2150-8925. DOI: 10.1002/ecs2.2210. URL: https://dx.doi.org/10.1002/ecs2.2210.

Roever, C. L., T. Delcurto, M. Rowland, M. Vavra, and M. Wisdom (2015). "Cattle grazing in semiarid forestlands: Habitat selection during periods of drought1". In: *Journal of Animal Science* 93.6, pp. 3212–3225. ISSN: 0021-8812. DOI: 10.2527/jas.2014-8794.

Roturier, S., S. Bäcklund, M. Sundén, and U. Bergsten (2007). "Influence of ground substrate on establishment of reindeer lichen after artificial dispersal". In: *Silva Fennica* 41. DOI: 10.14214/sf.296.

Rue, H., S. Martino, and N. Chopin (2009). "Approximate Bayesian inference for latent Gaussian models by using integrated nested Laplace approximations". In: *Journal of the Royal Statistical Society: Series B (Statistical Methodology)* 71.2, pp. 319–392. ISSN: 1369-7412. DOI: 10.1111/j.1467-9868.2008.00700.x. URL: https://dx.doi.org/10.1111/j.1467-9868.2008.00700.x.

Rue, H., A. Riebler, S. Sørbye, J. Illian, D. Simpson, and F. Lindgren (2017). "Bayesian Computing with INLA: A Review". In: *Annual Review of Statistics and Its Application* 4.1, pp. 395–421. ISSN: 2326-8298. DOI: 10.1146/annurev-statistics-060116-054045. URL: https://dx.doi.org/10.1146/annurev-statistics-060116-054045.

Sadykova, D., B. E. Scott, M. De Dominicis, S. L. Wakelin, A. Sadykov, and J. Wolf (2017). "Bayesian joint models with INLA exploring marine mobile predator–prey and competitor species habitat overlap". In: *Ecology and Evolution* 7.14, pp. 5212–5226.

Sánchez, M. C. M., S. A. Cushman, and S. Saura (2014). "Scale dependence in habitat selection: the case of the endangered brown bear (Ursus arctos) in the Cantabrian Range (NW Spain)".

In: *International Journal of Geographical Information Science* 28.8, pp. 1531–1546. DOI: 10.1080/13658816.2013.776684. eprint: https://doi.org/10.1080/13658816.2013.776684. URL: https://doi.org/10.1080/13658816.2013.776684.

Sarkar, M., A. Pandey, G. Singh, S. Lingwal, R. John, A. Hussain, G. Rawat, and R. Rawal (2018). "Multiscale statistical approach to assess habitat suitability and connectivity of common leopard (Panthera pardus) in Kailash Sacred Landscape, India". In: *Spatial Statistics* 28, pp. 304–318. DOI: 10.1016/j.spasta.2018.07.006.

Schrödle, B., L. Held, and H. Rue (2012). "Assessing the Impact of a Movement Network on the Spatiotemporal Spread of Infectious Diseases". In: *Biometrics* 68, pp. 736–744. DOI: https://doi.org/10.1111/j.1541-0420.2011.01717.x.

Seddon, P. J., D. P. Armstrong, and R. F. Maloney (2007). "Developing the Science of Reintroduction Biology". In: *Conservation Biology* 21.2, pp. 303–312. DOI: https://doi.org/10.1111/j.1523-1739.2006.00627.x. eprint: https://conbio.onlinelibrary.wiley.com/doi/pdf/10.1111/j.1523-1739.2006.00627.x. URL: https://conbio.onlinelibrary.wiley.com/doi/abs/10.1111/j.1523-1739.2006.00627.x.

Segurado, P., M. B. Araujo, and W. E. Kunin (2006). "Consequences of spatial autocorrelation for niche-based models". In: *Journal of Applied Ecology* 43.3, pp. 433–444. ISSN: 0021-8901. DOI: 10.1111/j.1365-2664.2006.01162.x. URL: https://dx.doi.org/10.1111/j.1365-2664.2006.01162.x.

Serrouya, R., B. N. Mclellan, H. Van Oort, G. Mowat, and S. Boutin (2017). "Experimental moose reduction lowers wolf density and stops decline of endangered caribou". In: *PeerJ* 5, e3736. ISSN: 2167-8359. DOI: 10.7717/peerj.3736. URL: https://dx.doi.org/10.7717/peerj.3736.

Shepard, D. B., A. R. Kuhns, M. J. Dreslik, and C. A. Phillips (2008). "Roads as barriers to animal movement in fragmented landscapes". In: *Animal Conservation* 11.4, pp. 288–296. ISSN: 1367-9430. DOI: 10.1111/j.1469-1795.2008.00183.x. URL: https://dx.doi.org/10.1111/j.1469-1795.2008.00183.x.

Simpson, D., J. B. Illian, F. Lindgren, S. H. Sørbye, and H. Rue (2016). "Going off grid: computationally efficient inference for log-Gaussian Cox processes". In: *Biometrika* 103.1, pp. 49–70. ISSN: 0006-3444. DOI: 10.1093/biomet/asv064. URL: https://dx.doi.org/10.1093/biomet/asv064.

Simpson, D., F. Lindgren, and H. Rue (2012). "In order to make spatial statistics computationally feasible, we need to forget about the covariance function". In: *Environmetrics* 23.1, pp. 65–74. ISSN: 1180-4009. DOI: 10.1002/env.1137.

Simpson, D., H. Rue, A. Riebler, T. Martins, and S. Sørbye (2017). "Penalising Model Component Complexity: A Principled, Practical Approach to Constructing Priors". In: *Statistical Science* 32.1, pp. 1–28. ISSN: 0883-4237. DOI: 10.1214/16-sts576.

Skarin, A. and M. Alam (2017). "Reindeer habitat use in relation to two small wind farms, during preconstruction, construction, and operation". In: *Ecology and Evolution* 7.11, pp. 3870–3882. ISSN: 2045-7758. DOI: 10.1002/ece3.2941. URL: https://dx.doi.org/10.1002/ece3.2941.

Skarin, A., Ö. Danell, R. Bergström, and J. Moen (2010). "Reindeer movement patterns in alpine summer ranges". In: *Polar Biology* 33.9, pp. 1263–1275. ISSN: 0722-4060. DOI: 10.1007/s00300-010-0815-y.

Skarin, A., C. Nellemann, L. Rönnegård, P. Sandström, and H. Lundqvist (2015). "Wind farm construction impacts reindeer migration and movement corridors". In: *Landscape Ecology* 30.8, pp. 1527–1540. ISSN: 0921-2973. DOI: 10.1007/s10980-015-0210-8. URL: https://dx.doi.org/10.1007/s10980-015-0210-8.

Song, L., A. E. Frazier, A. B. Estes, and L. D. Estes (2025). "A multi-scale approach for integrating species distribution models with landscape connectivity to identify critical linkage zones for African savanna elephants (Loxodonta africana)". In: *Ecological Modelling* 507, p. 111198. ISSN: 0304-3800. DOI: https://doi.org/10.1016/j.ecolmodel.2025.111198. URL: https://www.sciencedirect.com/science/article/pii/S0304380025001838.

Sørbye, S. H., J. B. Illian, D. P. Simpson, D. Burslem, and H. Rue (2019). "Careful prior specification avoids incautious inference for log-Gaussian Cox point processes". In: *Journal of the Royal Statistical Society: Series C (Applied Statistics)* 68.3, pp. 543–564. ISSN: 0035-9254. DOI: 10.1111/rssc.12321.

Soriano-Redondo, A., C. M. Jones-Todd, S. Bearhop, G. M. Hilton, L. Lock, A. Stanbury, S. C. Votier, and J. B. Illian (2019). "Understanding species distribution in dynamic populations: a new approach using spatio-temporal point process models". In: *Ecography* 42.6, pp. 1092–1102. ISSN: 0906-7590. DOI: 10.1111/ecog.03771.

Soulsbury, C. D. and P. C. L. White (2015). "Human–wildlife interactions in urban areas: a review of conflicts, benefits and opportunities". In: *Wildlife Research* 42.7, pp. 541–553. DOI: 10.1071/WR14229. URL: https://doi.org/10.1071/WR14229.

Spiegelhalter, D. J., N. G. Best, B. P. Carlin, and A. Van Der Linde (2002). "Bayesian Measures of Model Complexity and Fit". In: *Journal of the Royal Statistical Society Series B: Statistical Methodology* 64.4, pp. 583–639. ISSN: 1369-7412. DOI: 10.1111/1467-9868.00353.

Stanbury, A. (2011). "The changing status of the common crane in the UK". In: *British Birds* 104, pp. 432–447.

Stanbury, A. and N. Sills (2012). *Common Crane habitats in Britain*. Tech. rep. 23: 381. British Wildlife.

Storch, D., M. Konvicka, J. Benes, J. Martinková, and K. J. Gaston (2003). "Distribution patterns in butterflies and birds of the Czech Republic: separating effects of habitat and geographical

position". In: *Journal of Biogeography* 30.8, pp. 1195–1205. ISSN: 0305-0270. DOI: 10.1046/j.1365-2699.2003.00917.x.

Sun, X., Z. Long, and J. Jia (2022). "Identifying core habitats and corridors for giant pandas by combining multiscale random forest and connectivity analysis". In: *Ecology and Evolution* 12.2. ISSN: 2045-7758. DOI: 10.1002/ece3.8628.

Sunde, P., T. Kvam, P. Moa, A. Negård, and K. Overskaug (2000). "Space use by Eurasian lynxes Lynx lynx in central Norway". In: *Acta Theriologica* 45, pp. 507–524. ISSN: 0001-7051. DOI: 10.4098/at.arch.00-50.

Swain, D. and M. Friend (2013). "Opportunities for telemetry techniques in studies on the nutritional ecology of free-ranging domesticated ruminants". In: *Animal* 7, pp. 123–131. ISSN: 1751-7311. DOI: https://doi.org/10.1017/S1751731112000870. URL: https://www.sciencedirect.com/science/article/pii/S1751731112000870.

Tenan, S., P. Pedrini, N. Bragalanti, C. Groff, and C. Sutherland (2017). "Data integration for inference about spatial processes: A model-based approach to test and account for data inconsistency". In: *PLoS ONE* 12.10, e0185588. ISSN: 1932-6203. DOI: 10.1371/journal.pone.0185588. URL: https://dx.doi.org/10.1371/journal.pone.0185588.

Thompson, C. M. and K. Mcgarigal (2002). "The influence of research scale on bald eagle habitat selection along thelower Hudson River, New York (USA)". In: *Landscape Ecology* 17.6, pp. 569–586. ISSN: 0921-2973. DOI: 10.1023/a:1021501231182.

Timm, B. C., K. Mcgarigal, S. A. Cushman, and J. L. Ganey (2016). "Multi-scale Mexican spotted owl (Strix occidentalis lucida) nest/roost habitat selection in Arizona and a comparison with single-scale modeling results". In: *Landscape Ecology* 31.6, pp. 1209–1225. ISSN: 0921-2973. DOI: 10.1007/s10980-016-0371-0.

Tobler, W. R. (1970). "A Computer Movie Simulating Urban Growth in the Detroit Region". In: *Economic Geography* 46, p. 234. ISSN: 0013-0095. DOI: 10.2307/143141.

Torney, C. J., M. R. Laxton, D. J. Lloyd-Jones, E. M. Kohi, H. L. Frederick, D. C. Moyer, C. Mrisha, M. Mwita, and J. G. C. Hopcraft (2023). "Estimating the abundance of a group-living species using multi-latent spatial models". In: *Methods in Ecology and Evolution* 14.1, pp. 77–86. ISSN: 2041-210X. DOI: 10.1111/2041-210x.13941.

Turner, L., M. Udal, B. T. Larson, and S. Shearer (2000). "Monitoring cattle behavior and pasture use with GPS and GIS". In: *Canadian Journal of Animal Science* 80.3, pp. 405–413. ISSN: 0008-3984. DOI: 10.4141/a99-093.

Turunen, M., P. Soppela, H. Kinnunen, M.-L. Sutinen, and F. Martz (2009). "Does climate change influence the availability and quality of reindeer forage plants?" In: *Polar Biology* 32.6, pp. 813–832. ISSN: 0722-4060. DOI: 10.1007/s00300-009-0609-2.

Uhlenbeck, G. E. and L. S. Ornstein (1930). "On the Theory of the Brownian Motion". In: *Phys. Rev.* 36 (5), pp. 823–841. DOI: 10.1103/PhysRev.36.823. URL: https://link.aps.org/doi/10.1103/PhysRev.36.823.

Valente, S., A. Skarin, P. Ciucci, and A. Uboni (2020). "Attacked from two fronts: Interactive effects of anthropogenic and biotic disturbances generate complex movement patterns". In: *Arctic, Antarctic, and Alpine Research* 52.1, pp. 27–40. ISSN: 1523-0430. DOI: 10.1080/15230430.2019.1698251.

Van Niekerk, J., E. Krainski, D. Rustand, and H. Rue (2023). "A new avenue for Bayesian inference with INLA". In: *Computational Statistics & Data Analysis* 181, p. 107692. ISSN: 0167-9473. DOI: 10.1016/j.csda.2023.107692.

Van Niekerk, J. and H. Rue (2024). "Low-rank Variational Bayes correction to the Laplace method". In: *Journal of Machine Learning Research* 25.62, pp. 1–25. URL: http://jmlr.org/papers/v25/21-1405.html.

Wall, J., N. Hahn, S. Carroll, S. Mwiu, M. Goss, W. Sairowua, K. Tiedeman, S. Kiambi, P. Omondi, I. Douglas-Hamilton, and et al. (2024). "Land use drives differential resource selection by African elephants in the Greater Mara Ecosystem, Kenya". In: *Movement Ecology* 12.1. ISSN: 2051-3933. DOI: 10.1186/s40462-023-00436-8.

Waller, P. J. (2005). "Domestication of ruminant livestock and the impact of nematode parasites:possible implications for the reindeer industry". In: *Rangifer* 25.1, pp. 39–50. ISSN: 1890-6729. DOI: 10.7557/2.25.1.336.

Warton, D. I. and L. C. Shepherd (2010). "Poisson point process models solve the "pseudo-absence problem for presence-only data in ecology". In: *The Annals of Applied Statistics* 4.3, pp. 1383–1402. ISSN: 1932-6157. DOI: 10.1214/10-aoas331.

Watanabe, S. (2010). "Asymptotic Equivalence of Bayes Cross Validation and Widely Applicable Information Criterion in Singular Learning Theory". In: *Journal of Machine Learning Research* 11.116, pp. 3571–3594. URL: http://jmlr.org/papers/v11/watanabe10a.html.

Wathes, C., H. Kristensen, J.-M. Aerts, and D. Berckmans (2008). "Is precision livestock farming an engineer's daydream or nightmare, an animal's friend or foe, and a farmer's panacea or pitfall?" In: *Computers and Electronics in Agriculture* 64.1. Smart Sensors in precision livestock farming, pp. 2–10. ISSN: 0168-1699. DOI: https://doi.org/10.1016/j.compag.2008.05.005. URL: https://www.sciencedirect.com/science/article/pii/S0168169908001476.

Wiens, J. A. (1989). "Spatial Scaling in Ecology". In: *Functional Ecology* 3.4, p. 385. ISSN: 0269-8463. DOI: 10.2307/2389612.

Williamson, L. D., B. E. Scott, M. R. Laxton, F. E. Bachl, J. B. Illian, K. L. Brookes, and P. M. Thompson (2022a). "Spatiotemporal variation in harbor porpoise distribution and foraging across a landscape of fear". In: *Marine Mammal Science* 38.1, pp. 42–57. ISSN: 0824-0469. DOI: 10.1111/mms.12839.

Williamson, L. D., B. E. Scott, M. R. Laxton, J. B. Illian, V. L. Todd, P. I. Miller, and K. L. Brookes (2022b). "Comparing distribution of harbour porpoise using generalized additive models and hierarchical Bayesian models with integrated nested laplace approximation". In:

Ecological Modelling 470, p. 110011. ISSN: 0304-3800. DOI: 10.1016/j.ecolmodel.2022.110011.

Woodroffe, R., C. A. Donnelly, D. R. Cox, F. J. Bourne, C. L. Cheeseman, R. J. Delahay, G. Gettinby, J. P. Mcinerney, and W. I. Morrison (2006). "Effects of culling on badger Meles meles spatial organization: implications for the control of bovine tuberculosis". In: *Journal of Applied Ecology* 43.1, pp. 1–10. ISSN: 0021-8901. DOI: 10.1111/j.1365-2664.2005.01144.x. URL: https://dx.doi.org/10.1111/j.1365-2664.2005.01144.x.

Yamamoto, T., Y. Watanuki, E. L. Hazen, B. Nishizawa, H. Sasaki, and A. Takahashi (2015). "Statistical integration of tracking and vessel survey data to incorporate life history differences in habitat models". In: *Ecological Applications* 25.8, pp. 2394–2406. ISSN: 1051-0761. DOI: 10.1890/15-0142.1.

Yuan, Y., F. E. Bachl, F. Lindgren, D. L. Borchers, J. B. Illian, S. T. Buckland, H. Rue, and T. Gerrodette (2017). "Point process models for spatio-temporal distance sampling data from a large-scale survey of blue whales". In: *The Annals of Applied Statistics* 11.4, pp. 2270–2297. ISSN: 1932-6157. DOI: 10.1214/17-aoas1078.